



CRANFIELD UNIVERSITY  
COLLEGE OF AERONAUTICS  
DEPARTMENT OF AEROSPACE SCIENCE

**M.Phil. RESEARCH THESIS**

**MARK R. ROOTS**

**STRUCTURAL DESIGN FOR PASSENGER SAFETY**

Supervisor: Mr. J. C. Brown

May 1996

This thesis is submitted in fulfilment for the Degree of Master of Philosophy.

ProQuest Number: 10820908

All rights reserved

INFORMATION TO ALL USERS

The quality of this reproduction is dependent on the quality of the copy submitted.

In the unlikely event that the author did not send a complete manuscript and there are missing pages, these will be noted. Also, if material had to be removed, a note will indicate the deletion.



ProQuest 10820908

Published by ProQuest LLC (2018). Copyright of the Dissertation is held by Cranfield University.

All Rights Reserved.

This work is protected against unauthorized copying under Title 17, United States Code  
Microform Edition © ProQuest LLC.

ProQuest LLC  
789 East Eisenhower Parkway  
P.O. Box 1346  
Ann Arbor, MI 48106 - 1346





# Dedication

This thesis is dedicated to my father George Richard Roots who sadly passed away on 16th July 1994.

I owe my initial interest in aircraft, to my father, an interest spawned from his air force service. He served as an aircrewman for a period of three years during the Second World War with the Royal Australian Air Force (RAAF) and was stationed in England during this time. As a child I was always impressed by, and interested in, aircraft, especially those in which my dad flew which included Lancasters, Wellingtons and Fairey Battles to name a few. It was this interest which ultimately led me to study at Cranfield University and to gain my MSc in Aerospace Vehicle Design and to continue my studies to gain an MPhil (of which this thesis is part).

As a father he was patient and kind and he always had time to help or assist in any way he could. He took great interest in my studies here at Cranfield from the outset was always supportive and keen to help in any way he could.

I will always have fond memories of him as will the rest of my family. He was a man who loved to read and the following poem was selected from one of his many books. It sums up his thought on death and grief:

## *REMEMBER*

Christina Rossetti

Remember me when I am gone away,  
Gone far away into the silent land;  
Where you can no more hold me by the hand,  
Nor I half turn to go, yet turning stay.

Remember me, when no more day by day  
You tell me of the future that you plann'd:  
Only remember me; you understand  
It will be late to counsel then or pray.

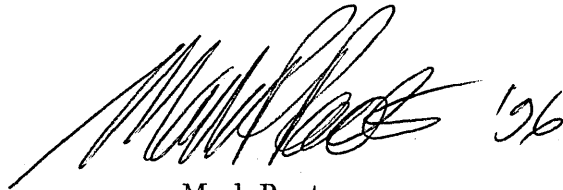
Yet if you should forget me for a while  
And afterwards remember, do not grieve:  
For if the darkness and corruption leave  
A vestige of the thoughts that once I had,  
Better by far you should forget and smile  
Than that you should remember and be sad.

# Acknowledgements

There are a number of people who were of great assistance during my time at Cranfield when undertaking my MPhil studies. Firstly I would like to thank my supervisor, Jason Brown, for providing endless guidance and advice during the course of my work, at all hours of the day and night. My computer skills (especially unix) were enhanced with the assistance Dr Les Oswald. The practical tests carried out as part of this thesis would not have been possible without the assistance of Barry Walker in setting up the instrumentation and sourcing equipment to enable me to carry out the required testing.

In addition there were many other people external to Cranfield who provided support and advice during my studied. In particular my sincere thanks goes to my late father, my mother and the rest of my family who provided encouragement and support during this time.

Joanne Melton deserves an extra special thank you and lots of hugs and kisses for her herculean effort in proof reading the text.



Mark Roots,  
Cranfield University,  
May 1996.



# Synopsis

This thesis covers the design and analysis of a roll cage structure for use on a sports racing car. The method used to design and verify the roll structure was novel as small automotive companies tend to use evolution as a design tool. Evolutionary design works well for certain problems, however, is not well suited to major structural modifications.

The method used in this report integrates the existing structure with the roll cage to improve the torsion stiffness and hence the handling of the vehicle. Careful integration of the roll cage with the rest of the chassis enabled the torsion stiffness to be increased by over 400 %. In addition the weight efficiency of the final chassis was increased over that of the original chassis by over 200 %. The investigation of the torsion stiffness was carried out using linear finite element analysis using the NASTRAN suite of programs.

The second stage of the investigation was to develop this design into a crashworthy roll cage. The resulting model and design are presented in this report. The design of the crashworthy roll cage was carried out using non linear finite element analysis with NASTRAN. The NASTRAN results were then verified with a full structural test on the chassis. The results of the tests are presented and compared to the NASTRAN analysis results. Good correlation was achieved and the method showed promise for applications in the small automotive industries.

The use of finite element analysis for the design of an integrated structure represented a novel application of a well established technique to an industry where experience is the main design tool. The results of the investigation were encouraging and a close correlation was achieved between the analysis and test results.

Finite element analysis represents a relatively cheap and quick method of investigating the effect of structural changes. This method could be used for the design and development of new structures and would give a good indication of the effect of these changes.

Small automotive companies, such as TVR, should find the technique particularly useful for both the design of new structures and for the modification of those already in use.

# Contents

<b>1</b>	<b>Introduction</b>	<b>1</b>
<b>2</b>	<b>Chassis Description</b>	<b>3</b>
2.1	Chassis Design . . . . .	4
2.2	Torsion Stiffness . . . . .	6
<b>3</b>	<b>Chassis Development</b>	<b>9</b>
3.1	Summary of Previous Investigations . . . . .	9
3.1.1	Griffith Torsion Analysis and Testing . . . . .	9
3.1.2	Sports Racing Chassis Torsion Stiffness Analysis . . . . .	11
3.2	Chassis Models Analysed for Torsion Stiffness . . . . .	12
3.2.1	Chimaera Chassis Model and Results . . . . .	12
3.3	Lengthened Chassis Models . . . . .	22
3.4	Roll Over Protection Development . . . . .	31
3.4.1	Roll Cage Development and Results . . . . .	32
3.5	Nonlinear Analysis of Roll Cage . . . . .	36
3.6	Analysis of Standard Chassis . . . . .	39
3.7	Analysis of Extralong Chassis . . . . .	40
3.8	Cerbera GT Chassis . . . . .	51
3.8.1	Investigation of Torsion Stiffness . . . . .	51
3.8.2	Modifications to Wanke's Model . . . . .	55
3.8.3	Full Width Diagonal and Lowered Door Bars . . . . .	57
3.8.4	Vertical Rear Hoop and Lowered Door Bars . . . . .	57
3.8.5	Improved Stiffening Members . . . . .	60
3.8.6	Improved Stiffeners with Gussets . . . . .	60

3.8.7	Final Model . . . . .	60
3.9	Non-Linear Analysis of the Roll Structure . . . . .	63
3.10	Hoop Vertical Loading . . . . .	82
<b>4</b>	<b>Model Setup in NASTRAN</b>	<b>89</b>
4.1	Introduction . . . . .	89
4.1.1	Elements Used for the Analysis . . . . .	90
4.1.2	Co-ordinate System Definition . . . . .	92
4.2	Development of Model in NASTRAN . . . . .	92
4.2.1	Modelling of the Restraints for the Torsion Tests . . . . .	94
4.2.2	Weight of Models . . . . .	94
4.3	Nonlinear Modelling . . . . .	95
4.3.1	General Recommendation on Nonlinear Modelling . . . . .	95
4.3.2	Development of the Nonlinear Model . . . . .	96
<b>5</b>	<b>Plastic Hinges</b>	<b>103</b>
5.1	Combined Bending and Axial Forces . . . . .	109
5.2	Inelastic Material Behaviour . . . . .	111
5.2.1	Maximum Shear Stress Theory (Tresca) . . . . .	112
5.3	Distortional Energy Density (von Mises) Criterion . . . . .	113
<b>6</b>	<b>Test Schedules for TVR Chassis</b>	<b>114</b>
6.1	Vertical Load Test . . . . .	114
6.2	Frontal Crush Loading . . . . .	123
6.3	Calibration of Instrumentation . . . . .	132
	<b>Discussion</b>	<b>136</b>
	<b>Conclusion</b>	<b>137</b>
	<b>Bibliography</b>	<b>139</b>
<b>A</b>	<b>RAC Motor Sports Requirements</b>	<b>140</b>
A.1	Technical Requirements - Section E . . . . .	140
A.2	Specific Technical Regulations for Car Racing - Section J . . . . .	143

A.3	Nomenclature and Definitions - Section P . . . . .	143
A.4	Safety Criteria - Section Q . . . . .	144
<b>B</b>	<b>Test Rig Design and Analysis</b>	<b>146</b>
B.1	Test Rig Design . . . . .	146
B.1.1	Design of Mounting Beam Clamps . . . . .	147
B.2	Chassis Attachments to Mounting Frame . . . . .	153
B.2.1	Bolts in Combined Shear and Tension . . . . .	156
B.3	Sizing of the Chassis Mounting Plates . . . . .	157
B.3.1	Bearing Stress . . . . .	158
B.3.2	Shear Tearout Failure . . . . .	159
B.3.3	Tensile Failure Stress . . . . .	160
B.3.4	Weld Design . . . . .	160
B.4	Friction Mounting of Beams . . . . .	161
B.4.1	Load Link Calibration . . . . .	163
B.5	Test Rig Design for Vertical Loading . . . . .	164
B.5.1	Bolt Diameters in Load Link . . . . .	164
B.5.2	Design of Load Bars . . . . .	166
<b>C</b>	<b>Material Properties</b>	<b>170</b>
C.1	Cold Finished Seamless (CFS) Tubing . . . . .	170
C.2	Carbon Manganese Steel Tube (T.45) Tubing . . . . .	170
C.3	Electrically Resistance Welded (ERW) Tubing . . . . .	171
C.4	Bolt Grades and Properties . . . . .	173
C.5	Standard Wire Gauges - SWG . . . . .	173
<b>D</b>	<b>Plastic Hinge Moment Calculations for Chassis</b>	<b>174</b>
D.1	Plastic Hinge Moment for a Circular Tube . . . . .	175
D.1.1	Thick Walled Tube . . . . .	176
D.2	Axial Force and Bending Moment Interaction . . . . .	178
D.2.1	Combined Bending and Axial Forces . . . . .	181
D.3	Comparison of Theoretical Results with NASTRAN Results. . . . .	183
<b>E</b>	<b>Nastran Plastic Hinge Model</b>	<b>185</b>

<b>F</b>	<b>Chassis Member Cross Sectional Properties</b>	<b>192</b>
F.1	Calculation of Cross Sectional Properties . . . . .	192
F.1.1	Cross Sectional Area . . . . .	192
F.1.2	Second Moments of Area . . . . .	193
F.1.3	Torsion Constants . . . . .	194
F.2	Cross Sectional Dimensions and Properties . . . . .	196
F.2.1	Cross Sectional Area . . . . .	196
F.2.2	Second Moment of Area . . . . .	196
F.2.3	Torsion Constant . . . . .	197
F.2.4	Tubular Sections . . . . .	197
<b>G</b>	<b>Torsion Load Calculation</b>	<b>198</b>
<b>H</b>	<b>RAC Safety Requirements</b>	<b>199</b>
<b>I</b>	<b>NASTRAN Data Files</b>	<b>210</b>
<b>J</b>	<b>Drawings</b>	<b>214</b>

# List of Figures

1.1	TVR Griffith . . . . .	1
2.1	TVR Chassis Arrangement . . . . .	4
2.2	Pawlowski's Chassis Structure . . . . .	5
2.3	Backbone Chassis Structure . . . . .	5
2.4	TVR Griffith Showing Chassis Structure . . . . .	7
2.5	TVR Chimaera . . . . .	8
2.6	TVR Cerbera . . . . .	8
3.1	Parallel Springs . . . . .	10
3.2	Chimaera Chassis with the gearbox crossmember and the plate . . . . .	13
3.3	Chimaera Chassis with the gearbox member and no plate . . . . .	14
3.4	Chimaera Chassis without the gearbox member or plate . . . . .	15
3.5	Chimaera Chassis without the gearbox member but with the plate . . . . .	16
3.6	Chimaera Chassis with the gearbox crossmember and the plate - Deflected Shape . . . . .	17
3.7	Chimaera Chassis with the gearbox member and no plate - Deflected Shape . . . . .	18
3.8	Chimaera Chassis without the gearbox member or plate - Deflected Shape . . . . .	19
3.9	Chimaera Chassis without the gearbox member but with the plate - Deflected Shape . . . . .	20
3.10	Graph of Deflections for the Different Chimaera Chassis Configurations . . . . .	21
3.11	Chassis (2,844mm) with the gearbox crossmember and the plate - Deflected Shape . . . . .	23
3.12	Chassis (2,844mm) without the gearbox crossmember and with the plate - Deflected Shape . . . . .	24
3.13	Chassis (2,844mm) with the gearbox crossmember and without the plate - Deflected Shape . . . . .	25
3.14	Chassis (2,844mm) without the gearbox crossmember and without the plate - Deflected Shape . . . . .	26



3.15 Chassis (2,844mm) with the gearbox member and plate with circular lower rails - Deflected Shape . . . . .	27
3.16 Graph of Deflections for the Different Chassis Configurations - Long (2,844mm) Chassis. . . . .	28
3.17 Graph of Deflections for the Different Chassis Configurations - Extralong (2,894mm) Chassis . . . . .	30
3.18 After Market Roll-Hoop . . . . .	31
3.19 After Market Roll-Hoop Joint . . . . .	32
3.20 Chimaera Chassis with Standard (After Market) Roll Hoop . . . . .	34
3.21 Chimaera Chassis with Front and Rear Roll Hoops <i>gearbox plate included</i> . . . . .	35
3.22 Extralong Chassis with Full Roll Cage . . . . .	37
3.23 Graph Showing Torsion Stiffness Variation - Chassis with Roll Structure . . . . .	38
3.24 TVR Chimaera Chassis with Roll Hoop - Aft Load. . . . .	41
3.25 TVR Chimaera Chassis with Roll Hoop - Forward Load. . . . .	42
3.26 Stress Distribution at Failure, TVR Chimaera Chassis with Roll Hoop - Aft Load. . . . .	43
3.27 Stress Distribution at Failure, TVR Chimaera Chassis with Roll Hoop - Forward Load. . . . .	44
3.28 Stress Distribution at Failure, TVR Chimaera Chassis with Roll Hoop - Aft Load with Elastic and Plastic Members . . . . .	45
3.29 Extralong Chassis with $\phi 44$ Circular Base Members - Stress Distribution at Failure, Load Acting Aft. . . . .	46
3.30 Extralong Chassis with $\phi 44$ Circular Base Members - Stress Distribution at Failure - Forward Acting Load . . . . .	47
3.31 Extralong Chassis with $\phi 55$ Circular Base Members - Stress Distribution at Failure - Aft Acting Load . . . . .	48
3.32 TVR Extralong Chassis with Full Roll Cage . . . . .	49
3.33 Extralong Chassis with Rollcage made from $\phi 44$ tubing - Stress Distribution at Failure	52
3.34 Extralong Chassis with Rollcage made from $\phi 25$ tubing - Stress Distribution at Failure	53
3.35 Extralong Chassis with Rollcage made from $\phi 32$ tubing - Stress Distribution at Failure	54
3.36 Final Chassis Arrangement . . . . .	55
3.37 Cerbera GT Chassis (Wanke) . . . . .	56
3.38 Cerbera GT Chassis with Full Rear Hoop Diagonal . . . . .	58
3.39 Cerbera GT Chassis with Vertical Rear Hoop and Lowered Door Bars . . . . .	59
3.40 Cerbera GT Chassis with Additional Front Stiffners . . . . .	61

3.41 Cerbera GT Chassis with Additional Stiffeners and Gussets . . . . .	62
3.42 Cerbera GT Chassis Final Model . . . . .	64
3.43 Torsion Stiffness Increase Achieved . . . . .	65
3.44 Stress Distribution in the Linear Analysis Cerbera GT Model . . . . .	67
3.45 Stress Distribution in the Fully Nonlinear Cerbera GT Model at Failure . . . . .	68
3.46 Stress Distribution in the Fully Nonlinear (T45 tubing) Analysis Cerbera GT Model at Failure . . . . .	69
3.47 Stress Distribution in the Partially Nonlinear Analysis Cerbera GT Model . . . . .	70
3.48 Stress Distribution in the Fully Nonlinear Analysis Cerbera GT Model with Single Elements Between Welded Joints . . . . .	71
3.49 Load Displacement Curve for Fully Nonlinear Cerbera GT Model . . . . .	72
3.50 Load Displacement Curve for Partially Nonlinear Cerbera GT Model . . . . .	73
3.51 Load Displacement Curve for Fully Nonlinear Cerbera GT Model with Single Ele- ments Between Welds . . . . .	74
3.52 Stress Distribution in the Fully Nonlinear Analysis Cerbera GT Model with the Webs Included (Elastic Webs) . . . . .	76
3.53 Stress Distribution in the Fully Nonlinear Analysis Cerbera GT Model with the Webs Included - Both Materials Modelled . . . . .	77
3.54 Deflected Shape (Isometric View) of the Fully Nonlinear Analysis Cerbera GT Model with the Webs Included - Both Materials Modelled . . . . .	78
3.55 Deflected Shape (Side View) of the Fully Nonlinear Analysis Cerbera GT Model with the Webs Included - Both Materials Modelled . . . . .	79
3.56 Deflected Shape (Front View) of the Fully Nonlinear Analysis Cerbera GT Model with the Webs Included - Both Materials Modelled . . . . .	80
3.57 Deflected Shape (Plan View) of the Fully Nonlinear Analysis Cerbera GT Model with the Webs Included - Both Materials Modelled . . . . .	81
3.58 Stress Distribution for Vertical Load on Rear Roll Hoop - Linear Cerbera GT Model, Applied Load 60,516 N . . . . .	83
3.59 Stress Distribution for Vertical Load on Rear Roll Hoop - Linear Cerbera GT Model, Applied Load 86,452 N . . . . .	84
3.60 Stress Distribution for Vertical Load on Rear Roll Hoop - Nonlinear Cerbera GT Model, Applied Load 59,670 N . . . . .	85
3.61 Vertical Displacement in the Centre of the Rear Roll Hoop - Linear Cerbera GT Model, Applied Load 86,452 N . . . . .	86
3.62 Vertical Displacement in the Centre of the Rear Roll Hoop - Nonlinear Cerbera GT Model, Applied Load 59,670 N . . . . .	87

4.1	NASTRAN BAR Element . . . . .	91
4.2	NASTRAN BAR Element Forces and Moments . . . . .	92
4.3	NASTRAN BEAM Element . . . . .	93
4.4	Chassis Restraints . . . . .	95
4.5	Chassis Showing Loading Bar Arrangement . . . . .	99
4.6	Combined Bending and Axial Forces . . . . .	101
4.7	Numerical Ill-Conditioning with Strain Hardening. . . . .	102
5.1	Cantilever Beam . . . . .	103
5.2	Loading Curve for Cantilever Beam . . . . .	104
5.3	Elastic-Perfectly Plastic Load Deflection Curve . . . . .	105
5.4	Moment-Curvature Diagram for the Cantilever Beam . . . . .	105
5.5	Ideal Moment Curvature Diagram for the Cantilever Beam . . . . .	106
5.6	Stress Strain Curve for Mild Steel . . . . .	107
5.7	Beam Cross Section and Yielding . . . . .	108
5.8	Plastic Zone in a Cantilever Beam . . . . .	109
5.9	Combined Bending and Axial Forces . . . . .	109
5.10	Rectangular Beam subjected to Axial and Bending Forces . . . . .	110
5.11	Bending Moment and Forces . . . . .	111
6.1	Rear Roll Hoop Test Setup on Chassis. . . . .	116
6.2	Rear Hoop Vertical Load-Displacement Curve - With Wooden Support Blocks. . . . .	117
6.3	Local Tube Crushing in the Rear Hoop . . . . .	118
6.4	Local Tube Flattening in the Rear Hoop . . . . .	119
6.5	Rear Hoop Vertical Load-Displacement Curve - Without the Wooden Support Blocks. . . . .	120
6.6	NASTRAN Model Vertical Load-Displacement Curve . . . . .	121
6.7	Vertical Test Setup - LVDT Location . . . . .	122
6.8	Test Rig Setup for the Frontal Crush Loading . . . . .	124
6.9	Load Deflection Curve for the Front Windscreen Corner. . . . .	126
6.10	NASTRAN Load Deflection Curve . . . . .	127
6.11	Hinge Locations in the "A" Pillar . . . . .	128
6.12	Order of Hinge Formation in the Roll Cage . . . . .	129
6.13	Details of the Buckling in the Front Roll Structure . . . . .	130

6.14	Detail of Closed up Buckle (No 1) in Roll Cage . . . . .	131
6.15	Detail of Buckle Number 4 in Roll Cage . . . . .	131
6.16	Load Cell Calibration . . . . .	133
6.17	LVDT Calibration . . . . .	134
A.1	RAC Approved Roll Cage Designs . . . . .	141
A.2	RAC Approved Roll Cage Designs . . . . .	142
B.1	Chassis Mounting for Tests . . . . .	146
B.2	Relative Location of Load Point to Chassis Mounting Beams for Tests . . . . .	147
B.3	Chassis Mountings in Relation to the Load . . . . .	148
B.4	Mounting Beam Loads . . . . .	149
B.5	Loading Plate Failure Modes . . . . .	157
B.6	Loading Plate Dimensions . . . . .	158
B.7	Loading Plate Failure Modes . . . . .	159
B.8	Fillet Weld Dimensions . . . . .	161
B.9	Forces acting on Mounting Beam . . . . .	162
B.10	Loadlink General Arrangement . . . . .	164
B.11	Calibration Curve for Load Link . . . . .	165
B.12	Loadlink Attachments . . . . .	166
B.13	Loading Arrangement . . . . .	167
C.1	Tensile Test Results - Chassis Roll Cage Tube . . . . .	172
D.1	Plastic Moment for Non-Symmetrical Section . . . . .	174
D.2	Circular Tube - Thick Wall . . . . .	175
D.3	Circular Chassis Tube . . . . .	177
D.4	Tube Subjected to Axial Force - Fully Plastic Collapse . . . . .	179
D.5	Tube Subjected to Axial Force . . . . .	179
D.6	Tube Subjected to Bending Moment . . . . .	180
D.7	Yield Surface for Combined Axial and Bending Stresses . . . . .	182
D.8	NASTRAN Cantilever Beam . . . . .	183
D.9	NASTRAN and Theoretical Results for Cantilever Beam . . . . .	184

E.1	NASTRAN Plastic Hinge Model . . . . .	186
E.2	NASTRAN Plastic Hinge Model Giving Locations of Lumped Masses. . . . .	187
E.3	Axial and Bending Strain on the Cross Section . . . . .	188
E.4	Bending Failure of Cross Section (Stage 1) . . . . .	189
E.5	Bending and Tensile Failure of Cross Section, Stage 2 . . . . .	190
E.6	Bending and Tensile Failure of Cross Section, Stage 3 . . . . .	190
E.7	Bending and Tensile Failure of Cross Section, Stage 4 . . . . .	191
E.8	Tensile Failure of Cross Section (Stage 5) . . . . .	191
F.1	Beam Cross Sections . . . . .	192
F.2	'C' Beam Cross Section . . . . .	195
H.1	RAC Safety Requirements . . . . .	200
I.1	Nonlinear Data File with Force Loading . . . . .	211
I.2	Nonlinear Data File with Displacement Loading . . . . .	212
I.3	Partially Nonlinear Model . . . . .	213

# List of Tables

3.1	Summary of Results from Gadola . . . . .	10
3.2	Summary of Results from Wanke . . . . .	11
3.3	Table of Results - Standard Chassis . . . . .	22
3.4	Table of Results for Long Chassis . . . . .	29
3.5	Table of Results for Extralong Chassis . . . . .	31
3.6	Table of Results for Chimaera Chassis with Roll Structure . . . . .	33
3.7	Table of Results for Extra Long Chassis . . . . .	36
3.8	Chimaera Chassis Results Table . . . . .	40
3.9	Extralong Chassis with Circular Base Tubes Results Table . . . . .	50
3.10	Extralong Chassis Results Table - Full Roll Cage . . . . .	50
3.11	Summary of Results from Wanke's Model . . . . .	57
3.12	Cerbera GT with full width diagonal in rear hoop and lowered door bars . . . . .	57
3.13	Cerbera GT with vertical rear hoop and lowered door bars . . . . .	57
3.14	Cerbera GT additional stiffeners in front . . . . .	60
3.15	Cerbera GT additional stiffeners in front . . . . .	60
3.16	Final Cerbera GT Model . . . . .	63
3.17	Cerbera GT Nonlinear Crush Results . . . . .	75
3.18	Cerbera GT Nonlinear Crush Results . . . . .	75
3.19	Cerbera GT Nonlinear Results - Load applied to rear hoop . . . . .	75
3.20	Cerbera GT Nonlinear Rear Hoop Loading Results . . . . .	88
6.1	Calibration Values for Tests . . . . .	132
B.1	Load Components Applied to Chassis . . . . .	147
B.2	Reaction Loads at the Lower Chassis Rails . . . . .	149
B.3	Mounting Beam Reaction Loads . . . . .	150

B.4	Reactions at Mounting Beam Base . . . . .	151
B.5	Tensile and Shear Maximum Loads . . . . .	151
B.6	Chassis Mounting Forces for 21kN Applied Load . . . . .	153
B.7	Chassis Mounting Forces for 35kN Applied Load . . . . .	154
B.8	Bolt Diameter Results for Grade 8.8 and 4.6 Steel with an applied load of 21kN . . .	155
B.9	Bolt Diameter Results for Grade 8.8 and 4.6 Steel with an applied load of 35kN . . .	156
C.1	CFS Tubing Material Properties . . . . .	170
C.2	ERW Tubing Material Properties . . . . .	171
C.3	Steel Bolt Material Properties . . . . .	173
C.4	Standard and Wire Gauges . . . . .	173
D.1	Plastic Hinge Moments for Roll-Cage Members . . . . .	178
E.1	NASTRAN Plastic Hinge Rod Areas and Locations . . . . .	187
F.1	Dimensions of the Chassis Tubes . . . . .	196
F.2	Cross Sectional Properties . . . . .	197

# Chapter 1

## Introduction

TVR Engineering is one of a handful of small automotive manufacturing companies in the United Kingdom. They specialise in the production of high performance vehicles for enthusiasts and their cars are aimed at this niche market.

The TVR vehicle body work is produced using glass reinforced polymers<sup>1</sup>. A tubular welded steel truss construction is used to produce the backbone chassis to which the body work is attached. Both of these components are produced by hand resulting in a low volume production in comparison to the large automotive manufacturers. Mechanical components are generally sourced from large manufacturers such as Ford and Rover which enables TVR to save on the development costs of these expensive components. This combination of in house production and external sourcing enables the company to keep the production costs to a minimum.

Current production rates are approximately 20 vehicles per week. The design and product sourcing detailed above enable TVR to produce their vehicles at competitive prices for the performance that is achieved. Current prices vary between £27,850 for a Chimaera to £33,700 for the new Cerbera<sup>2</sup>.

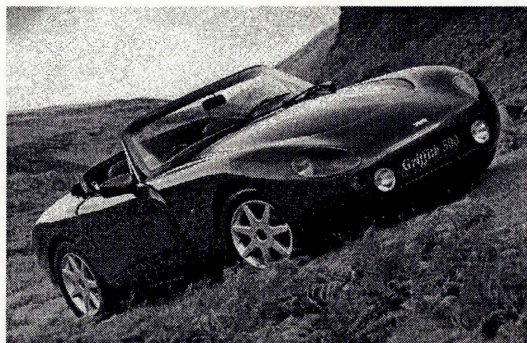


Figure 1.1: TVR Griffith

Historically, small sports car manufacturers have tended to use a combination of past experience and trial and error as design tools. This system of design has led to the development of a vehicle with adequate performance and handling characteristics. The incorporation of major design changes or new features such as crashworthiness are not particularly suited to the evolutionary

---

<sup>1</sup>Glass Reinforced Polymer (GRP) is often called Fibreglass.

<sup>2</sup>Price data from *Autocar* magazine 6th Sept. 1995



design methodology. If evolutionary design is used for these then the results may be inefficient or ineffective.

In racing there are now requirements<sup>3</sup> to fit vehicles with safety roll over structures. A major problem associated with the design and construction of this type of car is the achievement of an adequate torsion stiffness. Whilst the standard car without the roll over structure has a suitable torsion stiffness for general road usage it is not sufficient for the rigours of high performance racing. The incorporation of a roll cage into the existing chassis offers the manufacturer the ability to improve the torsion stiffness and consequently the handling performance of the vehicle, whilst additionally improving the roll over safety of the vehicle. This type of major structural modification is unsuitable for evolutionary design and a scientific approach is presented in this report to develop the roll cage and incorporate it into the overall vehicle structure.

In general the standard procedure in industry is to produce the two structures independently - the roll cage represents a consequent weight penalty without the stiffness contribution being properly utilised.

When the author commenced work on this thesis TVR were keen to investigate a lengthened version of the TVR Griffith<sup>4</sup> which is shown in Figure 1.1. This vehicle was initially being developed for racing and was to include a roll over structure to conform with the then proposed RACMSA requirements. Due to its good reception at the motor show a 2+2 seat car, the Cerbera, was the outcome of this investigation - albeit without the full roll cage. It is this chassis which was the basis of the original investigation.

After the author had completed the initial investigation other commitments led to a break in that work. In 1994 TVR received funding to produce a race version of the Cerbera for the BDRC 1995 Le-Mans 24 hour race (C2 class). At this stage Thomas Wanke, another student at Cranfield, undertook the work on this project. The main aim of this work was to improve the torsion stiffness of the chassis. He carried out an in depth study to increase the torsion stiffness of the vehicle without posing any serious weight penalty. This work is fully detailed in Ref. [4].

After the car had been produced for the 1995 Le-Mans race the author re-commenced his investigation into the design of the roll cage to the RAC requirements. The investigation consisted of three major parts:

- (1) the modelling of the tubular truss chassis and roll cage using static analysis to determine the torsion stiffness increase,
- (2) once a suitable torsion stiffness has been achieved the model was subjected to a nonlinear finite element analysis using material nonlinearity and,
- (3) verification of the results by carrying out a quasi-static crush test on the chassis with the pre determined loading cases<sup>5</sup>.

The loading specified by the RAC requirements [10] is a static load with a maximum deflection. There are no energy absorption requirements and consequently these are not dealt with in this report.

---

<sup>3</sup>RACMSA requirements from 1 January 1994 for all racing events in the UK and these requirements are in line with those introduced by the FIA. These requirements are for the safety of the competitors and the guidelines give designs for acceptable roll cages and the loading conditions to be satisfied.

<sup>4</sup>This TVR Griffith was introduced in Spring 1992 and was analysed by Gadola [5].

<sup>5</sup>The loading cases were based on the nonlinear finite element failure loads.

## Chapter 2

# Chassis Description

The backbone chassis is well established within the sports car market. TVR adopted this type of chassis early on with the production of the 'S' series vehicles. From this was developed the sports racing car, Tuscan, and then the Griffith, Chimaera, and soon to be released Cerbera<sup>1</sup>. This development highlights the evolutionary design process and illustrates its success in producing a succession of fine vehicles. This design methodology is suited to the minor changes which occur as models are developed and has included both structural and body work modifications.

The TVR chassis has the same basic structural form for all the variants. The major components and features of the chassis are described below and illustrated in Figure 2.1.

- triangulated front cage accommodating the radiator and wide based front double wishbones,
- large engine bay for the newly developed TVR engine. The engine bay tapers at the rear to the footwell,
- transmission tunnel designed as a tubular beam,
- a steel plate bolted underneath the transmission tunnel in order to protect the driveline and exhaust and most importantly to enclose the open section,
- triangulated rear cage accommodating the rear differential and the rear double wishbone suspension,
- outriggers which run underneath the occupant floor. These provide attachment for the GRP body sills and have the added advantage of providing some side impact protection to the occupants,
- outrigger stiffeners are attached at the front and rear and provide stiffness to these outriggers.

The entire chassis is constructed of steel tubes and sections. The material used for the chassis is CFS3<sup>2</sup> and all circular tubes are 16swg. The rectangular lower chassis members are 2mm wall thickness (14swg). All joints are hand MIG welded using a jig to hold the components.

---

<sup>1</sup>The BDRC Le-Mans 24 hour racing car developed and discussed in reference [4] is based on the Cerbera chassis.

<sup>2</sup>This material specification replaces the old designation CDS2 tubing and the material properties are contained in Appendix C

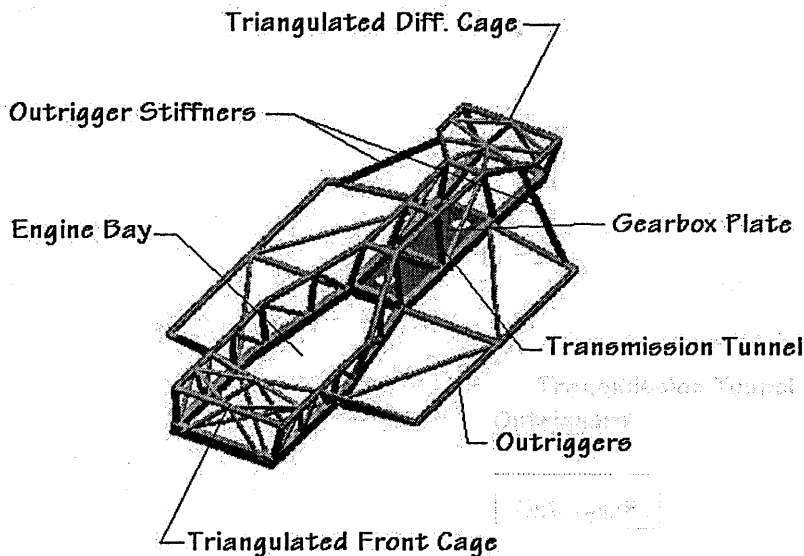


Figure 2.1: TVR Chassis Arrangement

## 2.1 Chassis Design

Pawlowski [6] categorizes vehicle structures as flat or punt types, closed integral types, or open integral types. The division does not, however, always correspond to the appearance of the body. The classification is dependent on the appearance of shear forces at the edges of the idealised structure as shown in Figure 2.2. In summary, the main types of structure are classed as:

- (1) **Closed** - if the main design surfaces form a closed system, and if shear forces occur between them when it is loaded in torsion. The simplest form of the closed structure is the rectangular parallelepiped. This type of structure is generally found in sedans and coupes etc.
- (2) **Open** - if it lacks the upper or front and rear structural surfaces in the parallelepiped system, and if edge shears do not arise between all the surfaces when loaded in torsion. Cabriolets and Roadsters fall into this category.
- (3) **Flat** - if all the torsion and bending loads are transferred through the floor because structural surfaces are not present. Sports cars with backbone style chassis' where the body and chassis cooperate in carrying the loads. This is the category of the TVR car analysed.

The essential elements of the flat structure are a floor plate with edge members (sills) and beams (cross members) which are used to mount the engine and suspension.

The backbone chassis works by having a central component of the structure taking the torsion loads from the front and rear of the vehicle as shown diagrammatically in Figure 2.3. In the case of the TVR chassis, the backbone is built up from a well triangulated truss arrangement in the transmission tunnel and the section is closed with a flat plate underneath. From the end of this structure are the beam cantilever elements which are used to hang the engine on and to provide a mountings for the suspension.

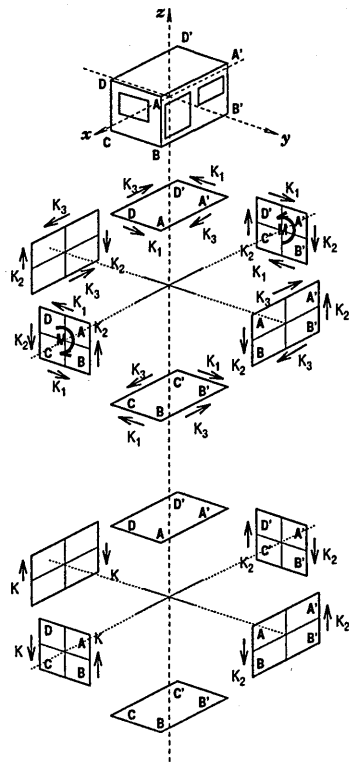


Figure 2.2: Pawlowski's Chassis Structure

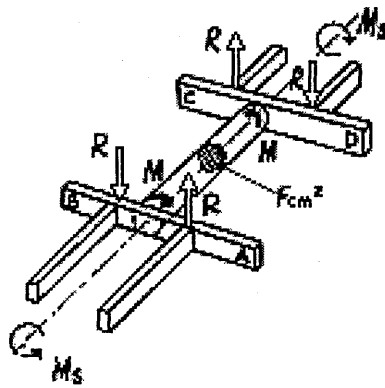


Figure 2.3: Backbone Chassis Structure

The advantage of the backbone frame chassis is the relatively high torsion stiffness at low cost and low weight. The disadvantage is the length of the outriggers needed to carry the body sides. These outriggers tend to introduce torsional vibration problems because of their high flexibility [7]. In the TVR chassis the outriggers have additional members connected back to the main chassis to minimise this effect. The body work is attached to the outriggers at a number of places which also assists in reduction of the vibrations. The co-operation of the remaining assemblies of the car body is ensured through the joint of the sill with the sidewall and the front and rear bulkheads with the cross members of the flat structure.

The amount of the load carried by the flat structure is dependent on how the body is attached to it. If the body is mounted with few elastic body mounts the chassis structure may carry 40-60% of the load. As the number of mounting points is increased (ie redundancy introduced) to a few dozen or more the load carried by the chassis structure is reduced to around 20-30%. Rigid mounts reduce this further and eventually this type of design becomes uneconomical and inefficient. This phenomenon is illustrated in the results from the work of Gadola [5]. A summary of this work is contained in Section 3.1.1.

## 2.2 Torsion Stiffness

As a general rule the value of the torsion stiffness is taken as a measure of the structural performance of a chassis. Typical values for torsion stiffness are given below.

The automotive chassis connects the four wheels to a structure which is, ideally, rigid in bending and torsion. In addition it has to support the engine and associated running gear, house the occupants, carry the body work and absorb all the external loads exerted on it without excessive deflection.

Practical experience has shown that the higher the stiffness of the car the better the handling characteristics will be. Whilst a high bending stiffness is the easiest to attain, a high torsion stiffness is probably the most important for handling. A high torsion stiffness is important to ensure that the tyres remain in contact with the road, that the car feels good to the driver and that the car reacts in a predictable and controlled manner. In general a good torsion stiffness will result in a more than adequate bending stiffness but the inverse is not true. It is possible to have a good bending stiffness with a low torsion stiffness (as occurs with a 'C' Beam). Torsion stiffness is also important for ensuring a good fatigue life although the two are not necessarily directly related.

Possibly the worst cars in terms of torsion stiffness on the road are the Triumph Herald and Spitfire which both have values around 2,200 Nm/deg. In today's climate a torsion stiffness of between 6,000 and 9,000 Nm/deg is considered adequate for a general purpose road car and is typical for a standard family sedan. A torsion stiffness of this order will allow the car to carry out its desired purpose satisfactorily without undue deflection, noise or vibration. Larger and more expensive cars have significantly higher values of torsion stiffness. This is achieved by way of refinement with a consequent lowering in the vibration and noise levels in the vehicle. Typical examples would be the Mercedes or BMW ranges which offer torsion stiffnesses in the range 12,000 - 15,000 Nm/deg.

Racing demands higher levels of torsion stiffness which is critical to the vehicle handling and performance at high speed and the maintenance of the correct suspension geometry. Rally vehicles require higher torsion stiffness to keep the wheels on the road in very rough conditions and normal values are in the range 15,000 to 20,000 Nm/deg. For road or track racing very stiff springs are



used in conjunction with rigid ball joints in the suspension in order to gain increased cornering power by keeping the tyre flat on the road. It is logical that as the suspension stiffness is increased the loads into the chassis are also increased which is another reason for the very high torsional stiffness requirements for the chassis. For Formula 1 vehicles the torsion stiffness is often in excess of 35,000 Nm/deg.

The chassis analysed was specifically for racing and it was realised that a significant improvement in the torsion stiffness was required. In order to comply with the race regulations a full roll cage had to be fitted and this provided the ideal method of improving the torsion stiffness.

The achievement of a satisfactory torsion stiffness required a closed box structure to be developed and incorporated into the design. The ideal structure is illustrated in Figure 2.2 which shows the load paths and the carrying of the torsion load as shear within the panels. If the box structure cannot be produced using flat panels (i.e. sheet metal) then the triangulated panel represents the next best option. For torsion stiffness the shear carrying capacity is of prime importance and as a consequence well triangulated panels are critical.

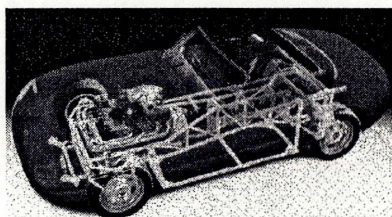


Figure 2.4: TVR Griffith Showing Chassis Structure

The standard chassis of the TVR is illustrated in Figure 2.1 and with the gearbox plate and crossmember incorporated it can be seen that the section aft of the engine bay represents a good torsion structure. The engine bay and the outriggers are not so good at carrying torsion loads due to their open nature. The arrangement of the chassis in the Griffith is shown in Figure 2.4. The incorporation of a roll cage structure can do a lot to improve the torsion stiffness of the weak engine bay.

Of prime importance in integrating the roll cage into the structure is the quality of the joints between it and the chassis. From the work of Wanke [4] it was found that a number of members were crucial in achieving a high torsion stiffness. These included the floor pans of the outriggers which form the base of the 'closed' chassis when the roll cage is incorporated and hence good triangulation is required. In addition the members incorporated between the front suspension points and the roll cage are crucial in taking the high loads in this region and redistributing them to the stiffer structure at the rear. This was investigated further by the author whilst also considering the constraint the body work presents to the structural design.

The work carried out by the author was a continuation and development into a more practical structure of the work in reference [4].

The TVR Le-Mans car which was analysed is based on the TVR Chimaera. The Chimaera is a high performance convertible two door road car (Figure 2.5) from which the Cerbera 2+2 car was developed (Figure 2.6). It is the Cerbera chassis which forms the basis of the Cerbera GT - the Le-Mans Racing Version. The Chassis consists of a tubular space frame truss arrangement to which



is attached a glass fibre (GRP) body. The bodywork is attached to the chassis at no fewer than 22 points and the combination of the two components gives a torsion stiffness in excess of the addition of the values for the two components [5] due to the high level of indeterminacy.



Figure 2.5: TVR Chimaera

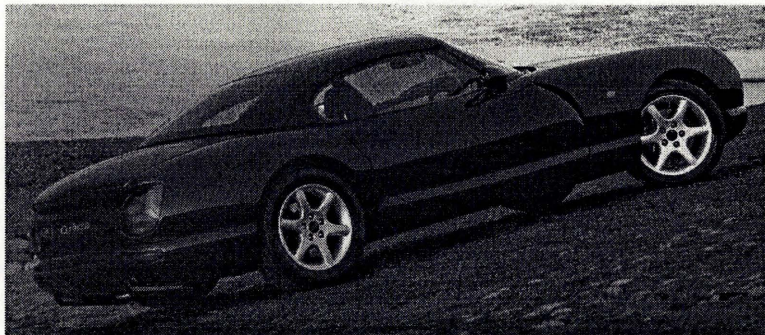


Figure 2.6: TVR Cerbera

## Chapter 3

# Chassis Development

The original chassis analysed by the author was that of the Chimaera. This chassis was identical to that of the Griffith which was analysed by Gadola [5]. Gadola investigated the stiffness contribution from the chassis, the body and the two combined.

The initial model analysed was based on the data from reference [5]. Gadola's data was verified in consultation with Neil Anderson from TVR and the model was generated using this data and drawings provided by TVR Engineering. This model was then used to investigate the torsion stiffness which was compared to the tests run by Gadola. The author's results for the chassis alone and the chassis with the plate were 11.6 % and 4.5 % higher respectively than the test results of Gadola. These results were considered within engineering limits and all further development was based on this mathematical model of the chassis.

### 3.1 Summary of Previous Investigations

Two past students have carried out work on various TVR chassis'. A brief summary of the results obtained and a description of the work is included below. The author's original work followed on from that of Gadola and looked at the incorporation of the roll cage into the overall structure. This was then investigated further by Wanke [4] during the development of a racing chassis.

#### 3.1.1 Griffith Torsion Analysis and Testing

In 1991/92 Marco Gadola [5] investigated the torsion stiffness of the TVR Griffith Chassis and bodywork. The analysis was carried out using the CRASHD software<sup>1</sup> and the theoretical results were verified with a series of tests. This model consisted of 76 nodes and 145 beam elements and the stiffening plate was modelled using beam elements. A general description of the chassis, its features and its evolution are contained in Section 2.1 and the general chassis is illustrated in Figure 2.1. The bare chassis analysed weighed 75kg and the bodywork 107kg.

The body work was attached to the chassis at 22 points and was found to contribute significantly to the overall torsion stiffness. The GRP bodywork incorporated deep closed section sills and a bonded windscreen which contributed to the overall stiffness of the body. It would be expected

---

<sup>1</sup>CRASHD is a large deformation code written by Cranfield Impact Centre which is used within Cranfield University.



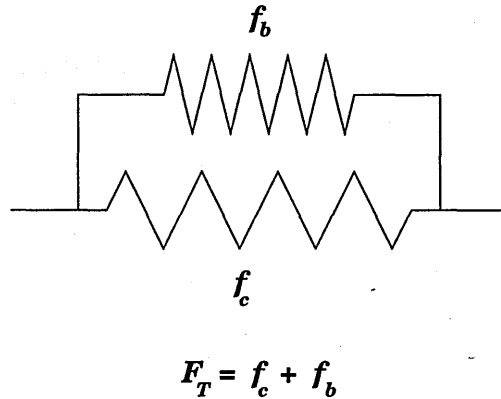


Figure 3.1: Parallel Springs

that the bodywork and the chassis would act as a pair of parallel springs as shown in Figure 3.1, however, the high level of redundancy of the attachments allows much more of the structure to carry the torsion load. As a consequence the load is transferred into much more of the total structure (the chassis and the body) and the result was an increase in stiffness of the overall structure. This illustrates the fact that redundant structures tend to be much stiffer than determinant ones as discussed in Section 2.1. The following torsion tests were carried out on the rolling chassis provided:

- (a) Chassis without the gearbox mounting plate or body.
- (b) Chassis with the gearbox mounting plate but no body.
- (c) GRP Body alone
- (d) Chassis with the gearbox plate and GRP body work.

The loaded length for the chassis torsion tests was 2,197 mm. This represented the distance between the suspension mounting points. It was not possible to produce a computer model of the GRP body and thus this was not able to be analysed and compared to the results of the physical tests. The loaded length for the torsion test on the bodywork was 2,810 mm. A summary of the results of this investigation are contained in Table 3.1.

TVR Griffith Chassis Analysis and Test					
Chassis Configuration	Theory Nm/deg	Test Nm/deg	Variation from test	Weight kg	Efficiency (Nm/deg)/kg
Chassis without gearbox plate	1,222	1,182	+3.4%	73.5	16.08
Chassis + gearbox plate	2,651	2,508	+5.7%	75	33.45
GRP Bodywork	-	373.5	-	107.5	3.47
Chassis + bodywork + plate	-	3,584	-	182.4	19.65

Table 3.1: Summary of Results from Gadola

### 3.1.2 Sports Racing Chassis Torsion Stiffness Analysis

The work carried out by Thomas Wanke [4] in 1994 was on a chassis developed from the Chimaera. The work of Wanke was essentially a continuation of the work which the author had concluded at the end of 1993. Wanke used the authors work and modified and developed it for the new vehicle arrangement. The chassis was specifically for racing, however, the road version of the chassis (more basic roll cage) will be used for the Cerbera. The race version is called the Cerbera GT and is bound for the 1996 BDRC Le-Mans 24 hour race. This vehicle used the company's newly developed AJP8 - V8 engine developing around 400bhp in race trim.

This chassis is longer by just over 350mm than that of the Griffith. This extra length consists of 280mm in the tunnel and 80mm in the engine bay. In addition to house the larger engine the engine bay had to be widened by 40mm. This investigation utilised the roll cage in improving the torsion stiffness of the chassis. Extensive modelling was carried out to improve the torsion stiffness and the results were verified with a series of torsion tests on the prototype chassis.

The loaded length of the chassis for nearly all the computer analyses was 2,446mm. The chassis tested had different load points to that of the F.E. model and the loaded distance was longer (2,586 mm). Consequently the measured overall torsion stiffness was less than that calculated. In addition, a number of the members that were modelled in the *improved rollcage* were not included in the test chassis. Due to these differences Wanke produced a separate model of the chassis to represent the test chassis<sup>2</sup>.

Table 3.2 summarises the results from a selected series of tests and analyses carried out. As can be seen from these results the torsion stiffness variation between the test and model (of the same configuration) was only 10%. It is to be expected that the Finite Element Model would yield a stiffer model as the joints are infinitely stiff. This result was good as was the correlation between test and theory.

TVR BDRC Racing Chassis Analysis and Test				
Chassis Configuration	Theory Nm/deg	Test Nm/deg	Weight kg	Efficiency (Nm/deg)/kg
Chassis without gearbox plate	1,478	-	71	20.8
Chassis with gearbox plate	2,935	-	74	39.7
Chassis + standard rollcage (no plate)	4,290	-	112	38.3
Chassis + standard rollcage + plate	5,715	-	115	49.7
Chassis + improved rollcage (no plate)	15,896	-	134	118.6
Chassis + improved rollcage + plate	16,278	-	137	118.8
Chassis + improved rollcage	9,548	8,772	121	79

Table 3.2: Summary of Results from Wanke

<sup>2</sup>The computer model here is representative of the test chassis and the loaded length is 2,586mm. In addition this model did not have the plate but used two rectangular crossmembers in its place.

## 3.2 Chassis Models Analysed for Torsion Stiffness

For the Chimaera chassis there were a number of models analysed to verify the correlation with the work of Reference [5]. The initial chassis was modelled on the production version of the Chimaera. This was then modified to incorporate the extra length proposed for the 2+2 seater and a roll over structure was developed for this new longer chassis.

In true TVR development style the chassis and bodywork were modified regularly during the analysis phase. This evolutionary design is suited to the company's structure but meant a lot of changes needed to be incorporated into the computer simulations. As a result of the changes many models were analysed and these are not all listed and detailed here for reasons of brevity. A few examples of the changing design are given along with their corresponding results. In essence the new chassis gained length and width. The final model analysed was 200mm (150mm in the tunnel and 50mm in the engine bay) longer and 100mm wider (across the outriggers) than the standard Chimaera chassis. Similar analyses were carried out on each chassis arrangement and the results compared.

### 3.2.1 Chimaera Chassis Model and Results

The Chimaera chassis has a gearbox crossmember and underbody plate both of which are in the tunnel section as shown in Figure 3.2. These members were found to be crucial in attaining a reasonable value for the torsion stiffness of this chassis. Their importance stems from the fact that they transform the tunnel section of the chassis from an open 'C' section to a closed 'torsion tube'. In all cases a load of 2,632N was used when determining the torsion stiffness. This was the same value used by Gadola in his analyses. He chose this value as it was a set number of divisions on the dynamometer used during testing and it gave a reasonable deflection of the chassis. This is in contrast to the method used by Wanke to determine the load which is summarised in Appendix G.

#### Case 1: Standard Chimaera Chassis (length 2,692 mm), Model A:

The following analyses were carried out on the standard Chimaera Chassis:

- (a) Chassis with the gearbox crossmember and the plate - Figure 3.2.
- (b) Chassis with the gearbox member and no plate - Figure 3.3.
- (c) Chassis without the gearbox member or plate - Figure 3.4.
- (d) Chassis without the gearbox member but with the plate - Figure 3.5 (as tested by Gadola).

The results of this investigation are contained in Table 3.3. Deflected plots for the chassis are contained in Figures 3.6 to 3.9. From these it is possible to see the variation in deflection for each arrangement. The gearbox member alone increased the chassis torsion stiffness by 38 %, the gearbox plate alone resulted in an increase of 103 % and the combination of the two resulted in a torsion stiffness increase of 122 %. A graph showing the torsion stiffness of each model is contained in Figure 3.10.

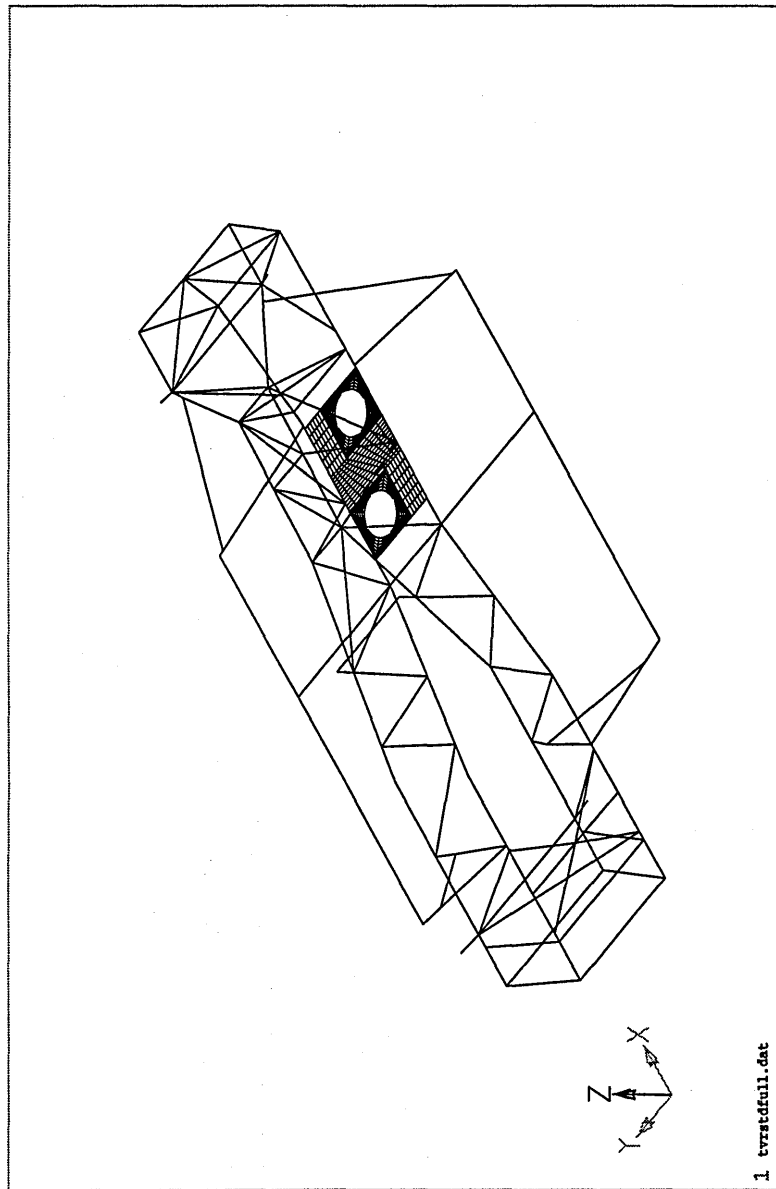


Figure 3.2: Chimaera Chassis with the gearbox crossmember and the plate

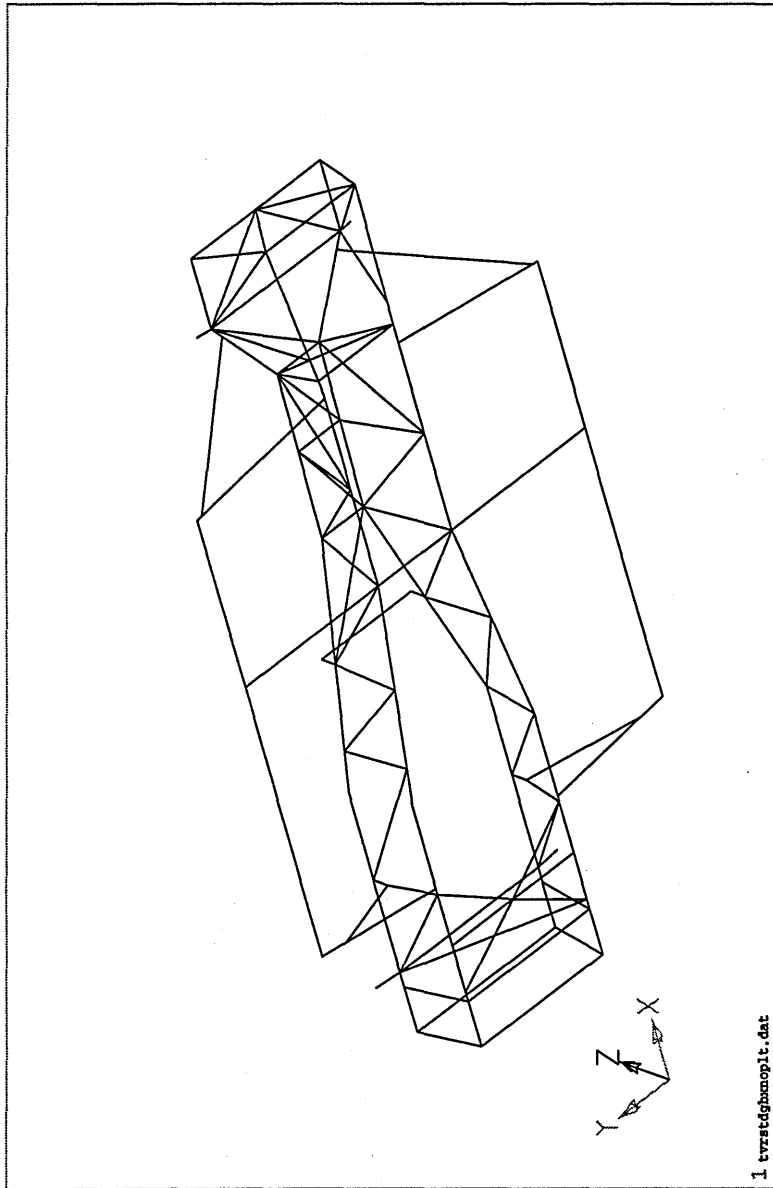


Figure 3.3: Chimaera Chassis with the gearbox member and no plate

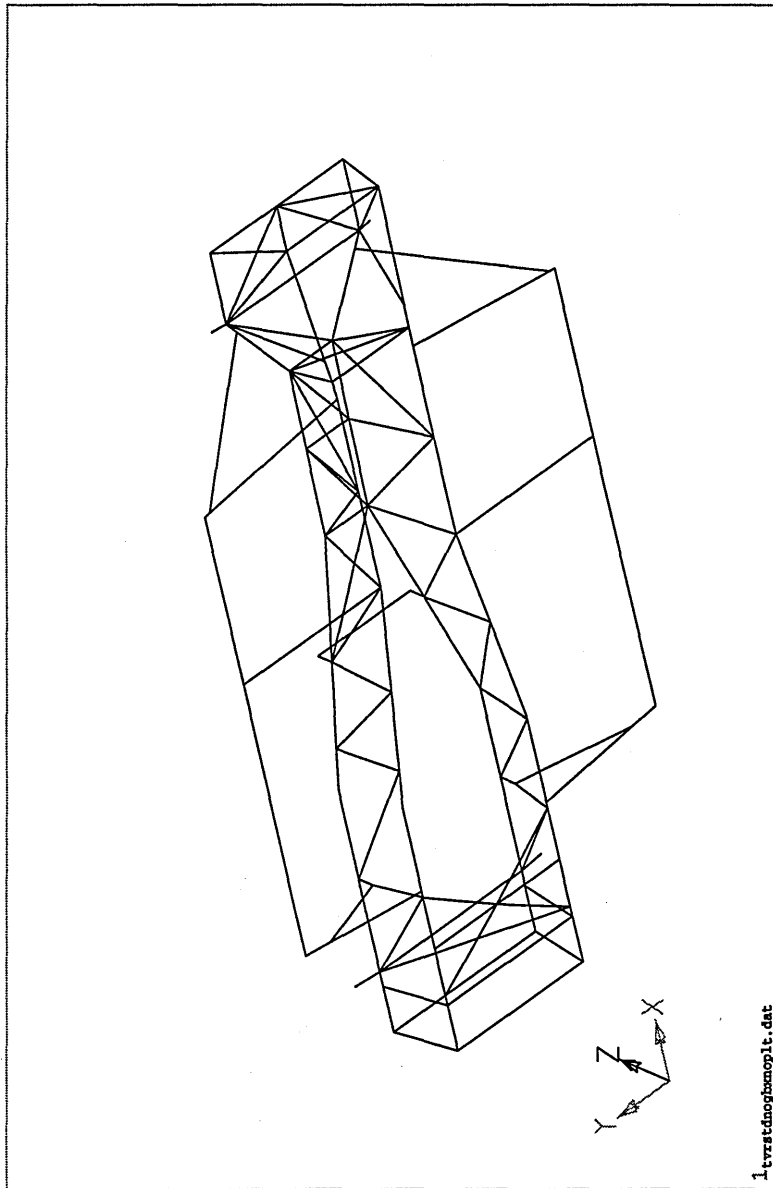


Figure 3.4: Chimaera Chassis without the gearbox member or plate

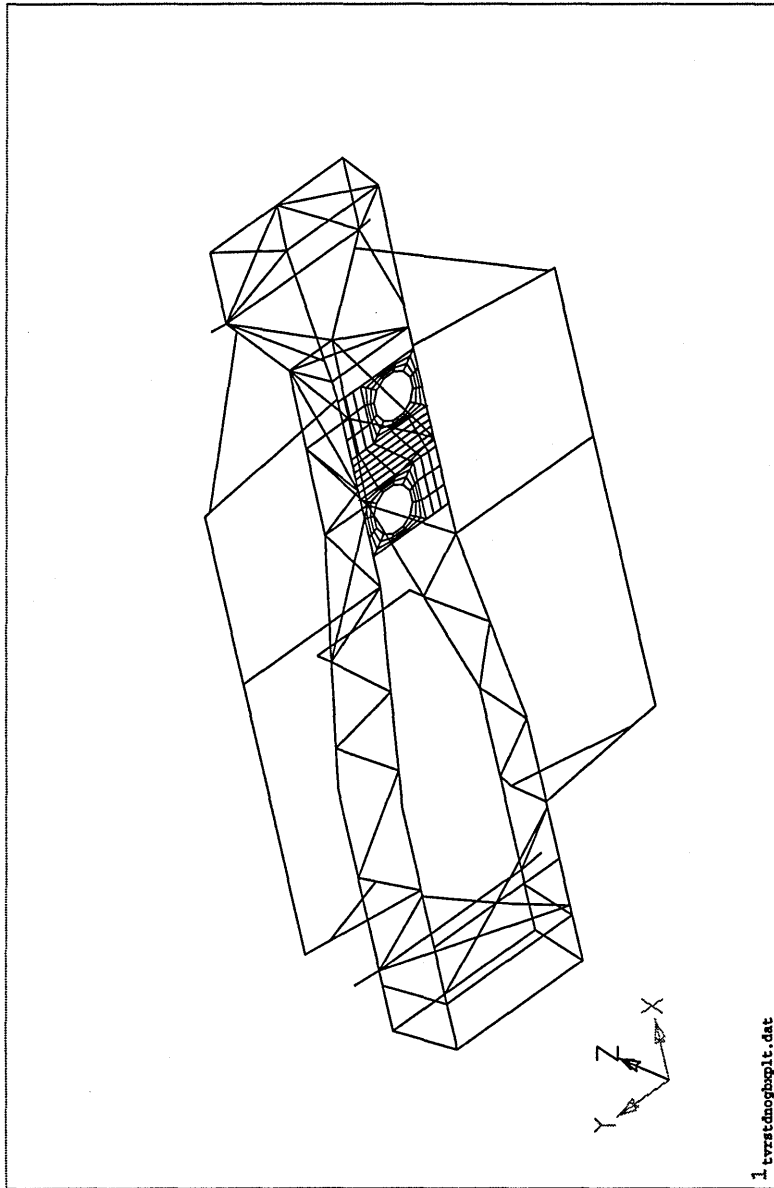


Figure 3.5: Chimaera Chassis without the gearbox member but with the plate

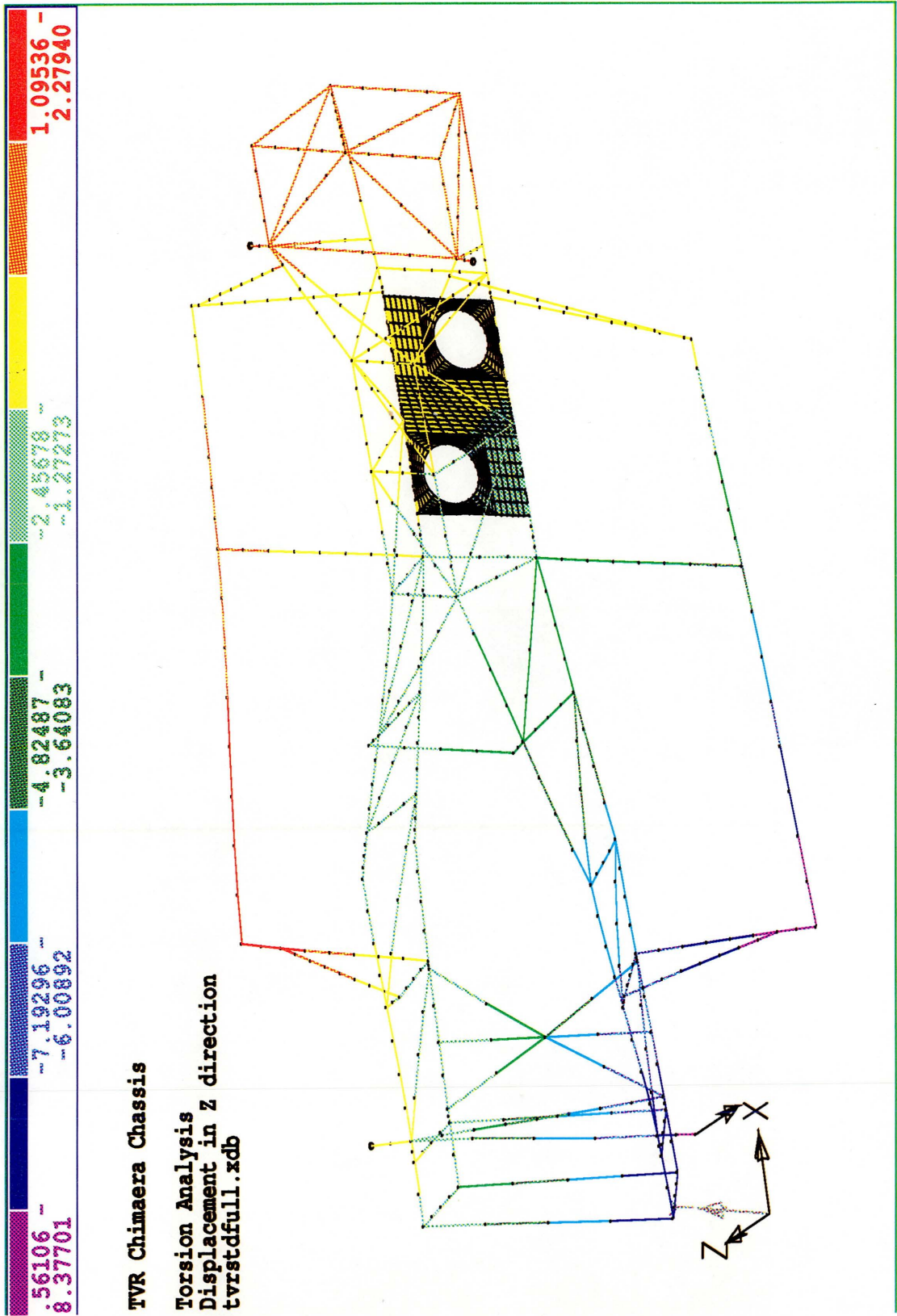


Figure 3.6: Chimaera Chassis with the gearbox crossmember and the plate - Deflected Shape



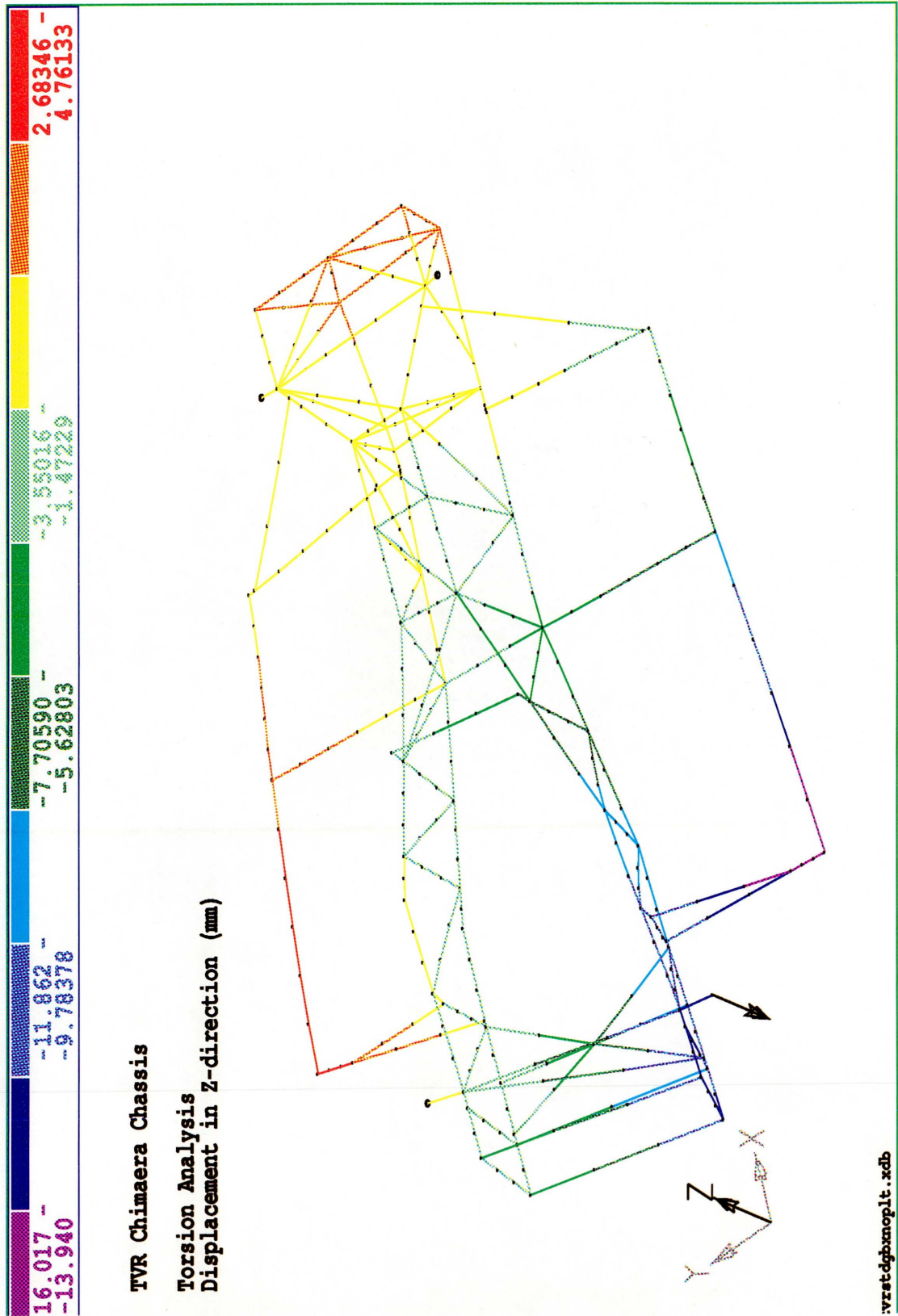


Figure 3.7: Chimaera Chassis with the gearbox crossmember and no plate - Deflected Shape

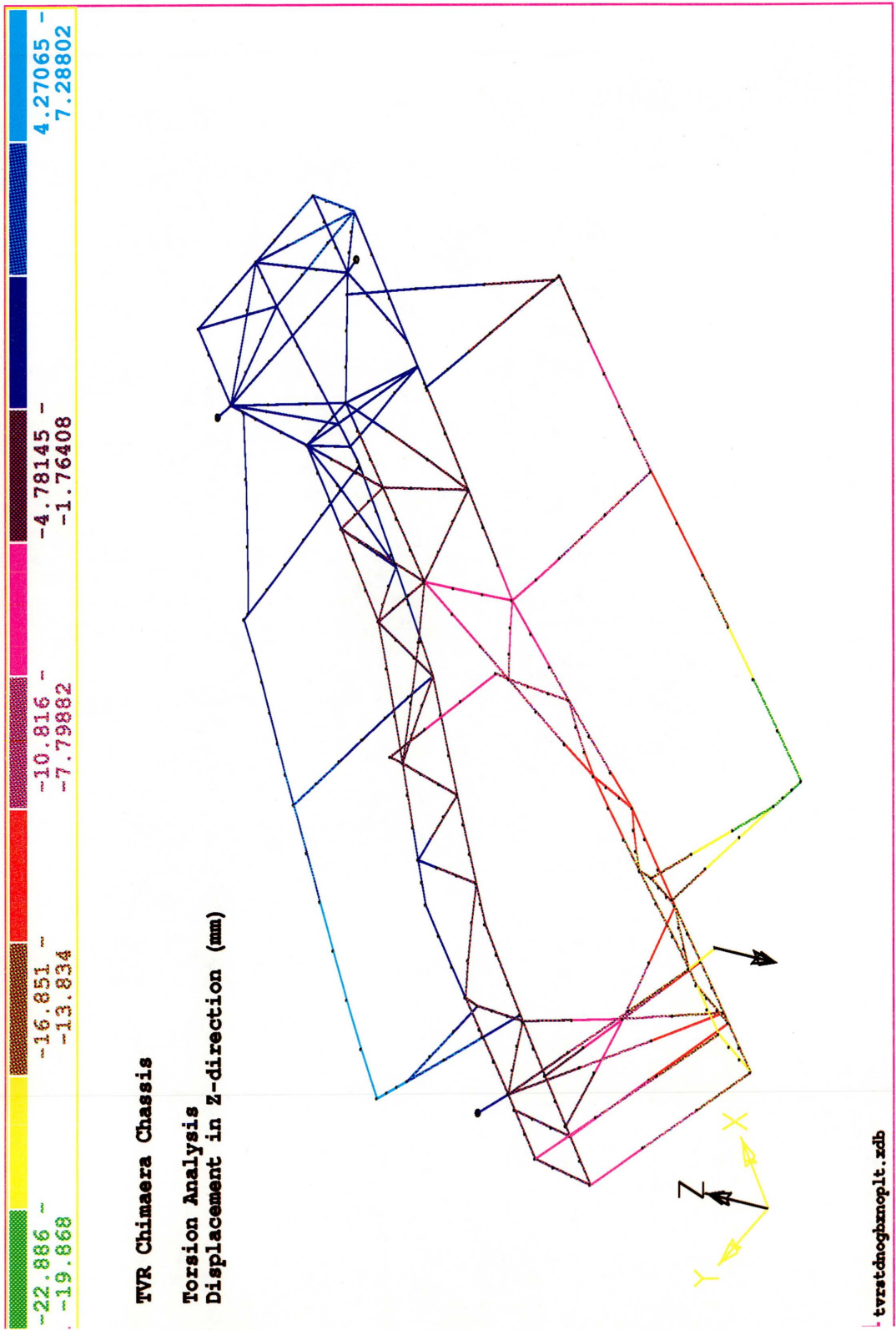


Figure 3.8: Chimaera Chassis without the gearbox crossmember or plate - Deflected Shape

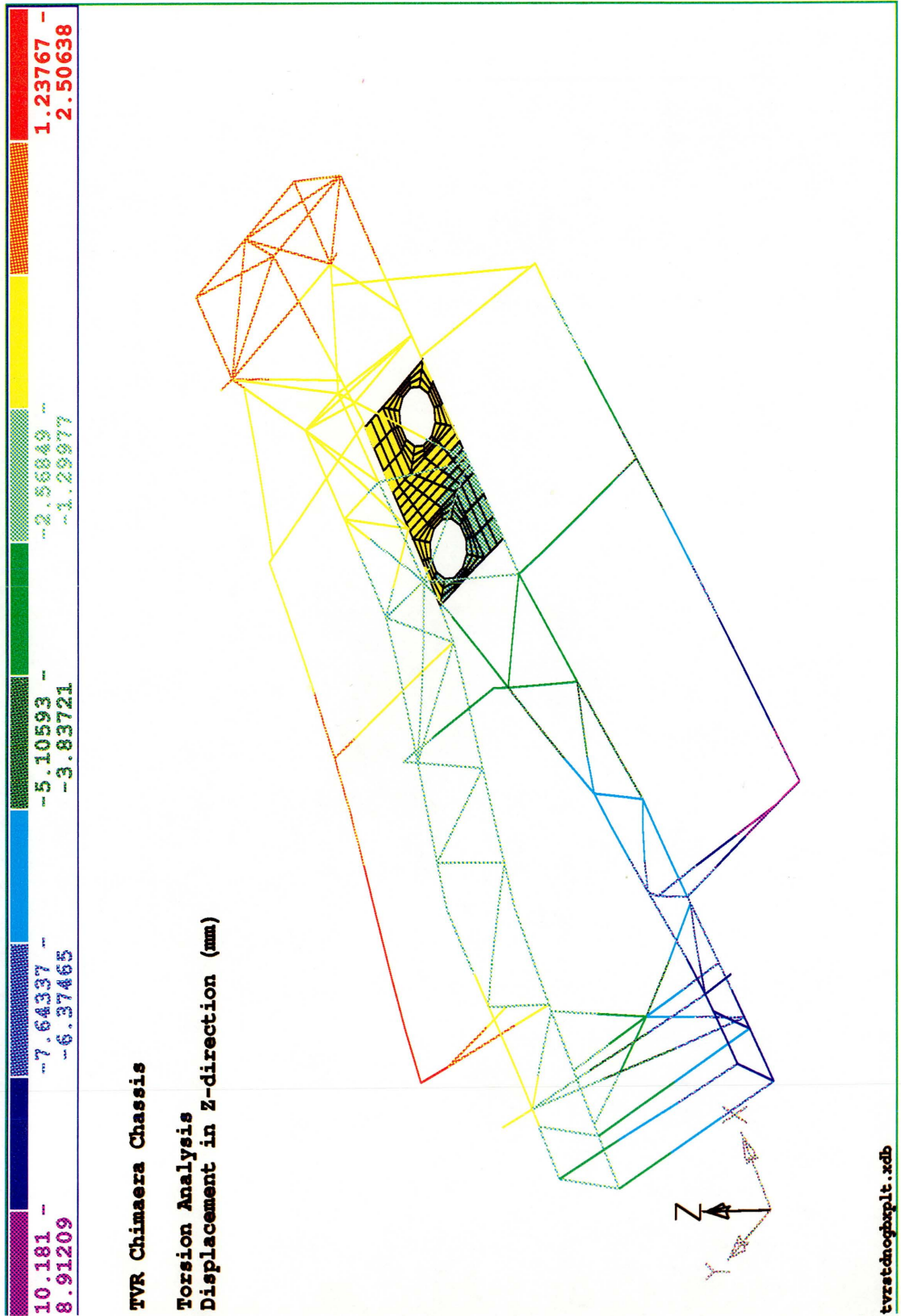


Figure 3.9: Chimaera Chassis without the gearbox member but with the plate - Deflected Shape

### Chimaera Chassis Torsion Stiffness

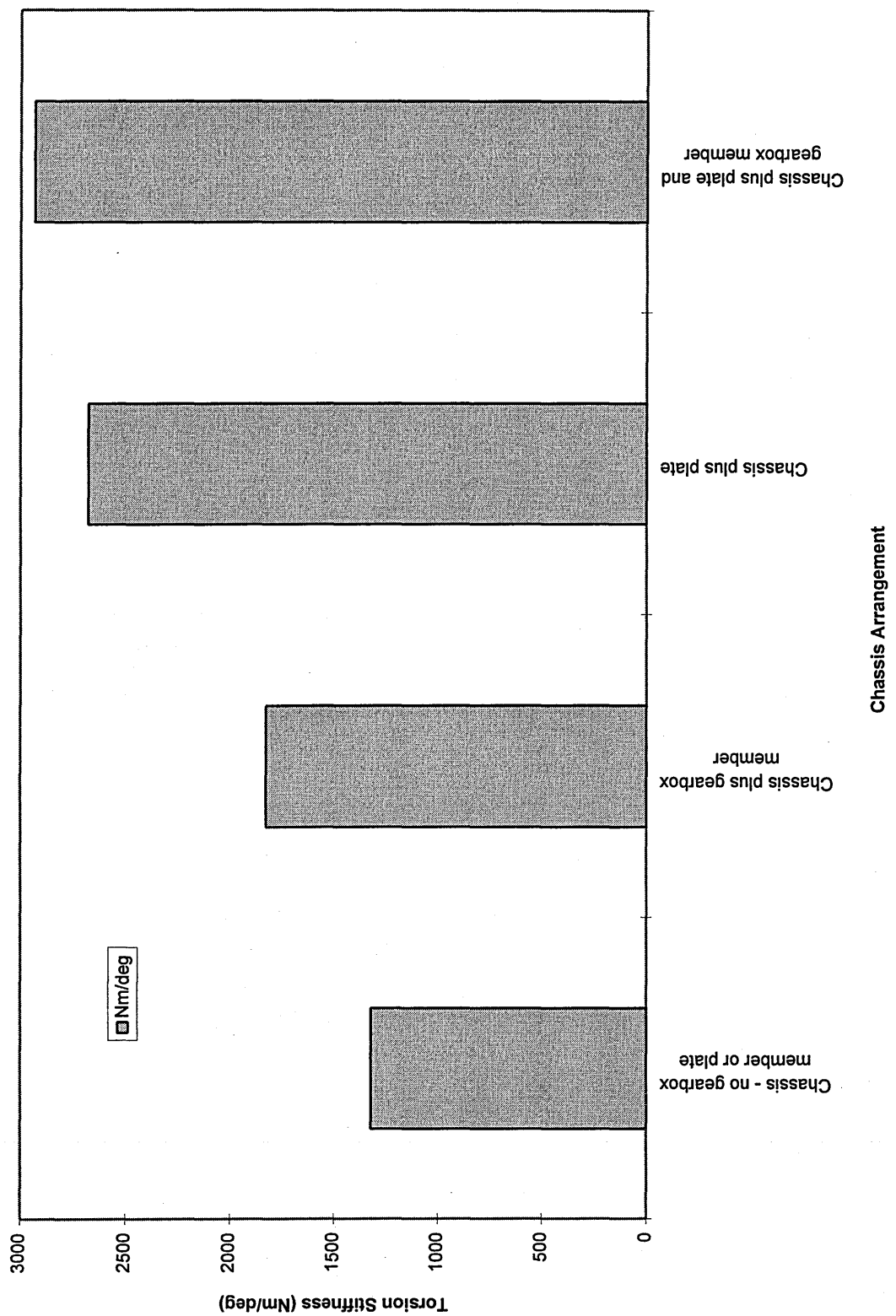


Figure 3.10: Graph of Deflections for the Different Chimaera Chassis Configurations

Chimaera Chassis					
Chassis Configuration	Deflection at load mm	Applied Torque Nm	Torsion Stiffness Nm/deg	Weight kg	Efficiency (Nm/deg)/kg
Chassis - no gearbox member or plate	19.06	1947.7	1320.47	63.2	20.9
Chassis + gearbox member	13.768	1947.7	1827.04	64.0	28.5
Chassis + plate	9.3996	1947.7	2676.36	64.8	41.3
Chassis + gearbox member + plate	8.581	1947.7	2931.99	65.3	44.9

Table 3.3: Table of Results - Standard Chassis

### 3.3 Lengthened Chassis Models

#### Circular Tubes for Chassis Rails

To ease the manufacture of the chassis and to limit the material carried in stock TVR requested an investigation into the use of circular tubes for the main chassis rails. The change from the standard rectangular sections (60mm × 40mm × 2mm) led to a variation in the torsion stiffness which was investigated.

This investigation highlighted the value of Finite Element Analysis (FEA) for the determination of the torsion stiffness. Initially TVR requested an investigation into the use of  $\phi 44 \times 1.6$  mm to replace the rectangular sections. As the torsion stiffness is related to the amount of material and its distance from the centroid of the section, it was intuitively felt that this arrangement would result in a reduction in the torsion stiffness. This analysis was only carried out on the lengthened and the extra long chassis'. A number of other tube cross sections were analysed, the aim being to achieve the same torsion stiffness as that for the chassis with rectangular members.

Two sets of analyses are included which illustrate the changes which occur as the chassis is lengthened to its final form.

#### Case 2: Lengthened Chassis by 150mm, Model B - (overall length 2,844 mm).

The chassis was extended in length (in the tunnel section) and the following analyses were carried out.

- Full long chassis with the gearbox member and the plate, Figure 3.11.
- Long chassis without the gearbox member but with the plate, Figure 3.12.
- Long chassis with the gearbox member but no plate, Figure 3.13.
- Long chassis without the gearbox member or plate, Figure 3.14.
- Long chassis with tubes for main chassis rails. The rectangular base members were replaced with a number of differing size circular tubes including  $\phi 44 \times 1.6$  mm,  $\phi 44 \times 3.0$  mm and  $\phi 55 \times 2.5$  mm, Figure 3.15.

The results for these models are contained in Table 3.4. Figures 3.11 and 3.15 show the variation in the deflection between models (a) and (e). This illustrates the effect of changing from rectangular base members to circular ( $\phi 44 \times 1.6$  mm) tubes. Figure 3.16 gives a graphical representation of the variation in torsion stiffness for the different models.



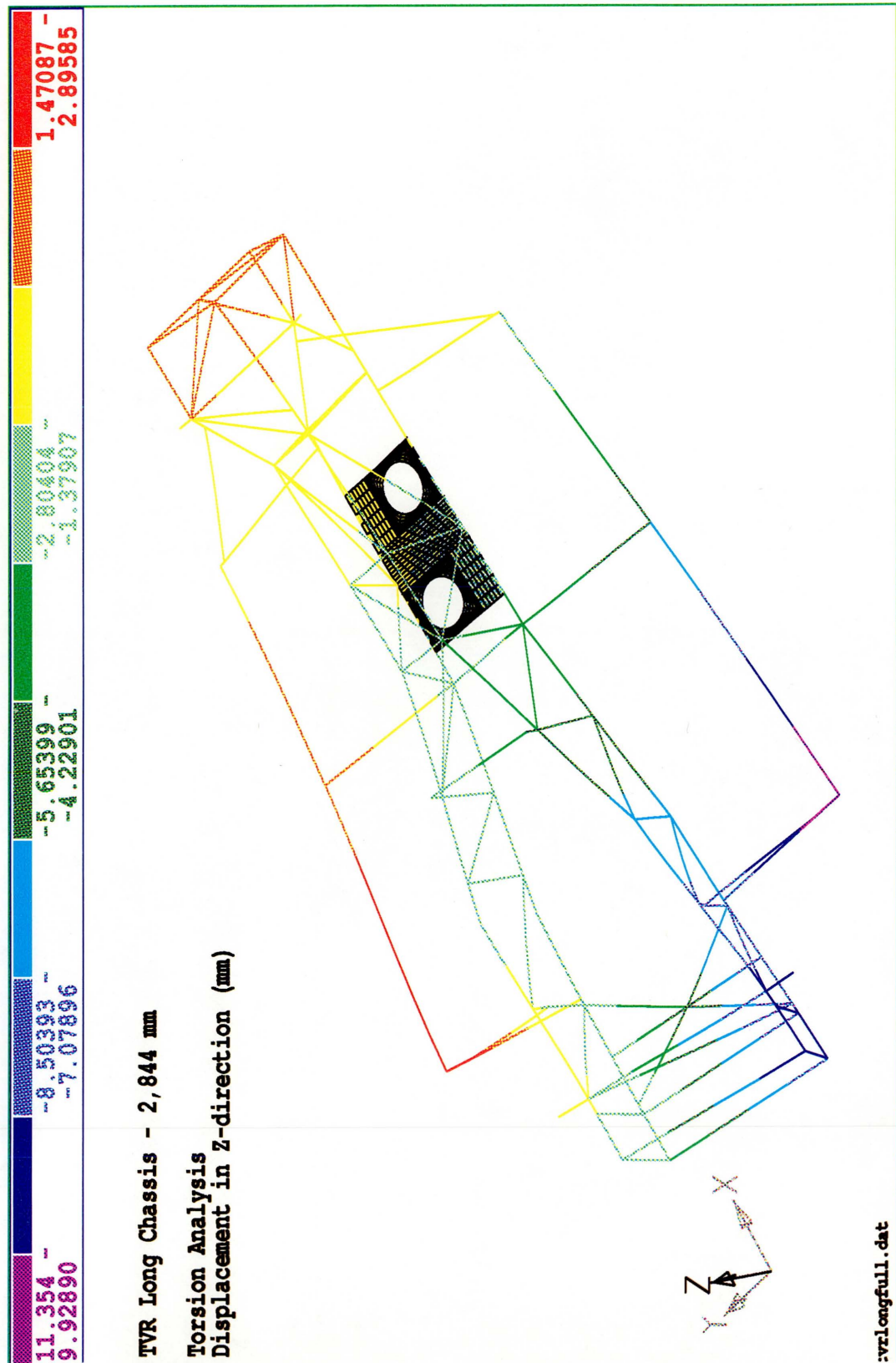


Figure 3.11: Chassis (2,844mm) with the gearbox crossmember and the plate - Deflected Shape

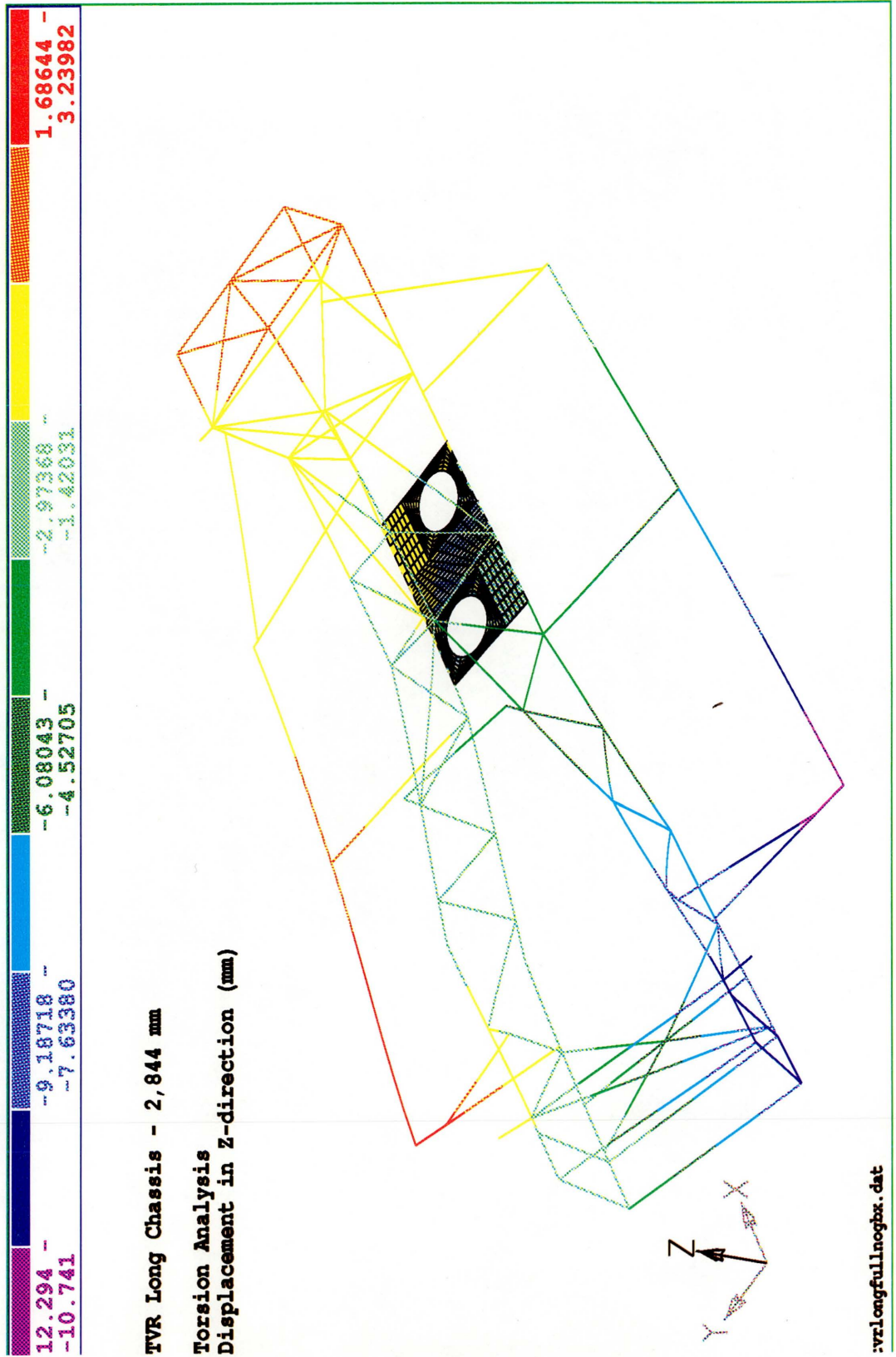


Figure 3.12: Chassis (2,844mm) without the gearbox crossmember and with the plate - Deflected Shape

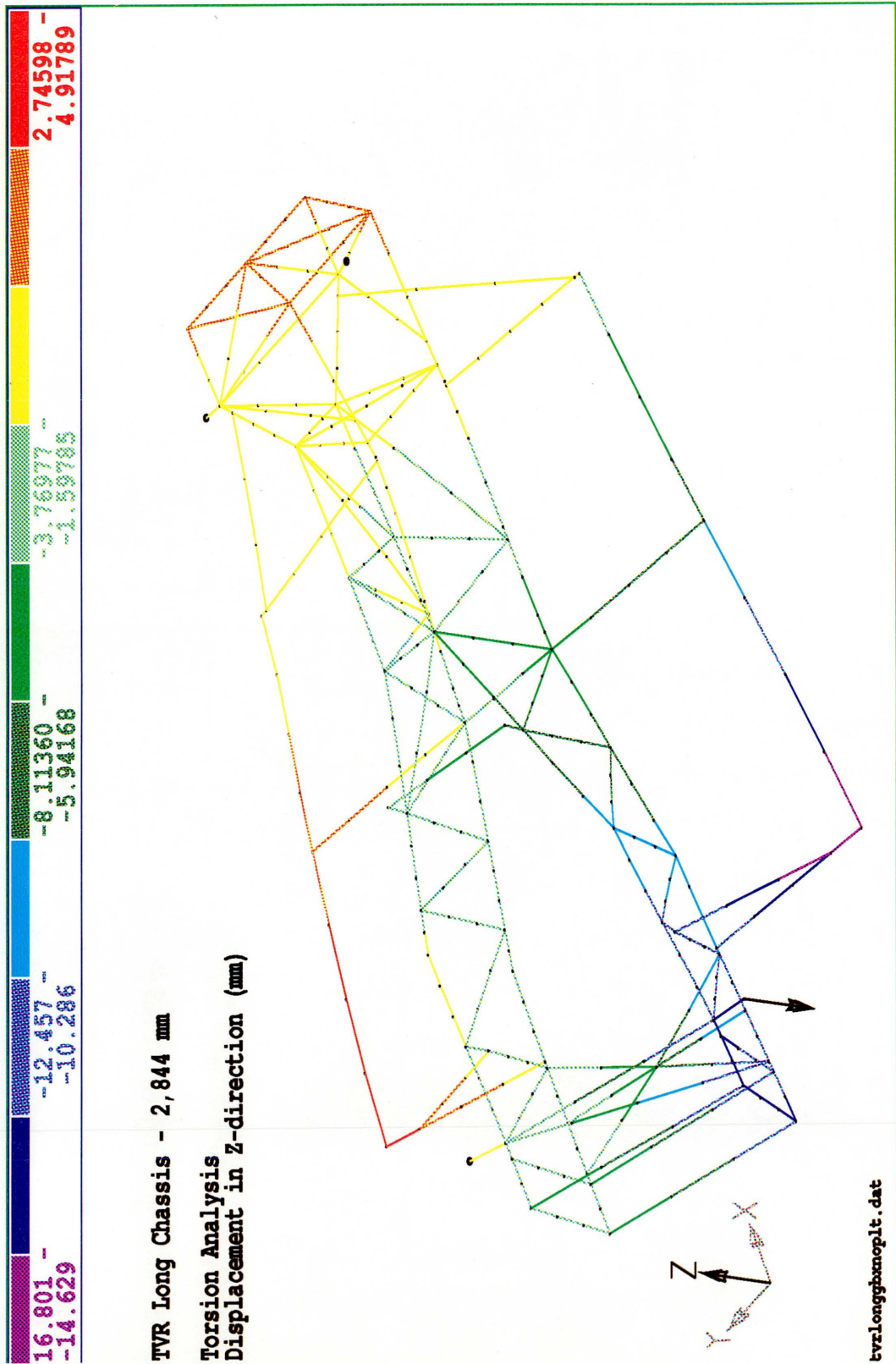


Figure 3.13: Chassis (2,844mm) with the gearbox crossmember and without the plate - Deflected Shape



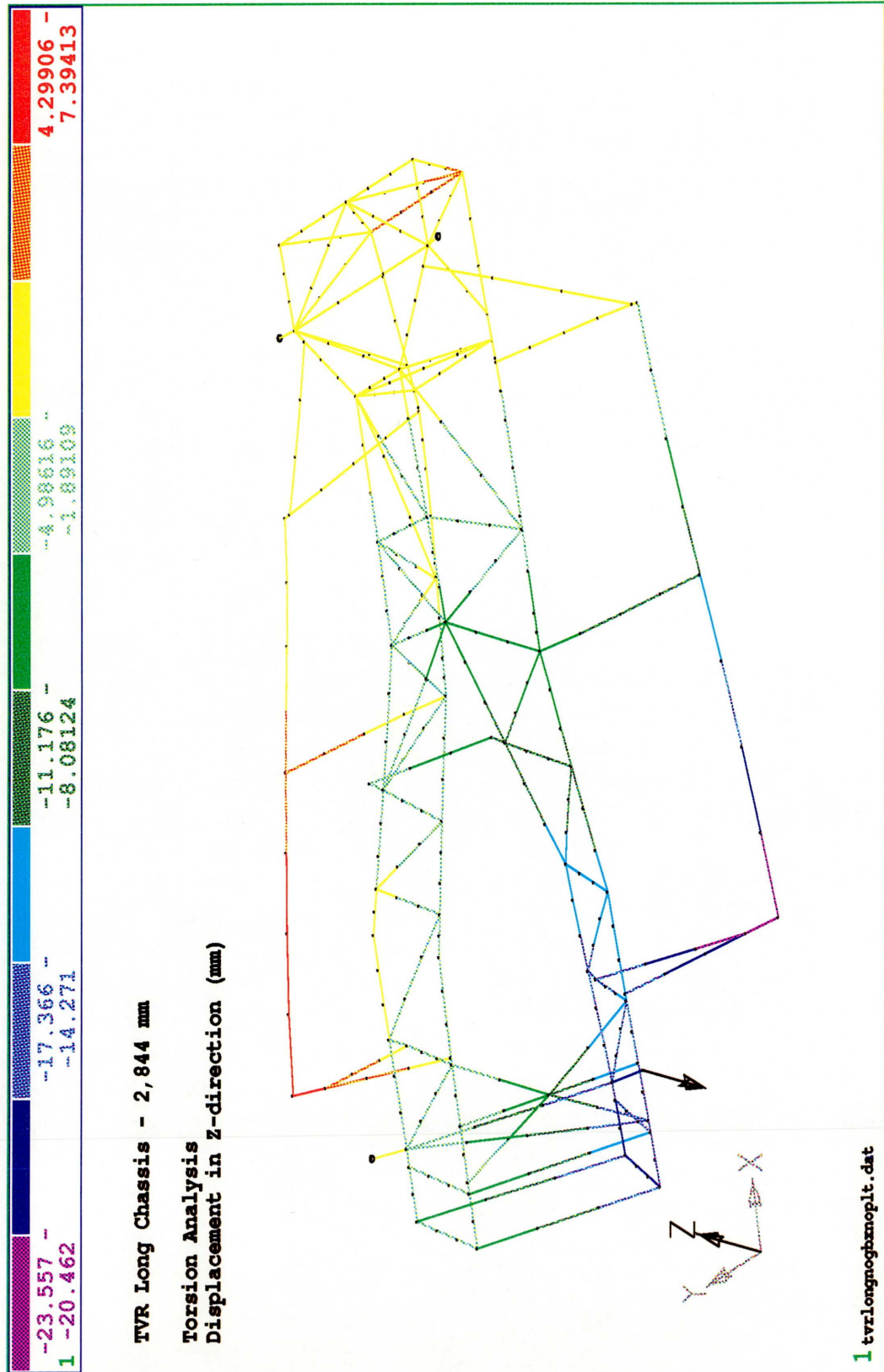


Figure 3.14: Chassis (2,844mm) without the gearbox crossmember and without the plate - Deflected Shape

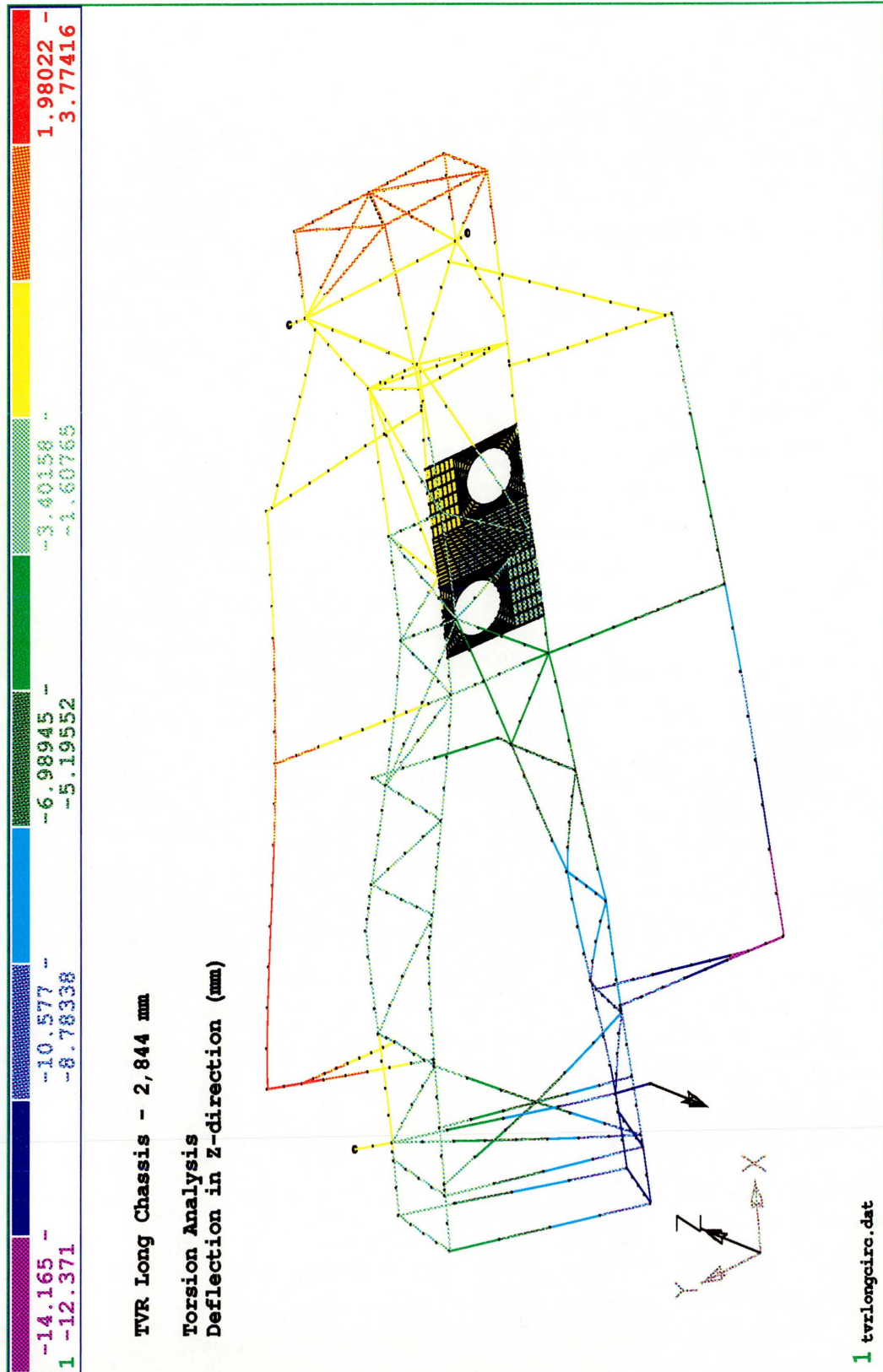


Figure 3.15: Chassis (2,844mm) with the gearbox crossmember and plate with circular lower rails- Deflected Shape

Long Chimaera Chassis - Overall Length 2,844mm

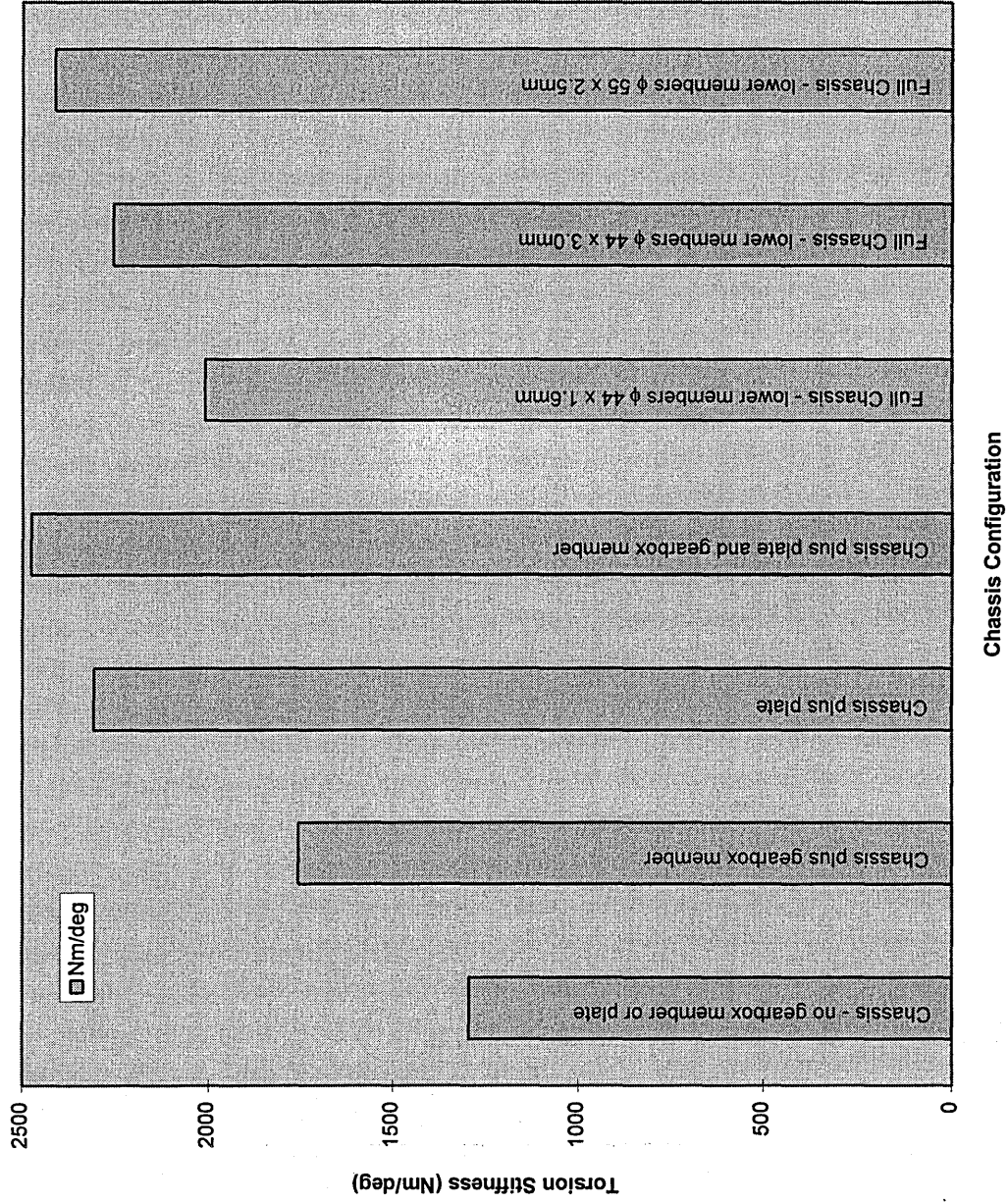


Figure3.16: Graph of Deflections for the Different Chassis Configurations - Long (2,844mm) Chassis

Long Chassis - overall length 2,844 mm					
Chassis Configuration	Deflection at load mm	Applied Torque Nm	Torsion Stiffness Nm/deg	Weight kg	Efficiency (Nm/deg)/kg
Chassis - no gearbox member or plate	19.44	1947.7	1294.3	66.4	19.5
Chassis + gearbox member	14.31	1947.7	1758.1	67.27	26.1
Chassis + plate	10.90	1947.7	2308.0	66.9	34.5
Chassis + gearbox member + plate	10.16	1947.7	2476.1	67.5	36.7
Full Chassis - lower members $\phi 44 \times 1.6 \text{ mm}$	12.52	1947.7	2009.4	59.2	33.9
Full Chassis - lower members $\phi 44 \times 3.0 \text{ mm}$	11.15	1947.7	2256.3	67.5	33.4
Full Chassis - lower members $\phi 55 \times 2.5 \text{ mm}$	10.43	1947.7	2412.0	67.8	35.6

Table 3.4: Table of Results for Long Chassis

**Case 3: Extralong chassis (overall length 2,894 mm) - (150mm in the tunnel, 50mm in the engine bay and 100mm wider across the outriggers), Model C.**

The chassis was extended by an additional 50mm in length and 100 mm in width. The following selection of models were run:

- (a) Full chassis, rectangular base members, with the gearbox member and the plate.
- (b) Long chassis with tubes for main chassis rails. The rectangular base members were replaced with a number of differing size circular tubes including,  $\phi 44 \times 1.6 \text{ mm}$ ,  $\phi 44 \times 3.0 \text{ mm}$  and  $\phi 55 \times 2.5 \text{ mm}$ .

Apart from the change in length and width the general appearance of the chassis was as for Model B. The results for the above models are contained in Table 3.5. Figure 3.17 gives a graphical representation of the variation in torsion stiffness for the different models.

From the preceding analyses it can be seen that extending the chassis by 150mm in length and widening it by 100mm (i.e. Model C) resulted in a 16 % drop in torsion stiffness over the standard Chimaera Chassis of Model A.

Using circular tubes ( $\phi 44 \times 1.6 \text{ mm}$ ) for the main chassis rails, as desired by TVR, resulted in a drop in the torsion stiffness over the same chassis with rectangular base members. For Model B this represented a 19 % drop in torsion stiffness and for Model C there was a 22 % drop in torsion stiffness.

Increasing the size of the tubular members enabled the torsion stiffness to be increased. It was necessary to use  $\phi 55 \times 2.5 \text{ mm}$  to achieve a comparable torsion stiffness to that of the chassis with rectangular lower members. Unfortunately using tubes of this size increased the overall weight of the chassis by 10 % and their use was rejected.

This investigation was of great use to TVR. Normally they would have built various chassis' and tested them which is an expensive business. Using Finite Element analysis the changes were made simply by altering the cross sectional properties for the lower chassis rails and then re-running the analysis. Each additional analysis took around half an hour in total. This included the modification, checking and running the model and analysing the results. This represents an effective method of looking at structural modifications and has the added advantage of being quick.



### Extralong Chimaera Chassis - Overall Length 2,894mm

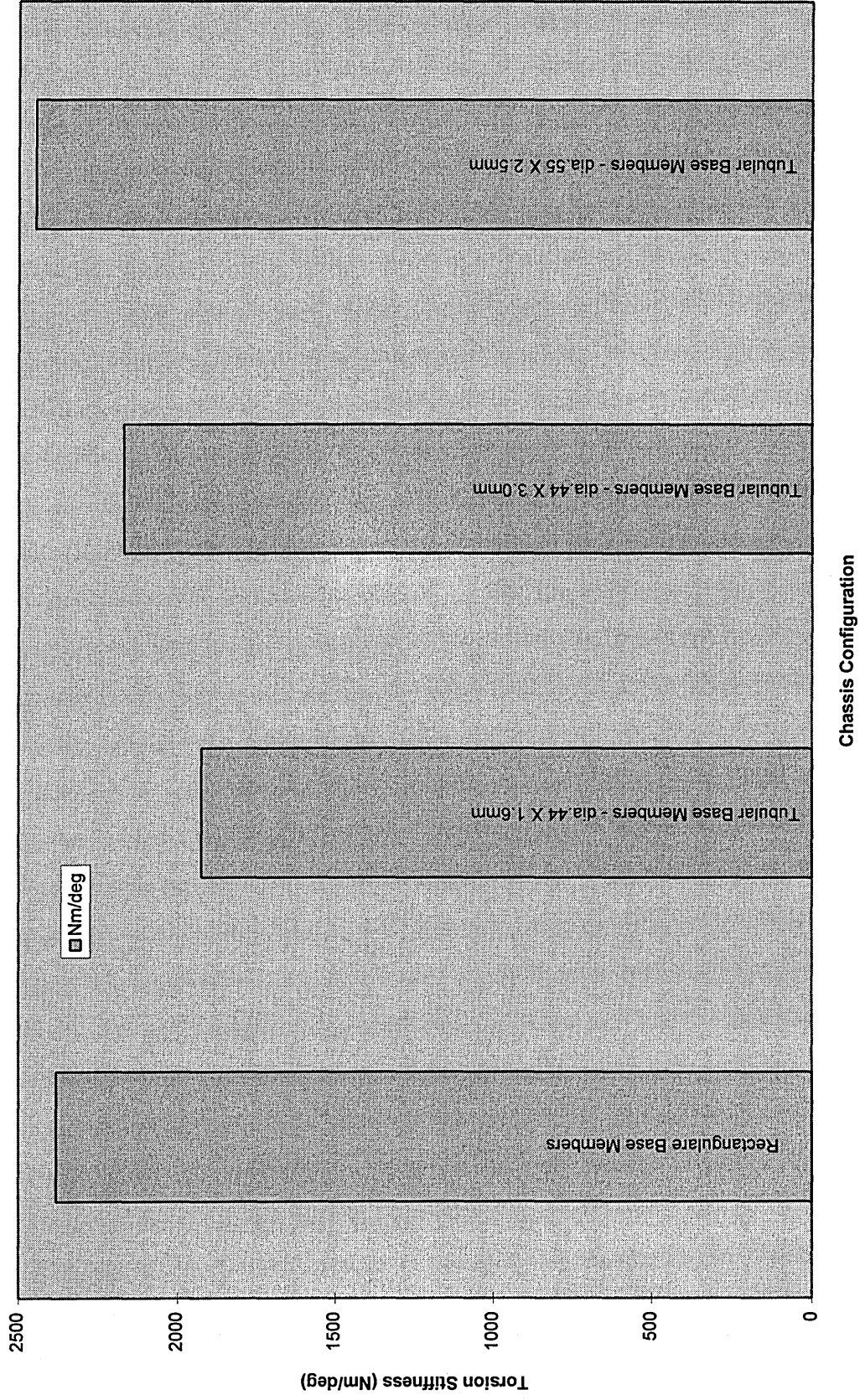


Figure 3.17: Graph for the Different Chassis Configurations - Extralong (2,894mm) Chassis



Extralong Chassis - overall length 2,894 mm					
Chassis Configuration	Deflection at load mm	Applied Torque Nm	Torsion Stiffness Nm/deg	Weight kg	Efficiency (Nm/deg)/kg
Rectangular base members	10.56	1947.7	2382.3	68.3	34.9
Circular base members $\phi 44 \times 1.6 \text{ mm}$	13.06	1947.7	1926.3	59.9	32.2
Circular base members $\phi 44 \times 3 \text{ mm}$	11.59	1947.7	2170.6	68.4	31.7
Circular base members $\phi 55 \times 2.5 \text{ mm}$	10.28	1947.7	2447.2	69.7	35.1

Table 3.5: Table of Results for Extralong Chassis

### 3.4 Roll Over Protection Development

TVR Engineering produce an after market rear roll-hoop for fitment to both the Griffith and Chimaera. This roll hoop had to be able to be fitted to the vehicle without the need to cut holes in the body work or to do any major structural modifications. The resulting roll hoop has poor attachments to the main structure and would provide only minimal protection in the event of a roll over. The roll hoop and its arrangement on the chassis is illustrated in Figure 3.18. From Figure

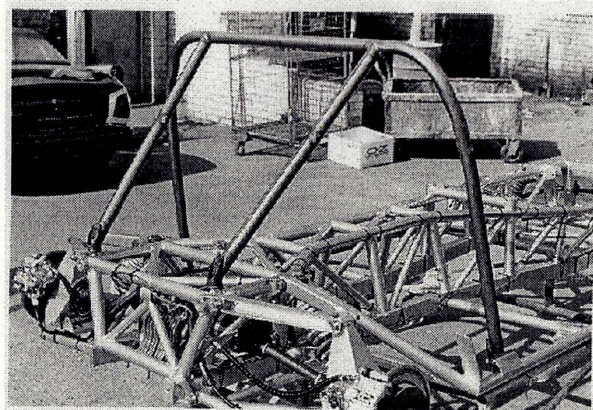


Figure 3.18: After Market Roll-Hoop

3.19 it can be seen that the attachments of the main hoop to the outriggers consists of a piece of flat plate and a welded and bolted joint. This represents a pin joint and as a consequence it would provide little lateral resistance to an impact. The rear mountings to the chassis at the differential cage were much more substantial and would provide much better resistance to impact.

This roll hoop was taken as the basis of the roll cage design. The initial modelling of the hoop assumed that the joints were rigid and not as detailed above. From this simple model a number of others were developed and the general progression of models was:

- Chassis with the standard roll hoop fitted, with ideal joints, Figure 3.20
- Chassis with a simple full roll cage - front and rear hoops tied together longitudinally and attached to the rear differential cage, Figure 3.21



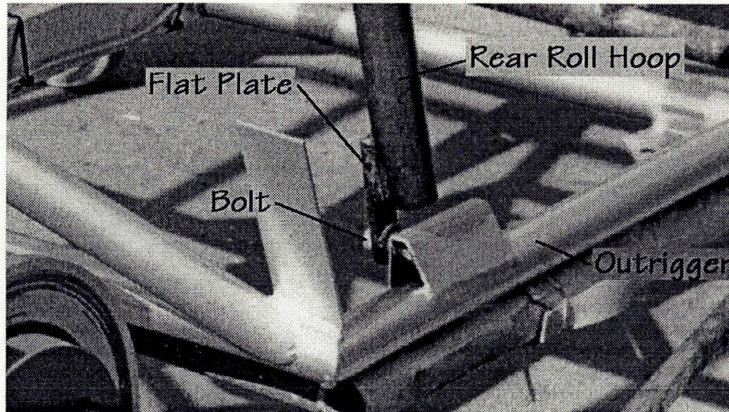


Figure 3.19: After Market Roll-Hoop Joint

- Chassis with a full roll cage attached at the front and rear ends and incorporating a side impact bar, Figure 3.22.

### 3.4.1 Roll Cage Development and Results

The modelling of the roll hoop and cage was carried out initially on the standard Chimaera chassis to give baseline figures. This was extended to the lengthened chassis with the more complex arrangements being carried out on the extralong chassis. The extralong chassis represented the 2+2 vehicle which was the subject of the overall study. The roll cage was analysed to see what increase in torsion stiffness was achievable. The roll cage was developed from a simple rear roll hoop to the full roll cage. On the final chassis model a number of analyses were conducted using circular tubes for the lower chassis rails. Whilst the models with rectangular members and the roll cage were always stiffer than those with the circular tubes it was found that a lower weight chassis could be produced with a reasonable torsion stiffness by using circular base members.

These analyses were an investigation of the additional torsion stiffness available using the roll cage as part of the torsion structure. A selection of the models analysed are detailed below.

The torsion stiffness results for the different arrangements are contained in Tables 3.6 and 3.7.

#### Standard (Chimaera) Chassis with the simple roll cage, Model D

The standard chassis with the rear roll hoop is shown in Figure 3.20. This model was then developed by adding a front roll hoop as shown in Figure 3.21, which was attached to the outrigger tubes. The front hoop was tied longitudinally to the rear hoop and a diagonal was included in the roof between the two hoops as shown. In this early model no front bracing or side impact bars were included. A selection of the models analysed are:

- Chimaera chassis with the standard roll hoop - no plate
- Chimaera chassis with roll hoop front and rear - no plate
- Chimaera chassis with roll hoop front and rear - with plate

Standard Chimaera Chassis with Roll Structure					
Chassis Configuration	Deflection at load mm	Applied Torque Nm	Torsion Stiffness Nm/deg	Weight kg	Efficiency (Nm/deg)/kg
No gearbox plate + rear roll hoop	13.41	1947.7	1877.5	70.7	26.6
No gearbox plate + front and rear hoops	10.88	1947.7	2312.2	80.4	28.8
Gerabox Plate + front and rear hoops	7.68	1947.7	3275.6	81.9	40.0

Table 3.6: Table of Results for Chimaera Chassis with Roll Structure

The results for the torsion stiffness of the standard chassis (Model D) with the roll structure were taken as the baseline values. These results which are contained in Table 3.6 were then compared to the results for the longer chassis arrangements.

#### Extralong Chassis (2,894 mm) with rear roll hoop, Model E

This chassis, Model E, was analysed with various tubular lower chassis rails and a single rear roll hoop. Whilst the chassis was longer than that analysed for the standard Chimaera Chassis the arrangement of the members was the same as that shown in Figure 3.20. A representative sample of the analyses carried out were:

- (a) Tubular lower chassis rails,  $\phi 44 \times 1.6 \text{ mm}$
- (b) Tubular lower chassis rails,  $\phi 44 \times 3.0 \text{ mm}$
- (c) Tubular lower chassis rails,  $\phi 55 \times 2.5 \text{ mm}$

The aim was to achieve the same torsion stiffness as the standard chassis in Model D with the gearbox member and roll hoop. The results of these analyses are presented in Table 3.7.

It was possible to achieve a higher torsion stiffness than the standard chassis, Model D, with a small weight reduction by using  $\phi 44 \times 1.6 \text{ mm}$  tubes. Needless to say larger diameter tubes resulted in higher values of the torsion stiffness - albeit with a weight penalty. However, the rectangular members were still found to give the best overall performance.

#### Extralong Chassis (2,894 mm) with full roll cage, Model F

The chassis of Model E was then modified to include the full roll cage with front and rear hoops. The front hoop was tied longitudinally to the rear cage with a 'V' brace in the roof section. The rear hoop was tied to the diff cage with a 'W' bracing arrangement. Side intrusion bars were incorporated and they consisted of longitudinal bars reinforced with a 'V' brace connecting this bar to the outriggers. The model arrangement can be seen in Figure 3.22. The following models were analysed:

- (a) Tubular lower chassis rails,  $\phi 44 \times 1.6 \text{ mm}$
- (b) Tubular lower chassis rails,  $\phi 38 \times 1.6 \text{ mm}$
- (c) Rectangular lower chassis rails,  $60 \times 40 \times 2 \text{ mm}$

From these analyses (Results in Table 3.7) it was found that the chassis with the rectangular base members still gave the most efficient structure of those analysed.

Compared to the chassis of Model D with the simple rear hoop, Model F with the full roll-cage was



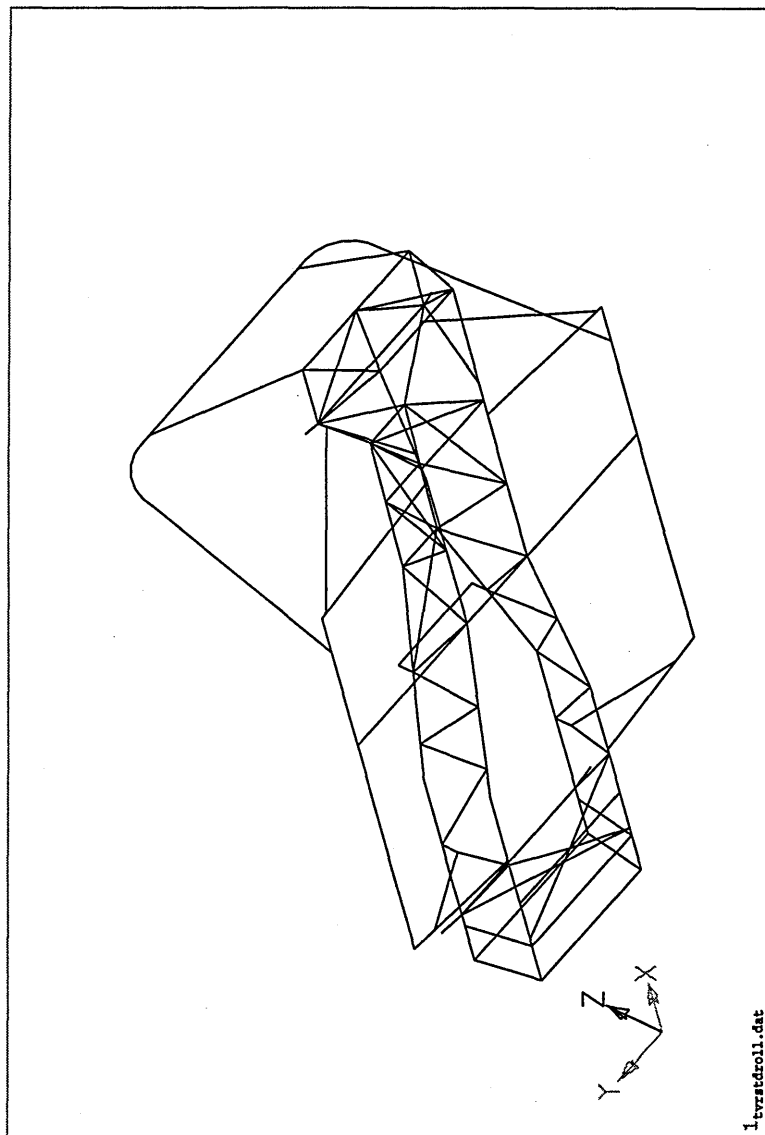


Figure 3.20: Chimaera Chassis with Standard (After Market) Roll Hoop

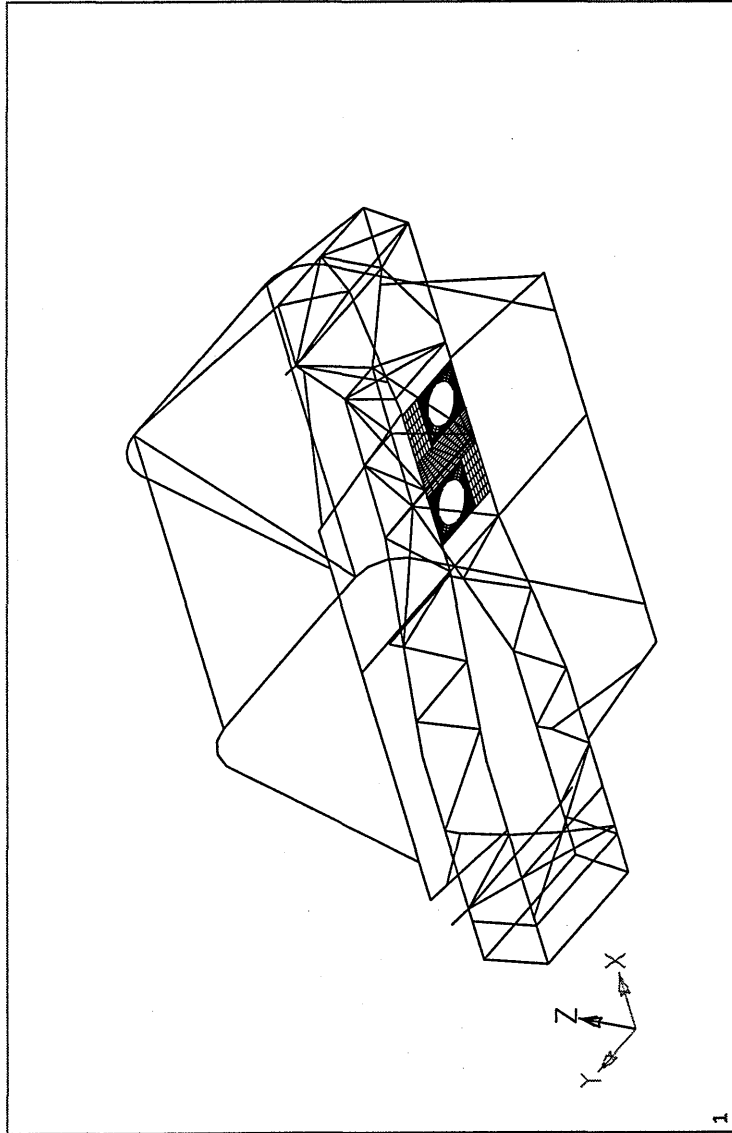


Figure 3.21: Chimaera Chassis with Front and Rear Roll Hoops *gearbox plate included*

Extra Long Chassis with Rear Roll Hoop					
Chassis Configuration	Deflection at load mm	Applied Torque Nm	Torsion Stiffness Nm/deg	Weight kg	Efficiency (Nm/deg)/kg
Chassis with rear roll hoop $\phi 44 \times 1.6 \text{ mm}$	12.84	1947.7	1959.3	68.3	28.7
Chassis with rear roll hoop $\phi 44 \times 3 \text{ mm}$	11.41	1947.7	2204.9	76.8	28.7
Chassis with rear roll hoop $\phi 55 \times 2.5 \text{ mm}$	10.14	1947.7	2481.0	78.1	31.8
Extra Long Chassis with Full Roll Cage					
Chassis with full roll cage $\phi 44 \times 1.6 \text{ mm}$	9.13	1947.7	2752.4	87.9	31.3
Chassis with full roll cage $\phi 38 \times 1.6 \text{ mm}$	10.16	1947.7	2476.1	85.4	29.0
Chassis with full roll cage $60 \times 40 \times 2 \text{ mm}$	7.82	1947.7	3216.9	96.4	33.37

Table 3.7: Table of Results for Extra Long Chassis

70% stiffer in torsion and this was achieved with a 30 % increase in weight. Careful integration of the roll cage with the extended chassis length of Model F (including the full roll cage) enabled a torsion stiffness only 1.8 % lower than that of the standard chassis with the full roll cage (Model D) to be achieved.

This illustrated the role of incorporating the roll cage into the structure and its ability to improve the torsion stiffness. The careful integration of the roll cage and the chassis structure into a complete structure is the best method of attaining an increase in torsion stiffness. This increased torsion stiffness then results in better handling on the track which was the desired result.

The variation between the models analysed is shown in Figure 3.23.

### 3.5 Nonlinear Analysis of Roll Cage

The analyses of Section 3.4 illustrated the important contribution which the roll cage can make to the overall structural stiffness of the chassis. The next step in designing the roll cage was to look at the overall load carrying capacity of the structure. The load to be carried by the roll cage was specified by the RACMSA and information on these requirements is contained in Appendix A.

Details of the nonlinear modelling process are contained in Chapter 4. The process of getting the models to run with the nonlinear load cases was challenging in itself. No one at Cranfield had much experience in using this capability of NASTRAN. Gaining an understanding of the format to be used for the analysis was particularly time consuming - the pre and post processor XL was not designed for these analyses and a lot of the required data had to be input into the data files by hand as there was no facility to do so using this package.

Once the roll cage had been developed its collapse was investigated using the non-linear material properties available in NASTRAN. The plausability of the early non-linear models was verified by running the same model using CRASHD. A good correlation was realised which gave confidence in the NASTRAN quasi-static loading method employed.

In excess of 200 models were run looking at the nonlinear collapse mechanism of the chassis and roll cage. A selection of illustrative analyses is included to show the main characteristics and problems.

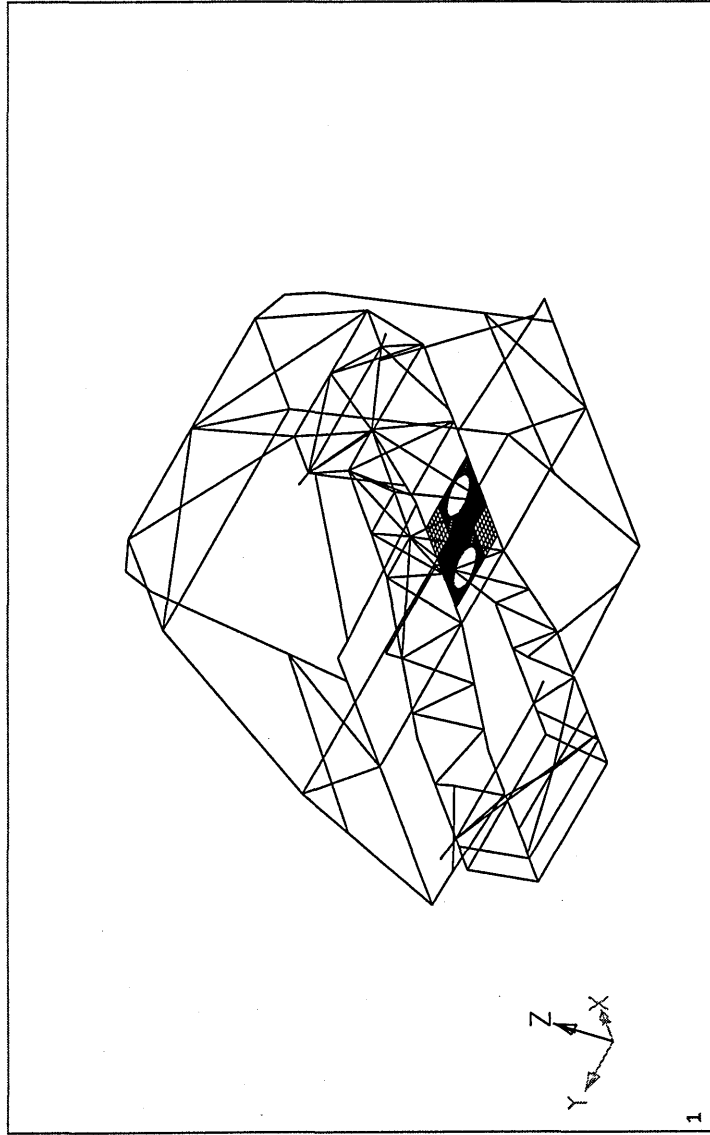


Figure 3.22: Extralong Chassis with Full Roll Cage

# Chimera Chassis' with Roll Structure

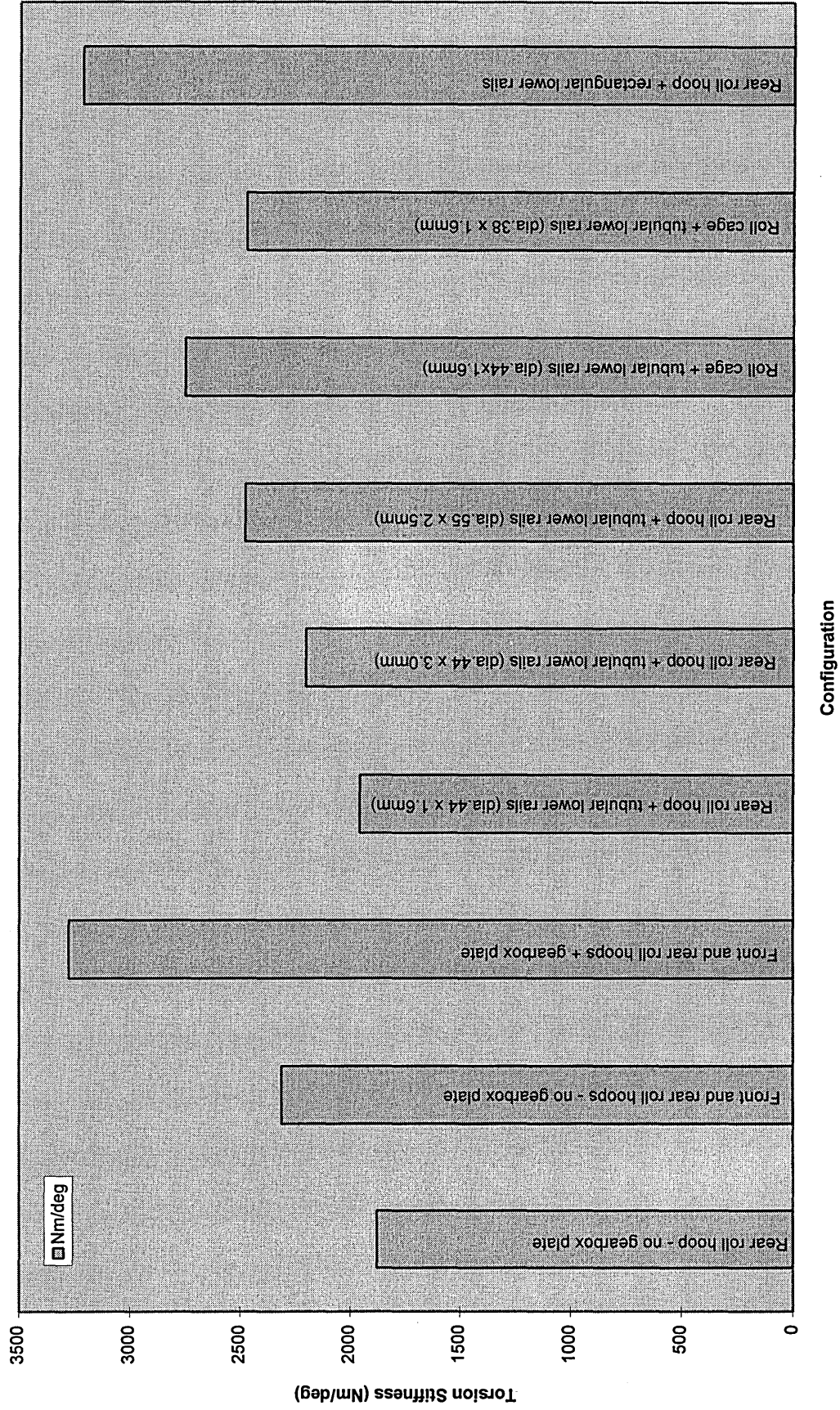


Figure 3.23: Graph Showing Torsion Stiffness Variation with Roll Structure

The initial analysis of the standard Chimaera chassis and the long chassis were carried out with the rear roll hoop only. In the nonlinear analyses the gearbox plate was removed as this increased the processing time manifold. The load was applied at the rear upper corner of the roll hoop in both the forward and aft directions. The design load which was to be carried [10] at any point on the top of the roll cage was 109,000 N (10 tonnes).

As more was learnt about the nonlinear analysis procedure other steps were taken to reduce the analysis times of the models. One procedure was to model the chassis as a combination of linear and nonlinear elements. The distribution of these was determined from the stress distribution in the early nonlinear models.

### 3.6 Analysis of Standard Chassis

The standard TVR Chimaera chassis was analysed with the rear roll hoop attached to the chassis. The roll cage was modelled as 38.1 mm diameter by 1.6mm (16swg) wall thickness CFS3 tubing<sup>3</sup>. Three representative models run using nonlinear elements were:

- Chimaera chassis with rear roll hoop. Load applied to rear hoop as shown in Figure 3.24 in the aft direction. All the elements in this analysis were nonlinear BEAM's.
- Chimaera chassis with rear roll hoop. Load applied to rear hoop as shown in Figure 3.25 in the forward direction. The roll cage and outriggers were modelled as nonlinear BEAM elements and the remaining structure was modelled as BAR (linear) elements.
- Chimaera chassis with rear roll hoop. Load applied to rear hoop as shown in Figure 3.24 in the aft direction. This model, however, is composed of both linear BAR elements and nonlinear BEAM elements.

The load was applied to the roll hoop using load increments via a number of subcases. The nonlinear analysis process in NASTRAN is discussed in Chapter 4 and is not reproduced here. Restraint was provided in the tunnel section of the model to represent the chassis mounting used for the actual tests.

The simple roll cage used on the standard chassis was braced back to the differential cage structure. The differential cage is quite stiff and is the ideal location to mount the roll cage stiffeners. As mentioned before the joints of the roll cage to the outriggers are quite poor, however, they are modelled as 'perfect' joints for the analysis.

The plastic moments for each member were calculated (see Appendix D) and the interaction between the bending and axial stresses was found to be of great significance with this being the primary cause of failure. This was only discovered much later in the analysis stage and is discussed in Appendix D.2.

The analysis gave the collapse load whence the structure could no longer restrain the applied load. At this point the stresses, bending moments and axial forces were all investigated to see which members were critical in the collapse mechanism. The resulting stress distribution for these three models are given in Figures 3.26 to 3.28 respectively. The maximum applied loads and the corresponding deflections are contained in Table 3.17.

<sup>3</sup>The material properties for this tube are summarized in Appendix C

Chimaera Chassis with Roll Hoop					
Model Arrangement	Max. Load (N)	Deflections (mm)			
		x	y	z	Total
Nonlinear - Aft Acting Load	12,117	60.65	22.37	-20.77	67.90
Nonlinear - Fwd Acting Load	9,352	-49.26	31.67	-26.52	64.29
Part Nonlinear - Aft Acting Load	11,500	49.57	13.92	-15.17	53.68

Table 3.8: Chimaera Chassis Results Table

As can be seen from the results there are significant differences in the ultimate load carried depending on the direction of loading on the rear hoop. With a forward acting load the roll hoop could carry a load 23 % less than if it was applied in the aft direction.

Using a partially nonlinear model also affected the results, but to within an acceptable limit. Applying the load in the aft direction on the partially nonlinear model resulted in an ultimate load 5 % less than on the fully nonlinear model and the maximum deflection was 20 % less.

These results were considered to be well within the limits of the modelling and serve to illustrate the variations that can be expected by making small modelling changes.

### 3.7 Analysis of Extralong Chassis

The extralong chassis model with a base length of 2,894 mm was analysed with the simple rear rollhoop but without the gearbox member and gearbox plate. The roll hoop was identical to that for the standard Chimaera Chassis as modelled in Section 3.6 and illustrated in Figure 3.24. In all the models below the main chassis structure was modelled as elastic BAR elements and the roll hoop and outrigger were nonlinear BEAM elements. The following three models are representative of those analysed:

- (1) Extralong Chassis with the lower chassis rails modelled with  $\phi 44 \times 1.6$  mm tubes. The simple rear roll hoop had the load applied in the aft direction as shown in Figure 3.29.
- (2) Extralong Chassis with the lower chassis rails modelled with  $\phi 44 \times 1.6$  mm tubes. The simple rear roll hoop had the load applied in the forward direction as shown in Figure 3.30.
- (3) Extralong Chassis with the lower chassis rails modelled with  $\phi 55 \times 1.6$  mm tubes. The simple rear roll hoop had the load applied in the aft direction as shown in Figure 3.31.

Deformed Stress Plots for these models at failure are contained in Figures 3.29, 3.30 and 3.31. The maximum loads and corresponding deflections are contained in Table 3.10.

The roll hoop was gradually developed into a full roll cage based on information provided by TVR Engineering. The full cage consisted of front and rear roll hoops tied together longitudinally. In addition it incorporated stiffeners in the roof and had side intrusion bars as detailed in Section 3.4.1. The entire roll cage, outriggers and attachments to the main chassis were modelled as nonlinear BEAM elements. The main chassis structure was predominantly elastic BAR elements.

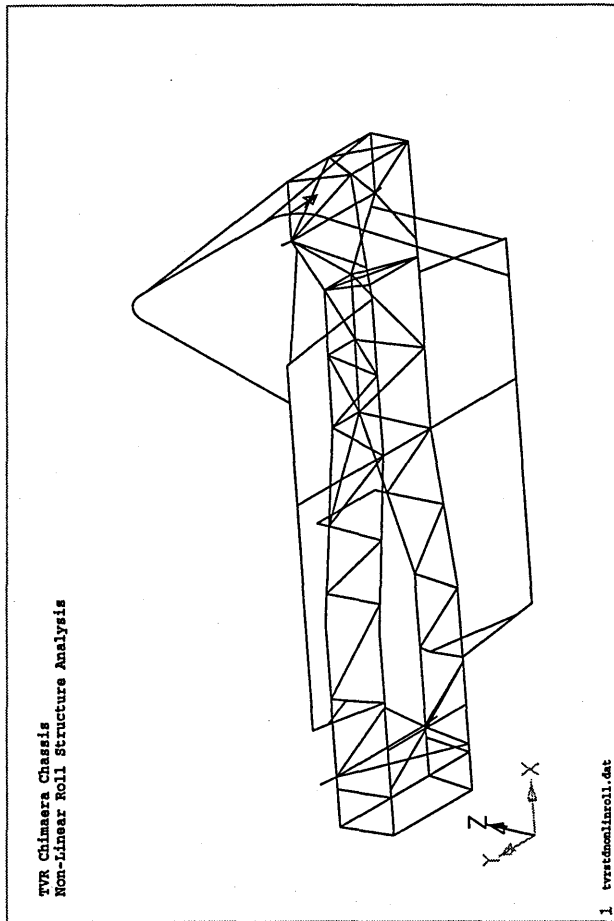


Figure 3.24: TVR Chimaera Chassis with Roll Hoop - Aft Load.



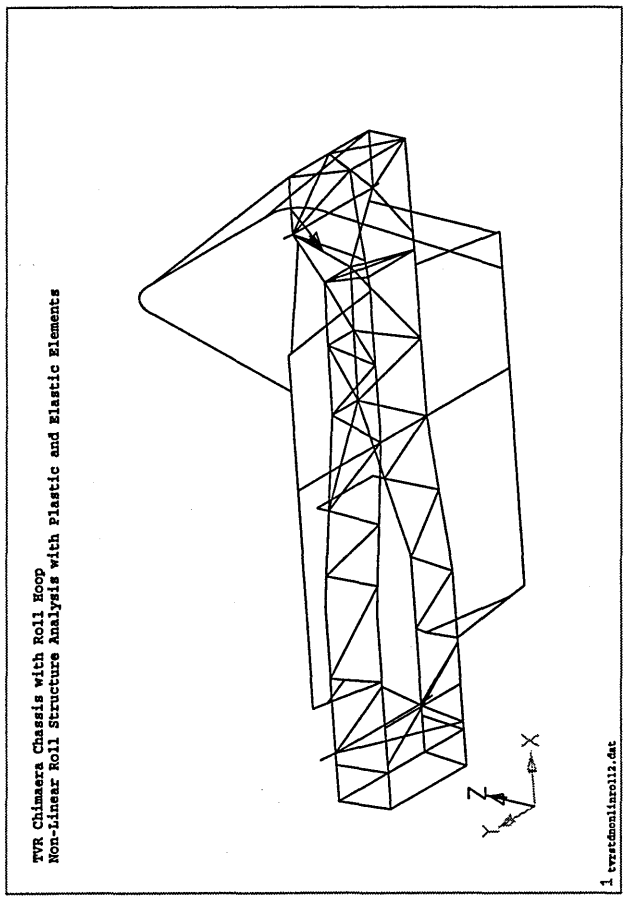


Figure 3.25: TVR Chimaera Chassis with Roll Hoop - Forward Load.

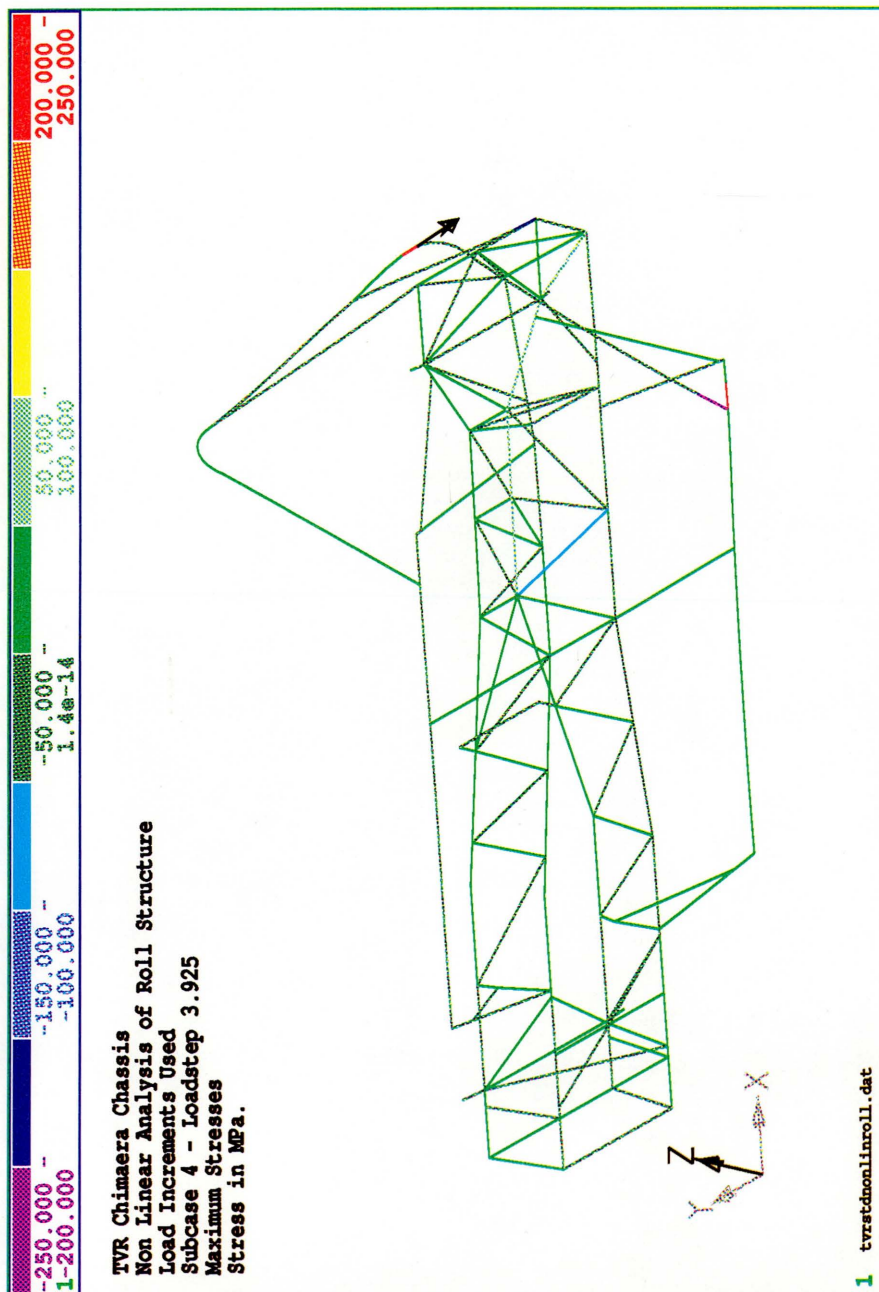


Figure 3.26: Stress Distribution at Failure, TVR Chimaera Chassis with Roll Hoop - Aft Load

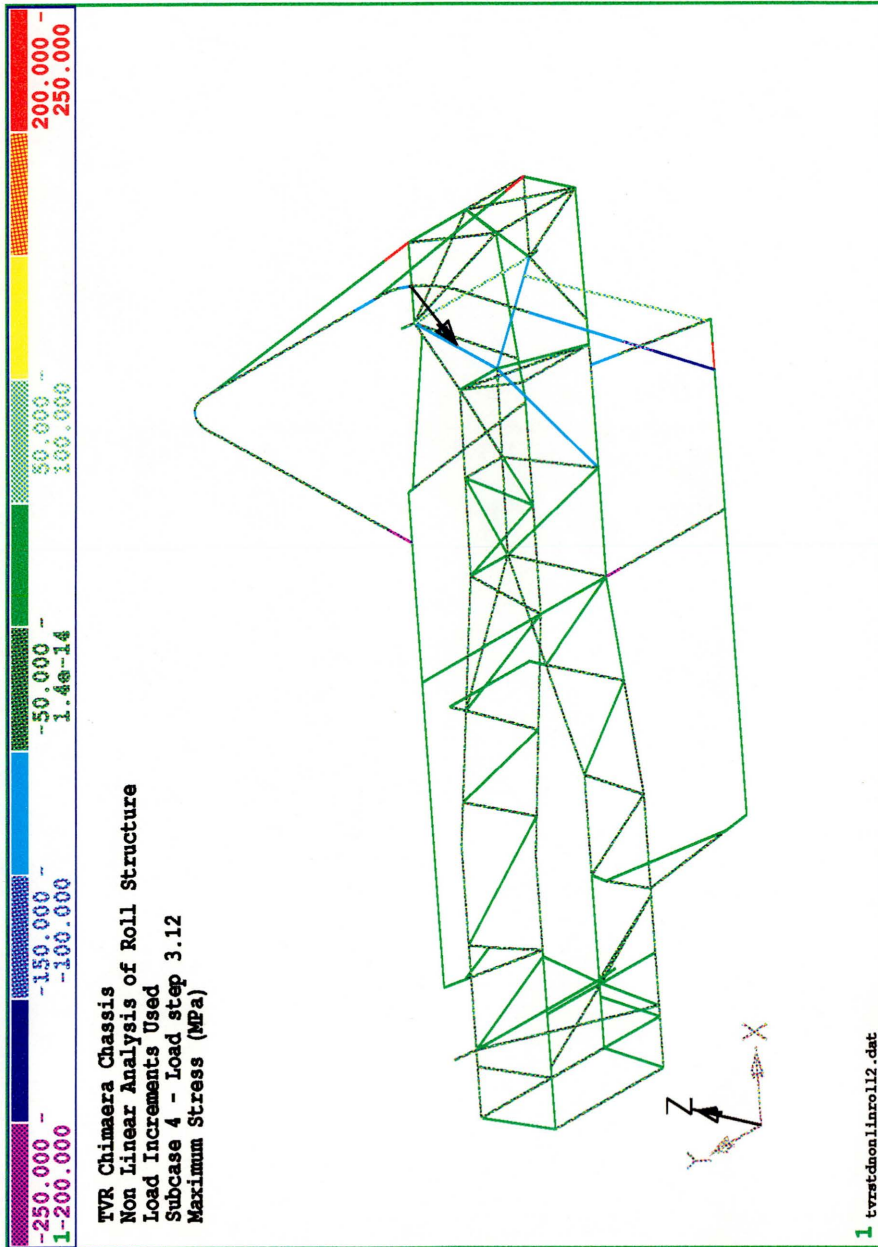


Figure 3.27: Stress Distribution at Failure, TVR Chimaera Chassis with Roll Hoop - Forward Load

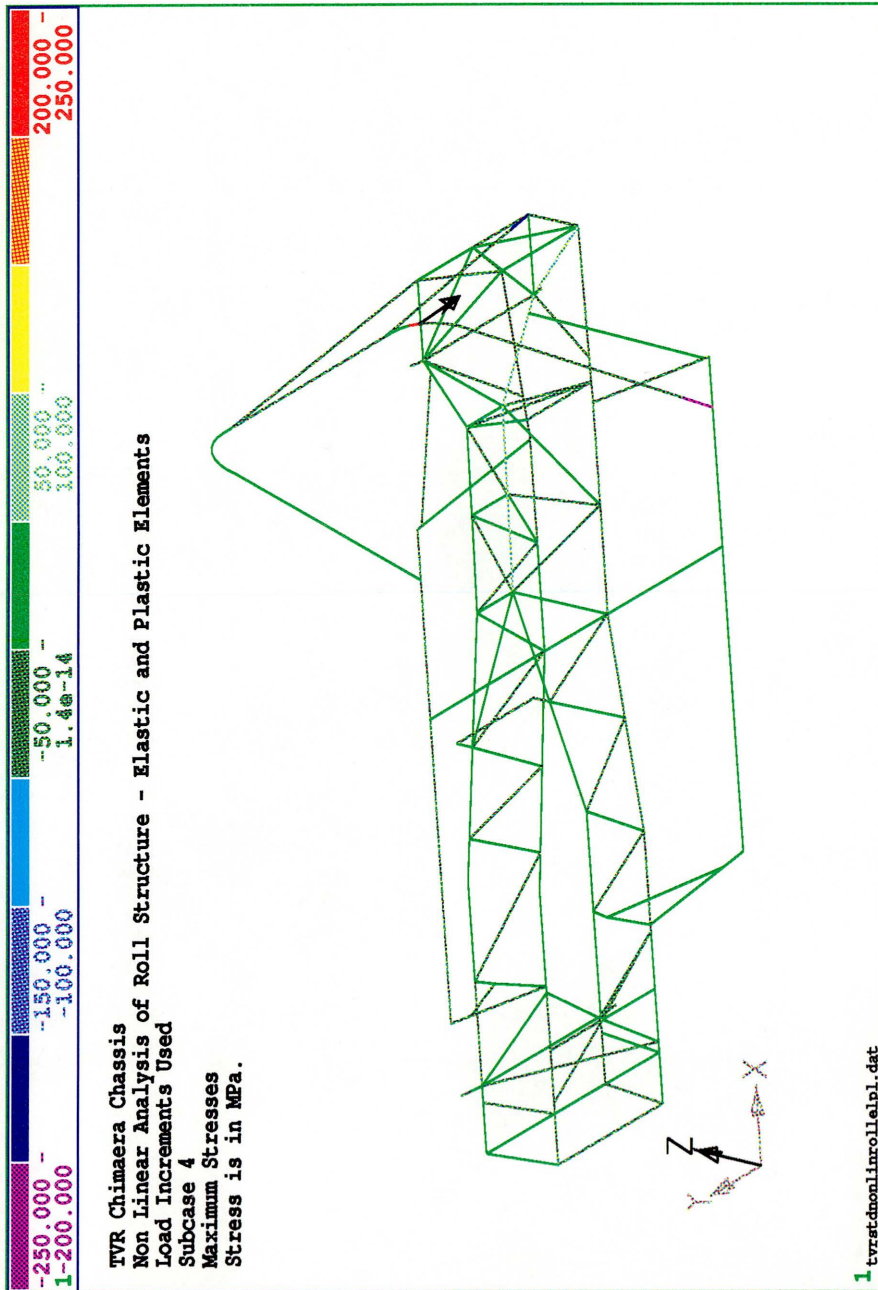


Figure 3.28: Stress Distribution at Failure, TVR Chimaera Chassis with Roll Hoop - Aft Load with Elastic and Plastic Members

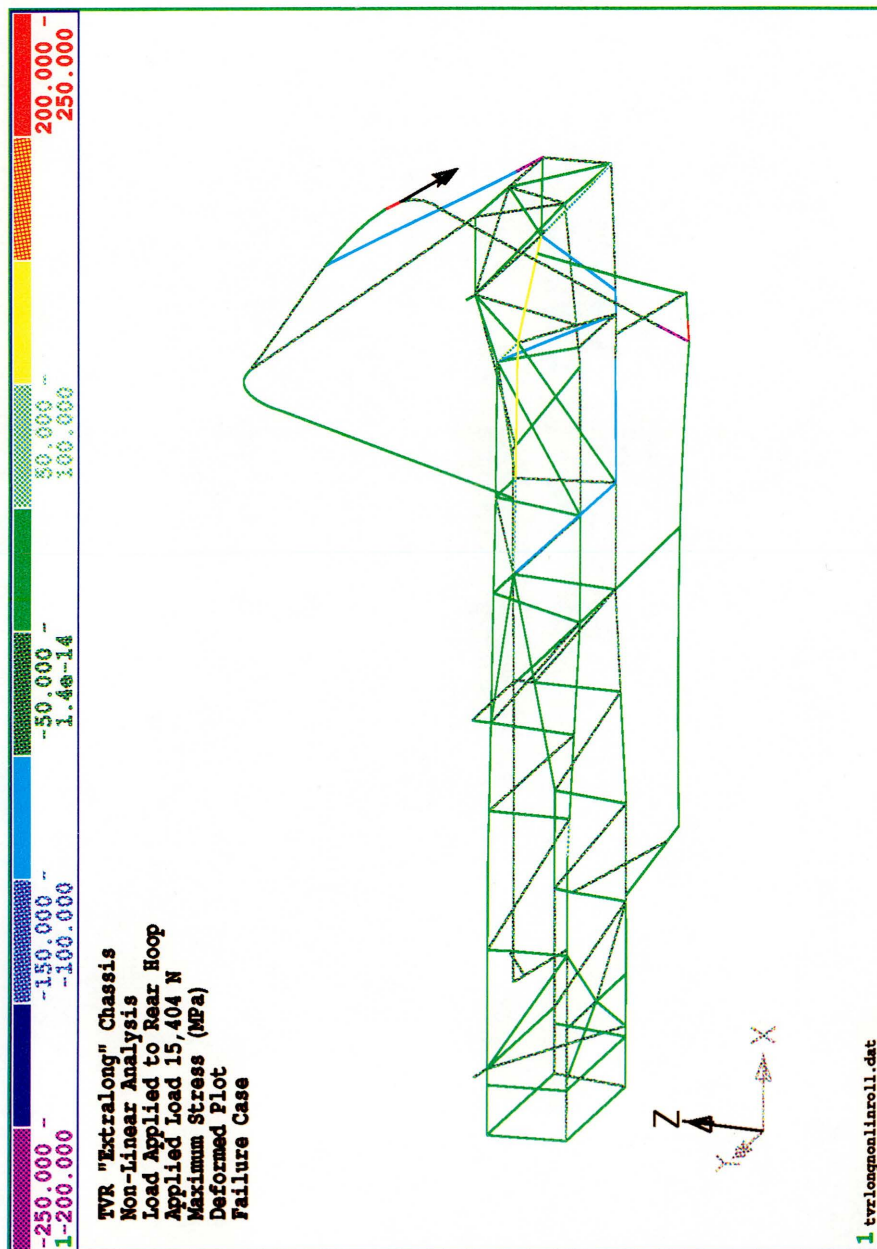


Figure 3.29: Extralong Chassis with  $\phi 44$  Circular Base Members - Stress Distribution at Failure - Load Acting Aft



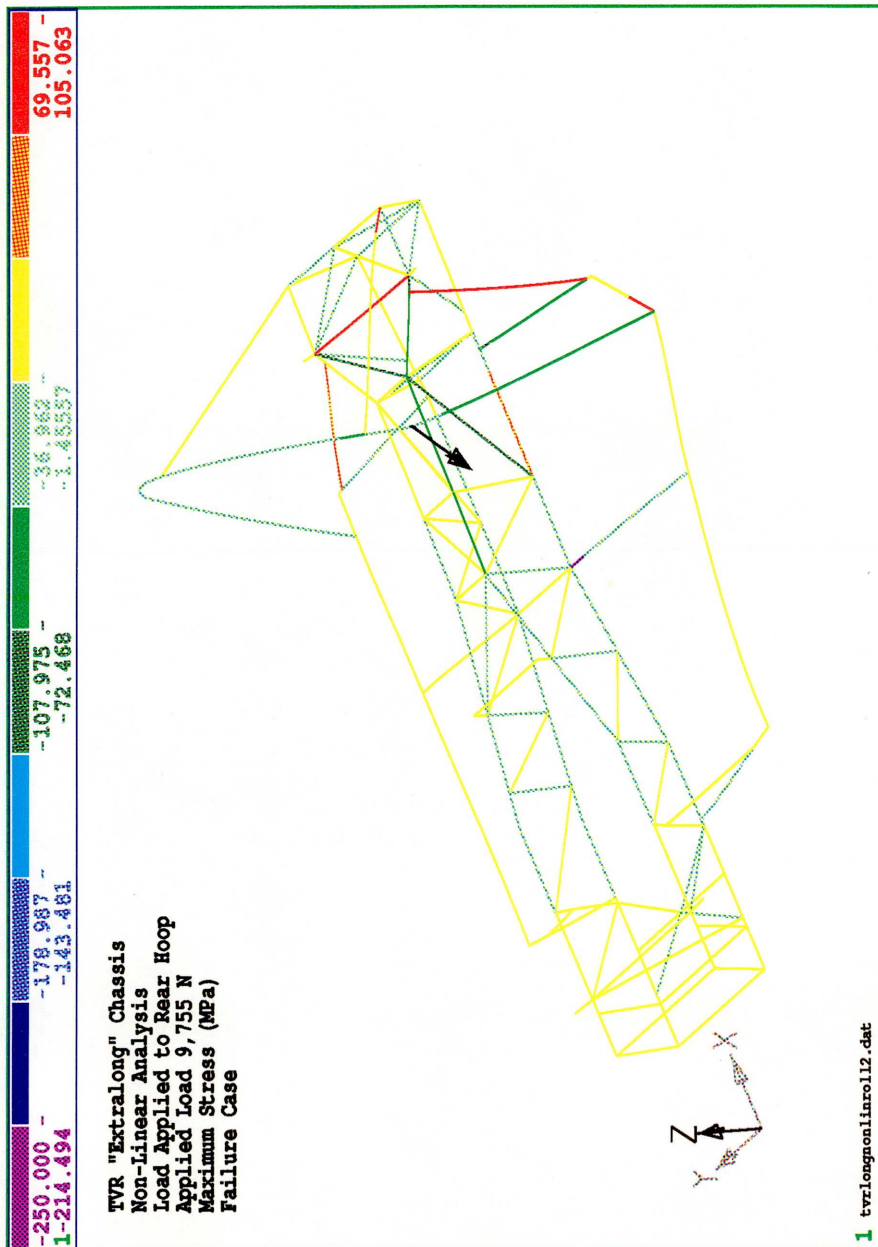


Figure 3.30: Extralong Chassis with  $\phi 44$  Circular Base Members - Stress Distribution at Failure - Forward Acting Load

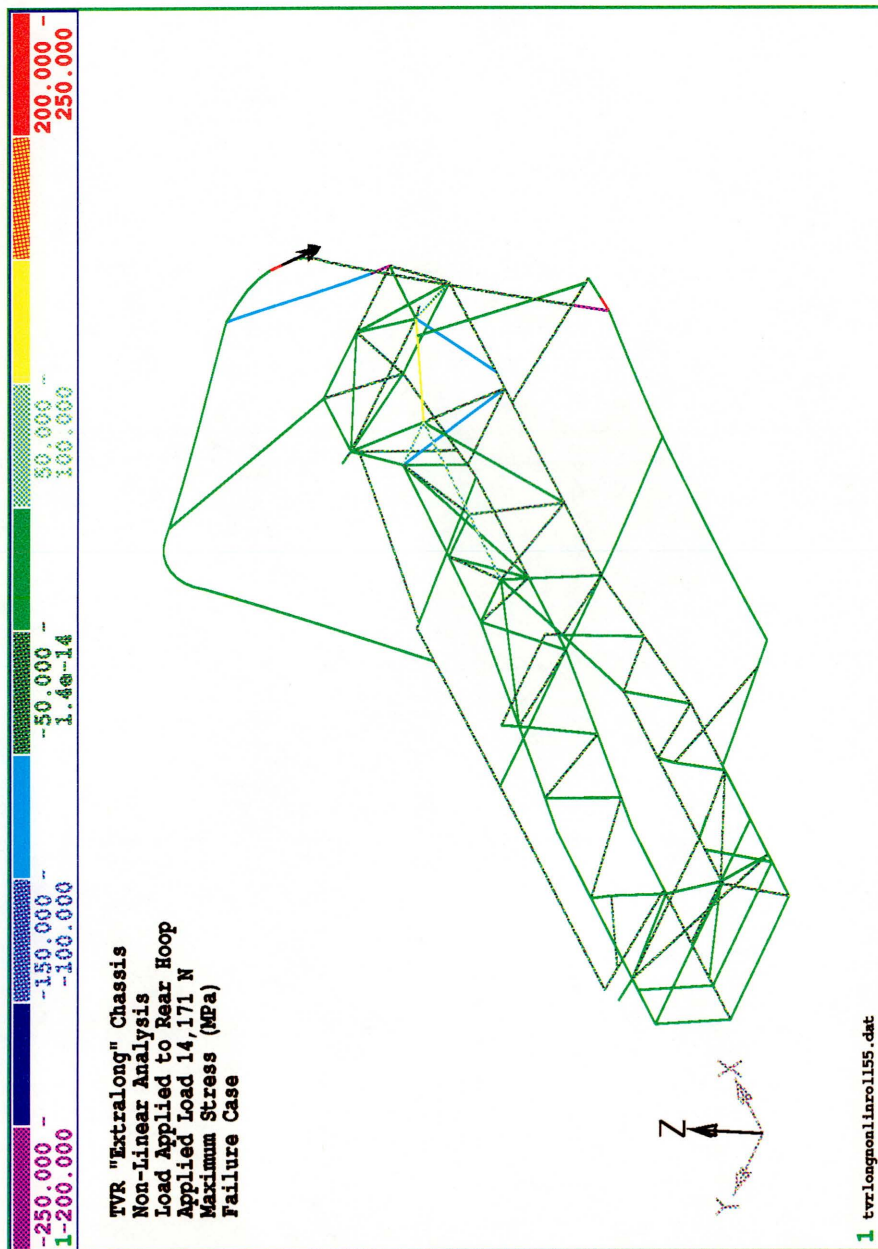


Figure 3.31: Extralong Chassis with  $\phi 55$  Circular Base Members - Stress Distribution at Failure - Aft Acting Load

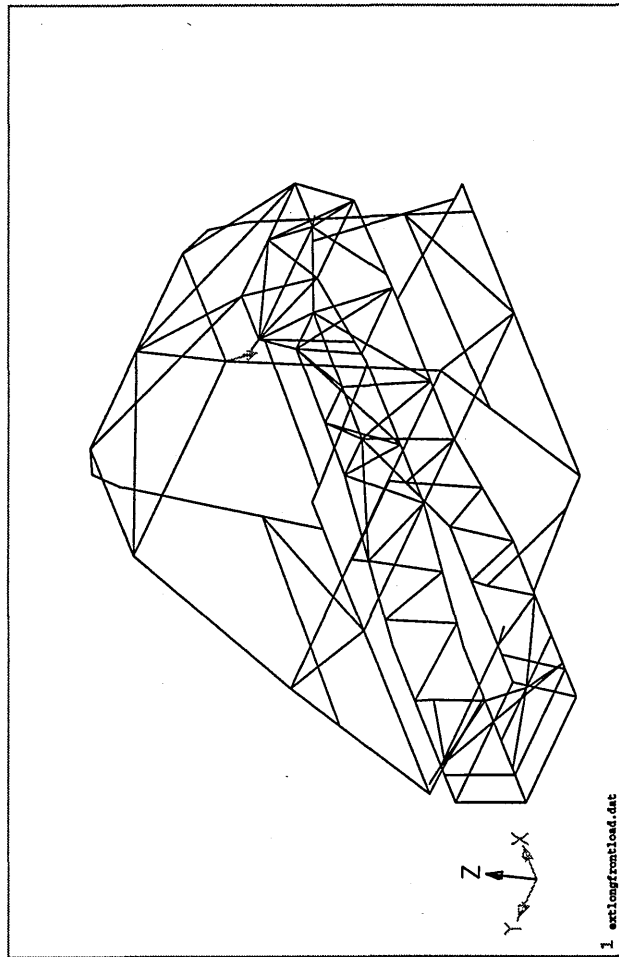


Figure 3.32: TVR Extralong Chassis with Full Roll Cage



Extralong Chassis with Roll Hoop					
Model Arrangement	Max. Load (N)	Deflections (mm)			
		x	y	z	Total
Circular Base $\phi 44 \times 1.6$ - Aft Load	15,404	86.39	36.40	-34.23	99.80
Circular Base $\phi 44 \times 1.6$ - Fwd Load	9,755	-34.19	10.01	-22.83	42.56
Circular Base $\phi 55 \times 2.5$ - Aft Load	14,171	56.20	16.39	-19.31	61.64

Table 3.9: Extralong Chassis with Circular Base Tubes Results Table

Extralong Chassis with Roll Cage					
Model Arrangement	Max. Load (N)	Deflections (mm)			
		x	y	z	Total
Roll Cage $\phi 44 \times 1.6$	17,223	8.87	-1.88	-24.06	25.72
Roll Cage $\phi 25 \times 1.6$	9,869	18.0	-3.92	-35.23	39.76
Roll Cage $\phi 32 \times 1.6$	13,900	15.51	-1.55	-43.42	46.13

Table 3.10: Extralong Chassis Results Table - Full Roll Cage

The chassis was restrained along the main tunnel section. The general arrangement can be seen in Figure 3.32. A representative selection of the models run was:

- (1) Extralong Chassis with a full roll cage as shown in Figure 3.33. The load was applied to the front upper windscreen corner in an aft direction. The rollcage was manufactured from  $\phi 44 \times 1.6mm$  and the lower chassis rails were rectangular sections.
- (2) Extralong Chassis with a full roll cage as shown in Figure 3.34. The load was applied to the front upper windscreen corner in an aft direction. The rollcage was manufactured from  $\phi 25 \times 1.6mm$  and the lower chassis rails were rectangular sections.
- (3) Extralong Chassis with a full roll cage as shown in Figure 3.35. The load was applied to the front upper windscreen corner in an aft direction. The rollcage was manufactured from  $\phi 32 \times 1.6mm$  and the lower chassis rails were rectangular sections.

The results for these investigations are contained in Table 3.10. The maximum load which could be carried by each of these examples varied significantly and, as would be expected, the larger diameter tubes could carry much higher loads with much lower deflections.

The results from the above investigations showed that it was not possible to carry the load specified by the RACMSA on the rear roll hoop.

It would be expected that increasing the lower chassis rail dimensions would be beneficial to the structure carrying more load. This was not found to be so in the models of Figure 3.29 and Figure 3.31. The possible reason for this is that increasing the lower chassis rail size also increases the stiffness of the chassis as already noted. This increase in torsion stiffness consequently leads to smaller deflections under applied loads and this can be seen from the results in Table 3.10. A result of lowered overall deflections is that some members may become more highly stressed and this can be seen from Figures 3.29 and 3.31. Consequently the load which can be carried by the chassis

which was expected to be stronger is in actual fact diminished.

The incorporation of the full roll cage enabled a substantial load to be carried at what was the weakest point on the roll cage structure (the front upper windscreen corner). It was possible to carry a load similar in magnitude (15 % higher) to that carried by the stiff rear hoop when loaded in an aft direction. The deflections of the front corner prior to complete collapse were smaller (32 % lower) than those experienced by the rear hoop in the early models when using the same size tubing for the roll structure.

### 3.8 Cerbera GT Chassis

Once the initial investigation had been completed work was discontinued for some time. Wanke [4] undertook an investigation of the torsion stiffness of the TVR Chassis and this work is summarised in Chapter 3.1.2. The final stage of the chassis modelling carried out by the author followed on from the work of Wanke and is detailed in this Section of the report.

Initially Wanke's final chassis model was modified to improve the access for the driver. The access for the driver was crucial for egress in the case of emergency. Each stage of these modifications was modelled and analysed to investigate the implications. Details of a representative sample of models are contained below.

#### 3.8.1 Investigation of Torsion Stiffness

The model of Wanke [4] was verified against the current car structure from information provided by TVR. The modifications to the chassis to improve access and exit from the vehicle were then carried out on this chassis model.

Over 30 runs were carried out investigating the effect of moving various structural members. In all of these analyses the torsion stiffness was the test criteria. It is not possible to detail all of the models and a representative sample are included.

Once a structure satisfying the entry and exit requirements, which could be easily manufactured (i.e. minimising the complex tube intersections in the door bars), was designed further improvements were investigated. To achieve improved entry and exit to the cockpit the door bars were re-arranged and lowered and the rear hoop was rotated aft to make it vertical.

Further investigations were made in an attempt to increase the torsion stiffness by getting the high loads from the torsionally weak engine bay back into the stiff torsion structure of the roll cage and chassis. This modelling resulted in an achievable increase in the torsion stiffness of 20 % with the addition of a few extra members. This highlighted the gains in torsion stiffness that could be realised if it were possible to triangulate this area of the chassis. This however was not possible as there were systems and components for the vehicle in the spaces required for the bars.

The final chassis arrangement which was provided for the physical test is shown in Figure 3.36. This chassis represented the best compromise for this vehicle and gave an adequate, weight efficient, torsion stiffness with suitable openings for entry and exit of the driver.

Once the final structure was decided on this was taken as the nonlinear model and analysed accordingly. The details of the analysis are contained in Chapter 4.

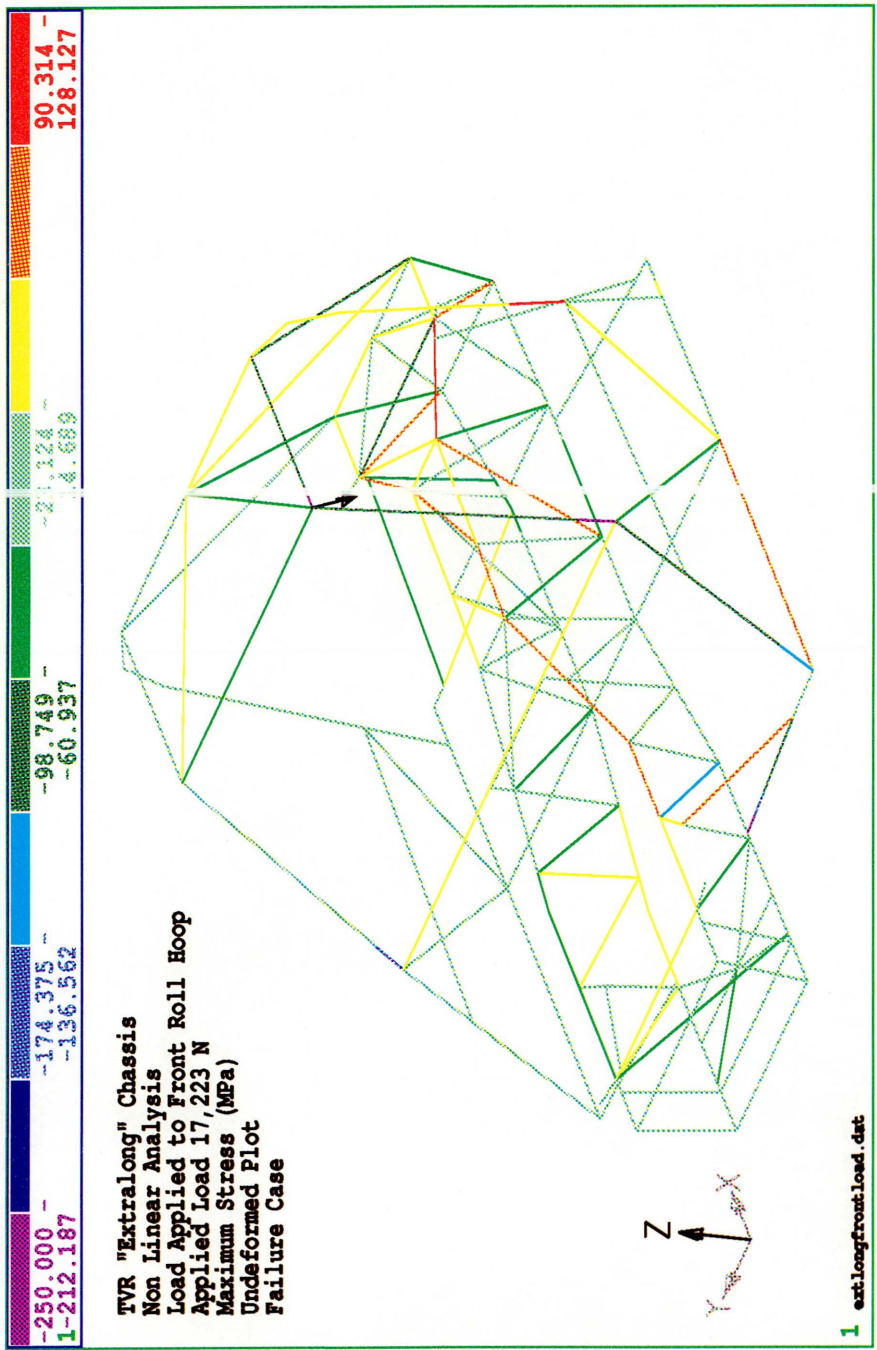


Figure 3.33: Extralong Chassis with Rollage made from  $\phi 44$  Tubing - Stress Distribution at Failure

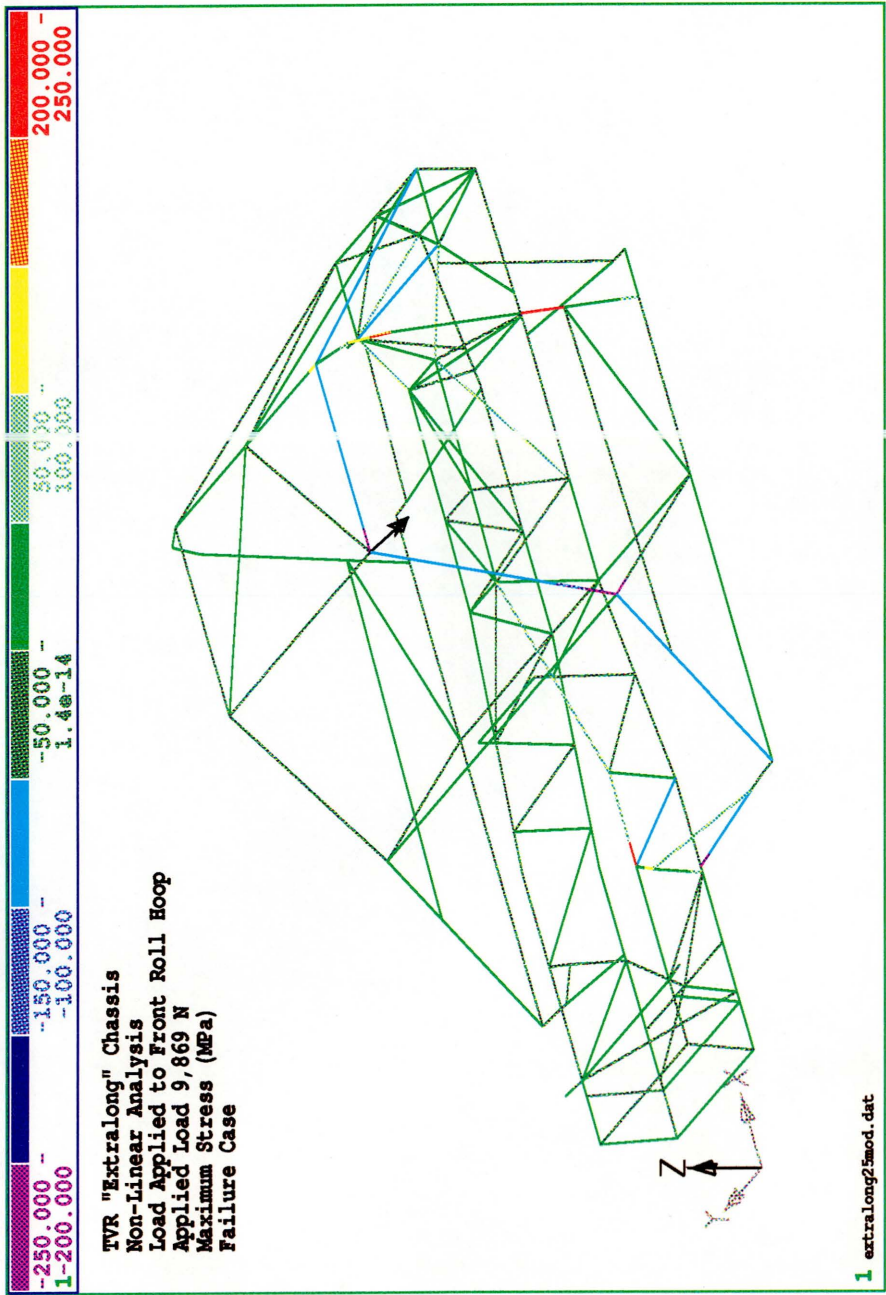


Figure 3.34: Extralong Chassis with Rollcage made from  $\phi 25$  Tubing - Stress Distribution at Failure

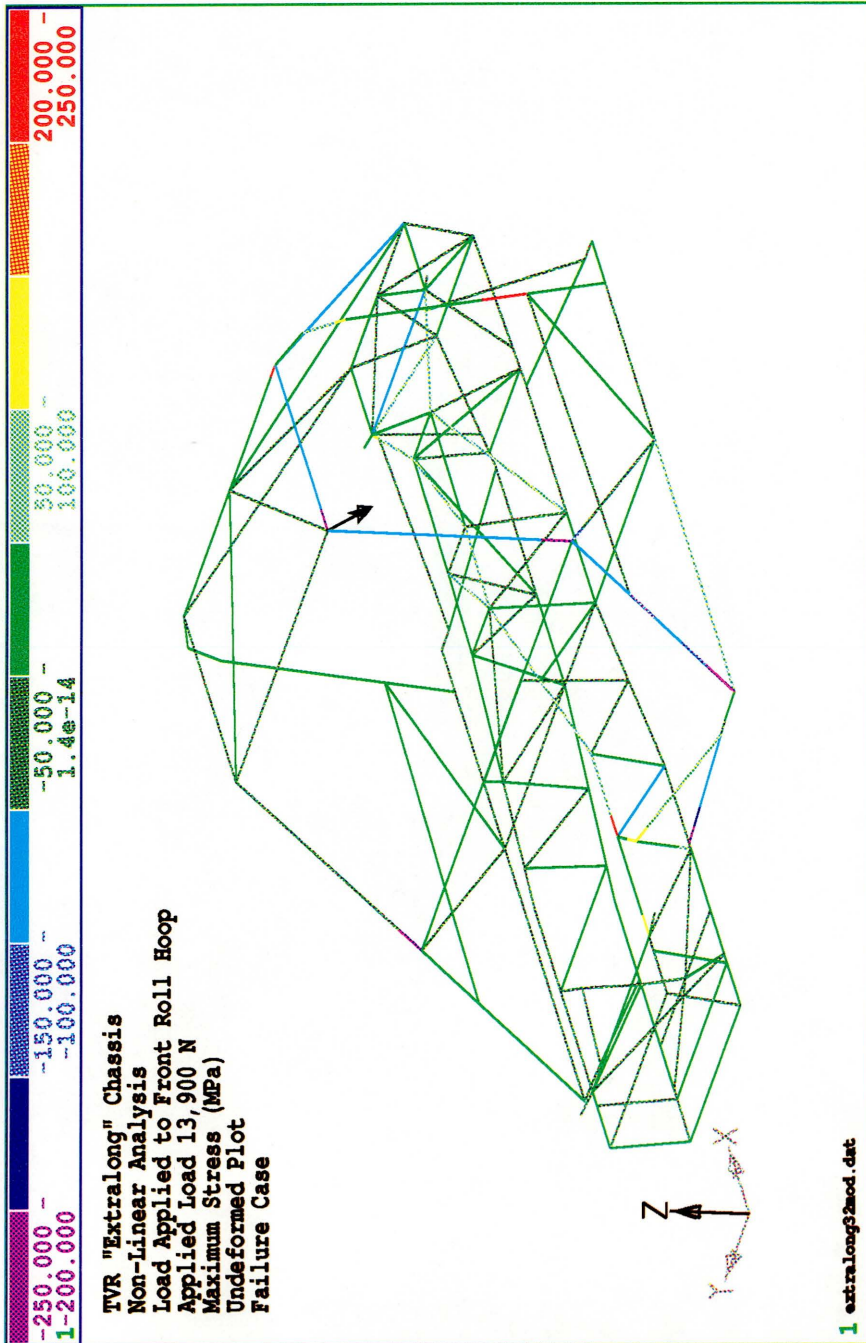


Figure 3.35: Extralong Chassis with Rollcage made from  $\phi 32$  Tubing - Stress Distribution at Failure



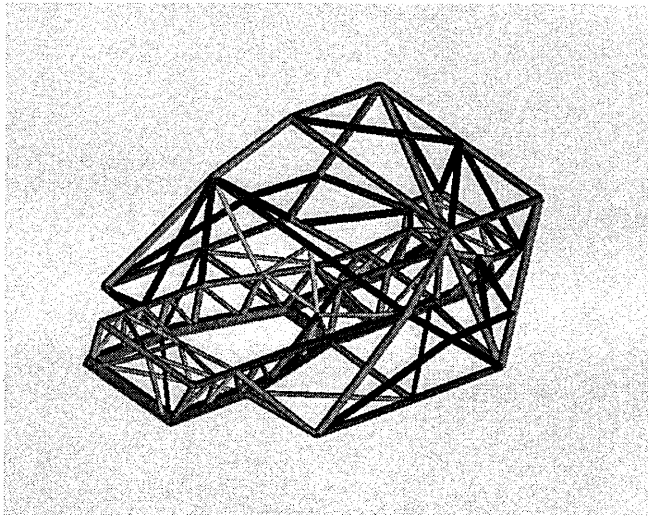


Figure 3.36: Final Chassis Arrangement

### 3.8.2 Modifications to Wanke's Model

The work of Wanke [4] followed on from the initial work (see Chapter 3.2) of the author. The investigation by Wanke concentrated on increasing the torsion stiffness of the racing chassis. The chassis in its final form, as analysed by Wanke is shown in Figure 3.37 and this was the first model run to give baseline values.

As mentioned in Section 3.1.2 the chassis tested by Wanke had a loaded length which was longer than that in the actual chassis. Prior to analysing this model the loaded length of the model was changed so as to represent the real car structure. The data in Table 3.11 is a summary for this chassis. All subsequent models were compared to these results and this model is referred to as the *Original Model*.

The major structural modifications carried out on this chassis (Figure 3.37) in order to make it more practical were:

1. Fitting of a full width diagonal to the rear hoop - this is more structurally efficient and does not put large bending loads into the rear hoop structure,
2. The door bars were lowered and rearranged to ease access to the cockpit and to ease manufacture of the roll cage,
3. The rear roll hoop was rotated aft so that it was vertical giving more head room in the vehicle (*for the Managing Director*),
4. Front stiffeners were modelled to increase the torsion stiffness,
5. Gussets were added to the joints to investigate their effect,
6. Different material grades and sizes were modelled to investigate their effect on the chassis.

Models illustrating the modifications carried out are discussed below and illustrated in Figures 3.37 to 3.42. The results from the analyses are contained in Tables 3.11 to 3.16.

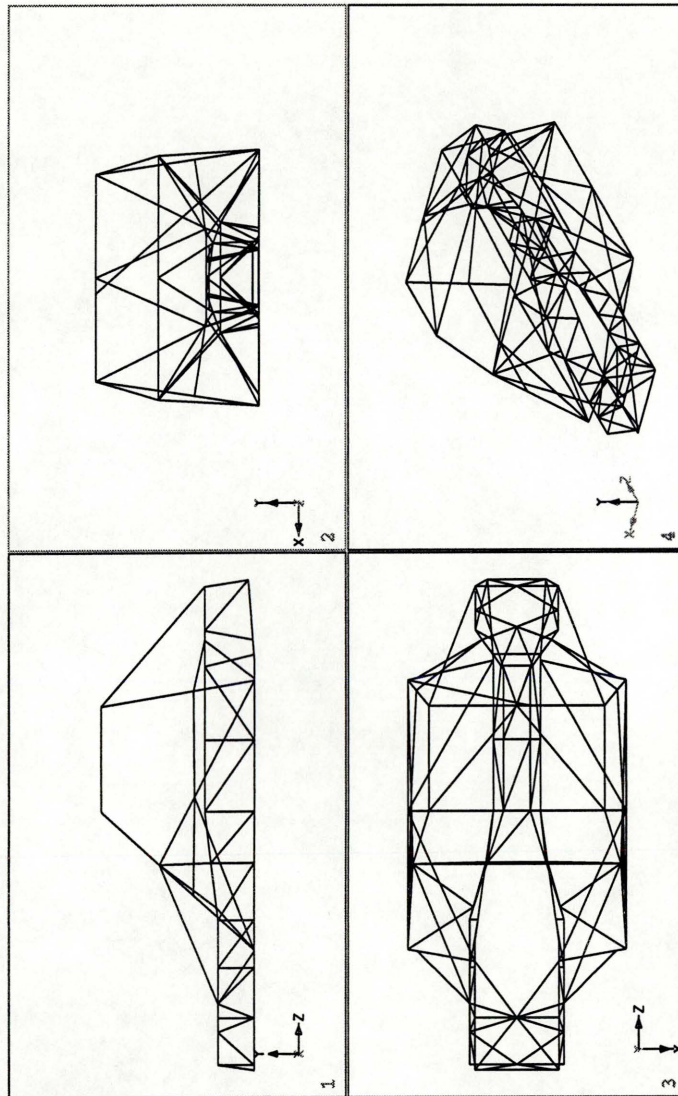


Figure 3.37: Cerbera GT Chassis (Wanke)

Cerbera GT Inital Model		
Loaded Length	mm	2,446
Applied Load	N	1,000
Torsion Load	Nm	600
Torsion Stiffness	Nm/deg	10,595
Weight	kg	121
Efficiency	(Nm/deg)/kg	87.56

Table 3.11: Summary of Results from Wanke's Model

Cerbera GT		
Loaded Length	mm	2,446
Applied Load	N	1,000
Torsion Load	Nm	600
Torsion Stiffness	Nm/deg	10,444
Variation from Original	%	-1.4
Weight	kg	120
Efficiency	(Nm/deg)/kg	87.03

Table 3.12: Cerbera GT with full width diagonal in rear hoop and lowered door bars

### 3.8.3 Full Width Diagonal and Lowered Door Bars

The model in Figure 3.37 was modified to include a full width diagonal in the rear hoop. The door bars were lowered by 61mm at the rear to improve the access to the car cockpit. The arrangement is shown in Figure 3.38. The results data for this model is contained in Table 3.12.

### 3.8.4 Vertical Rear Hoop and Lowered Door Bars

The model was the same as that in Figure 3.38 with the exception that the rear hoop was rotated aft to make it vertical. The door bars were essentially the same as those of the previous model. This model is illustrated in Figure 3.39. The results data for this model can be found in Table 3.13.

Cerbera GT		
Loaded Length	mm	2,446
Applied Load	N	1,000
Torsion Load	Nm	600
Torsion Stiffness	Nm/deg	10,246
Variation from Original	%	-3.2
Weight	kg	120
Efficiency	(Nm/deg)/kg	85.38

Table 3.13: Cerbera GT with vertical rear hoop and lowered door bars



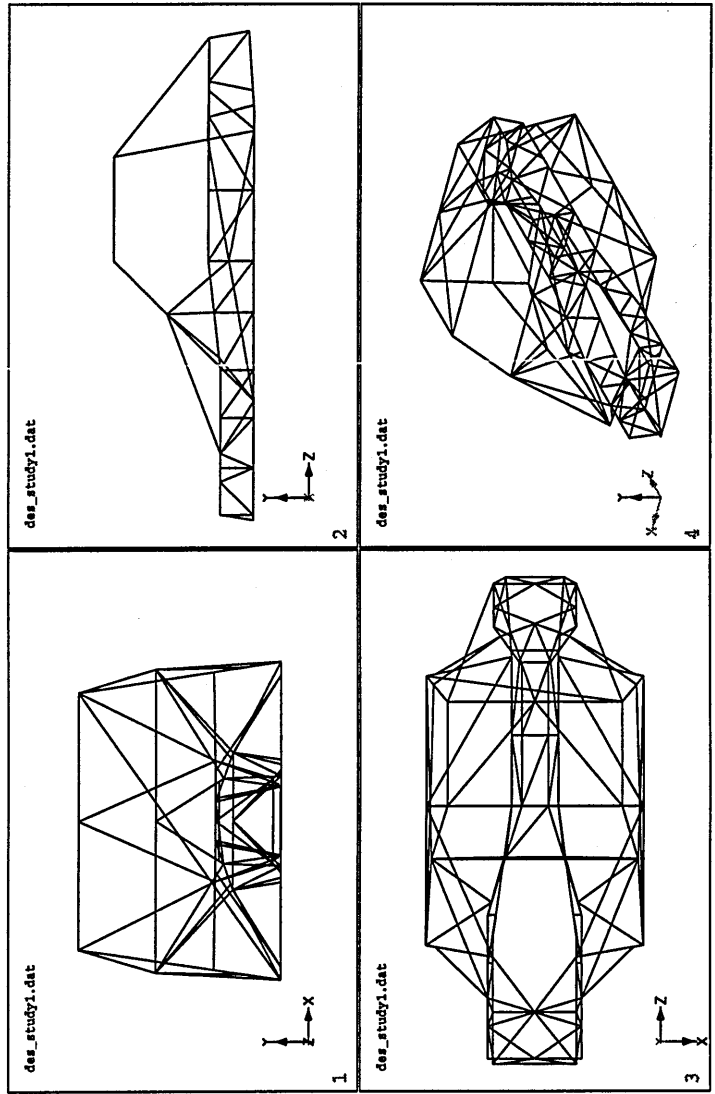


Figure 3.38: Cerbera GT Chassis with Full Rear Hoop Diagonal

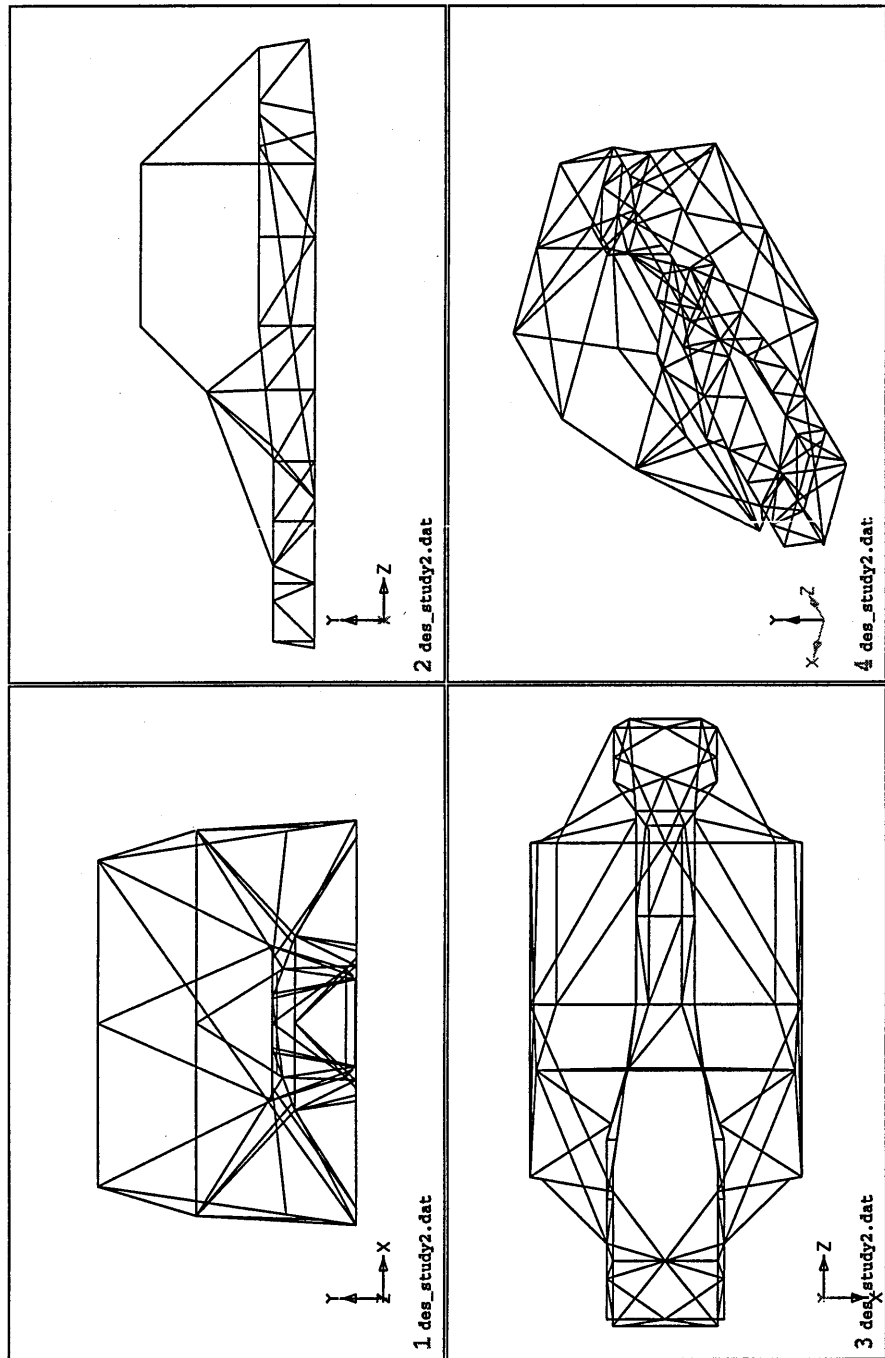


Figure 3.39: Cerbera GT Chassis with Vertical Rear Hoop and Lowered Door Bars

Cerbera GT		
Loaded Length	mm	2,446
Applied Load	N	1,000
Torsion Load	Nm	600
Torsion Stiffness	Nm/deg	12,637
Variation from Original	%	+19
Weight	kg	126
Efficiency	(Nm/deg)/kg	100.30

Table 3.14: Cerbera GT additional stiffeners in front

Cerbera GT		
Loaded Length	mm	2,446
Applied Load	N	1,000
Torsion Load	Nm	600
Torsion Stiffness	Nm/deg	13,776
Variation from Original	%	+30
Weight	kg	129
Efficiency	(Nm/deg)/kg	106.79

Table 3.15: Cerbera GT additional stiffeners in front

### 3.8.5 Improved Stiffening Members

To increase the torsion stiffness further methods of getting the high loads from the torsionally weak engine bay back into the stiff roll cage structure were investigated. Several members were added to take the load from the front suspension mount and direct it back to the cage. The general arrangement is shown in Figure 3.40. Whilst the bars were carefully arranged so as to not encroach on the space required for the body work it was found that they encroached on space required for other subsystems and thus the gain in torsion stiffness was not practical. The results data for this model is contained in Table 3.14.

### 3.8.6 Improved Stiffeners with Gussets

The model in Figure 3.40 was then taken and modified to include gussets in the rear roll cage corners between the roll hoop and the longitudinal members and in the front upper windscreen corners. These modifications increase the joint stiffness and a small increase in torsion stiffness over the above model was realised. The chassis arrangement is illustrated in Figure 3.41. The results for this model are listed in Table 3.15.

### 3.8.7 Final Model

The final arrangement was derived from the preceding models. As mentioned above the additional stiffening members were not able to be added to the structure as space in the front section of the car is well utilised to incorporate the sub-systems for the vehicle. It was decided to raise the door

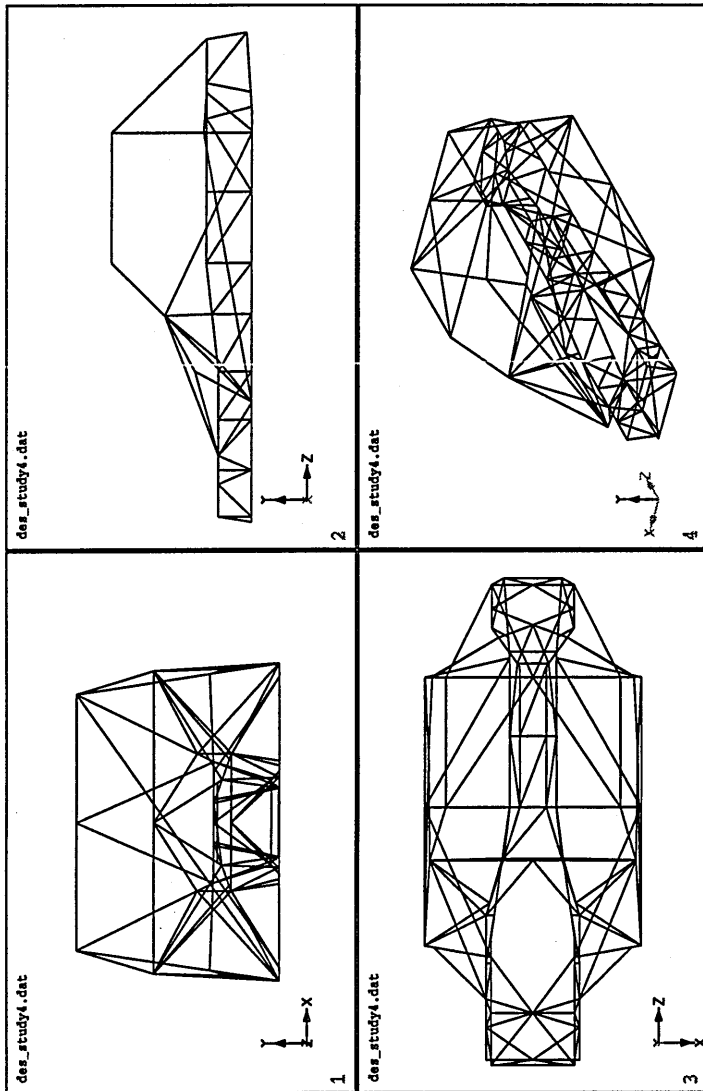


Figure 3.40: Cerbera GT Chassis with Additional Front Stiffeners

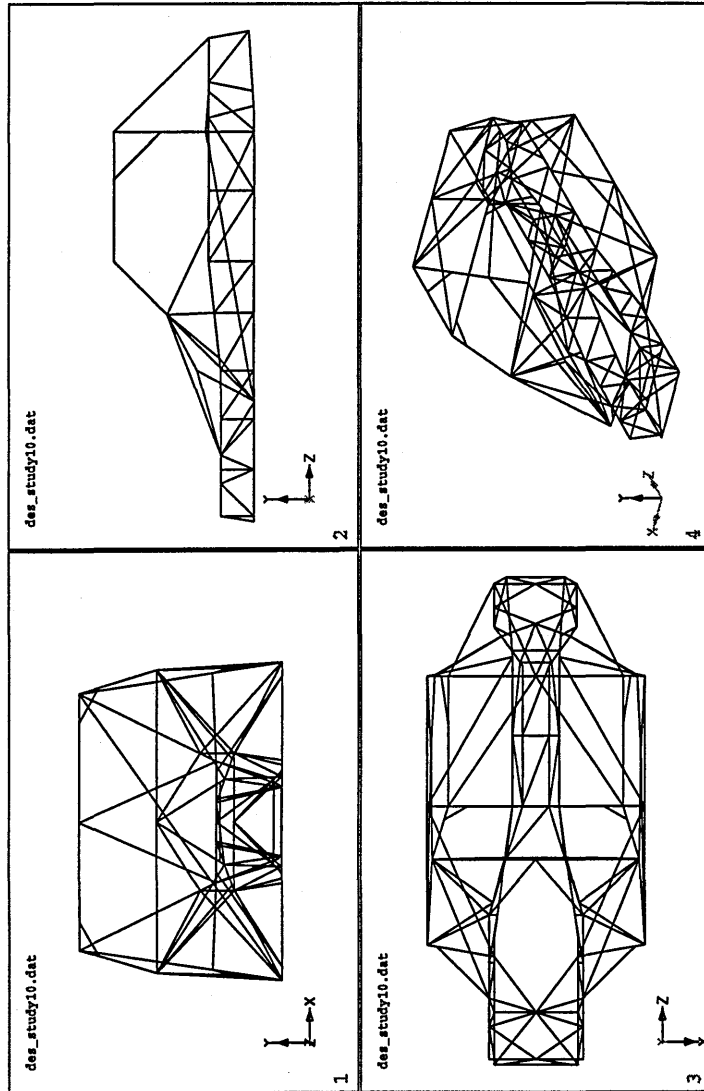


Figure 3.41: Cerbera GT Chassis with Additional Stiffeners and Gussets

Cerbera GT		
Loaded Length	mm	2,446
Applied Load	N	1,000
Torsion Load	Nm	600
Deflection at Load	mm	0.631
Torsion Stiffness	Nm/deg	9,947
Variation from Original	%	-6
Weight	kg	108
Efficiency	(Nm/deg)/kg	92.10

Table 3.16: Final Cerbera GT Model

bars so that the side intrusion bar was horizontal. This was easier to manufacture than two angled members. Lowering the side intrusion bar as shown added quite a bit of room to the entry and exit area of the car once the rear hoop was moved aft to give more headroom for the managing director.

The final arrangement is shown in Figure 3.42. The results for this structure are given in Table 3.16. Whilst this arrangement had a torsion stiffness 6% lower than the model of reference [4], the ease of access for the driver and ease of manufacture were considered more important.

The torsion stiffness increase achieved through the development of the chassis from the standard Chimaera chassis to the final Cerbera arrangement is summarised in Figure 3.43. This model was used in the next stage of the analysis to investigate the crush resistance of the roll cage.

### 3.9 Non-Linear Analysis of the Roll Structure

The final chassis arrangement shown in Figure 3.42 was converted to run as a nonlinear model. The nonlinear modelling incorporated material nonlinearity and made allowances for large displacements. In the early stages of modelling the load was applied using load increments. Later in the analysis stage this strategy was changed and displacement incrementation was used to try to get the deep collapse mechanism. Full details of the non-linear analysis with NASTRAN and the associated problems are contained in Chapter 4.

Both fully nonlinear models and some partially nonlinear ones were run for comparison and representative models are presented below. The advantage of running partially nonlinear models was that they were much more efficient in terms of time to run. A typical fully nonlinear run would take between 7 and 10 hours on the Sun 630 MP computer or between 5 and 7 hours when running on the Cray YMP computer.

For part nonlinear models the highly stressed areas needed to be identified so as to ensure that nonlinear elements were used where they were required. This was achieved by running a linear analysis with incremental loads (this took about 10 minutes on the Sun computer). The highly stressed areas were then converted to nonlinear elements and the part nonlinear models run. These part nonlinear models took 4-5 hours on the Sun or 1-4 hours on the Cray which was a marked reduction in the run time from that of a fully nonlinear model. Running the nonlinear models with one element between each tube joint was found to give quite good results with a minimum of running time. For these models the run time was about 2 hours on the Sun computer and 1.5 hours on the Cray.

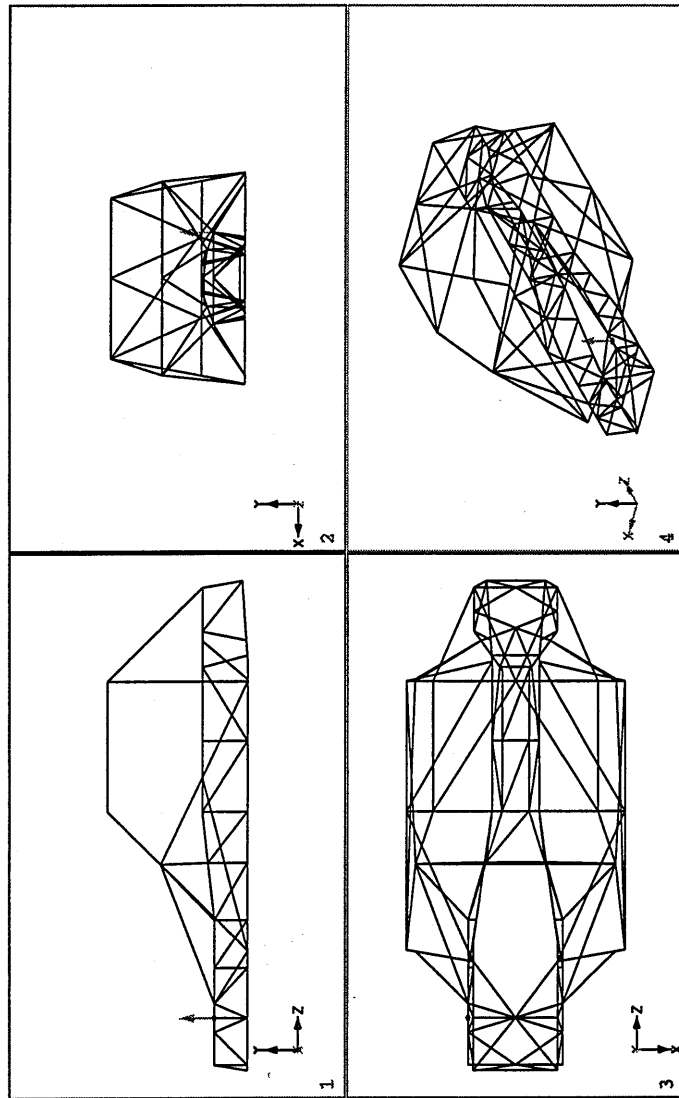


Figure 3.42: Cerbera GT Chassis Final Model

TVR Chassis Torsion Stiffness Increase

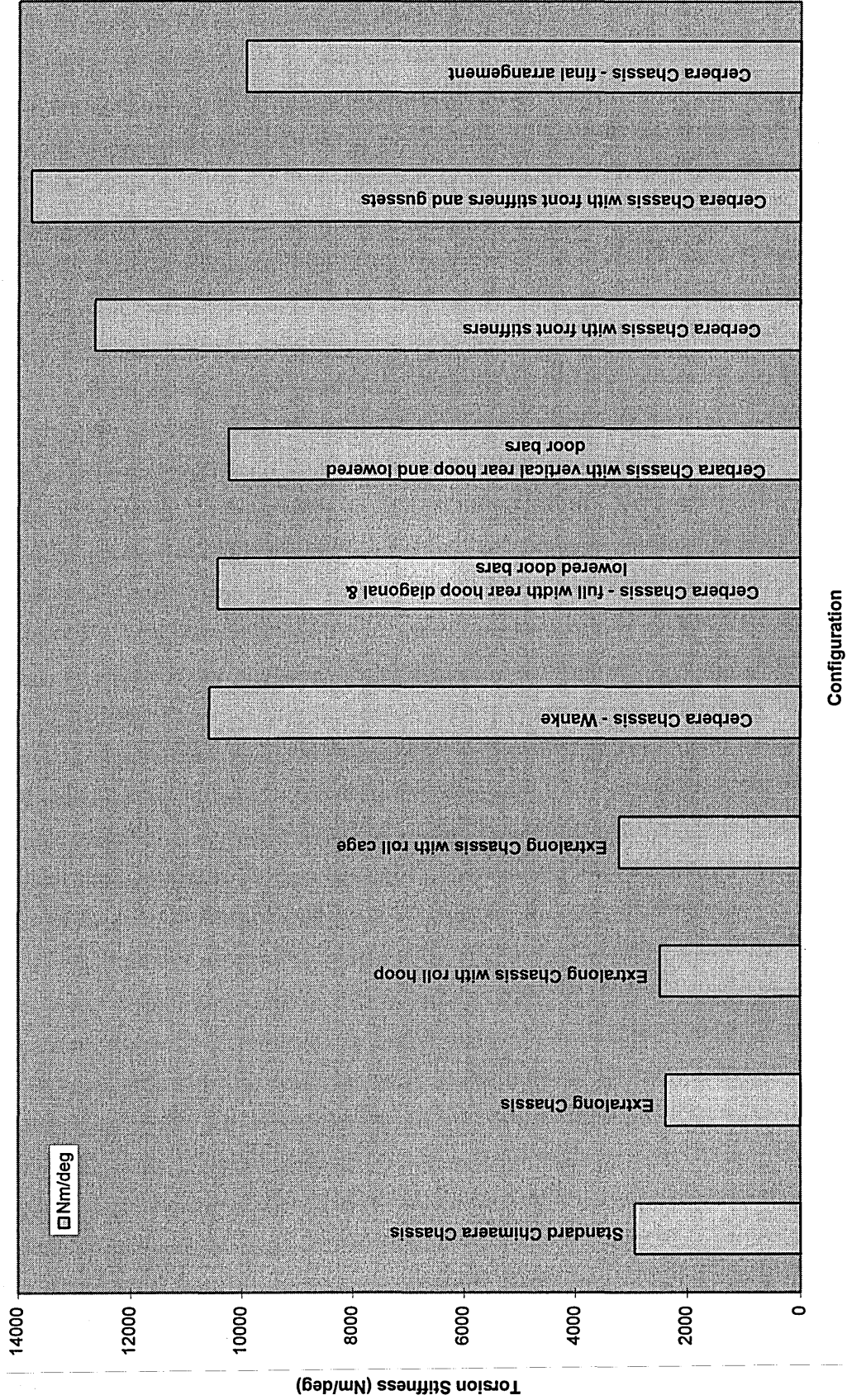


Figure 3.43: Torsion Stiffness Achieved



Of the many analyses carried out on different Chassis' the following were selected as being representative of the structural variations.

- Model consisting entirely of BEAM elements thus representing a fully nonlinear model of the chassis.
- Model consisting of both BEAM and BAR elements thus representing a partially non-linear model of the chassis.
- Model consisting of a single element between each welded joint in the structure.

The material provided for the test roll cage was ERW 1 tubing which had a yield strength of 200 MPa and this was used in all the models listed above. This enabled the analysis results to be compared directly to the test results as they used the same material properties.

For racing purposes, however, the roll cage was to be manufactured from T45 tubing which has a yield of 620 MPa, consequently models with these material properties were run as both a fully nonlinear and partially nonlinear analysis for comparison.

Using a linear model to predict the collapse load of the nonlinear structure yields, as expected, quite erroneous results. The linear model estimates ultimate loads which are much higher than those for the nonlinear models. In Table 3.17 the load and displacement for subcase 20 of the linear analysis are given. This corresponds to the point where the linear model indicated that the stress in the roll cage rear stay just exceeded 200 MPa (the yield value assumed). The linear analysis indicated that the highly stressed areas occur in the off side front windscreen stay, longitudinal roof member and backstay. This is shown graphically in Figure 3.44.

These contrast to the results using nonlinear elements. The applied load for the linear case to achieve the results of Figure 3.44 was 37,497 N. The failure load when using a fully nonlinear model as shown in Figure 3.45 was 19,162 N. The maximum deflection for these models were 16.82 mm and 24.32 mm respectively. Consequently it can be seen that the linear analysis over estimated the load carrying capacity by 96% and under estimated the deflection which would occur in the structure by 31%.

Partially nonlinear results were comparable to those for the fully nonlinear analyses. The results in Figure 3.47 compare favourably with those in Figure 3.45. The maximum deflection for the partially nonlinear analysis was 19.40 mm with an applied load of 20,155 N. The deflection was 20% lower and the load was 5.2% higher than the results for the fully nonlinear model and these were considered to be acceptable.

Both the partially nonlinear results and the fully nonlinear results with many elements compared favourably to the ultimate load and stress results for the chassis with one element between each tube joint. This single element model deflected 38.21mm when subjected to a load of 19,635 N. The load estimates with the single elements were much more comparable with the fully nonlinear model (being only 2.5% lower) and the partially nonlinear analysis (being 2.6% higher). The deflection with one element between each tube joint was higher than that estimated from both the nonlinear and partially nonlinear analyses by 57% and 97% respectively.

In all the preliminary models the gussets which were fitted to the test chassis were left out of the analysis as it was thought that they would not play a major role in the collapse mechanism as they represented a local stiffening only. To check their influence, however, a model was run with the gussets as used in the test and the results are presented in Table 3.18. In all three models with

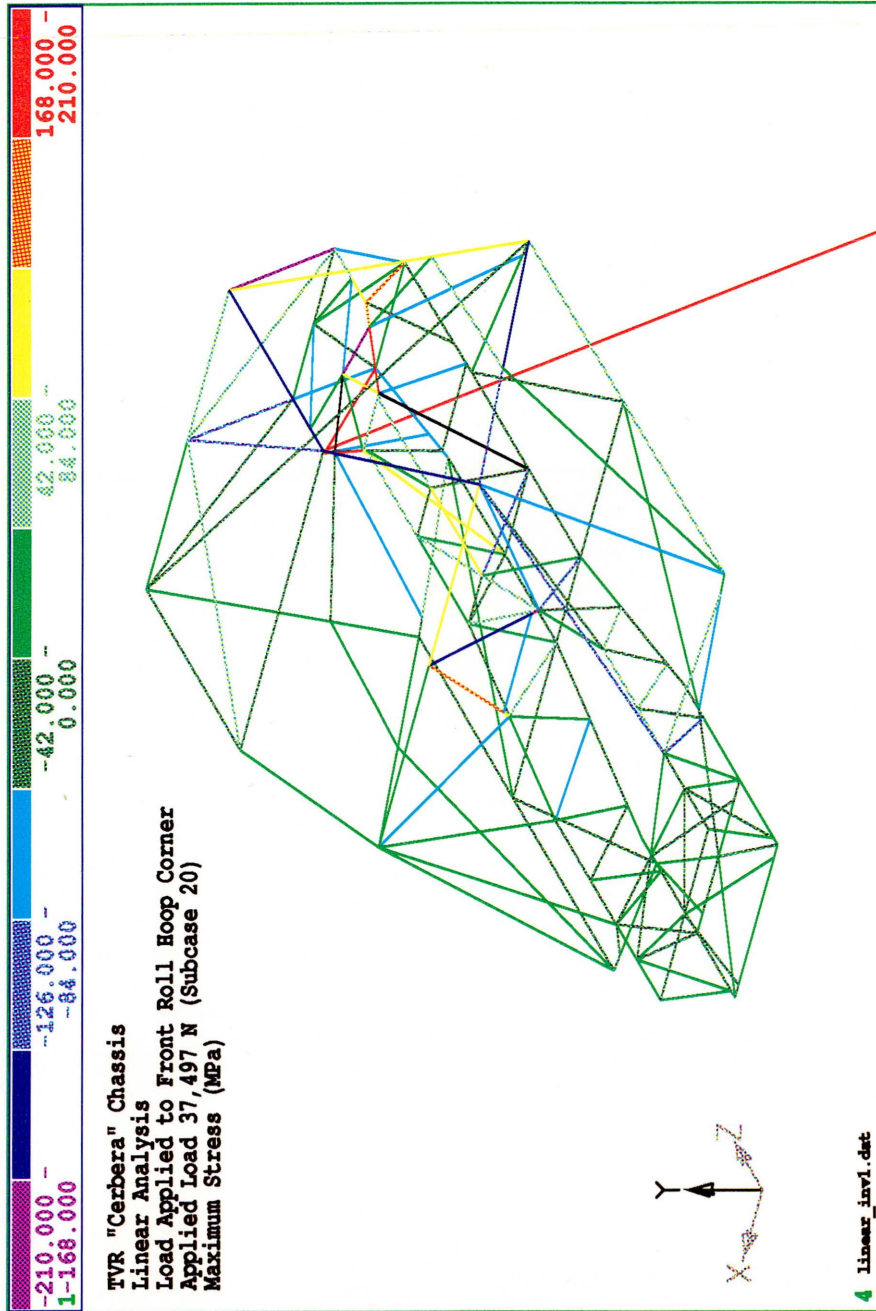


Figure 3.44: Stress Distribution in the Linear Analysis Cerbera GT Model

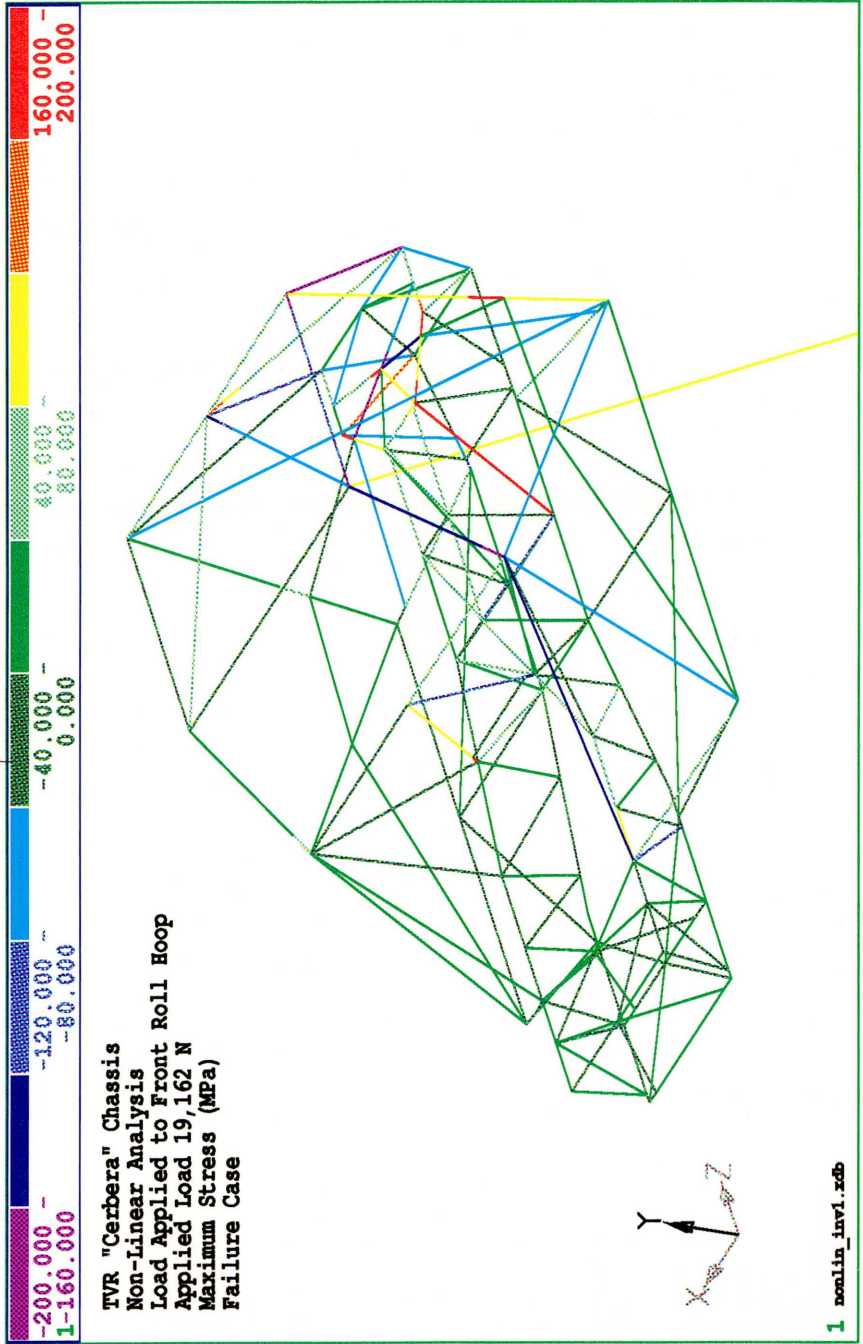


Figure 3.45: Stress Distribution in the Fully Nonlinear Cerbera GT Model at Failure

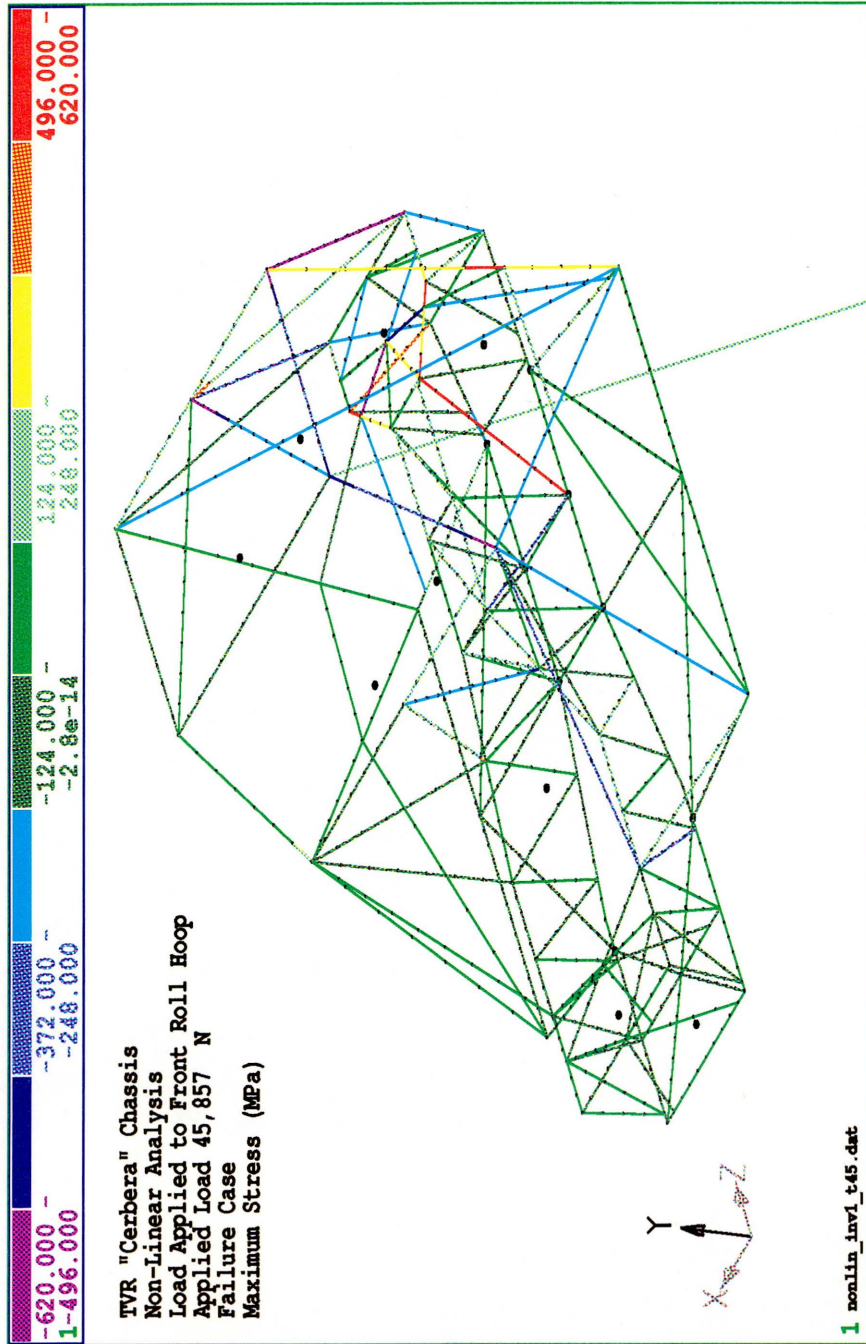


Figure 3.46: Stress Distribution in the Fully Nonlinear (T45 tubing) Analysis Cerbera GT Model at Failure



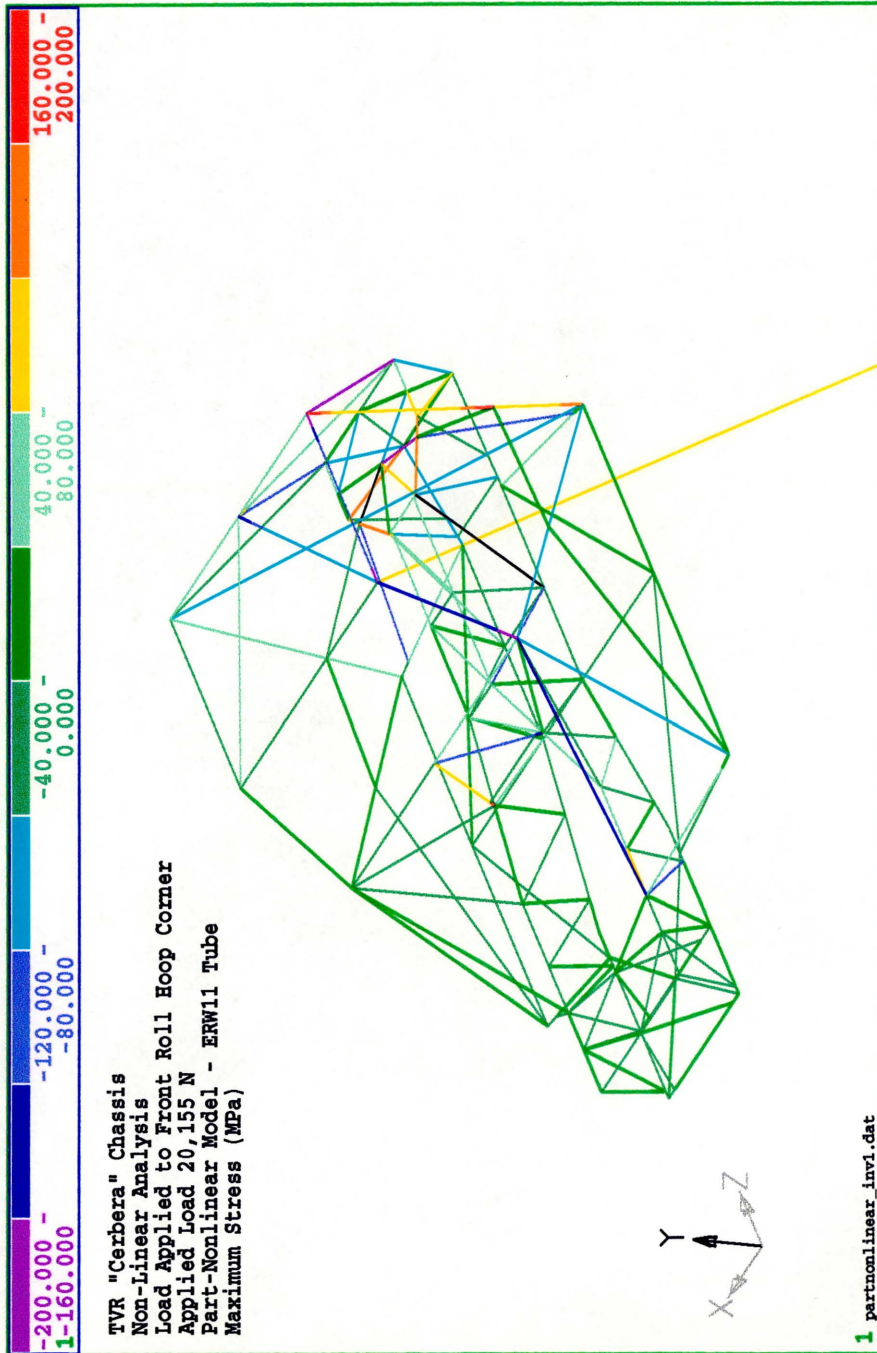


Figure 3.47: Stress Distribution in the Partially Nonlinear Analysis Cerbera GT Model

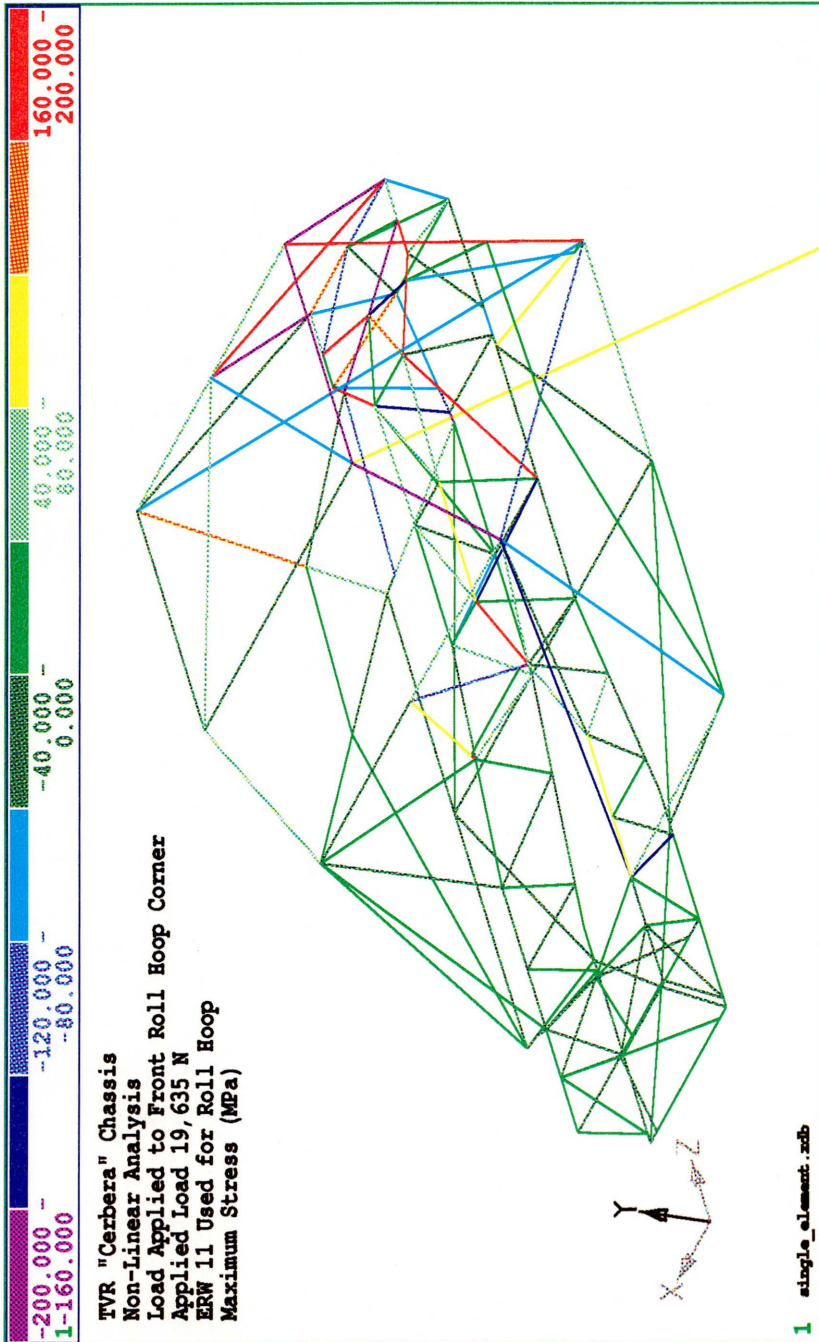


Figure 3.48: Stress Distribution in the Fully Nonlinear Analysis Cerbera GT Model with Single Elements Between Welded Joints



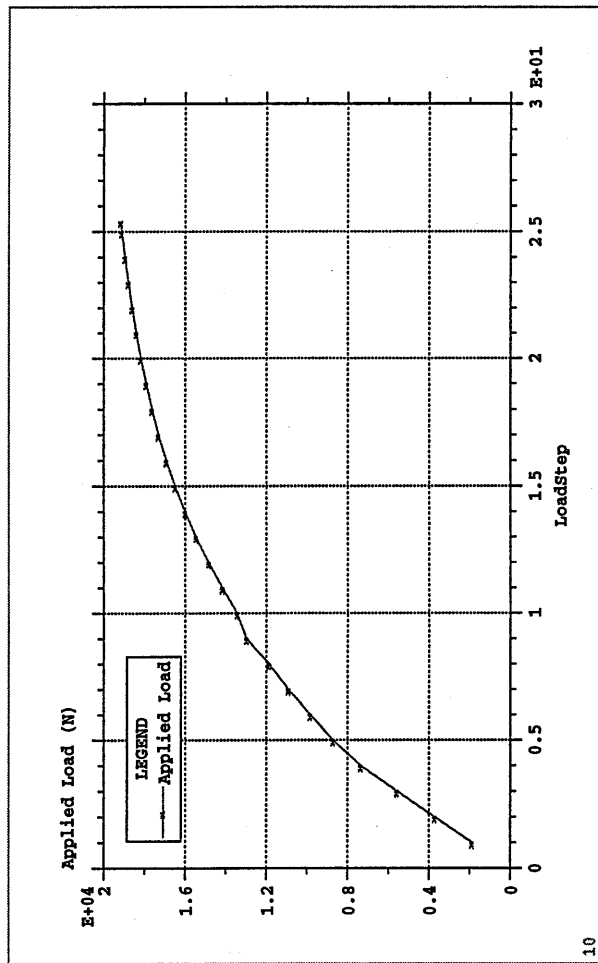


Figure 3.49: Load Displacement Curve for Fully Nonlinear Cerbera GT Model

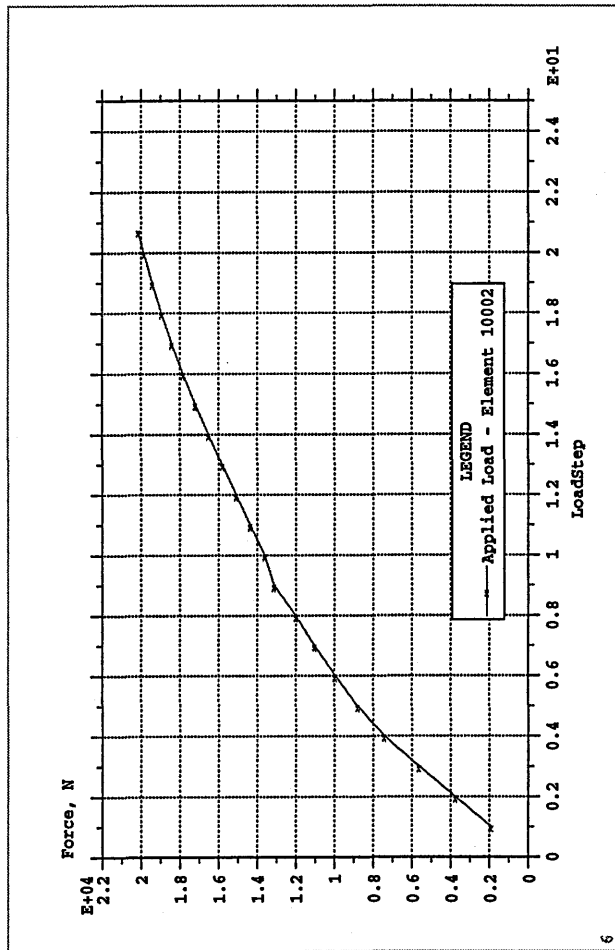


Figure 3.50: Load Displacement Curve for Partially Nonlinear Cerbera GT Model

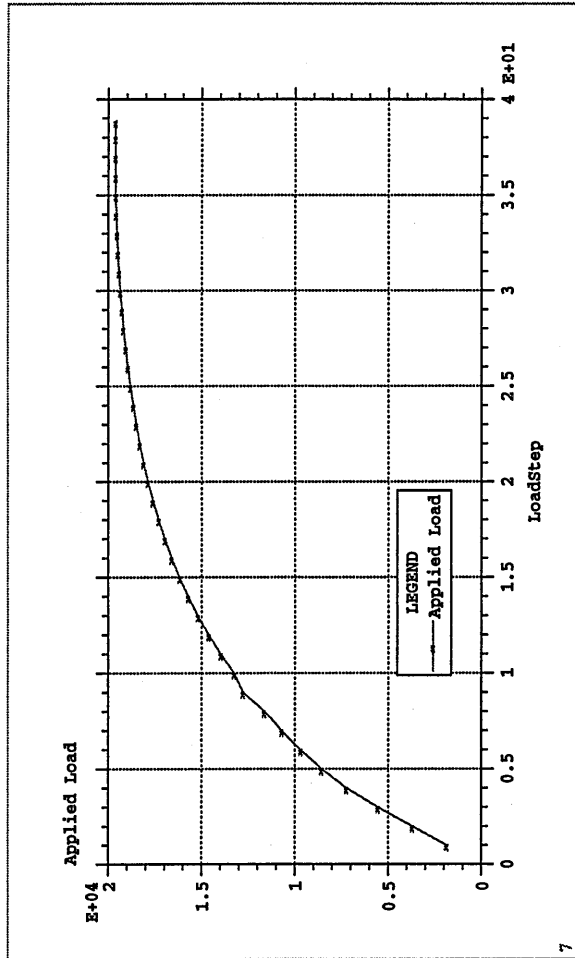


Figure 3.51: Load Displacement Curve for Fully Nonlinear Cerbera GT Model with Single Elements Between Welds

Nonlinear Results Table					
Model Arrangement	Max. Load (N)	Deflections (mm)			
		x	y	z	Total
Linear	37,497	-2.23	-13.45	9.85	16.82
Full Nonlinear	19,162	-2.79	-19.75	13.92	24.32
Full Nonlinear (T45)	45,857	-6.29	-58.70	36.84	69.59
Full Nonlinear + Strainhardening	19,369	-2.99	-21.06	14.89	25.96
Part Nonlinear	20,155	-2.36	-16.00	10.71	19.40
Part Nonlinear + Strainhardening	19,858	-2.26	-15.4	10.32	18.68
Single Elements	19,635	-4.21	-30.94	22.03	38.21
Single Elements (T45)	36,187	-7.00	-108.88	61.68	125.33

Table 3.17: Cerbera GT Nonlinear Crush Results

Nonlinear Results Table - Gusseted Models					
Model Arrangement	Max. Load (N)	Deflections (mm)			
		x	y	z	Total
Nonlinear Model - linear gussets	18,730	-2.73	-23.09	12.39	26.35
Nonlinear Model - nonlinear gussets	18,405	-2.86	-27.04	13.62	30.41
Nonlinear Model - nonlinear gussets (2 materials)	19,380	-2.64	-22.96	11.53	25.83

Table 3.18: Cerbera GT Nonlinear Crush Results

the gussets were run, one had elastic gussets added, the second was a fully plastic model and the third model used all nonlinear elements and modelled the chassis using CDS3 material properties and the roll cage as having ERW 1 properties. The results of these three analyses are contained in Table 3.18.

Using nonlinear gussets and the two materials in the structure resulted in a maximum load which was only 1.1% higher than that for the fully nonlinear model without gussets. The maximum deflection was approximately 1% higher than the model without gussets.

By running a number of different load cases it was possible to determine the least stiff load point. This was found to be the front near-side windscreen corner and the majority of the analysis concentrated on loading at this point.

To compare the range of load carrying capacity the stiffest load point (off-side rear hoop upper corner) was analysed also. This model was illustrative of the differences in load carrying capacity between the stiffest and most flexible. As was done above the model was run with material

Nonlinear Results Table - Different Load Cases					
Model Arrangement	Max. Load (N)	Deflections (mm)			
		x	y	z	Total
Part Nonlinear Model Rear Hoop	33,658	-0.96	-1.34	0.76	3.29
Part Nonlinear Model Rear Hoop (T45)	103,720	-2.97	-4.20	2.46	5.70

Table 3.19: Cerbera GT Nonlinear Results - Load applied to rear hoop

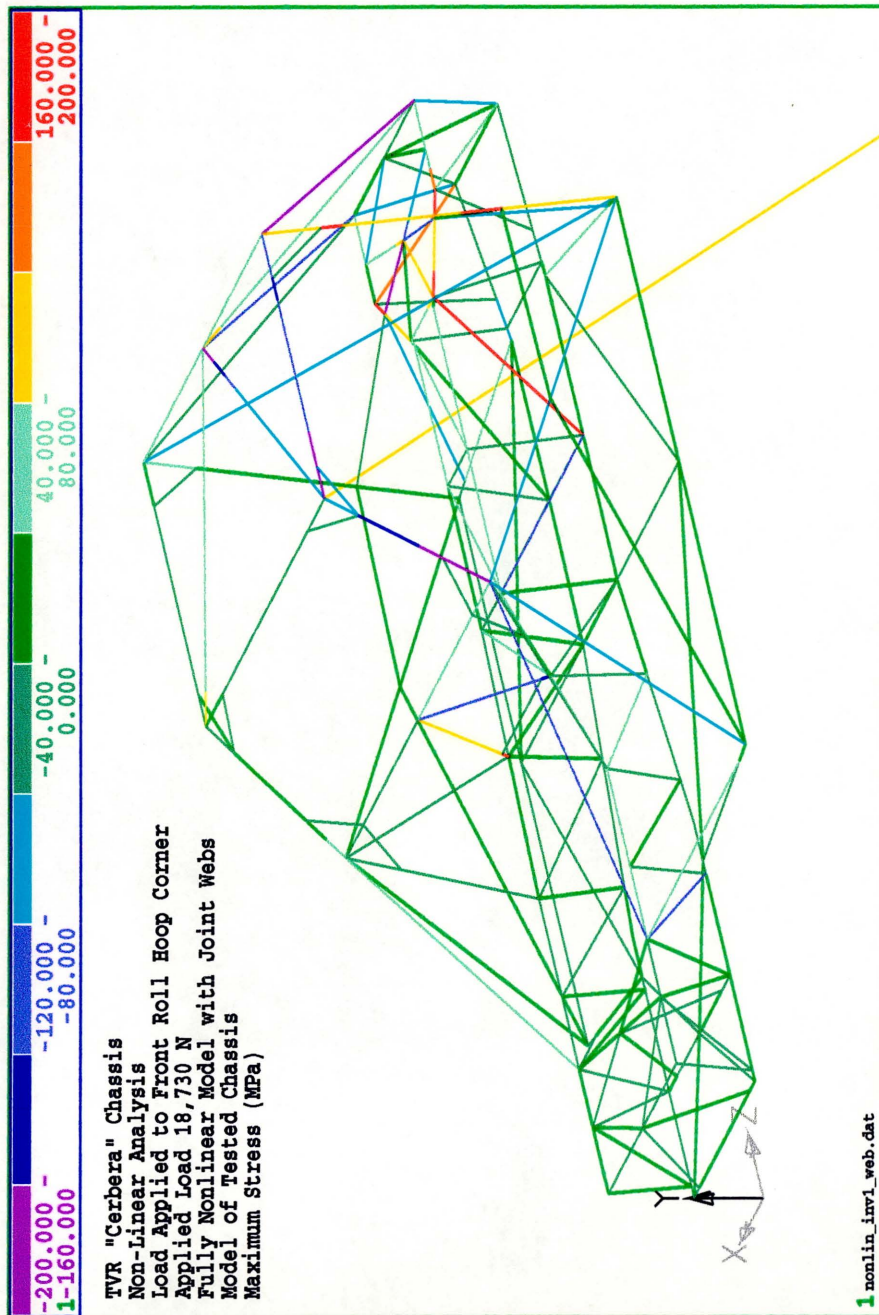


Figure 3.52: Stress Distribution in the Fully Nonlinear Analysis Cerbera GT Model with the Webs Included (Elastic Webs)

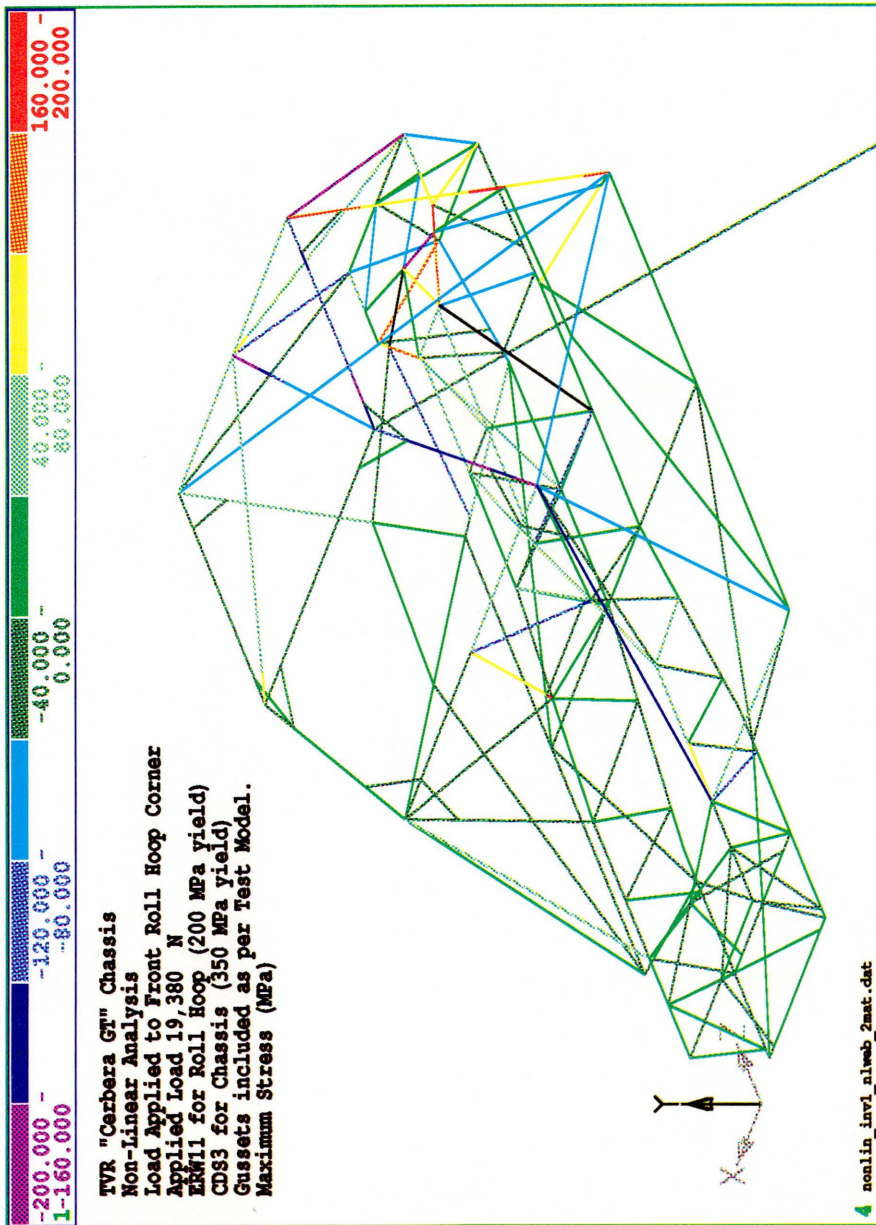


Figure 3.53: Stress Distribution in the Fully Nonlinear Analysis Cerbera GT Model with the Webs Included - Both Materials Modelled



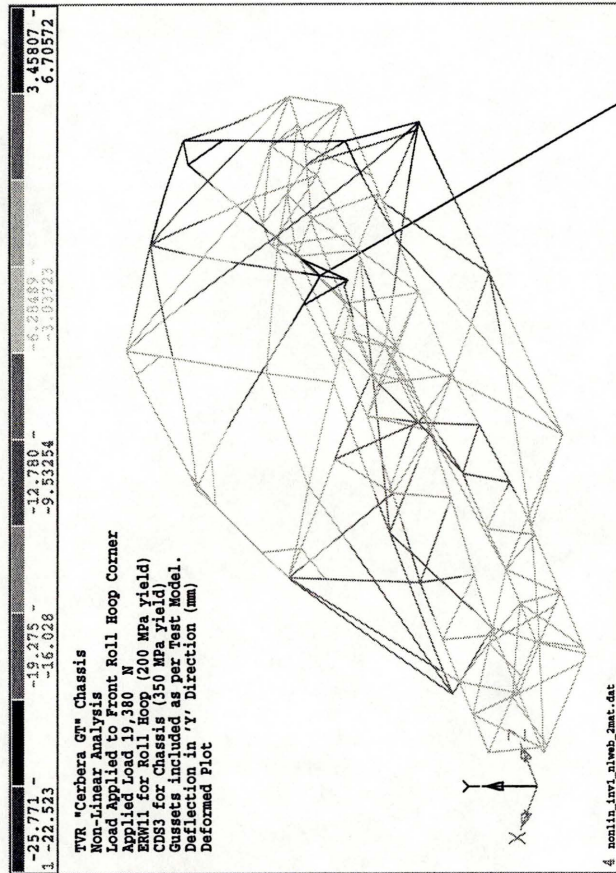


Figure 3.54: Deflected Shape (Isometric View) of the Fully Nonlinear Analysis Cerbera GT Model with the Webs Included - Both Materials Modelled

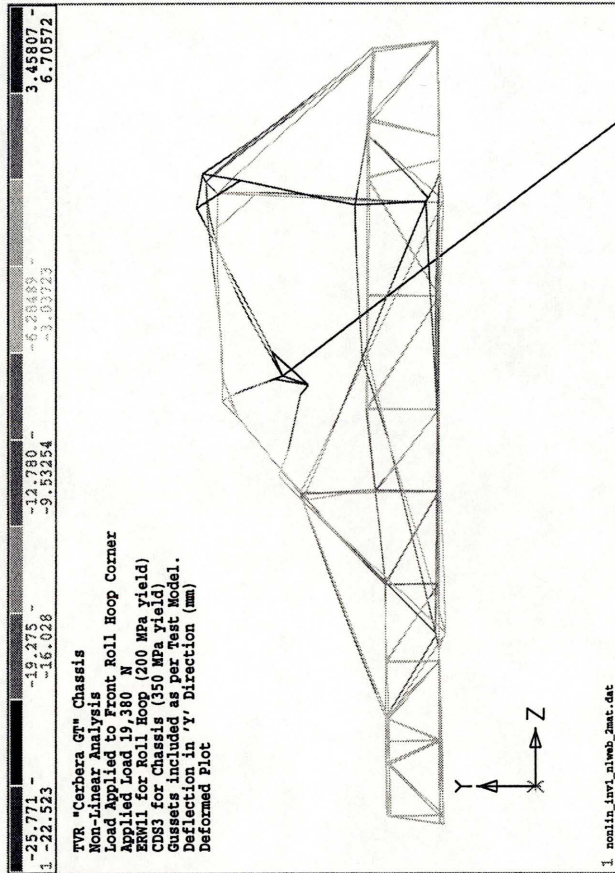


Figure 3.55: Deflected Shape (Side View) of the Fully Nonlinear Analysis Cerbera GT Model with the Webs Included - Both Materials Modelled

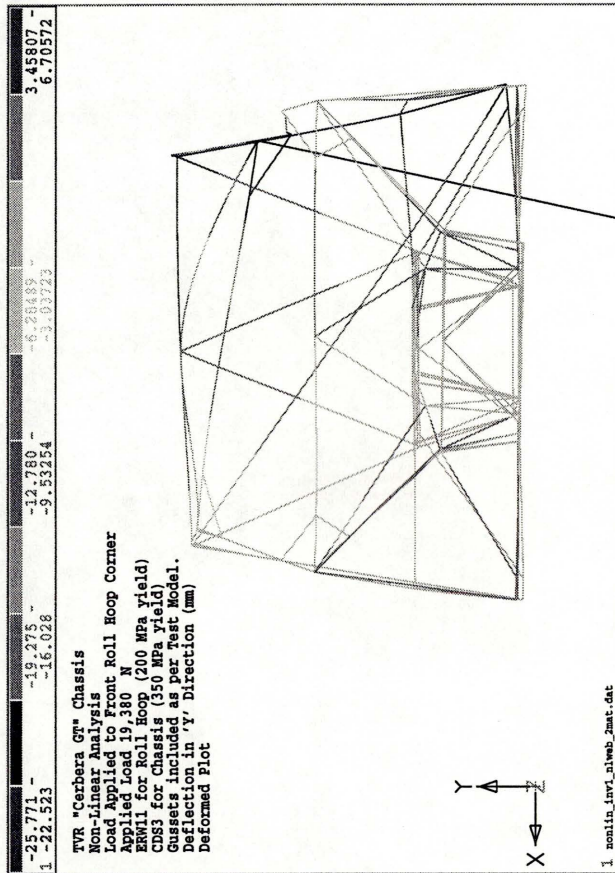


Figure 3.56: Deflected Shape (Front View) of the Fully Nonlinear Analysis Cerbera GT Model with the Webs Included - Both Materials Modelled



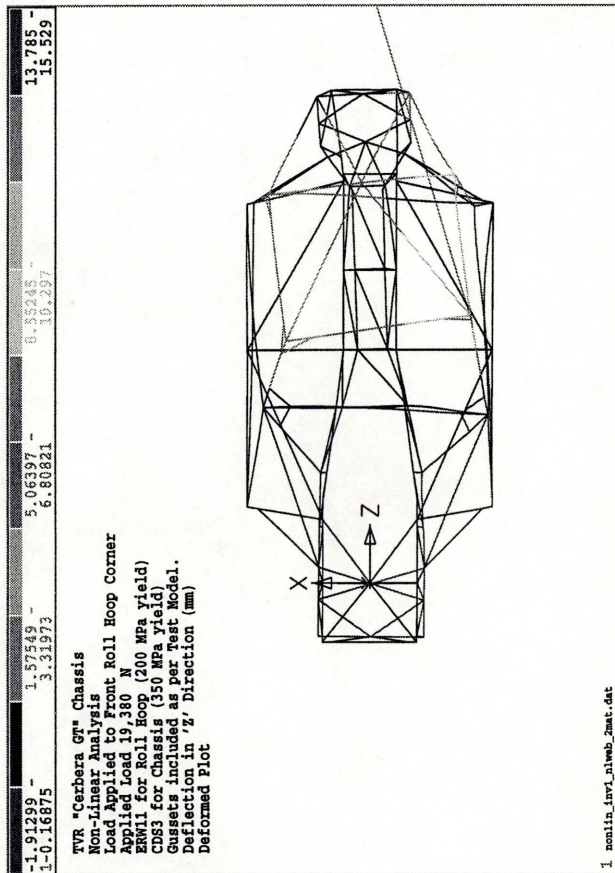


Figure 3.57: Deflected Shape (Plan View) of the Fully Nonlinear Analysis Cerbera GT Model with the Webs Included - Both Materials Modelled

properties for ERW 1 and for T45 Tubing and the results are tabulated in Table 3.19.

Application of the load to the front windscreen corner and the rear hoop corner yielded significantly different results. Applying the load to the rear hoop enabled the structure to carry a load 76 % higher than if it had been applied to the front windscreen corner. In addition the deflection with the load at the rear was reduced by 86 % from that with the load at the front windscreen corner.

This highlights the sensitivity of the overall load carrying capacity of the structure to the load application point.

### 3.10 Hoop Vertical Loading

It was discovered that when tests are carried out in industry to verify a roll cage the normal practice is to apply the vertical load on the rear hoop. This vertical load is that which is specified by the RACMSA of  $7.5W^4$  which equates to 86,452 N for the TVR Chassis.

The application of this load on the rear hoop was proposed as part of the test. Initially linear models were run with this load applied incrementally to the hoop as two point loads. This was then verified by running a fully nonlinear model to see when yield and failure occurred. Results for both of these analyses are contained in Table 3.20.

The linear analysis predicted that the rear hoop would take the required load without yield occurring in the rear hoop or associated members. This again highlights the danger of using linear analysis when nonlinear behaviour is expected in the structure. Two sets of data are given for the linear analysis in Table 3.20, one is when one of the outrigger support members reaches a stress of 200 MPa and the other is the complete load application of 86,452 N. Plots of the local stresses in the elements are shown in Figures 3.58 and 3.59 for applied loads of 60,156 N and 86,452 N respectively.

Figure 3.62 is a fully nonlinear model with an applied load of 59,760 N. This load corresponds to the failure case for the structure. It can be seen that a number of members have reached their yield point of 200 MPa. The stress distribution shown by the nonlinear model contrasts to the results from the linear analysis as shown in Figure 3.58.

The linear analysis gave some insight into the stress distribution for the nonlinear model. It can be seen from this comparison that the differences between the two analysis methods are quite significant. If the appearance of the first stress above the yield limit was taken as the failure criterion for the linear analysis then the linear and nonlinear results for the load capacity are reasonable (i.e. the maximum load was within 1.4 %) - but the stress distribution was quite different. It should also be noted that the deflections were vastly different (i.e. the linear analysis gave deflections 68 % lower than those for the nonlinear analysis) between the two models. To take the linear results at any stage past this point are erroneous and misleading.

---

<sup>4</sup>See Chapter A

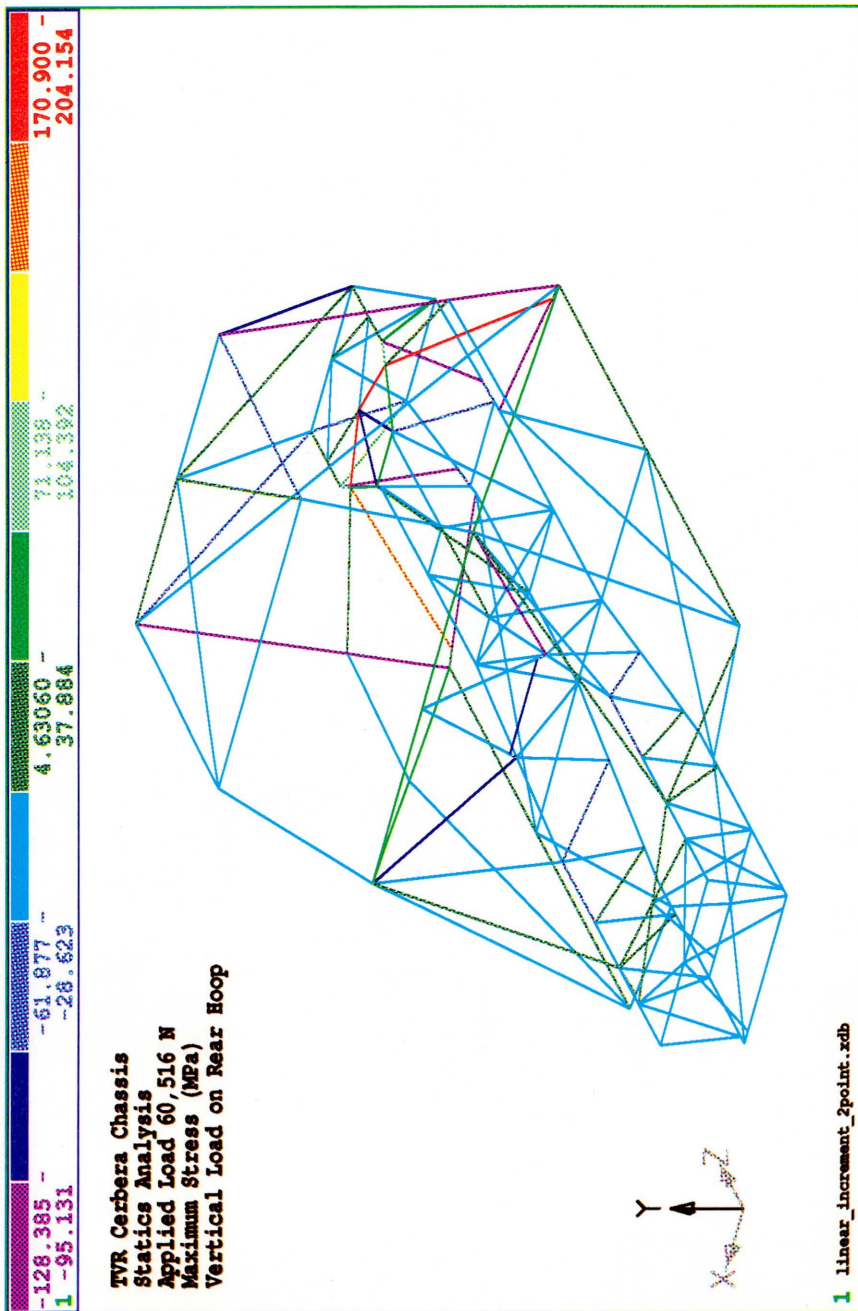


Figure 3.58: Stress Distribution for Vertical Load on Rear Roll Hoop - Linear Cerbera GT Model, Applied Load 60,516N



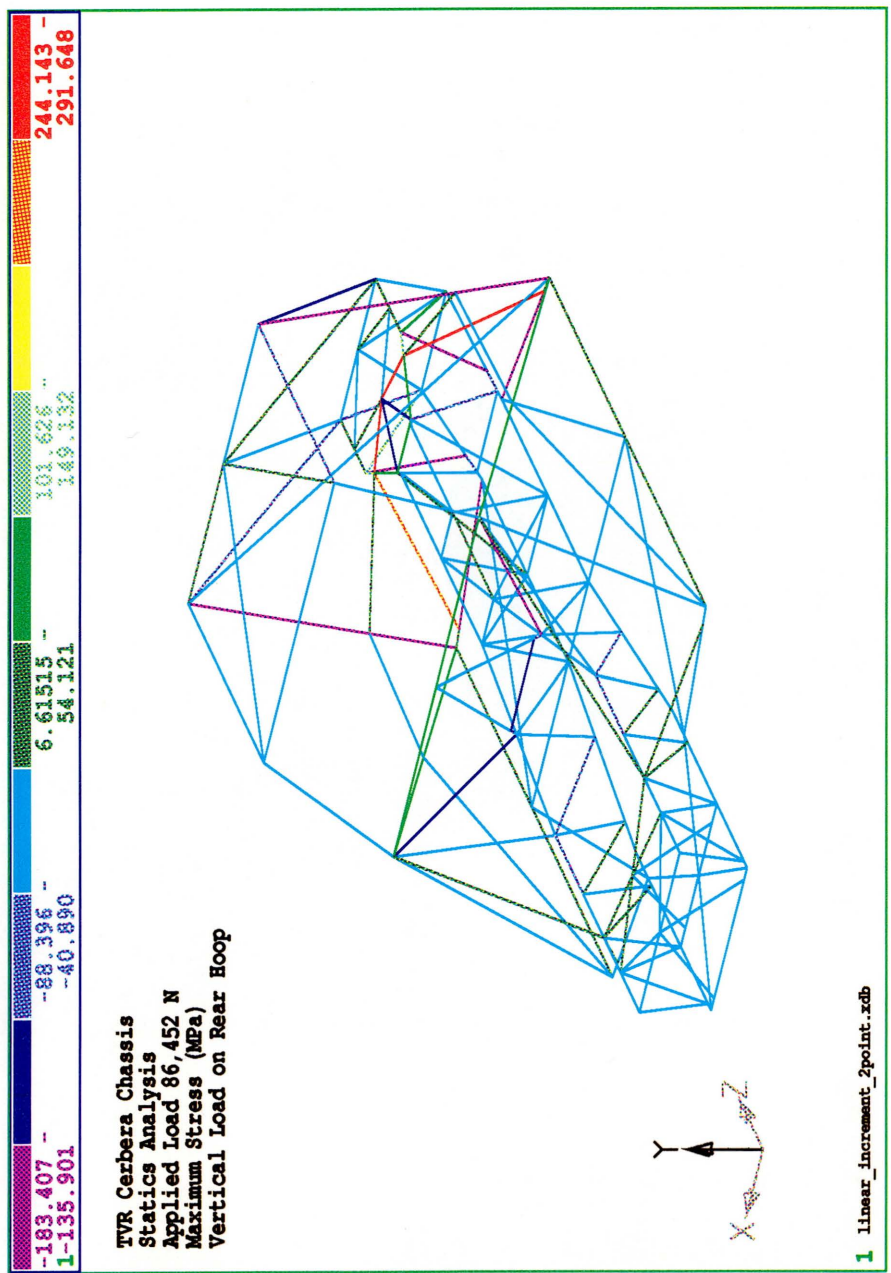


Figure 3.59: Stress Distribution for Vertical Load on Rear Roll Hoop - Linear Cerbera GT Model, Applied Load 86,452N

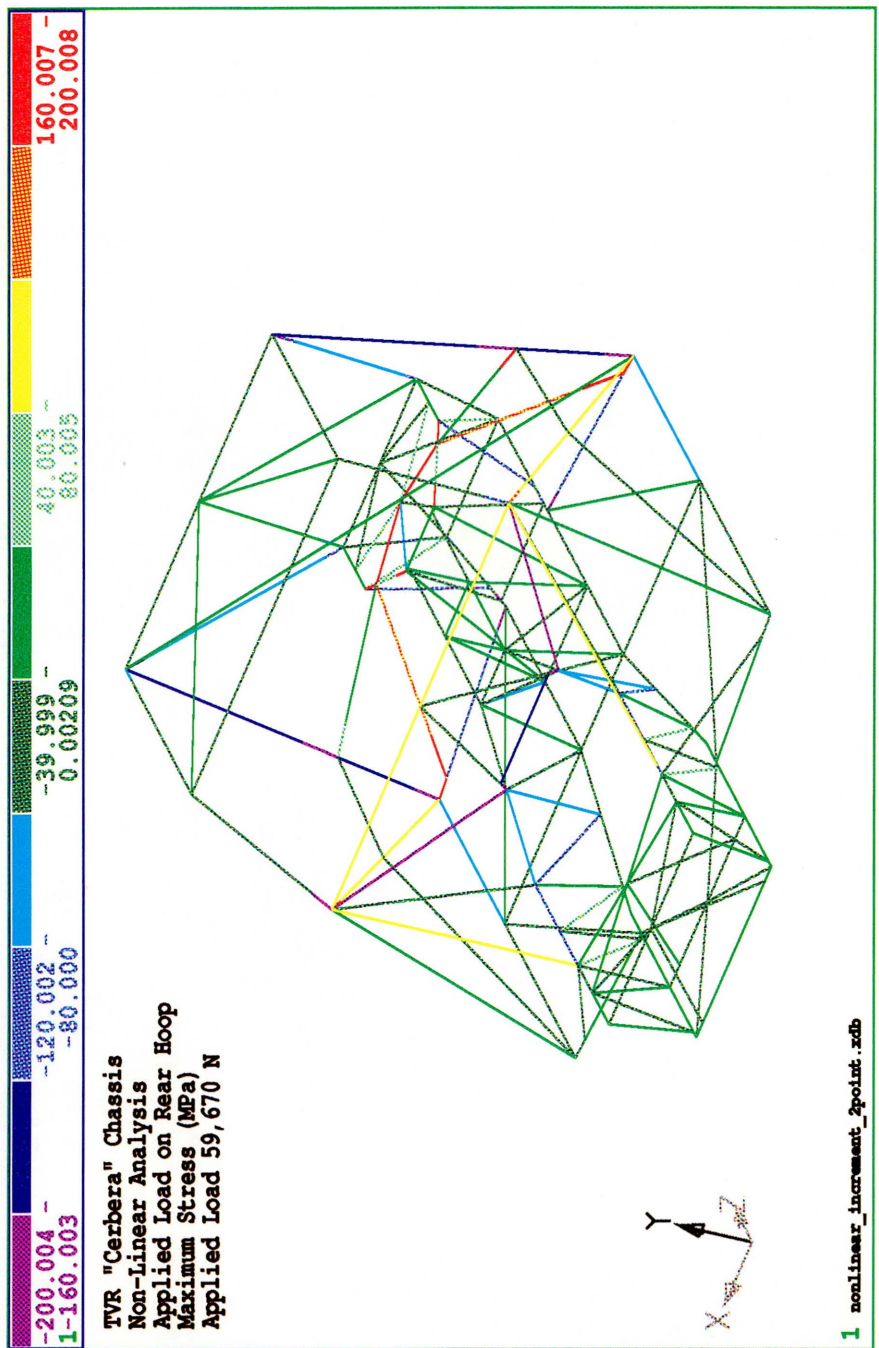


Figure 3.60: Stress Distribution for Vertical Load on Rear Roll Hoop - Nonlinear Cerbera GT Model, Applied Load 59,670N

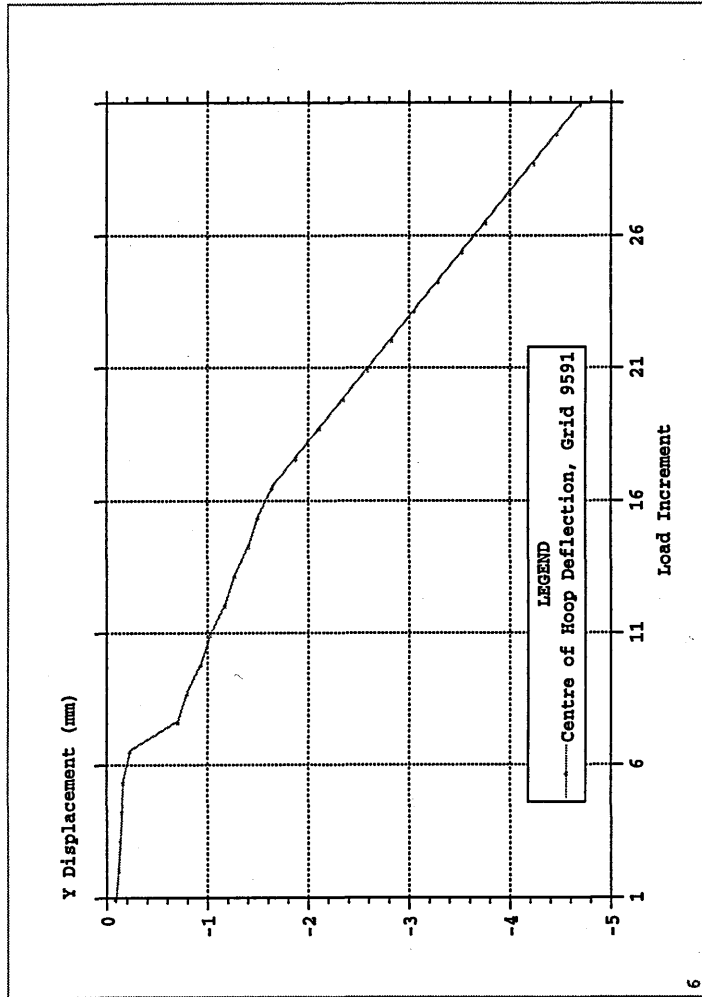


Figure 3.61: Vertical Displacement in the Centre of the Rear Roll Hoop - Linear Cerbera GT Model, Applied Load 86,452 N

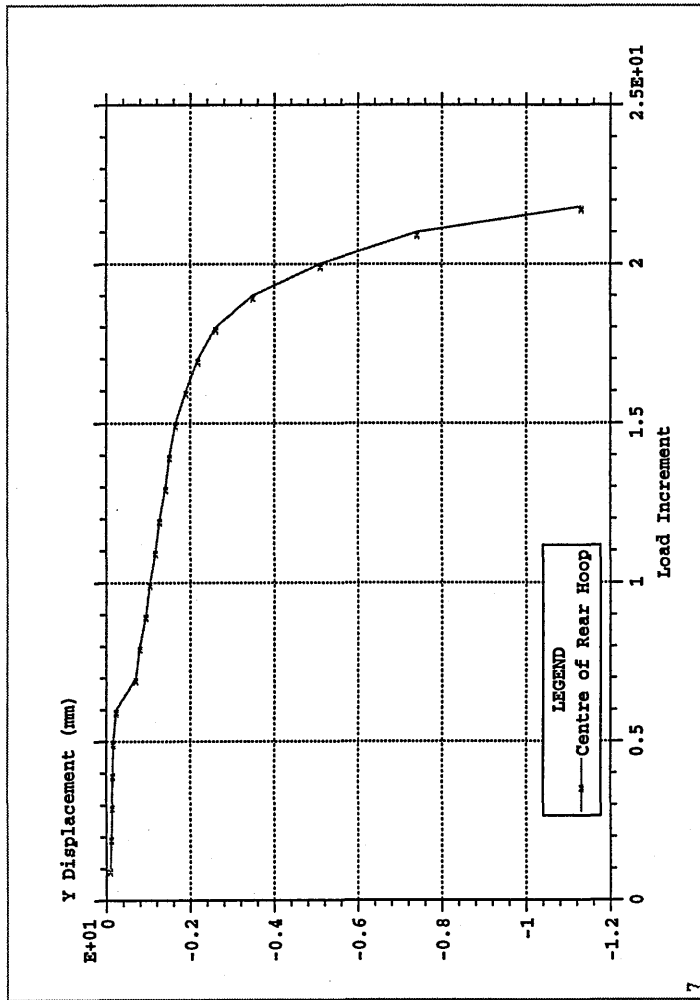


Figure 3.62: Vertical Displacement in the Centre of the Rear Roll Hoop - Nonlinear Cerbera GT Model, Applied Load 59,670 N

Rear Hoop Vertical Loading					
Model Arrangement	Max. Load (N)	Deflections (mm)			Total
		x	y	z	
Linear Elastic 1	60,516	0.32	-4.04	-2.74	4.89
Deflection Grid 9577		0.34	-3.78	-2.24	4.38
Centre Grid 9591		0.32	-3.29	-2.33	4.04
Linear Elastic 2	86,452	0.46	-5.77	-3.92	6.99
Deflection Grid 9577		0.48	-5.40	-3.20	6.30
Centre Grid 9591		0.45	-4.70	-3.33	5.78
Nonlinear Plastic	59,670	0.13	-12.21	-9.41	15.42
Deflection Grid 9577		0.10	-12.04	-8.90	14.97
Centre Grid 9591		0.12	-11.31	-8.94	14.42

Table 3.20: Cerbera GT Nonlinear Rear Hoop Loading Results

## Chapter 4

# Model Setup in NASTRAN

### 4.1 Introduction

All TVR cars have the body shell manufactured from glass-fibre reinforced plastic (GRP). The vehicle styling and modelling was carried out by hand and the production moulds were taken directly from the resulting prototype. Consequently there were no drawings of the bodywork and the testing and modelling carried out was confined to the tubular space frame chassis.

NASTRAN (NAsa STRuctural ANalysis) was developed in the 1960's by NASA to carry out structural analysis using the finite element method. The code used for the TVR analysis was that of MSC/NASTRAN the propriety version of NASTRAN, marketed by MacNeal Schwendler Corporation (MSC). The majority of the pre and post processing was carried out using MSC-XL.

The finite element (F.E.) method of analysis requires a mathematical model of the structure to be formed by subdividing the real-world structure into a finite number of small parts or regions called elements. Each element is connected to its surrounding neighbours by a finite number of grid points. The only interaction between elements is through the forces that they exert on these grid points.

The design and analysis of the structure was carried out in a number of steps gradually increasing in complexity. The initial analyses were carried out using linear elastic analysis on the TVR Griffith chassis. Gradually a full roll cage was developed and integrated with the chassis. The final stage was an analysis of the structure which included material nonlinearity and looked at the roll cage crush.

The data was input into the pre-processor XL and this graphical interface allowed the geometric data to be entered and viewed. It additionally provided an easy and user friendly method of meshing the Finite Element Model. The data required for the linear modelling of the chassis was:

- Definition of the chassis in three dimensions using points and curves,
- Generation of grid points and the orientation of the coordinate systems which were used to record components of displacement and forces at the grid points,
- Identification of the grid points connecting the elements resulting in the mathematical model of the structure,



- Definition of the element properties including the cross sectional area and the inertial properties of the sections,
- Definition of the material properties including the density, Young's and Bulk moduli and Poisson's ratio,
- Definition of the restraints for the structure - these had to model the testing phase and provide restraint of all rigid body modes,
- Definition of the loads on the structure,
- Definition of the solution methods to be used.

As the analysis was to be carried out for the entire structure it was considered sufficiently accurate to use Bar and Beam elements to model it. In addition the plate was modelled using thin isoparametric<sup>1</sup> shell elements (QUAD4) in all cases where it was used<sup>2</sup>. All elements assumed that the joints were stiff and that there were no local instabilities in the tubes or plates. It was considered overkill to model the structure using full three dimensional elements. This would have been an inefficient use of computer time and the solution time for the nonlinear analyses would have been increased many times.

Prior to the analysis the required output data was requested from that which was available. NASTRAN produces the following data from which this was selected:

- components of displacement at grid points,
- components of stress within elements and related information (i.e. strain, strain energy, internal forces and moments),
- components of force and moment at the grid points due to the various sources (i.e. applied loads, constraints and finite elements).

The output data was requested using the relevant Case Control Cards.

The NASTRAN suite of programs was used for nearly all the analyses (with the exception of a verification model based on CRASHD and some investigative work with DYTRAN in the final stages of the modelling). Postprocessing was carried out using XL which enabled the deformations and stresses to be looked at in graphical form. This was used in conjunction with the detailed data in the output files.

#### 4.1.1 Elements Used for the Analysis

For linear elastic analyses the BAR element was used. The BAR element is derived from classical beam theory (plane cross-sections remain plane under deformation). It provides exact results for end loads of any kind. The BAR element is a one-dimensional bending and axial force element.

---

<sup>1</sup>Isoparametric elements use the same shape function to interpolate both the displacement and the geometry. This has the advantage that the displacement field is invariant to the orientation of the cartesian co-ordinate system in x and y.

<sup>2</sup>The plate was neglected in all the non-linear analyses as it was found to slow the analysis process down significantly and the plate was found to be not too important in these analyses - based on early models run

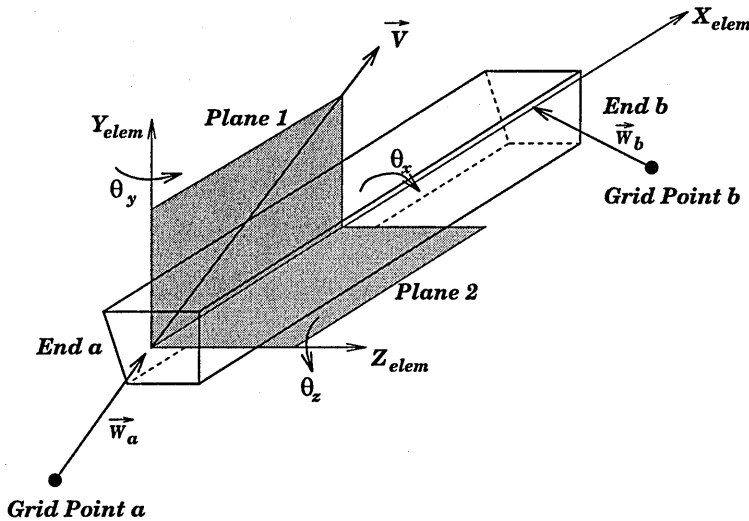


Figure 4.1: NASTRAN BAR Element

In addition the shear centre and neutral axis coincide and the torsional stiffening effect of the out of plane cross-sectional warping is neglected. The average axial force, torque about the bar axis, shear force in the two reference planes and bending moments and displacements at both ends can be determined. The element and its arrangement are shown in Figure 4.1.

The available output from the BAR element were the forces and moments shown in Figure 4.2 and the axial stresses  $\sigma_x$  at a maximum of four cross sectional points at end A and the same four points at end B. These points are defined by the user.

Non linear analysis is not supported for the BAR element and as a consequence the BEAM element was used for the non-linear analyses. The BEAM element includes extensional and torsional stiffness, bending stiffness and transverse shear flexibility in two perpendicular planes.

The BEAM element contains all the capabilities of the BAR element and, in addition, a number of optional capabilities are also present, none of which were required for this investigation. It is up to the user to determine which of these additional capabilities is required and to activate them. The output that was requested from the BEAM elements for these analyses included,

- bending moments in the two reference planes at the neutral axis,
- axial force at the neutral axis,
- real longitudinal stress at four user defined points for each cross section defined along the length of the the beam,
- maximum and minimum longitudinal stresses.

Non linear element formulation is also different for the BEAM element. The element is assumed to have a plastic zone which is one third of its length at each end. The collapse of the bar is idealised as a series of 8 rod elements which occupy this third of the beam. These rods are located according to an elliptical model which is discussed in Appendix E and this gives an approximation to the theoretical collapse of the beam.

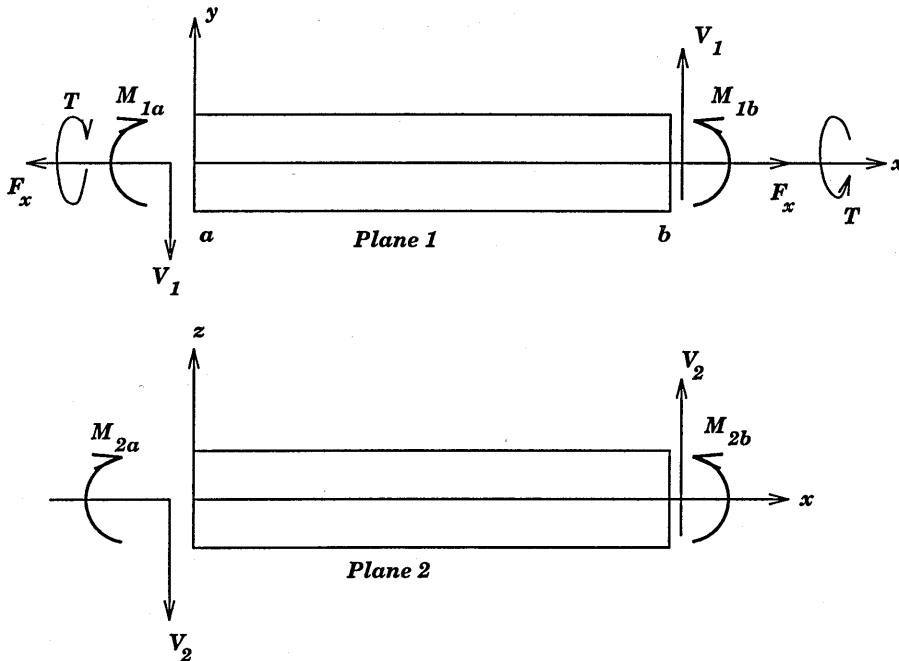


Figure 4.2: NASTRAN BAR Element Forces and Moments

### 4.1.2 Co-ordinate System Definition

Co-ordinate systems are required to define the locations of the grid points in space and to orient the displacement vector in space. NASTRAN has one implicitly defined co-ordinate system called the *Basic Co-ordinate System*. It is a rectangular cartesian system and this system is frequently sufficient to define the entire model. If it is not sufficient it is possible to define many other co-ordinate systems *Local Co-ordinate Systems* that may ease the definition of the model. They can be defined as rectangular, cylindrical or spherical co-ordinate systems. It should be noted that all of the co-ordinate systems must be able to be transformed back to the *Basic Co-ordinate System*. Consequently when defining a new co-ordinate system it must reference the basic system.

Co-ordinate systems are also required to orient the components of stresses, forces and moments within the elements and also to orient the section properties of line elements. Each element has its own implicitly or explicitly defined *Element Co-ordinate System* which is defined with reference to the grid point connectivity of the element.

The union of all the local directions for the components of motion at the grid points is called the *Global Co-ordinate System*. This is a useful concept which is employed when specifying the directions that the components of motion will have when printed or plotted as output.

## 4.2 Development of Model in NASTRAN

The location and length of each bar was defined by two nodes - one at either end. These nodes were defined in the global co-ordinate system within the finite element program. In the initial modelling carried out on the TVR Griffith and Chimaera chassis the origin was taken at the front centre of the chassis. This was to ease the determination of the point and element location as it required

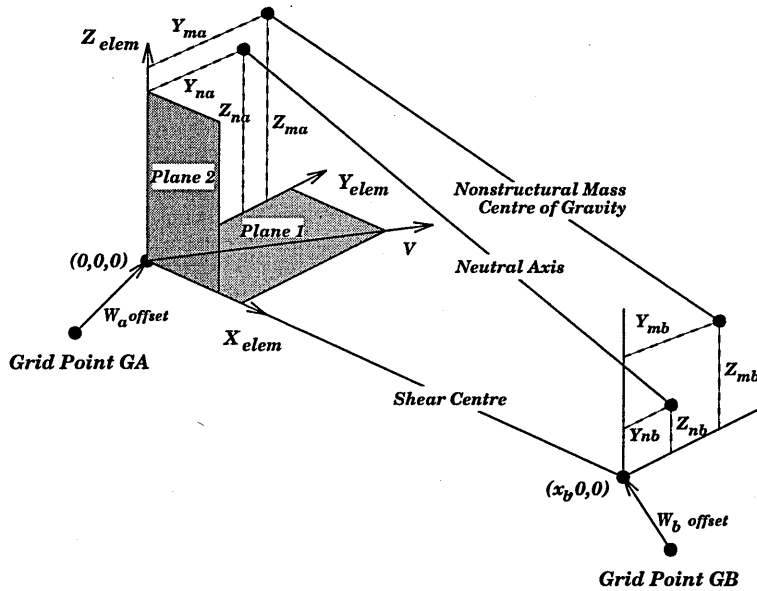


Figure 4.3: NASTRAN BEAM Element

only positive values to be used. The standard right hand cartesian co-ordinate system was taken and this had the longitudinal axis of the vehicle as the x-direction, the lateral direction was taken as the y-direction and vertical was taken as the z-direction. The centre line of the chassis was taken as y=0 and as a consequence the left and right halves of the chassis were easily identified when checking the data by their differing sign. It should be noted that the drawings provided by TVR take the front axle as the zero point and thus the data used had to be taken from these and converted to the authors system.

In later work the final model of Wanke [4] was used and developed further. The co-ordinate system used by Wanke was different and took the zero point as that defined in the TVR drawings. In addition the x-axis was taken directed at the front right hand wheel and the positive z-direction was to the aft of the car. Using a right hand set of axes resulted in the vertical direction being the y-axis. The reader should bear this in mind to avoid confusion with the data contained in the various figures and tables in this report.

Nearly all of the chassis members were circular tubes with the exception of the lower chassis rail members (rectangular) and one cross member consisting of an open 'C' section.

When defining elements it was important to align or orient the element local co-ordinate systems. This was achieved by aligning the two reference planes, Plane 1 and Plane 2 using the vector  $\vec{v}$ . This vector was defined using an orientation point in plane 1. This was most important for the non-circular sections where the incorrect definition of the second moments of area would result in large errors in the results. The orientation of the elemental co-ordinate system and reference planes are illustrated in Figure 4.1 and 4.3.

A number of simplifying assumptions were made in the modelling process and these were aimed at speeding up the analysis and providing an efficient solution to the model analysed. These included:

- all welded joints were modelled as rigid in all degrees of freedom,
- multiple joints (of which there are many) all intersected at the neutral axis,

- small offsets were ignored between bars of differing sections,
- initially the bend radii were modelled in a crude way (in the roll cage rear hoops) these were neglected in subsequent models,
- material specifications were assumed to be as published i.e. no material property modification due to the welding and fabrication and for plastic analysis minimum published strength values were used.

It was expected that these assumptions would result in a stiffer model than was realised in the tests. This was found to be true in all cases where tests were carried out for the torsion stiffness - the reader is referred to references [5] and [4], a summary of which can be found in Tables 3.1 and 3.2. More detailed analysis of the joints is contained in reference [4] but the additional complications of these were not considered to be of any real advantage in the models analysed.

#### 4.2.1 Modelling of the Restraints for the Torsion Tests

In restraining the model for calculation of the torsional stiffness it was important to use the same loaded length as had been used for the previous tests. This was to ensure that the results were directly comparable between the different analyses. The loading points used in Ref.[5] were the suspension mounting points and these were used for all torsion calculations carried out by the author.

It was necessary to restrain the chassis to only remove the rigid body modes of motion. If this was not done then an 'overstiff' structure would result. In essence a restraint system was required that was statically determinant. This meant that the number of restraints had to be the same as the number of equations for equilibrium. In three dimensions there are six unknown degrees of freedom and thus six equations of motion (three translations and three rotations). The system of restraints is shown in Figure 4.4 and it can be seen that restraint 123 restrains the three translations in the x, y and z directions, restraint 23 restrains the rotations about z and y-axes respectively, restraint 2 then provides the final rotational restraint about the x-axis. The remaining suspension mount at the front of the chassis is available to apply the load. This load and the resulting torsion was then used in conjunction with the calculated deflection to give the torsion stiffness.

#### 4.2.2 Weight of Models

To determine the weight of the various chassis models a 1g gravity load was applied. The material densities were specified in the material input (MAT1) data and the gravity load was specified using the GRAV input card which is used to define the acceleration vector and its magnitude.

NASTRAN distributes the element mass along the element neutral axis. The resulting forces at the model restraints (SPC) were retrieved from the analysis results and summed to give the chassis mass. The weight of each model analysed can be found in the relevant tabulated data for that model.

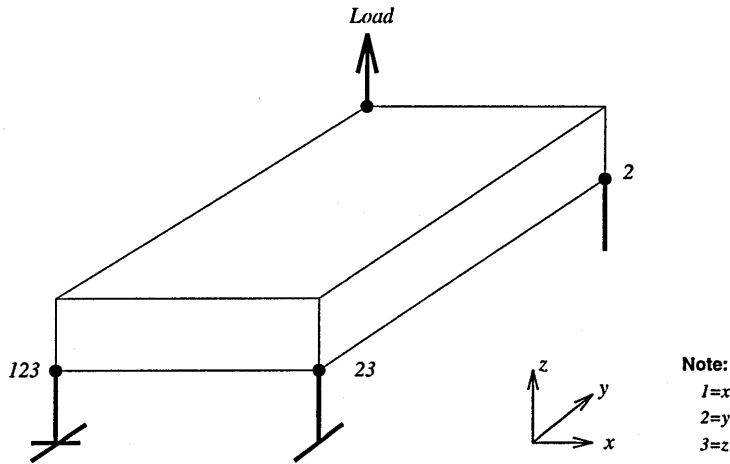


Figure 4.4: Chassis Restraints

### 4.3 Nonlinear Modelling

As with all finite element modelling there are a number of guidelines which need to be followed to try to minimise modelling errors. The following modelling practice is recommended for both linear elastic and nonlinear modelling:

- A simple model should be the starting point for any analysis of this nature, especially if the analyst does not have much insight into the behaviour of the structure,
- The size and complexity of the model needs to be considered in relation to the purpose of the model and the trade off between accuracy and efficiency,
- Prior thought should be exercised in contemplating the geometric modelling of the structure. This should include considerations of the coordinate systems, number of nodal points and geometry, arranging of model into different layers or parts during modelling. This will save time in the long run and allows easy identification of sections of the model.
- Consider where the high stress concentrations will occur, or determine them from a simple model. Areas of high stress, in general, need to have a finer mesh used.
- If using two or three dimensional elements avoid highly stretched and distorted elements (tapered etc.) and use TRIA3 elements only for geometric reasons.
- Use the graphical display to verify the model prior to running. The graphical display can be used to hide various parts and to zoom in and look at different locations in the model.

#### 4.3.1 General Recommendation on Nonlinear Modelling

Whilst the above recommendations apply to all Finite Element Models there are a number of points which are more important for nonlinear modelling. Nonlinear modelling requires better insight into the structural behaviour and the type of nonlinearity expected must be determined. For nonlinear analysis the following points should be considered:



- Local contacts which occur during deformation will effect the constraint set and these should be identified before analysis.
- Geometric nonlinear effects can be substantial and again these should be identified and their effect quantified prior to analysis.
- Localise the nonlinear region for computational efficiency. If unsure perform a linear analysis prior to the nonlinear analysis to gain insight into the structural behaviour, but be aware of the limitations of linear elastic analysis.
- In general the nonlinear region will require a finer mesh if severe element distortions or stress concentrations are anticipated.
- Divide the analysis into discrete steps. This is convenient for running restarts and is of assistance for changing loading paths and constraints if this is required.
- The load increments in the subcases should be divided into increments with the NLPARM card.
- Use the default options on the NLPARM card until some experience is gained in its use.
- Gain some understanding of the basics of plasticity and plastic collapse before using these capabilities.

### 4.3.2 Development of the Nonlinear Model

Converting the linear elastic files to run with material nonlinearity presented a few minor problems. The graphical interface, XL, was predominantly designed for use with linear materials. As a result a number of the options required to run the nonlinear analysis had to be input into the data file by hand which was a time consuming process.

The nonlinear solution sequence in NASTRAN requires an incremental and iterative process to achieve a solution. The increment size for loads has a very significant effect on the efficiency and accuracy of the model. Whilst an excessively small increment reduces the computing efficiency without a significant increase in accuracy, a large increment may result in less accuracy or even divergence of the solution.

For nonlinear analysis the loads and solution sequence can be changed from subcase to subcase on an incremental basis. Constraints can only be changed via the subcase data for static analyses. Thus the subcase structure allows the user to determine the loading sequence, constraints and solution sequence for the analysis.

It is impossible to optimize the incremental step size without prior knowledge of the structural response. It was thus necessary to use good engineering judgement to determine the step size based on the severity of the nonlinearity. Ideally a uniform change in the strains or stresses for material nonlinear problems and a uniform rate of change of displacement for geometric nonlinear problems was required. In this case uniform displacement increments were used to load the chassis. As the collapse load was approached the increments were subdivided to try to get a uniform change in the strains and stresses. In all the nonlinear analyses carried out the NLPARM card was used to control the solution by setting limits on the divergence and number of iterations. The increment size was also set on this card and was varied during the analysis by specifying different NLPARM

cards for each subcase. This allowed the solution sequence to be refined as the collapse load was approached.

If the selection of input data on the NLPARM card resulted in a step size which was too large then warning messages were generated in the results data. Typical warnings were,

- EXCESSIVE INCREMENTAL LOAD IS APPLIED.....
- ERROR EXCEEDED 20% OF CURRENT YIELD STRESS

Initially the default settings were accepted on the NLPARM card. In some instances the solution required more iterations for convergence than the default setting on the NLPARM card. Consequently the step size had to be decreased to improve the solution. In general small increments were used when the stiffness was drastically changing such as occurred at the onset of plastic hinge formation.

Restraint of the nonlinear model was along the base as this was envisaged as the method of restraining the test chassis. The restraint on the final models was modified to be a number of discrete points to model more closely the chassis test mountings.

Initial models used load increments for the analysis. These were controlled and incremented using the combination of FORCE and LOAD cards. The FORCE card specified the load and the load vectors (i.e. direction of load application) to be used. The LOAD card specified what fraction (or percentage) of the FORCE to apply in each subcase. An example of this approach is given in Appendix I.

It was found that the analysis of nonlinear models would often stop partway through the subcases and would give FATAL error warnings due to the matrices becoming singular. The normal type of error message was:

- \*\*\* SYSTEM FATAL MESSAGE 4549,  
SINGULAR (C+KBRR) MATRIX ENCOUNTERED FOR BEAM ELEMENT 1144  
DMAP INFORMATION MESSAGE 9005 (NL-UPDT) -  
THE SOLUTION FOR THE LAST CONVERGED LOOPID=143 IS SAVED FOR RESTART

In the early investigations the error message (4549) was taken to mean that the chassis model had reached its ultimate load carrying capacity. The author's interpretation (in physical terms) of the error, which seemed reasonable from the results data, was that the structure had formed a mechanism and the application of further load on the structure with essentially zero stiffness was an infinite rotation. This would then cause the numerical solver some problems (i.e. singular matrices).

In the initial phase of the analysis this load application method was used and the author's interpretation of the error message was assumed correct. In the second stage of the analysis (after the work of ref [4]) when the Cerbera GT was analysed the method of load application was changed. The author's supervisor suggested investigation of the deep collapse mechanism on this chassis and a displacement load was used to deform the structure.

The application of a displacement load presented several new problems. NASTRAN needs to have the load applied in set directions which must be defined using the Basic Co-ordinate System. Thus to apply a displacement load in the required direction specified by the RACMSA (see Appendix

A) it was necessary to calculate each displacement increment in three orthogonal directions. The SPCD card was then used to apply these increments, however, three entries for each displacement corresponding to the x,y and z components were required for each subcase. Due to the limitation of XL mentioned above these had to be added to the data file by hand and this procedure was very time consuming.

The SPCD card defines an enforced displacement. A co-ordinate referenced on the SPCD card must also be referenced by an SPC card and selected by the SPC Case Control command. The displacement value given on the SPCD card overrides that specified on the SPC Bulk Data entry. Each displacement was to be defined using increments in the three orthogonal directions defined using the Global Coordinate system. A novel way of applying the displacement in a relatively constant direction was to apply them through a long BAR element. This BAR element was positioned in three dimensions to lie on the load line required. By incrementing the lower end of this BAR it was possible to maintain the correct load path even if small errors in the displacements occurred. This proved to be a successful method of applying the displacements and the applied load was given by the axial load in the BAR element. This arrangement is shown in Figure 4.5.

By using displacement increments it was thought that the error (4549) due to singularity in the matrix would cease to be a problem. As the error message persisted a more detailed investigation was carried out. It was noted that the plastic hinge moments tended to be lower than the theoretical value and that they dropped as the load was increased. The cause of this phenomenon was not initially apparent to the author or his supervisor for some time.

As a result of these problems an investigation into the nonlinear collapse modelling used in NASTRAN was carried out. Firstly a simple cantilever beam was used to predict the plastic hinge moment at collapse. The results were found to be in good agreement with theory and these are discussed in Appendix D.3 and shown in Figure 4.6. MSC were contacted with this problem and they too were initially unclear as to the cause of the problem. It took a lot of investigation and dealing with MSC in England, Germany and the United States to discover the cause of the error message and to gain a understanding of the limitations associated with using NASTRAN for modelling nonlinear materials.

Bob Harder<sup>3</sup> provided more insight into the problems and what the error message signified. It was confirmed that the error message represented the ultimate load of the structure. To test that this was the case it was suggested that a very low value of strain hardening be included in the material plasticity model.

When strain hardening was introduced the initial singularity error disappeared but the analysis revealed signs of numerical ill-conditioning which resulted in the last subcase for each of these analyses being disregarded. The results prior to the last subcase seemed to agree well with those from the analyses without strain hardening. The load-deflection results for a typical analysis with strain hardening are shown in Figure 4.7. The inclusion of the very small value of strain hardening in the model showed that the structure had reached its ultimate load when the error message (4549) occurred. The nonlinear element formulation for the BEAM element does not support strain hardening which explains the poor solution results (i.e. the dogleg in the load deflection curve) as shown in Figure 4.7.

The reason found for the lowering of the plastic hinge moment as the load was increased was the interaction between bending and axial forces on the collapse mechanism. This was verified by

---

<sup>3</sup>MSC element specialist for nonlinear material properties

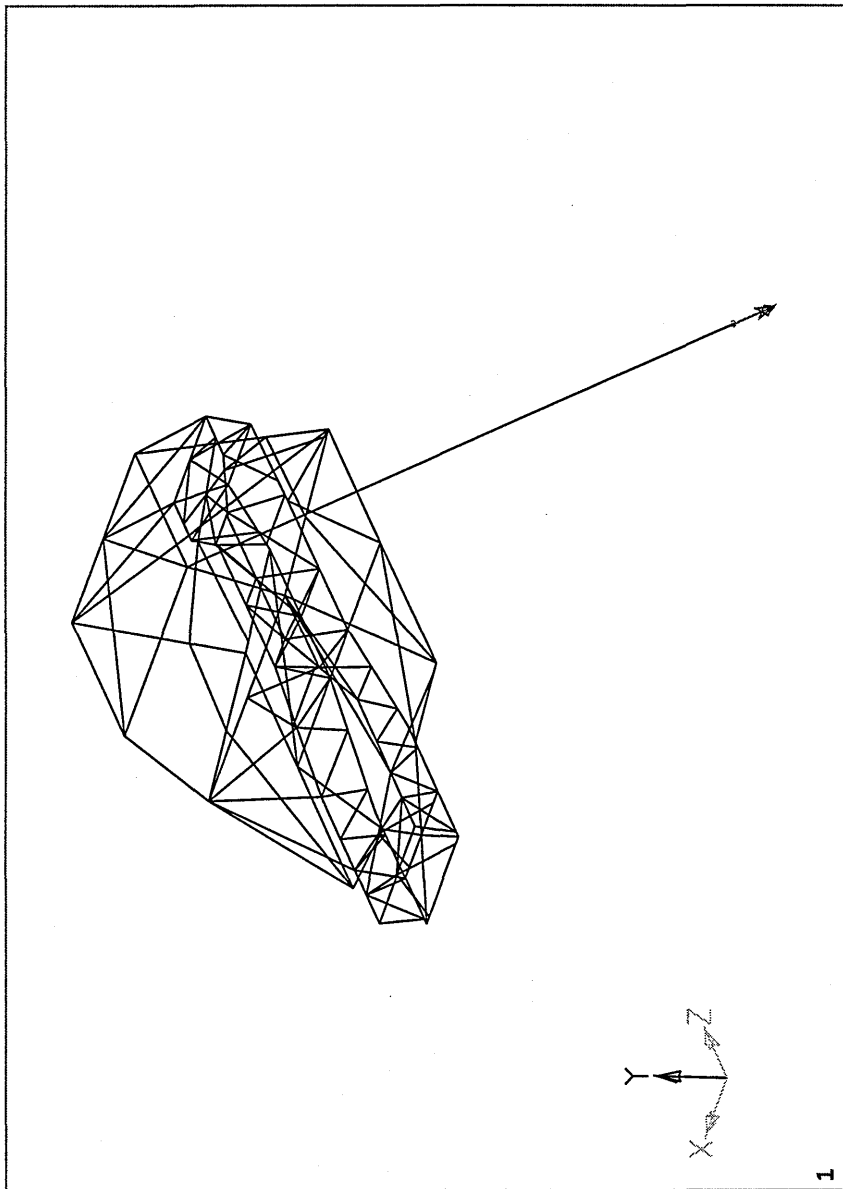


Figure 4.5: Chassis Showing Loading Bar Arrangement

investigating the modelling of plastic hinges for tubular members using the default NASTRAN plastic hinge formulation. A simple (tubular) cantilever beam was loaded with increments of bending moment and axial force using NASTRAN. The same calculation was carried out by hand with expressions being derived for the interaction as detailed in Appendix E. The resultant load curve was extracted from the NASTRAN analysis and compared to the theoretical results. The results can be seen in Figure 4.6.

Investigation and solving of this problem was quite time consuming and took approximately eight weeks. During this time many hundreds of models were run with both finer and coarser meshes to see what influence these had on the solution. The results of this investigation are contained in Chapter 3.8.

Bending Moment Ratio vs Axial Force Ratio - Comparison of NASTRAN and theoretical data.

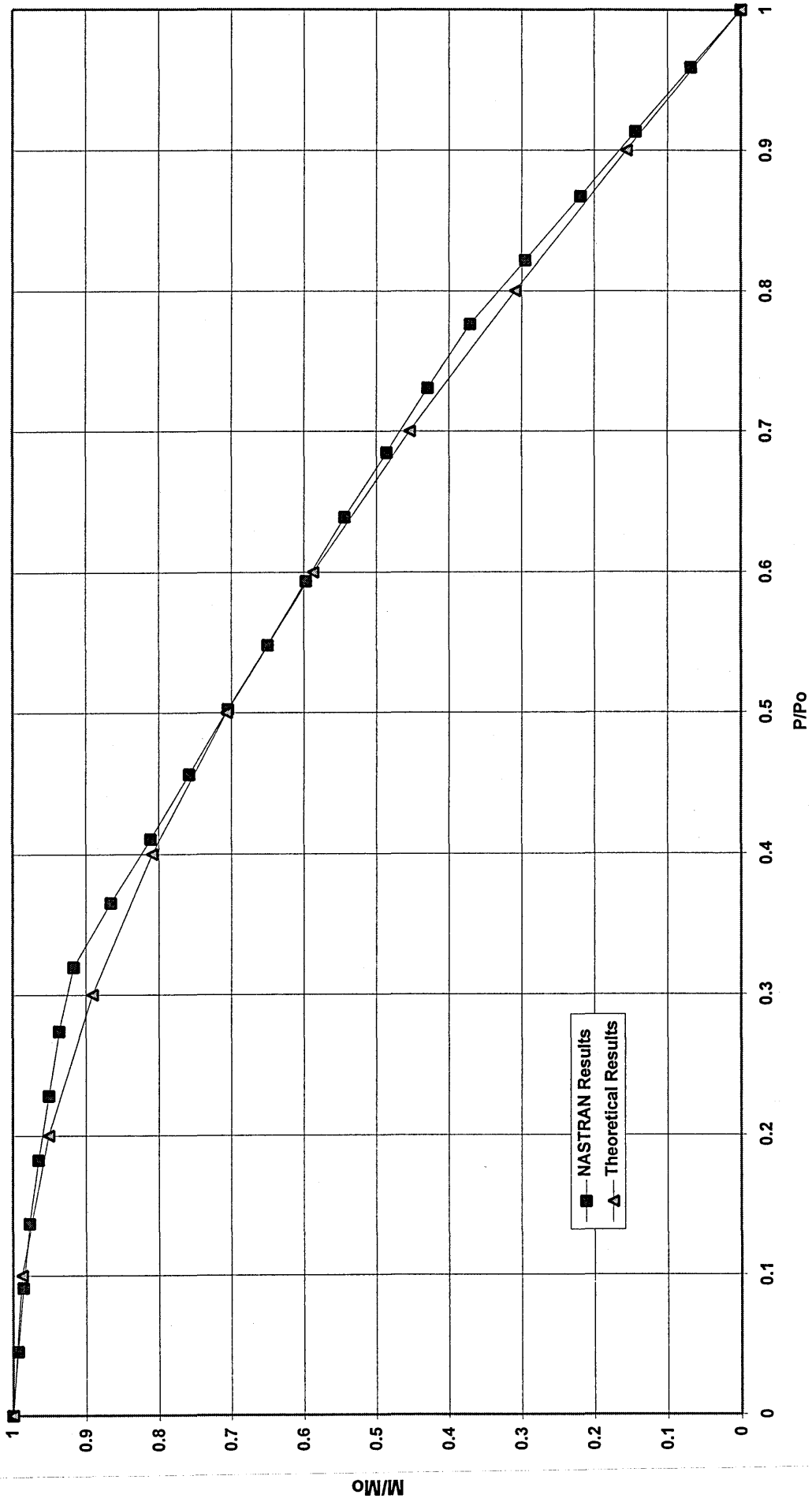


Figure 4.6: Combined Bending and Axial Forces



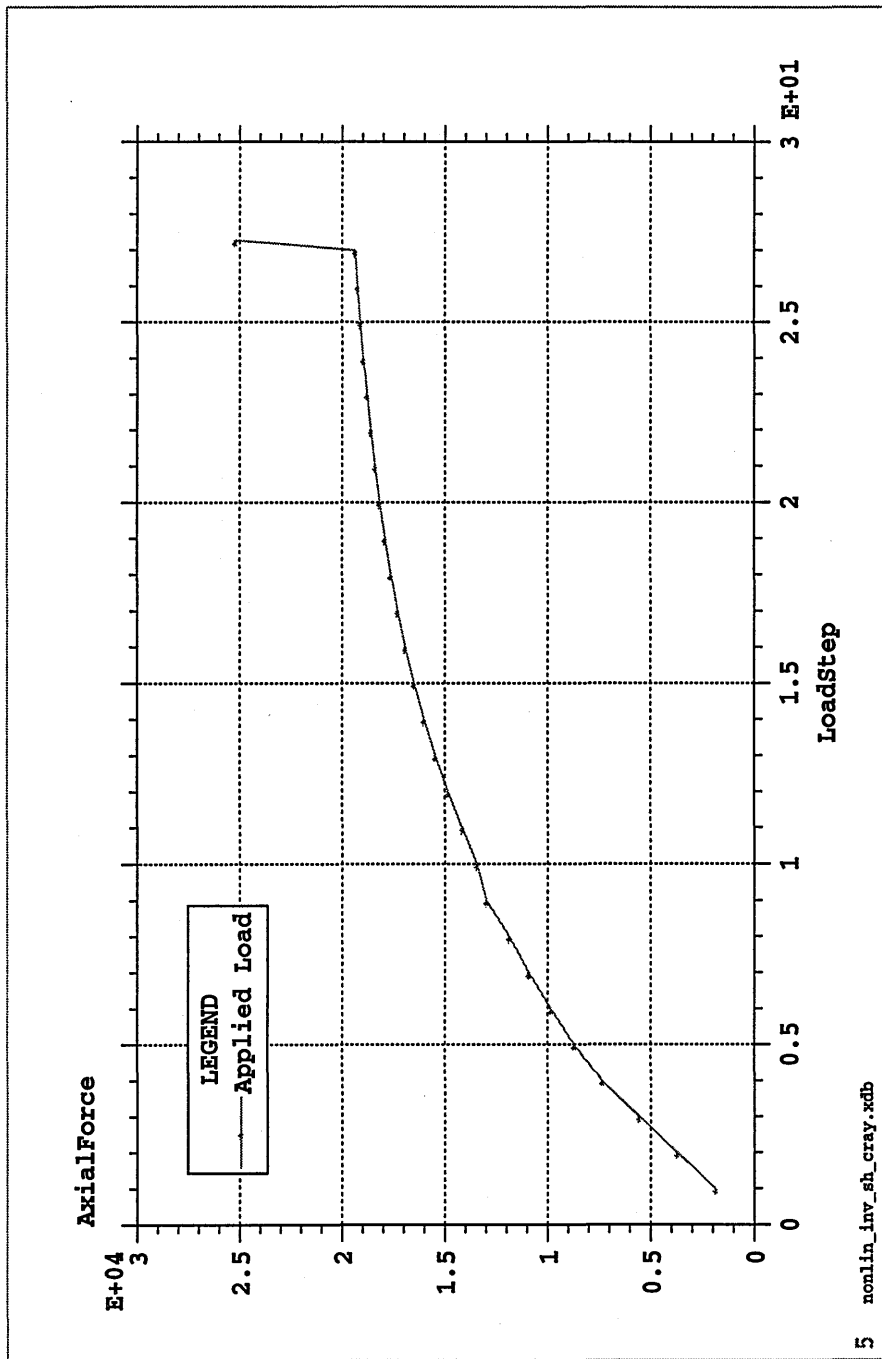


Figure 4.7: Numerical Ill-Conditioning with Strain Hardening.

## Chapter 5

# Plastic Hinges

Engineering structures are required to perform many tasks. Of these the most important are that it shall be strong enough to resist the external loading without collapse and that it is stiff enough so that it doesn't deflect unduly under loading and unloading.

Generally engineering design is concerned with the elastic behaviour of the materials and structures. Thus the structure is designed to have no permanent deformation even under the harshest of design loading conditions. The strength of the structure is thus often assessed by calculating how close the structure or any part of it is to yielding.

This assessment of strength is suitable for most engineering structures. If the loading is increased so that part of the structure yields then a permanent deformation results. This is often used as a safety net as the structure has a significant load carrying capacity once it has began to yield thus safety factors for ductile structures calculated using the yield strength will be conservative.

In automotive and aircraft design the fact that structures have a significant load carrying capacity beyond their yield strength is used to advantage. In the case where a collision may occur the deciding factor on the survivability may be the preservation of an uncrumpled zone and low decelerations. This is where the plastic deformation and energy absorption of the material is used to advantage. If a portion of the structure can be sacrificed then the safety or survival cell may be preserved with the majority of the energy of impact being absorbed by the crumpling, or plastic deformation, of the structure.

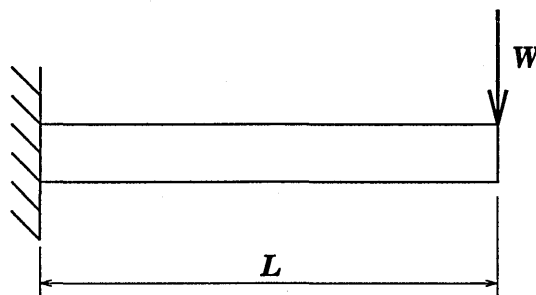


Figure 5.1: Cantilever Beam

For metal components it is possible to illustrate the load carrying capacity in excess of the yield strength by an example. Consider a simple cantilever beam as shown in Figure 5.1. A plot of the load versus the deflection is given in Figure 5.2. From points O to A the beam is behaving elastically

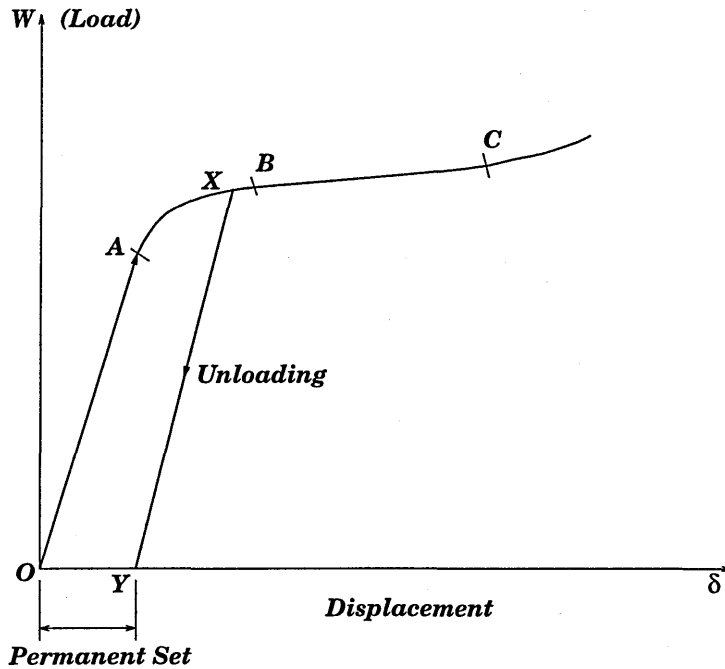


Figure 5.2: Loading Curve for Cantilever Beam

and the deflection of the beam is fully recoverable on unloading of the beam and no permanent deformation occurs. As the load is increased past point  $A$ , however, there is some permanent set taking place in the beam and the deflection begins to increase more rapidly with increasing load. If the loading is removed during this phase, the unloading of the beam will occur elastically along a line such as that of  $XY$ . The permanent set of the beam is represented by the deflection  $OY$ . As the load is increased the deflection increases more rapidly with increasing load and there is a gently rising characteristic in the load deflection curve due to strain hardening of the material.

If the strain hardening of the material is relatively small then it is easy to approximate this stage of the deformation using an elastic perfectly plastic material as shown in Figure 5.3. This models a material that has a maximum load carrying capacity,  $W_u$  after which the displacement increases without increasing load. Consequently, in the case of a cantilever beam as shown Figure 5.2, the bending moments are also constant since the load is constant. The majority of the deformation is taking place in the vicinity of the restrained end and this area behaves much like a hinge. Thus, once the full collapse load acts, the hinge begins to turn and deflection increases. It must be noted however, that if the load is reduced slightly then the hinge ceases to rotate and the beam can support the new load indefinitely if it is below the load required to rotate the hinge. This hinge is called a *plastic hinge* and it occurs at the section of the beam with the largest bending moment.

For this simple example the collapse load of the structure,  $W_u$ , is indicative of the strength and is not directly related to the elastic material behaviour. The elastic limit given by point  $A$  in Figure 5.3 is in a more or less definite ratio to the ultimate collapse load for the cantilever beam but it will not be the same ratio necessarily for a different structure. The mere onset of yielding does not imply that complete collapse is imminent.

The load deflection curve of Figure 5.2 is a result of a particular moment-curvature relationship for the cross section of the cantilever beam in this example. This relationship is shown in Figure 5.4 and is of a similar shape to the load deflection curve of Figure 5.2.

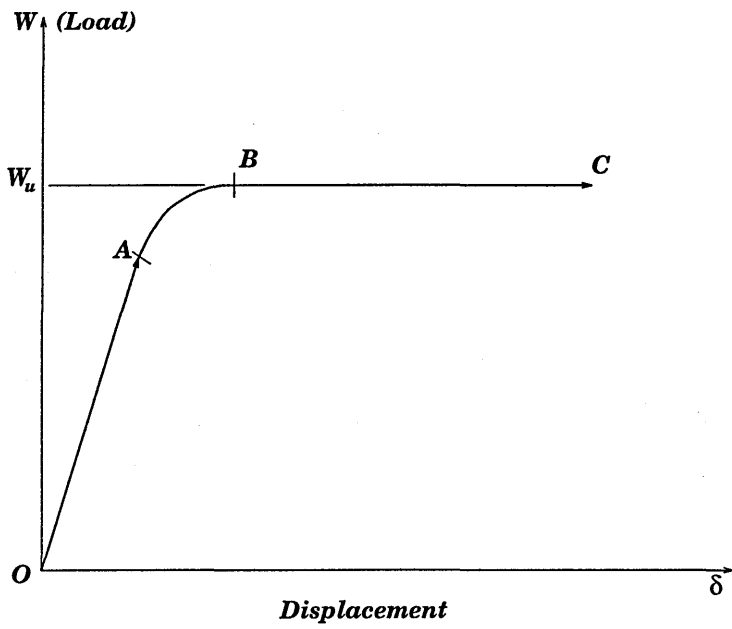


Figure 5.3: Elastic-Perfectly Plastic Load Deflection Curve

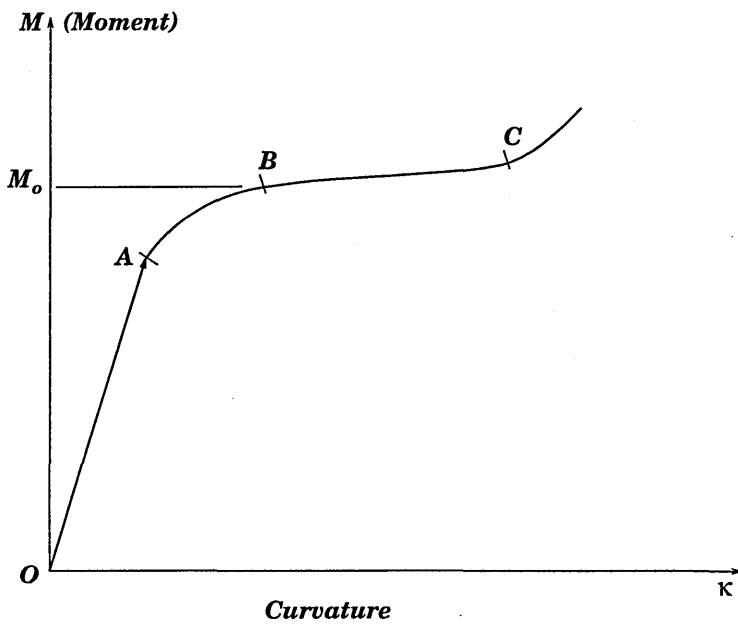


Figure 5.4: Moment-Curvature Diagram for the Cantilever Beam

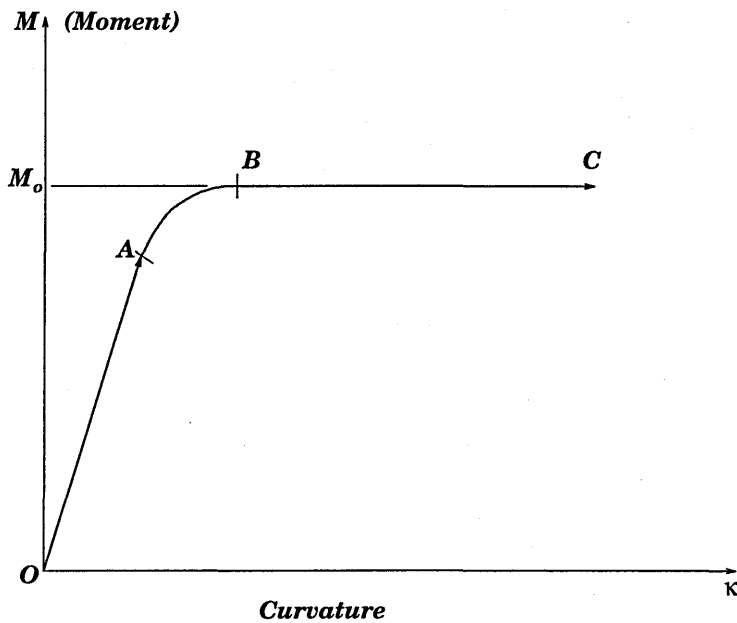


Figure 5.5: Ideal Moment Curvature Diagram for the Cantilever Beam

As was done above an “idealised” form of the moment-curvature curve can be proposed as shown in Figure 5.5. In this figure the curvature is taken to increase infinitely at a constant value of bending moment,  $M_o$ . It is clearly seen that the value of  $M_o$  corresponds to the moment acting at the plastic hinge - this moment is known as the *full plastic moment* or *plastic hinge moment*.

Whilst being able to plot the moment-rotation diagram for a particular beam or set of beams withing a structure is of use, it is better to have a relationship between the loading of the structure and the yield stress of the beam. By determining the relationship between the tensile stress-strain curve and the fully plastic bending behaviour it is possible to determine the set of applicable plastic moduli, which, when multiplied by the yield stress give the required values of the plastic hinge moment.

For a structural mild steel the stress strain curve is as shown in Figure 5.6. Elastic extension occurs until the yield stress,  $\sigma_o$  is reached. The stress then remains almost constant for increasing strain until quite large strains are reached whence strain hardening occurs. The further straining in this final region results in a slight increase in the stress levels. At very large strains necking and fracture occur and represent the final failure of the material. Typically the strain at the yield point is of the order of  $10^{-3}$  (0.1%). The strain at the end of the plastic range is at least 10 times this value for structural mild steel, lying between 1 and 2%. (The total elongation to fracture may be as high as 50%). The plastic range is of sufficient length for the adoption of the earlier assumption of indefinite rotation at constant moment - and to negelect the strain hardening effect. It can be argued that neglecting the strain hardening is on the safe side anyhow. It has been reported [1] that in general the full plastic moment is essentially attained prior to the onset of strain hardening. This is relevant to the NASTRAN model of the plastic hinge used which assumes no strain hardening is present.

In the ensuing analysis and in all the calculation a number of simplifying assumption are made which include:

- The material behaviour is tension is identical to that in compression,

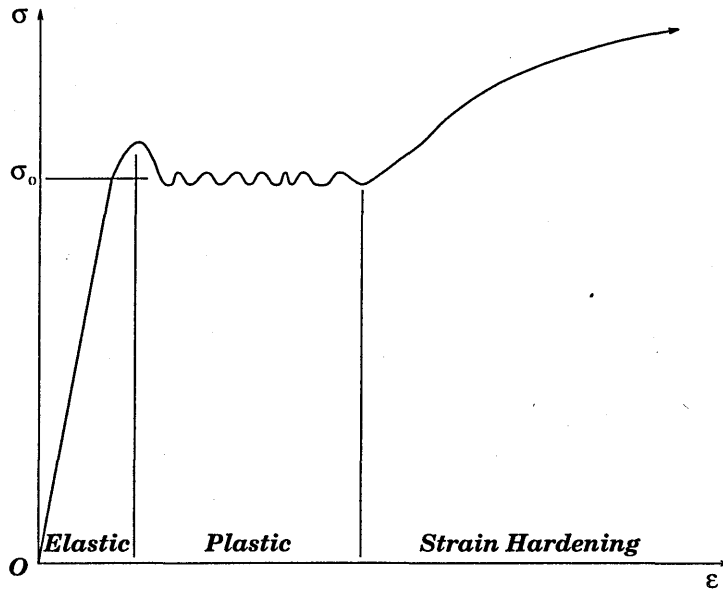


Figure 5.6: Stress Strain Curve for Mild Steel

- Strain varies linearly across the cross section (plane sections remain plane),
- Adjacent fibres do not effect each other and the effect of shearing stress on the bending can be ignored,

As an example of the plastic deformation of a beam the rectangular cross section of Figure 5.7 is analysed. The dimensions of this cross section are taken to be  $b \times 2d$  At the onset of yield the value of the moment is,

$$M_y = \frac{1}{2}bd\sigma_o \left( \frac{4}{3}d \right) = \frac{2}{3}bd^2\sigma_o \quad (5.1)$$

The elastic modulus ( $Z_e = I/y$ ) of this beam is thus,  $\frac{2}{3}bd^2$ . In the partially plastic state the value of the moment of resistance of the beam can be calculated in terms of the parameter  $\zeta$  defining the depth of the elastic zone:

$$M_h = (1 - \zeta)bd\sigma_o [(1 + \zeta)d] + \frac{2}{3}\zeta^2bd^2\sigma_o \quad (5.2)$$

Simplifying,

$$M_h = bd^2\sigma_o \left( 1 - \frac{1}{3}\zeta^2 \right) \quad (5.3)$$

This equation reduced to that of equation (5.1) when  $\zeta = 1$ .

As the value of  $\zeta$  approaches zero it can be seen that more and more of the cross section passes from the elastic into the plastic state and the value of the moment of resistance approaches the limiting value:

$$M_p = bd^2\sigma_o \quad (5.4)$$

The plastic modulus ( $Z_p$ ) is taken to be the quantity that is multiplied by the yield stress of the material to give the full plastic moment,  $M_p$ . For the case above it can be seen that the plastic



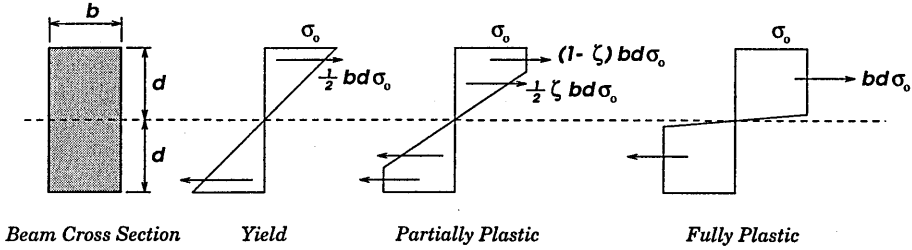


Figure 5.7: Beam Cross Section and Yielding

section modulus for this rectangular section is  $Z_p = bd^2$ . The shape factor, defined as the ratio of the plastic to the elastic modulus,  $Z_p/Z_e$ , thus has a value of 1.5 for a beam of rectangular cross section. The value of the shape factor is a function of the geometry of the cross section only.

At the full state of plasticity with  $\zeta = 0$  in equation (5.2) there is the implication of infinite strain in the cross section. It can be seen for the partially plastic cases of Figure 5.7 that the strain in the outer fibres of the cross section is  $1/\zeta$  times the yield strain. For a mild steel having a plastic range as short as 10:1, however, for which the strain in the outer fibres can reach ten times the yield strain before strain hardening, the value of the moment increases to almost the fully plastic value before strain hardening sets in. Setting  $\zeta = 0.1$  in equation (5.2) it can be seen that the factor in the brackets varies from unity by only 0.3%. Thus although the theory requires the impossible condition of infinite strain it is sufficiently accurate to assume that the plastic hinge can form and can undergo indefinite rotation under the constant value of the resisting moment  $M_o$ .

Equation (5.2) and (5.4) can be combined to give the general expression for the moment of resistance in the partially plastic state:

$$M_h = M_p \left( 1 - \left( \frac{1}{3} \right) \zeta^2 \right) \quad (5.5)$$

From this equation it is possible to determine the shape of the plastic zones for a simple beam of rectangular cross section. Assuming the simple cantilever in Figure 5.1 is loaded by a point load,  $P$  at the free end which just causes the full plastic moment to be developed at the built in end. The bending moment at any section  $x$  of the beam will then be given by,

$$M = M_p - M_p \left( \frac{x}{l} \right) = M_p \left( 1 - \frac{x}{l} \right) \quad (5.6)$$

Equating (5.5) and (5.6) gives,

$$\zeta = \sqrt{\left( \frac{3x}{l} \right)} \quad (5.7)$$

From equation (5.7) it can be seen that with  $x/l = 0.33$  the value of  $\zeta = 0.99$ . This is shown graphically in Figure 5.8.

The plastic zone shown in Figure 5.8 decays quite quickly. Thus the plastic hinge is confined to a finite and infinitesimal length. In reality, however, the rotation of the hinge will cause the material to strain harden and the bending moment will increase above the theoretical fully plastic value. Consequently the plastic zone will spread from the hinge position and this increases the area over which the plastic hinge is spread.

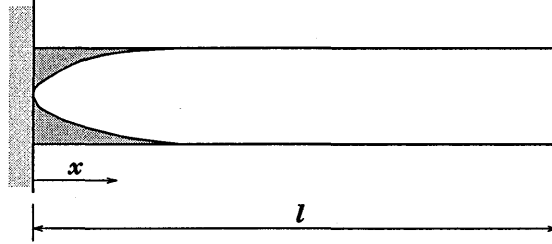


Figure 5.8: Plastic Zone in a Cantilever Beam

### 5.1 Combined Bending and Axial Forces

It was found that the axial load was important in the collapse mechanism of the chassis and the combined effect of axial force and bending moment were investigated.

If an axial (tension) force is applied to a beam then a uniform tensile stress will occur in the cross section due to this. If a small bending moment is then added to the beam this will add a linear variation to the elastic stress acting across the beam cross section. This is shown diagrammatically in Figure 5.9. As the bending moment is increased with the axial load remaining constant then

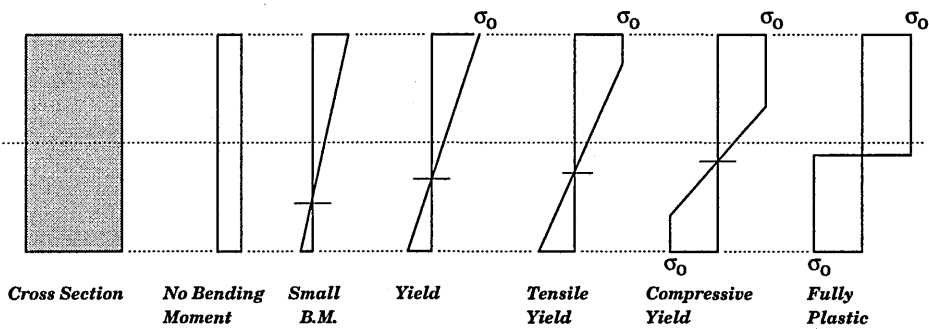


Figure 5.9: Combined Bending and Axial Forces

yield will eventually occur on one face of the section. This will be followed by yield on the other face and eventually the entire section will yield. This process is accompanied by the zero stress axis moving until it reaches its final location for the fully plastic state. The zero stress axis actually lies outside the cross section for very small values of bending moment. It is the fully plastic state which is of interest for the nonlinear collapse of the beams. Consider a beam of rectangular cross section as shown in Figure 5.10. Once the beam has reached a level where the full plastic moment has occurred, the addition of an axial load results in the beam then the zero stress axis moving from the centre line by an amount, say  $\beta d$ . In essence an axial stress distribution has been added to the cross section which results in this shift of the zero stress axis. To gain some insight into what is happening the stress distribution can be broken down into a component from the bending and one from the axial force. This *fictitious* distribution is shown in Figure 5.10.

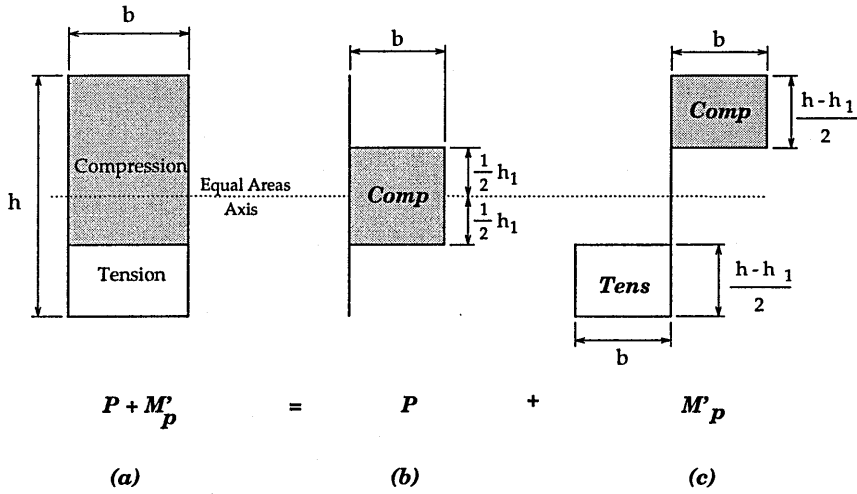


Figure 5.10: Rectangular Beam subjected to Axial and Bending Forces

The resultant stress on the beam cross section due to the axial force in Figure 5.10 (b) must be equal to the applied axial load,  $P$  which acts over the area shown in Figure 5.10. Thus, the area is:

$$A_{af} = 2 \left( \frac{h_1}{2} \right) b = bh_1$$

and the force acting on this area due to the stress  $\sigma_y$  is,

$$P = \sigma_y(bh_1) \tag{5.8}$$

The axial load at the onset of yield in the cross section is denoted as  $P_0$  (axial collapse load) which would act over the entire cross section and is given by the relationship,

$$P_0 = \sigma_y(b)(h) \tag{5.9}$$

Defining the ratio of the axial force acting on the section to that of the axial collapse load as  $n$  gives the relationship,

$$\frac{P}{P_0} = n \tag{5.10}$$

Rearranging equation (5.8) gives,

$$P = \frac{h_1}{h} \sigma_y(b)(h) \tag{5.11}$$

and since  $\sigma_y(b)(h)$  is the axial collapse load,  $P_0$ , Equations 5.8 and 5.11 can be combined to give, expressed as,

$$\therefore \frac{P}{P_0} = \frac{h_1}{h} = n$$

The resultant of Figure 5.10 (c) is a couple which is equal and opposite to the applied moment,  $M'_p$ . The force acting on each of the segments subjected to the bending force (as shown in Figure 5.11) is given by,

$$P_b = (b) \left( \frac{h - h_1}{2} \right) \sigma_y \tag{5.12}$$

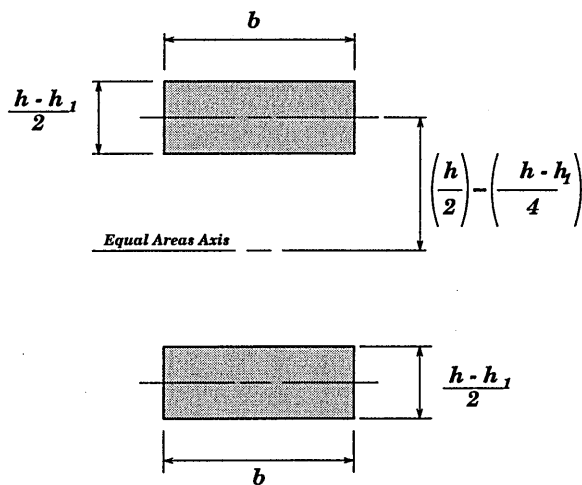


Figure 5.11: Bending Moment and Forces

Taking moments about the equal area axis,

$$M'_p = \left( \sigma_y b \left[ \frac{h-h_1}{2} \right] \left[ \frac{h+h_1}{4} \right] + \left[ \frac{h-h_1}{2} \right] \left[ \frac{h+h_1}{4} \right] \right)$$

$$\therefore M'_p = \frac{\sigma_y b h^2}{4} - \frac{\sigma_y b h_1^2}{4} \tag{5.13}$$

Since  $n = \frac{h_1}{h}$  equation (5.13) can be rewritten as,

$$M'_p = (1 - n^2) M_p \tag{5.14}$$

where  $M_p$  is the plastic moment for pure bending and  $M'_p$  is the plastic moment in the presence of the axial force.

Substituting for  $n = \frac{P}{P_0}$  into this equation yields,

$$\frac{M'_p}{M_p} + \left( \frac{P}{P_0} \right)^2 = 1 \tag{5.15}$$

Which is the general solution for combined axial and bending forces.

## 5.2 Inelastic Material Behaviour

Ductile materials have the inherent ability to deform and remain intact well beyond the level of stress which causes yield. Engineering design and analysis is usually based upon elastic behaviour which requires, in general, the use of a factor of safety with the aim being to avoid any plastic deformation.

Failure of a structure occurs when the stresses in any part of the structure exceed some predetermined limit (often taken as the yield stress). When combined stress states are present, the

interaction of the inelastic stress components become very complicated analytically. Failure theories have been postulated for the purpose of identifying stress situation which may lead to material failure.

For a general biaxial-stress state a yield criterion needs to be used. The two most popular failure theories are discussed as applied to two dimensional stress states. The maximum shear stress theory sometimes referred to as the Tresca (1864) failure theory is a principal stress theory. The derivation of the theory is straightforward but care must be used when applying the theory. The maximum distortion energy theory is often referred to as the Von Mises (1913) failure theory and is also a principal stress theory. The derivation is more involved but the use of the failure criterion is straightforward. A principal stress theory requires principal stresses to be computed before the failure criterion can be used.

### 5.2.1 Maximum Shear Stress Theory (Tresca)

The maximum shear stress theory is also known as the Tresca Criterion and states that yielding begins when the maximum shear stress at a point equals the maximum shear stress at yield in uniaxial tension or compression. The maximum shear stress for a multiaxial stress state can be defined as:

$$\tau_{max} = \left( \frac{\sigma_{max} - \sigma_{min}}{2} \right) \quad (5.16)$$

Where  $\sigma_{max}$  and  $\sigma_{min}$  are the maximum and minimum principal stress components respectively.

For the state of uniaxial tension ( $\sigma_1 = \sigma$ ,  $\sigma_2 = \sigma_3 = 0$ ), the maximum shear stress is given by  $\tau_{max} = \frac{\sigma}{2}$ . Defining the yield strength of the material in uniaxial tension (or compression) as  $Y$  then yield begins when  $\sigma_1 = Y$ . Consequently the yield stress associated with this state is  $\tau_{max} = \frac{Y}{2}$ .

A yield criterion is a descriptive statement defining the conditions under which yielding will occur and is often expressed in a mathematical form as a yield function of the form  $f(\sigma_{ij}, Y)$ . In this case  $\sigma_{ij}$  defines the stress state and  $Y$  is the yield strength in uniaxial tension or compression. The yield function is satisfied when  $f(\sigma_{ij}, Y) = 0$ . The material behaviour is elastic when  $f(\sigma_{ij}, Y) < 0$  and it is undefined when  $f(\sigma_{ij}, Y) > 0$ . In developing the yield function the components of the multiaxial stress state are combined into a single quantity known as the effective stress which is then compared to the yield stress,  $Y$ , to determine if yield has occurred.

Hence, if the yield is defined as occurring when  $\tau_{max} = \frac{Y}{2}$  and the effective stress is defined as  $\sigma_e = \tau_{max}$  then the yield function can be defined as,

$$f = \sigma_e - \frac{Y}{2}$$

The magnitude of the extreme values of the shear stress can be obtained from Mohr's Circle for a three dimensional stress state (see Ref. [2]).

$$\tau_1 = \frac{|\sigma_2 - \sigma_3|}{2}$$

$$\tau_2 = \frac{|\sigma_3 - \sigma_1|}{2}$$

$$\tau_3 = \frac{|\sigma_1 - \sigma_2|}{2}$$

The maximum shear stress is the largest of  $\tau_1, \tau_2, \tau_3$ . If the principal stresses are not in any order then yielding can occur in any one of the following situations:

$$\begin{aligned}\sigma_1 - \sigma_3 &= \pm Y \\ \sigma_3 - \sigma_1 &= \pm Y \\ \sigma_1 - \sigma_2 &= \pm Y\end{aligned}\tag{5.17}$$

From this information in the equations (5.17) above the yield surface for the maximum shear-stress criterion is a regular hexagon in the principle stress space. In the biaxial state ( $\sigma_3 = 0$ ) the yield surface takes the form of an elongated hexagon in the  $(\sigma_1, \sigma_2)$  plane. The Tresca theory gives good agreement with experimental results for ductile materials.

### 5.3 Distortional Energy Density (von Mises) Criterion

This theory states that yielding begins when the distortional strain energy density at a point equals the distortional strain energy at yield in uniaxial tension or compression.

The mathematical derivation of this failure theory is not undertaken here and full details can be found in ref.[2]. It can be shown that the Yield function for the distortional energy density (von Mises) criterion (where  $Y$  is the yield strength in uniaxial tension) is,

$$f = \frac{1}{6} [(\sigma_1 - \sigma_2)^2 + (\sigma_2 - \sigma_3)^2 + (\sigma_3 - \sigma_1)^2] - \frac{1}{3} Y^2\tag{5.18}$$

For a biaxial stress state the von Mises yield surface reduces to an ellipse in the  $(\sigma_1, \sigma_2)$  plane. The von Mises criteria is fairly accurate at predicting yield of ductile materials and is more accurate than Tresca for pure shear failures. For pure shear,  $\sigma_1 = -\sigma_2 = \sigma, \sigma_3 = 0$  and from equation (5.18),

$$3\sigma^2 = Y^2\tag{5.19}$$

and for maximum shear stress from equation (5.16),

$$\tau_{max} = \left( \frac{\sigma_1 - \sigma_2}{2} \right) = \sigma\tag{5.20}$$

Thus at yield,  $\sigma = \tau_{max} = \tau_y$  and substitution into equation (5.19) gives,

$$\tau_Y = \frac{Y}{\sqrt{3}} = 0.577Y$$

Compared to the Tresca value of,

$$\tau_Y = \frac{Y}{2}$$



## Chapter 6

# Test Schedules for TVR Chassis

To verify the finite element model two tests were carried out. Whilst the purpose of these two tests were similar they were carried out on different parts of the roll cage and the loading was quite different.

The first test was a verification of the rear roll hoop design and was carried out using the method<sup>1</sup> used in industry for proving roll cage structures. This involved loading the main roll hoop with 8,812 kg (86,451 N) in the vertical direction. This value is taken from the required roll cage load carrying capacity in the RACMSA requirements as detailed in Appendix A. It should be noted, however, that very few roll cages or roll bars are tested due to the high costs involved and most design is done by calculation and by using the requirements and design guidelines of the RACMSA.

The second test was using the full load as specified by the RACMSA (see Appendix A and FIA for roll cage approval. For the TVR Chassis tested ( $w = 1,175$  kg) the load consisted of:

17,290 N Laterally  
63,397 N Longitudinally  
86,451 N Vertically

The RACMSA stipulate that this load must be able to be carried at *any* point on the top of the roll cage. From the author's investigation of different loading cases it would appear that the load applied to the upper front windscreen corner represents the worst case. The main contributing factors were found to be the large open sections present in this region. As this was least stiff point on the roll cage it was chosen as the load application point for the nonlinear finite element analysis and for the test. This would be the worst loading case in a roll over accident.

### 6.1 Vertical Load Test

This test was arranged to verify the vertical load carrying capacity of the final roll cage fitted to the Cerbera GT chassis supplied by TVR.

A finite element analysis was carried out on the chassis with this loading to identify the onset of yield and the location of the highly stressed members. This analysis was then used for the subsequent design of the test equipment and mountings.

---

<sup>1</sup>The industry standard method is based on information from a leading roll cage design company

There were two material grades<sup>2</sup> used in the chassis structure supplied for test. The main chassis members and truss structure (including the outriggers) were manufactured from CFS 3 and the roll cage was manufactured from ERW 1.

ERW 1 was used for the roll cage in this instance to reduce the cost of the test chassis. The purpose of the test was to compare the finite element models to the physical test chassis and the material grade was not considered crucial to the results. In the production chassis the roll cage is to be made of high strength steel (BS T45) and a finite element model was run with the roll cage made from this material and the results are discussed in Section 3.5.

Whilst the material grade used may make a significant difference to the load carried, it should not effect the overall structural behaviour. Consequently if it could be shown that the nonlinear finite element analysis modelled the ultimate load carrying capacity of the structure and the deformed shape found from the test then its value as a design tool for this class of problem would be apparent.

If the NASTRAN analysis results, using the materials of the test chassis, were comparable to the test results then it should be possible to read the results across to structures designed using different materials but the same techniques (provided the failure mechanisms of the new material used is similar to that of the test case).

The theoretical results for the chassis are contained in Section 3.5. The results from the analysis are compared to the test results below. The design of the test rig and all the attachments is contained in Appendix B. The reaction load results from the nonlinear analysis were used for the test rig design. The final arrangement for the test setup is shown in Figure B.1.

For the test the chassis was set up as shown in Figure 6.1. The load was applied using a hydraulic ram, arranged as shown, to the rear roll hoop. The horizontal bar was mounted on wooden blocks in an attempt to prevent local crushing of the tube. This proved to be futile due to the thin gauge of the material used and local crushing occurred during the test.

It was estimated (from the nonlinear analysis) that the rear hoop manufactured in ERW 1 tube would carry a vertical load of 59,670 N at failure. The vertical load testing was carried out first and, as the chassis was required for the nonlinear crush, no permanent deformation was desired at this stage. In order to minimise the chassis deformation the load was increased progressively up to a maximum load of approximately 55kN (i.e. below the predicted ultimate load).

The load was applied and the data logged, with the results being given in Figure 6.2. At approximately 45kN the tube in the rear hoop locally collapsed as shown in Figure 6.3 in the vicinity of the wooden blocks used in the loading setup. This type of failure (i.e. buckling/local crushing) was found to be significant for the roll structure due to the thin wall thickness (18swg) of the tubes used. The local collapse occurred at a load below the predicted failure load in this case.

The wooden blocks were then removed and the bar placed directly on the rear hoop. The load was reapplied and, as would be expected, the tube was locally flattened as shown in Figure 6.4. As can be seen in Figure 6.4 the local collapse occurred in areas where there were a lot of tube joins. The join was quite stiff and the thin walled tubes (flexible) were the first to collapse under the high loads in this region.

In practice, however, the buckles would close up and at this point the structure would stiffen again and carry an increasing load until the next buckle developed.

---

<sup>2</sup>The relevant material properties can be found in Appendix C

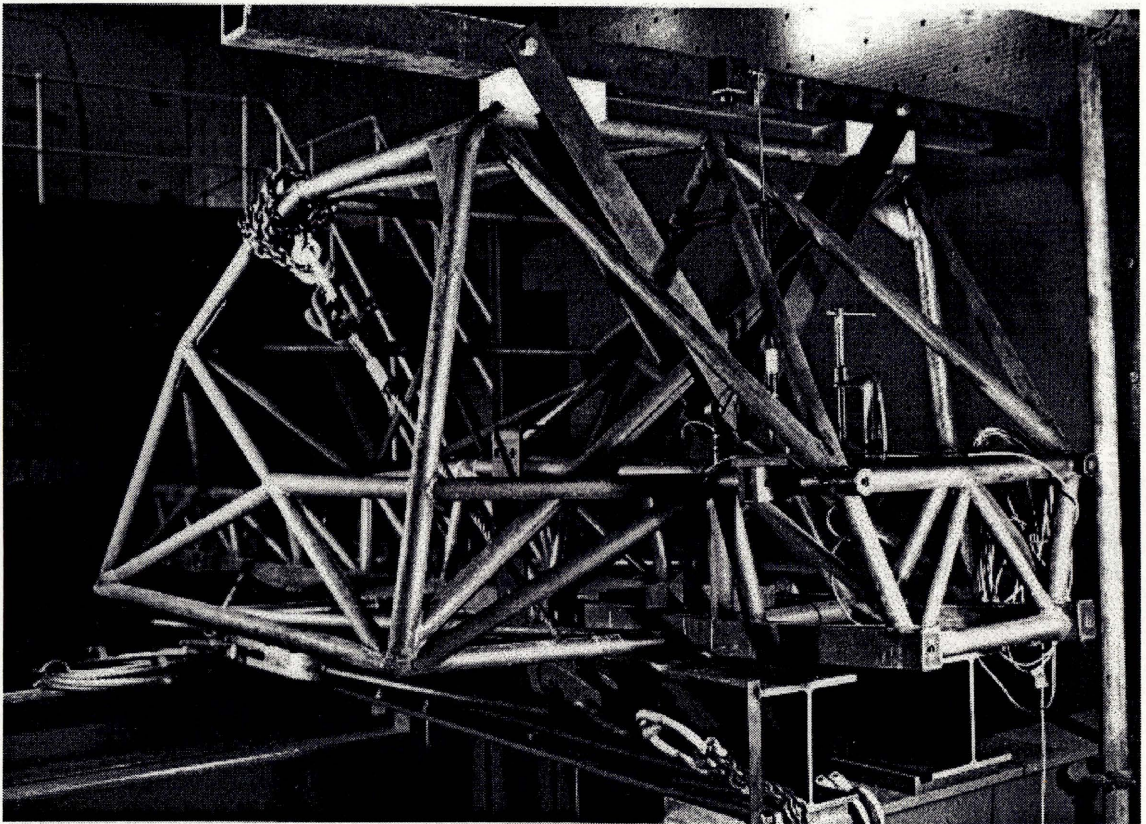


Figure 6.1: Rear Roll Hoop Test Setup on Chassis.

### TVR Rear Hoop Test 1

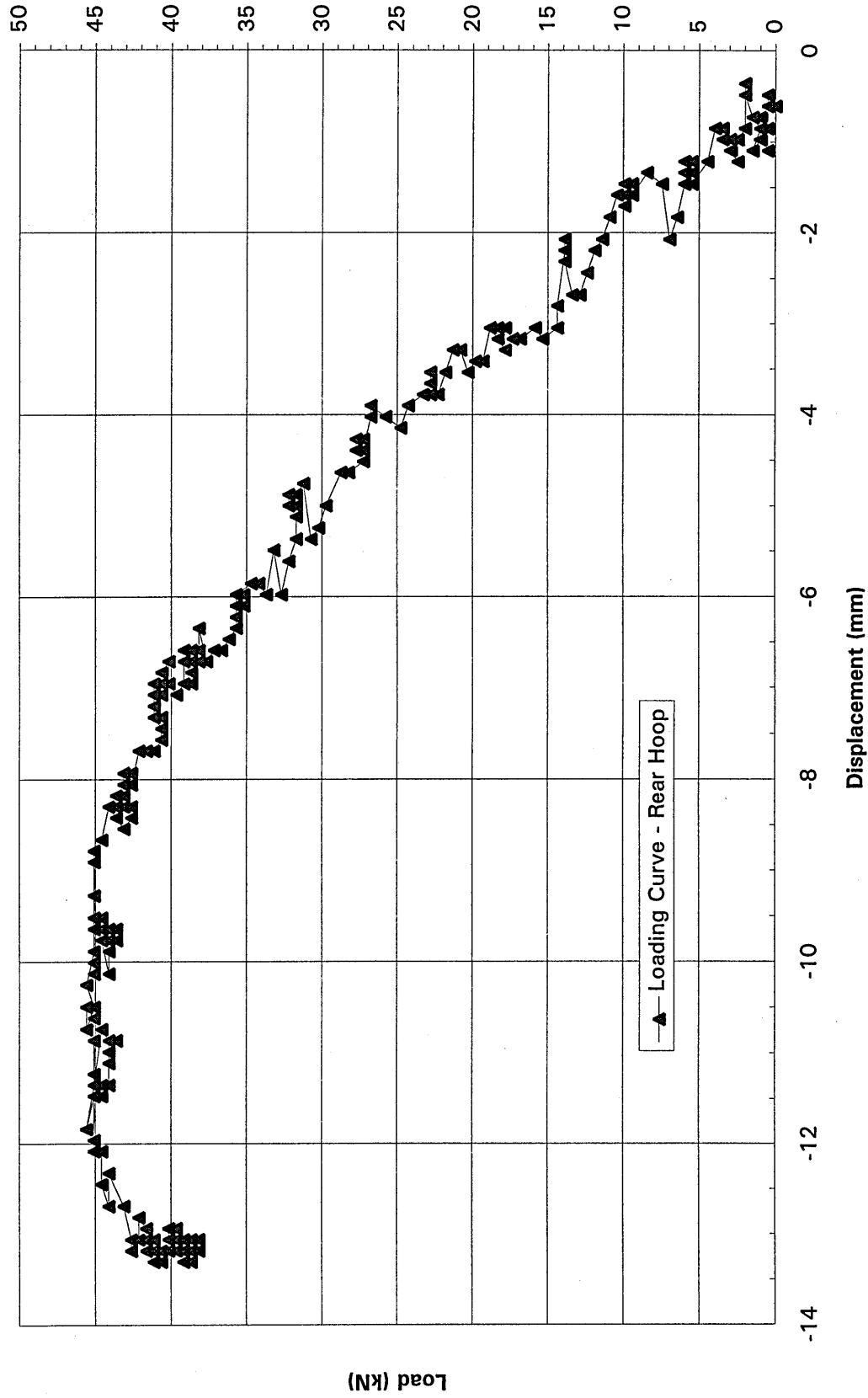


Figure 6.2: Rear Hoop Vertical Load-Displacement Curve with Wooden Support Blocks



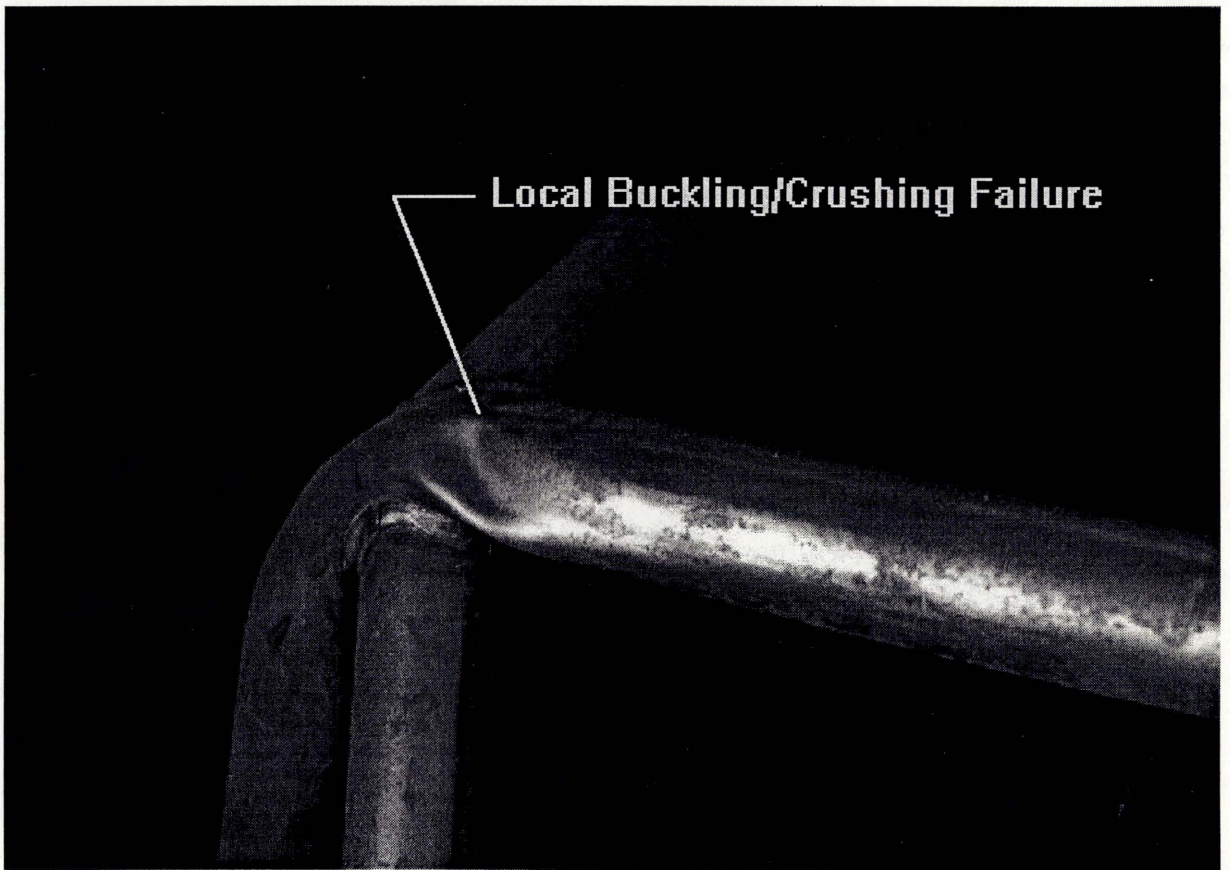


Figure 6.3: Local Tube Crushing in the Rear Hoop

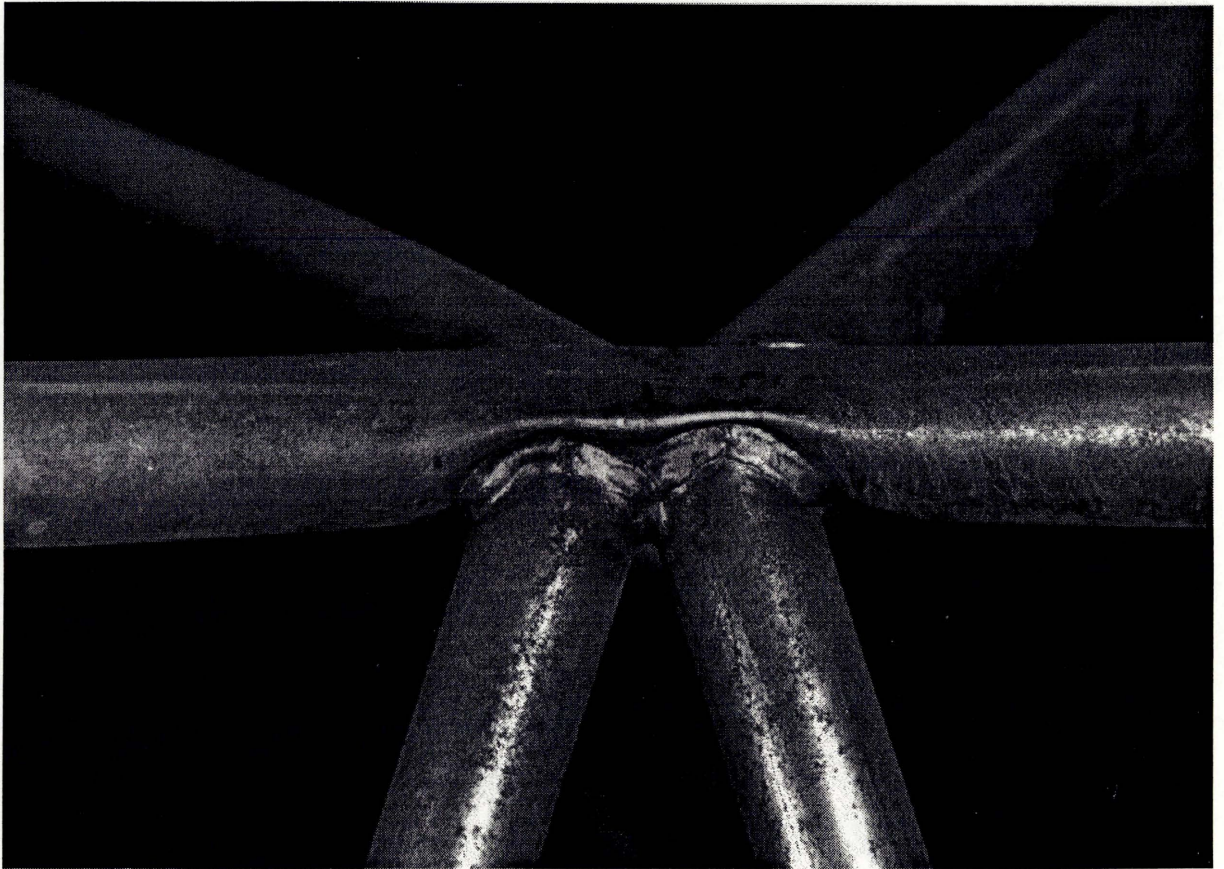


Figure 6.4: Local Tube Flattening in the Rear Hoop



TVR Rear Hoop Test 2

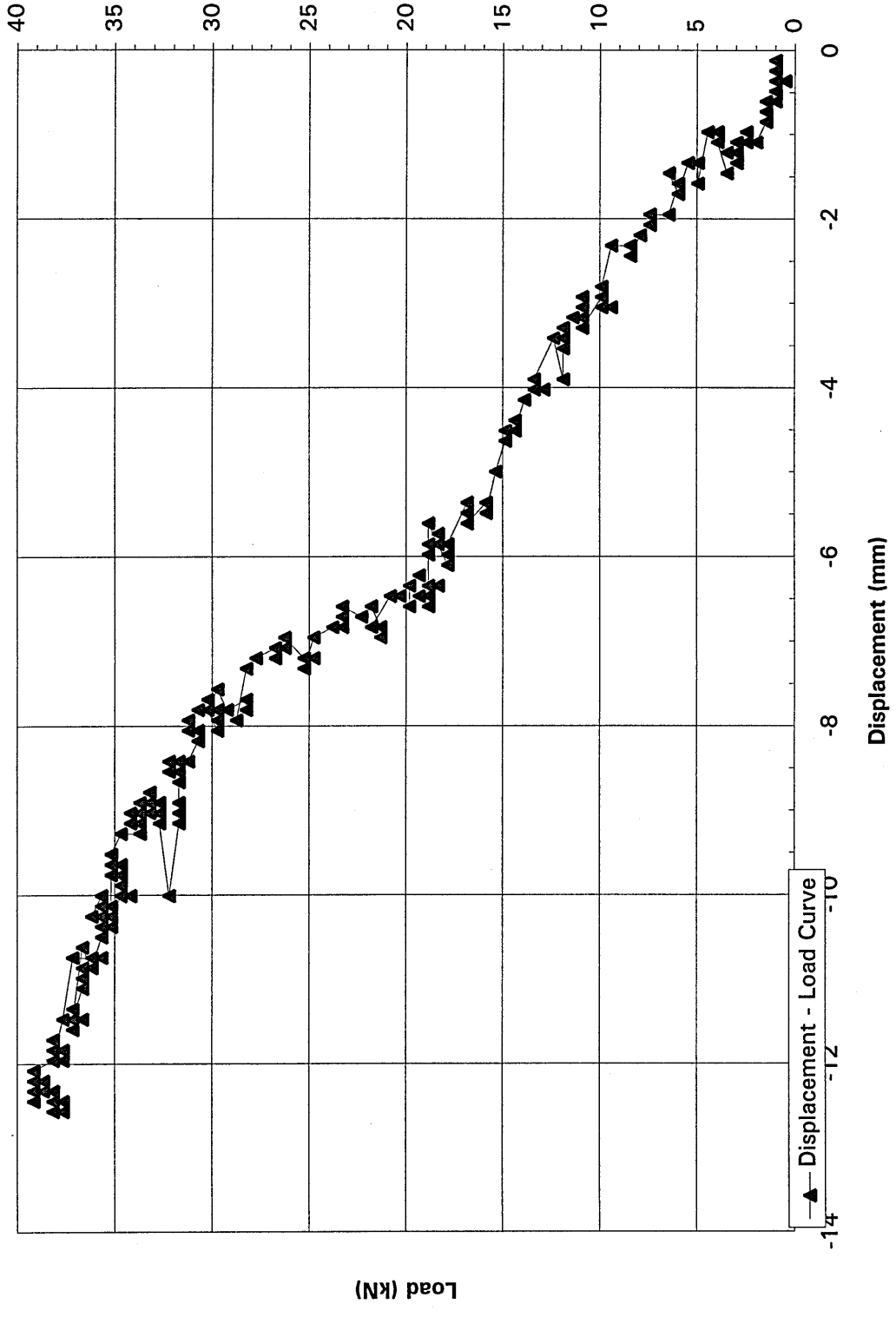


Figure 6.5: Rear Hoop Vertical Load-Displacement Curve - Without the Wooden Support Blocks

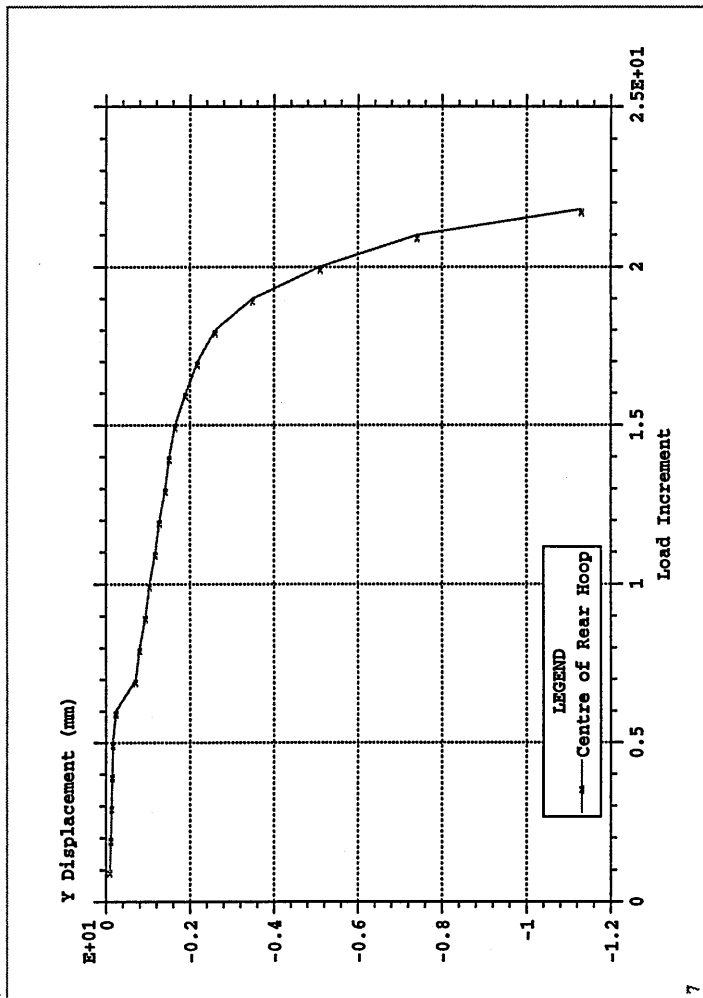


Figure 6.6: NASTRAN Model Vertical Load-Displacement Curve

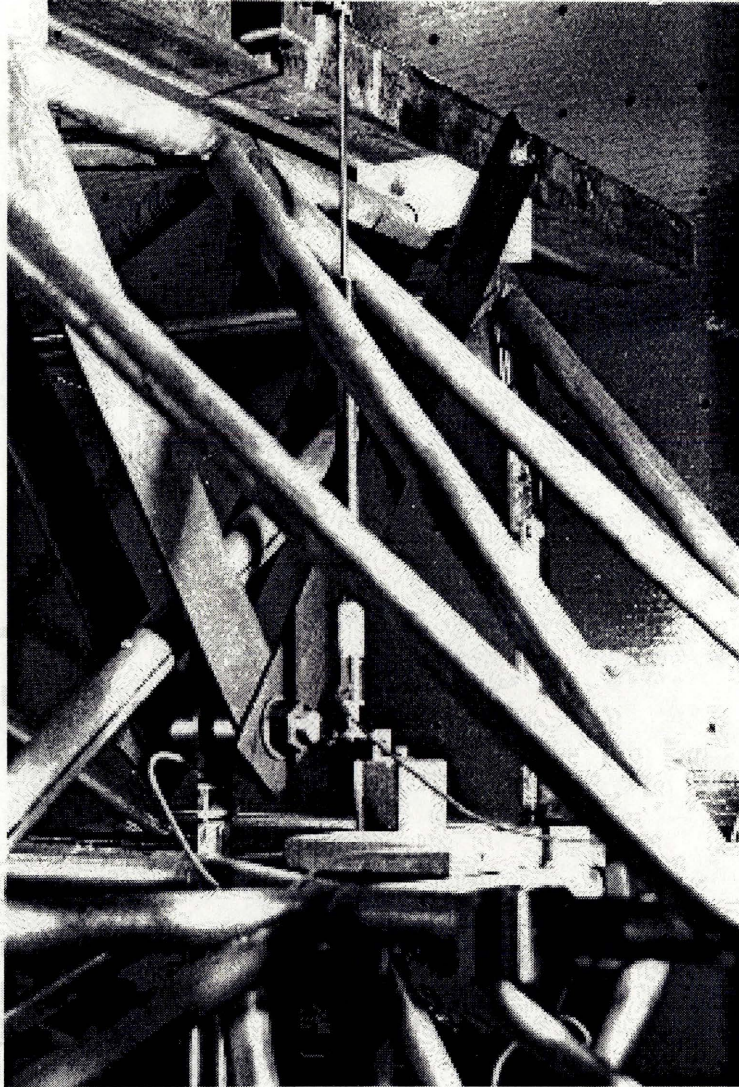


Figure 6.7: Vertical Test Setup - LVDT Location

Once the hoop was deformed for the second time with the structure taking minimal plastic deformation the test was terminated. The nonlinear collapse of the roll hoop under the application of the proof load was to be carried out subsequently and thus the deformation in the rear hoop had to be minimised.

The load was applied steadily to the rear hoop and the load displacement for the two parts of the test are given in Figures 6.2 and 6.5. The displacement was measured using an LVDT mounted as shown in Figure 6.7. These results can be compared to the load displacement curve for the NASTRAN model in Figure 6.6.

From the load displacement data from the test as presented in Figure 6.2 the maximum load carried by the rear hoop, prior to local collapse, was 45.6 kN with a corresponding deflection of 10.7mm. The predicted ultimate collapse load for this arrangement using NASTRAN nonlinear analysis was 59.7 kN with a displacement of 15.4mm. For the test, however, the maximum load to be applied was 55 kN so as to minimise the plastic deformation in the structure. The load applied was thus 17% less than this value.

It is difficult to make a direct comparison between the NASTRAN data and the test results in this instance as the applied load cannot be equated to a particular point in the NASTRAN analysis. It can be seen from the data in Figure 6.2 that the load displacement curve is linear up to approximately 45 kN, and it would thus appear that this is the load at which the local collapse commenced.

Overall the results were favourable considering the simplifications assumed in the modelling and the limitations of the analysis. In addition the material tested had a yield stress which was approximately 25% less than the value assumed for the analysis. The value assumed for the testing was taken from published data as presented in Appendix C.

## 6.2 Frontal Crush Loading

The chassis setup for this test is shown in Figure 6.8. The test was carried out on the same rig as that for the rear hoop test. The test rig was designed based on the loads predicted from the relevant NASTRAN analyses and details of the design are contained in Appendix B.1.

The application of the oblique load on the front windscreen corner of the chassis posed several problems. A simple test apparatus was desired which would allow a displacement of 150mm with an applied load of three tonnes. Several methods were considered for applying the load:

- Use of a three tonne hydraulic cylinder,
- Use of the 150 tonne press in the College of Aeronautics,
- Use of a Tirfor winch and pulleys.

The problem with using a hydraulic cylinder was finding one with the required load capacity combined with a suitable stroke. In the College of Aeronautics it was possible to find cylinders with a suitable capacity but not a suitable stroke. For this reason this option was discounted.

The 150 tonne press was not suitable because the load needed to be applied to the front windscreen corner. The geometry of the chassis would have made this impossible without a large purpose built (and designed) loading frame.



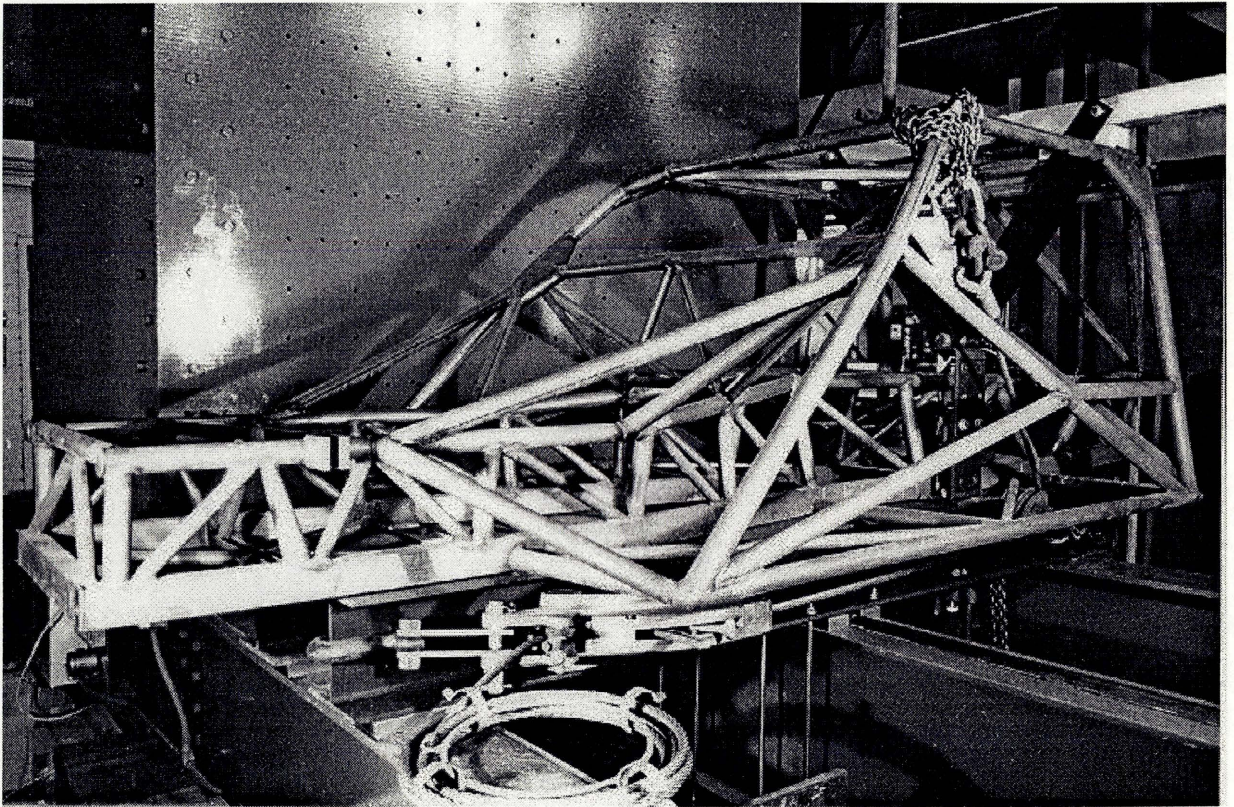


Figure 6.8: Test Rig Setup for the Frontal Crush Loading

The application of the load to the structure also required some design work. A flat plate with attachments to apply the load to the front windscreen corner was considered and several designs were postulated. In all cases a simple method of keeping the plate central on the load point proved to be difficult to design. This was due to the geometry of the bars and their joins in the vicinity of the front windscreen corner. This proposal was discarded in favour of using a set of lifting chains to apply the load. Whilst this may have looked "messy" it seemed to provide the most cost efficient solution for applying the load to the structure.

The final test setup is shown in Figure 6.8. The load was applied with a Tirfor winch<sup>3</sup> which was attached via the load link and a set of chains to the front windscreen corner.

The load was gradually applied by hand, using the winch, and the load and deflection were recorded. The load deflection curve is presented in Figure 6.9. The results from the NASTRAN analysis are presented in Figure 6.10 for comparison.

As the load was applied the deflection increased and the collapse began at the loaded corner. The first hinge formed on the front 'A' Pillar at the lower end of the Gusset. With increasing load a number of other hinges formed in the roll cage and these are all numbered in Figure 6.12. The hinges on the 'A' Pillar occurred in the numerical order indicated (i.e. 1 - 5) and can be seen in detail in Figure 6.11. However, the order of formation for the other hinges (numbered 6 - 8) was not determined as it was difficult to see where they had occurred until the load was removed. In all 5 major buckles occurred as indicated in Figure 6.11 (numbered 1 - 5) and the test was concluded when the limit of travel of the LVDT was reached.

Again it was apparent that the local collapse (buckling) was a major failure mechanism in the collapse. Whilst local buckling was not accounted for with the nonlinear analysis in NASTRAN reasonable results were obtained. The frontal crush load expected from the NASTRAN analysis was approximately 19.38 kN for the model which most closely resembled the test chassis. This model used the two different materials for the Chassis and roll cage and included the webs as per the test chassis. With this load the expected displacement was 25.8mm.

The test results in Figure 6.9 show that the peak load was 20.8 kN and the corresponding deflection was 10.6mm. Thus the measured maximum load was only 7% above that predicted. However, the measured displacement was 60% less than that predicted by the NASTRAN model.

Some caution needs to be exercised when trying to make a direct comparison between the NASTRAN and test results. The theoretical load-displacement curve is presented in Figure 6.10. From this it can be seen that the results are well behaved and approximate an ideal perfectly-plastic model (which is what NASTRAN allows for). The NASTRAN model only allows for plastic hinges to form, no local instability or collapse is allowed for.

Local collapse formed part of the mechanism of failure for the test chassis. The load deflection curve (Figure 6.9) from the test was in contrast to that from the NASTRAN analysis. The test results gave a load peak of 20.8kN and this was followed by a rapid drop in stiffness and load capacity to a minima of 10kn is at a displacement of 25mm. The stiffness then increases again and a maxima of 20 kn is reached at a deflection of 75mm which is followed by another drop to 12kn at a displacement of approximately 107mm (the test was stopped at this point as the LVDT had run out of travel). This phenomena would appear to be consistent with local collapse occurring, the buckle then closes up, the stiffness increases and the load carrying capacity of the structure increases. This will occur several times prior to complete collapse occurring.

---

<sup>3</sup>Compliments of Mr Barry Walker who made it available for the test

# TVR Roll Hoop Crush

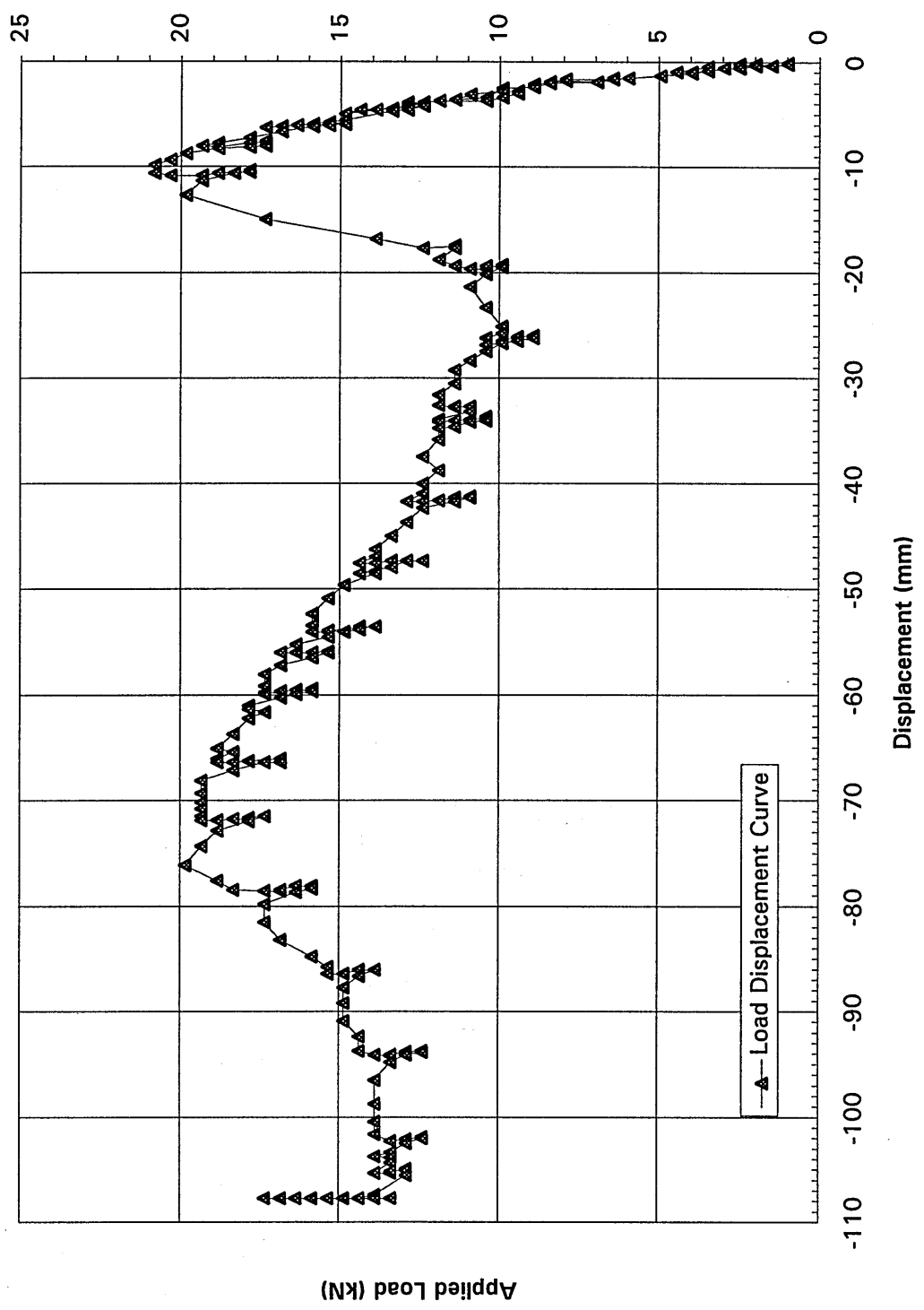


Figure 6.9: Load Deflection Curve for the Front Windscreen Corner.



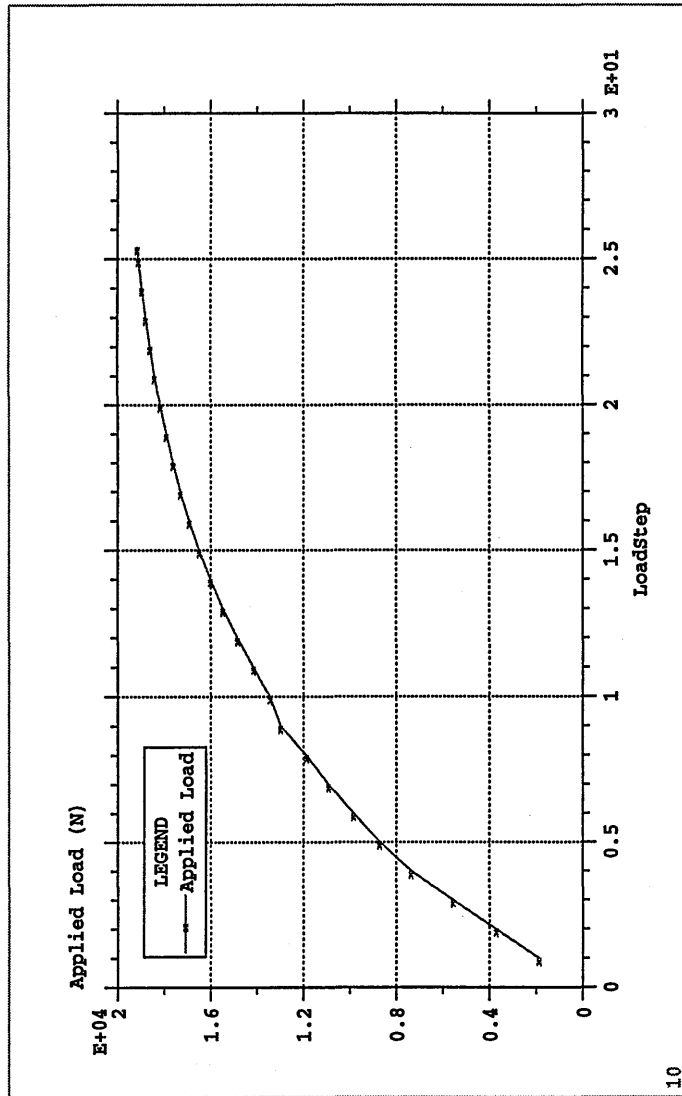


Figure 6.10: NASTRAN Load Deflection Curve

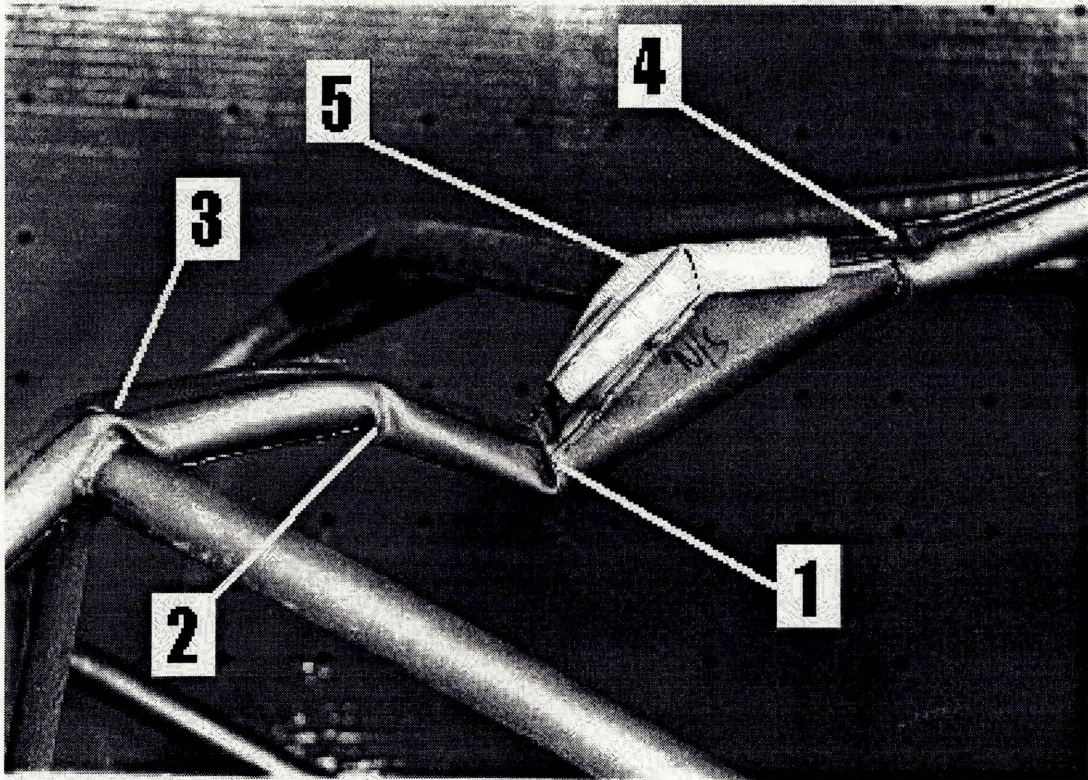


Figure 6.11: Hinge Locations in the "A" Pillar



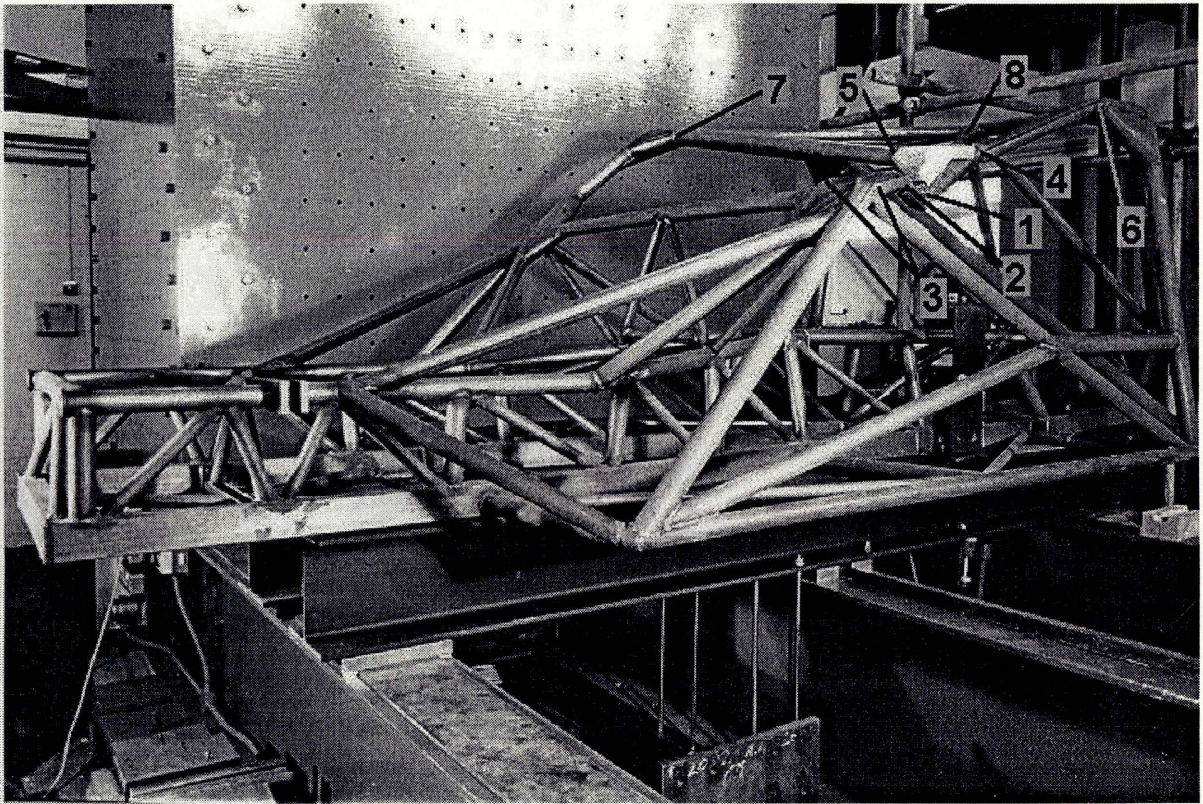


Figure 6.12: Order of Hinge Formation in the Roll Cage





Figure 6.13: Details of the Buckling in the Front Roll Structure



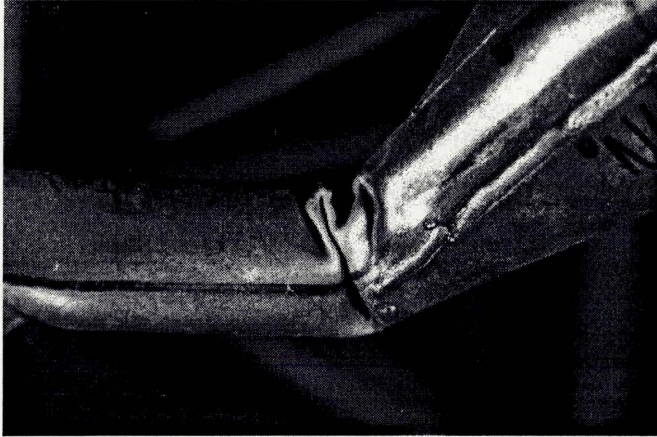


Figure 6.14: Detail of Closed up Buckle (No 1) in Roll Cage



Figure 6.15: Detail of Buckle Number 4 in Roll Cage

As a result of this local collapse occurring the displacement recorded with the peak load does not represent the final collapse displacement and it can be seen that this will be in excess of 107mm. Thus the NASTRAN model, whilst giving a good indication of the load carrying capacity gave a poor indication of the ultimate displacement.

### 6.3 Calibration of Instrumentation

The load was measured using the load cell shown in Figures B.1. The load cell was calibrated prior to the test in order that the loads applied could be determined. The load cell calibration is given in Table 6.1.

The displacements were measured using an LVDT. This was calibrated using known displacement intervals and the displacement calibration figures are given in Table 6.1.

Instrument Calibration Figures		
Instrument	Measurement Units	Calibration Units/Volt
LVDT	mm	25 mm/Volt
Load Cell	kN	101.54 kN/Volt

Table 6.1: Calibration Values for Tests

The calibration figures for these two devices are shown in Figures 6.16 and 6.17 respectively for the load cell and LVDT. These calibration figures were entered into the analysis and logging software which was used to log all the data.



# Load Cell Calibration

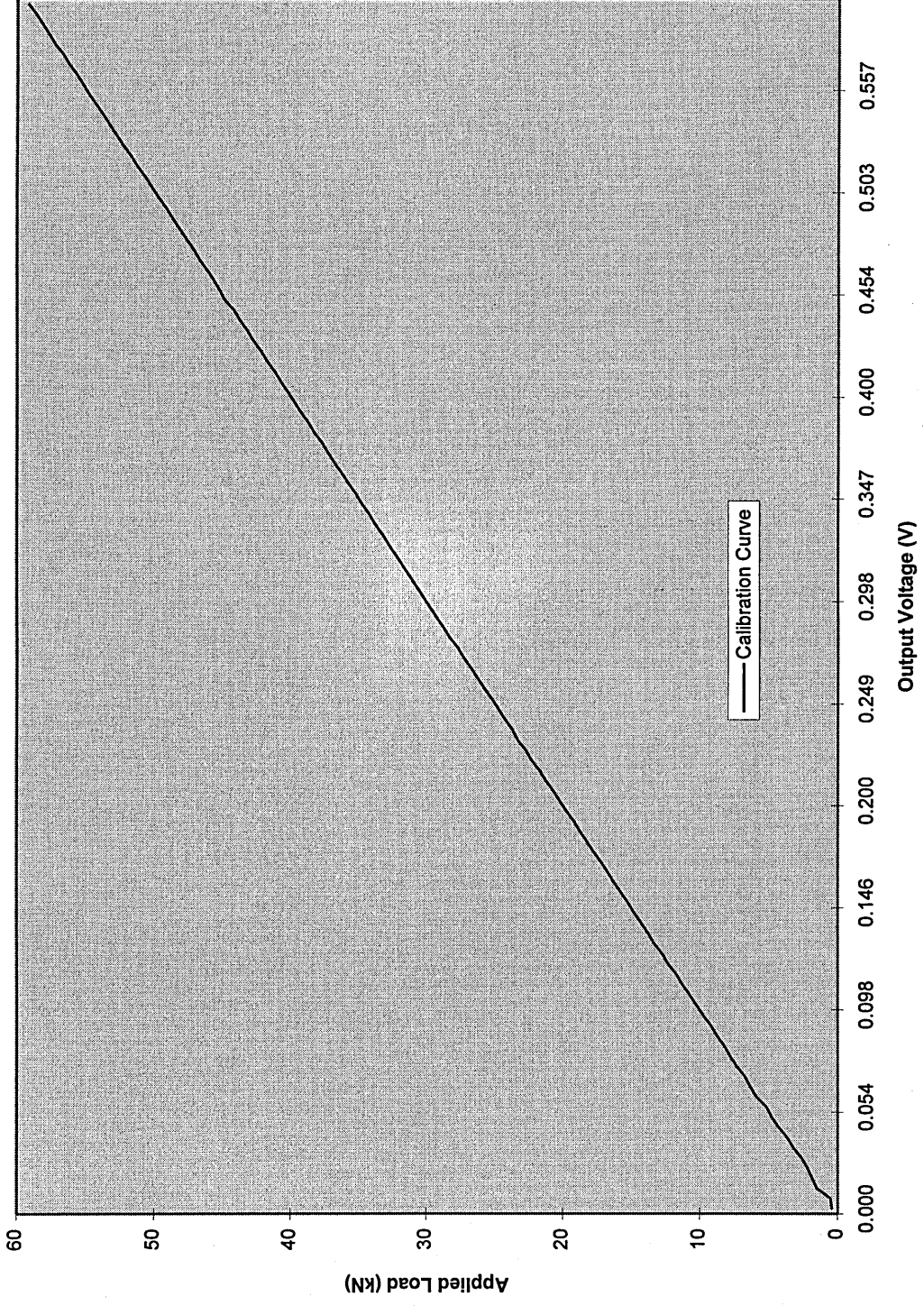


Figure 6:16: Load Cell Calibration Curve

# LVDT Calibration

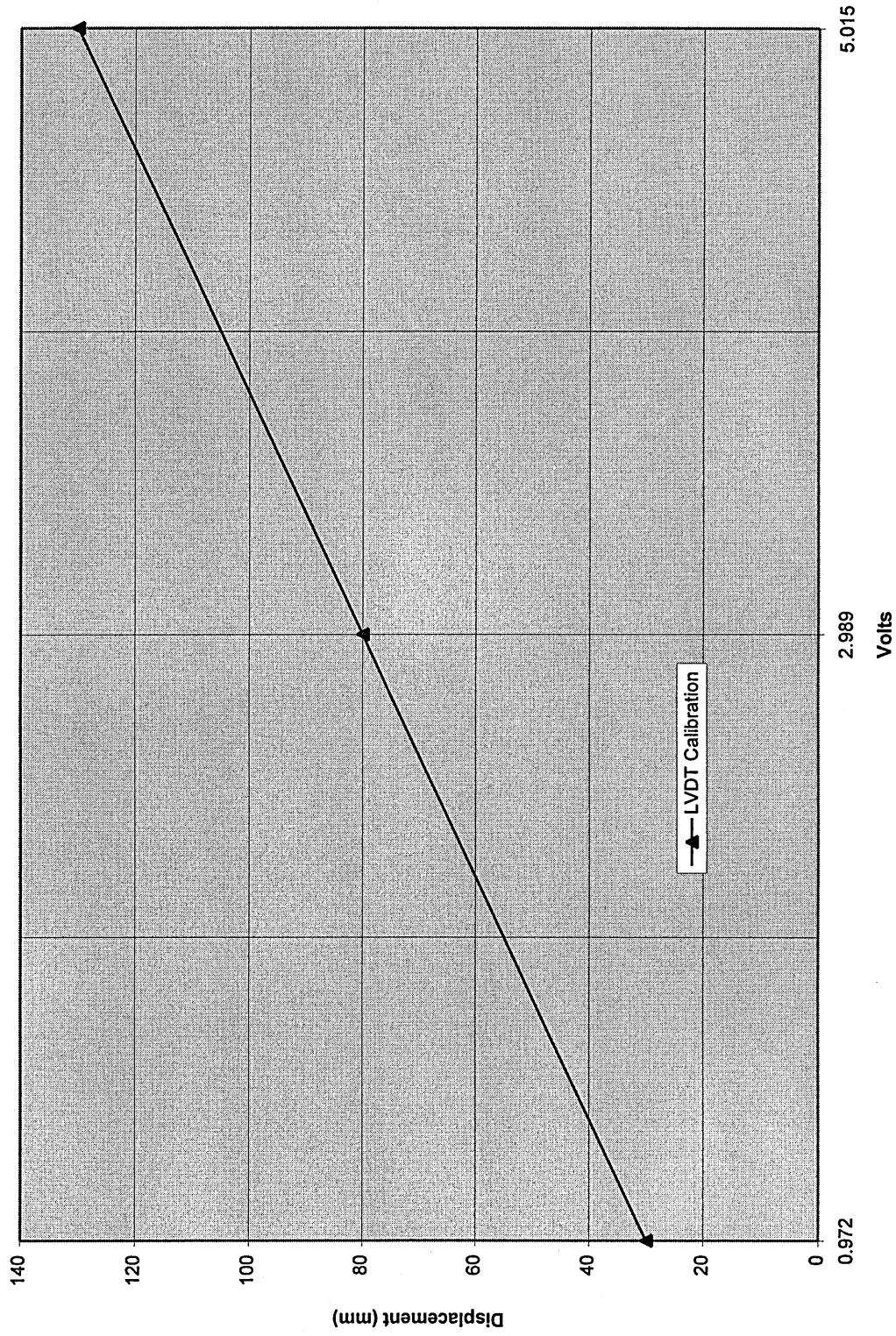


Figure 6.17: LVDT Calibration

# Discussion

The results from each part of the investigation are summarised in the relevant section. The use of Finite Element Analysis to model the torsion stiffness of the chassis gave encouraging results. The value of this technique was evident from the work of Gadola [5] and Wanke [4].

Using the roll structure to improve the torsion stiffness of the chassis proved to be very successful. The torsion stiffness of the original Chimaera chassis of Model A, was 1,827 Nm/deg. This was increased to a maximum value of 13,776 Nm/deg for the Cerbera GT model with front stiffeners detailed in Table 3.14. This represented an increase of over 650% in the torsion stiffness. Due to limitations on space, the maximum practical value of torsion stiffness (which corresponded to the test chassis) was 9,947 Nm/deg. Consequently the torsion stiffness was increased by over 440% from the initial chassis to the final arrangement for the test.

The efficiency of the structure was also increased significantly from 28.5 (Nm/deg)/kg to 92.1 (Nm/deg)/kg which represented an increase of over 220%. This highlighted the value of simple linear analysis for the investigation of the chassis torsion stiffness and the incorporation of major structural modifications to the chassis.

The nonlinear analysis was successful in increasing the load carrying capacity of the roll cage. For the standard Chimaera chassis with a simple roll hoop the maximum load carried was 12,117 N with a deflection of 67.9mm. The load was applied to the rear hoop in an aft direction which represented the stiffest load point. The material for the roll hoop was thicker than that used for the final Cerbera GT models, yet it was still possible to make a significant difference to the load carrying capacity of the rear roll hoop. In the Cerbera GT with the load applied to the rear hoop (with the full roll cage incorporated) it was possible to increase the applied load to 33,658 N with a deflection of 3.29mm. This represented an increase of 178% in load carrying capacity with a reduction in the deflection of 1958%. Even when loading the chassis at the front windscreen corner (the least stiff point on the top of the roll cage) it was possible to achieve load capacities above those for the Chimaera chassis. For the Cerbera GT the maximum load capacity at the front windscreen corner was 19.4kN with a deflection of 25.8mm. This was for a full roll cage of thinner wall than the roll structure for the Chimaera Chassis (i.e. 18swg not 16swg).

The deflected shape of the nonlinear NASTRAN was in close agreement with the test results. The data in Figure 3.54 to 3.57 can be readily compared to the collapsed shape of the test chassis as shown in Figure 6.11 and 6.12. This gave confidence in the ability to use other materials in the structure which had similar collapse mechanisms to those of the ERW 1 tubing. The results for the analysis with T45 materials would thus give a reasonable first estimate as to the collapsed shape of the structure. The location of the plastic hinges will also be in close agreement with the results for the actual chassis.

The model with T45 material properties gave an ultimate load capacity of 45.9kN with a displace-

ment of 69.6mm when the roll cage was loaded at the front windscreen corner. This represented a load 60% below the required RACMSA load capacity of 109 kN, however, this was when loading the structure at its weakest point. Applying the load at the rear hoop corner of the same model (this was the strongest point on the top of the roll structure) resulted in an ultimate load of 103.7kN being carried with a deflection of 5.7mm. This load was only 5% below the required RACMSA value and use of a larger diameter tube in the critical areas would enable the RACMSA load to be carried.

The overall results from the NASTRAN analysis were in good agreement with those from the test as discussed in Section 6.2. Finite element analysis provided an ideal tool for this development work. A small automotive manufacturer would find the cost of testing many chassis' uneconomical, whereas running a series of models would be more efficient and cost effective. This applies to both the linear and nonlinear analyses as detailed above.

# Conclusion

This work illustrates the application of the finite element method to the design and development of an automotive chassis. Traditionally automotive manufacturers of this size would rely on experience for design and development and this would be an evolutionary process. Evolutionary design is not well suited to major modifications as were carried out in this investigation. Finite Element analysis is an ideal method of assisting the design process in a company of this size.

The use of finite element analysis to develop the chassis and roll structure enabled the torsion stiffness of the original Chimaera Chassis to be increased by over 440%. In addition it was possible to increase the weight efficiency of the chassis by over 220% in the final Cerbera GT model.

This type of development was beyond the scope of evolutionary design and the number of analyses performed would not have been possible if they had to be built and tested. It was possible to investigate the difference made by changing the cross section of structural components within the chassis. This investigation resulted in TVR not adopting tubular sections for the main chassis rails due to increase in weight with no real increase in torsion stiffness being realised.

The nonlinear collapse of the chassis in the test was comparable to the results from the NASTRAN analyses. The ultimate load carried and the collapse mechanism were comparable and the results were thus particularly encouraging. It was possible from the results of the analysis on the test chassis to say that the NASTRAN modelling gave a close approximation to the collapsed shape of the structure and located the major plastic hinge nodes. This meant that the results from analyses with different materials should also yield results that were in close agreement with what would be the results for the actual structure. Consequently running models with T45 material would give a good indication as to the structural response of the chassis with a roll cage manufactured from this material attached. This ability would make the use of finite element analysis within a small company cost effective in gaining insight into the structural collapse of simple structures such as the chassis analysed. The ability to analyse a range of structures with differing materials would represent a major cost saving over full scale testing. The technique of non linear analysis using finite element analysis thus shows a great deal of promise to this area of application.

The use of finite element analysis in this instance was a new application of an existing technique. The use of material nonlinear analysis was found to be of great benefit in gaining an insight into which material to use for the roll cage structure. This type of analysis was time consuming in terms of run time, however, still represented a cost effective method of analysing the structure.

It is hoped that this application of FE analysis to an old problem will encourage other users to investigate the application of computer analysis in new areas where it can offer cost effective solutions to engineering problems.

# Bibliography

- [1] Baker, J. & Heyman, J. *Plastic Design of Frames Part 1 - Fundamentals*, Cambridge University Press, 1969.
- [2] Boresi, A.P.; Schmidt, R.J.; Sidebottom, O.M. *Advanced Mechanics of Materials - 5th edition*, John Wiley and Sons, 1993.
- [3] Buchanan, G.R. *Mechanics of Materials*, Holt Rinehard and Winston Inc., 1988.
- [4] Wanke, T.R. *Finite Element Analysis of the Torsional Stiffness of a Sports Racing Car Chassis*, MSc Thesis, Cranfield University, 1994.
- [5] Gadola, M. *Sports Racing Car Chassis Analysis*, MSc Thesis, Cranfield Institute of Technology, 1992.
- [6] Pawlowski, J. *Vehicle Body Engineering*, Business Books Ltd., London, 1969
- [7] Newton, K; Steeds, W; Garrett, T.K. *The Motor Vehicle*, 10th Edition, Butterworths, London, 1983.
- [8] MacNeal Schwendler Corporation, *Handbook of Nonlinear Analysis*
- [9] MacNeal Schwendler Corporation, *Handbook of Linear Analysis*
- [10] RAC Motor Sports Association Ltd., *British Motor Sports Yearbook 1994*, Royal Automobile Club Motor Sports Association, 1994.
- [11] Young, W.C. *Roark's Formulas for Stress and Strain*, 6th Edition, McGraw Hill Inc., 1989.
- [12] Deutschman, A.D.; Michels, W.J.; Wilson, C.E. *Machine Design - Theory and Practice*, Macmillan Pub. Co., 1975.
- [13] Timoshenko, S.P.; Gere, J.M. *Mechanics of Materials*, 2nd Edition, Wadsworth Int., 1985.
- [14] Coates, R.C.; Coutie, M.G.; Kong, F.K. *Structural Analysis*, 2nd Edition, Thomas Nelson & sons Ltd., 1980.
- [15] Shigley, *Mechanical Engineering Design?*
- [16] Bruhn, *Analysis and Design of Flight Vehicle Structures*, Jacobs Publishing Inc, 1973.
- [17] Barstow, D & Howard, G.P. *Car Suspension and Handling*, 3rd Edition, Pentech Press, London, 1993.
- [18] Ellis, J.R. *Vehicle Handling Dynamics*, Mechanical Engineering Publications, London, 1993



- [19] Staniforth, A. *Competition Car Suspension*, Haynes Publications Inc., Somerset, UK, 1988.
- [20] Ford, H., *Advanced Mechanics of Materials*, Longman Group, London, 1972.
- [21] Collins, J.A., *Failure of Materials in Mechanical Design*, Wiley Interscience Publication, 1981.
- [22] Hoole, G.A.; Kinne, W.S., *Stresses in Framed Structures*, McGraw Hill Company, 2ed, 1942.
- [23] Oberg, E.; Jones, F.; Horton, H., *Machinery's Handbook*, 21st Edition, Industrial Press Inc, NY, 1979.

## Appendix A

# RAC Motor Sports Requirements

In the United Kingdom the control of automobile sports is governed by the Royal Automobile Club Motor Sports Association (RACMSA). This took effect on 1st January 1979 and was with agreement of the Royal Automobile Club (RAC) and the RAC British Motor Sports Council and is recognised by the world governing body, Federation Internationale de l'Automobile (FIA).

In the United Kingdom the British Motor Sports Yearbook, familiarly known as the *Blue Book*, contains all the basic regulations required to take part in four wheeled Motor Sport in the United Kingdom. Whilst the RACMSA is the controlling body for motor sport in the UK, the FIA is the International controlling body. The FIA have there own set of rules which are contained in the FIA Yearbook of Automobile Sport, usually known as the *Yellow Book*.

The *Blue Book* also provides design guidelines for the production of roll bars and cages for racing events. These guidelines specify a minimum material grade and sizes to be used. In conjunction with these there are "approved" designs of roll cages which don't need certification if produced as shown in Figures A.1 - A.2. Additionally there are figures showing approved joints, mountings and minimum bolt sizes and grades. Thus, the whole design process for roll cages for these events is somewhat of a "cookbook" approach. This is not necessarily a bad approach as it ensures that competitors produce a roll cage that experience has shown will provide at least the minimum required protection in the case of a roll over accident.

Should an individual wish to design their own roll cage for use in racing under these rules then it is necessary to get an approval which is based on a set load carrying capacity. The determination of the suitability is based on calculations by a recognised expert (approved by the RACMSA) and/or by a physical test. Generally the loading applied to a new roll cage/bar is a vertical load as specified in the *Blue Book* applied to the main roll hoop.

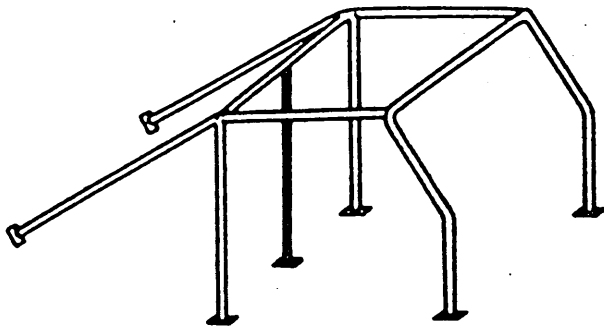
The rollcage requirements from both the *Blue* and *Yellow Book* were considered and the major design criteria are noted in this section.

### A.1 Technical Requirements - Section E

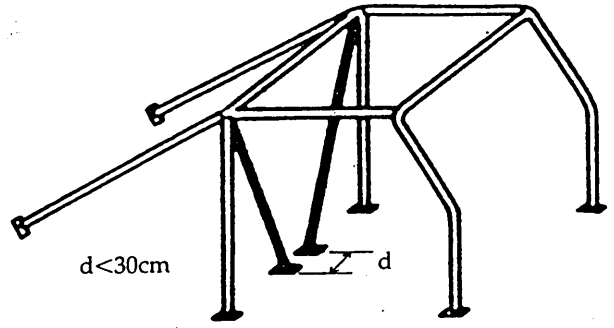
The following mandatory requirements were considered to be applicable to roll cage design as applied to the TVR Chassis.

Q

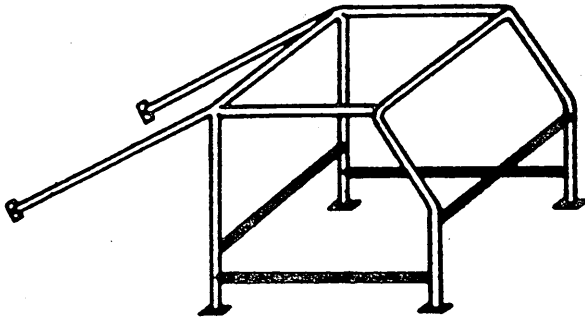
GENERAL REGULATIONS



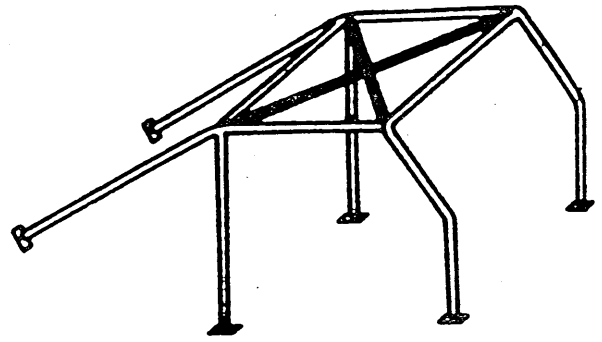
Drawing No. 7



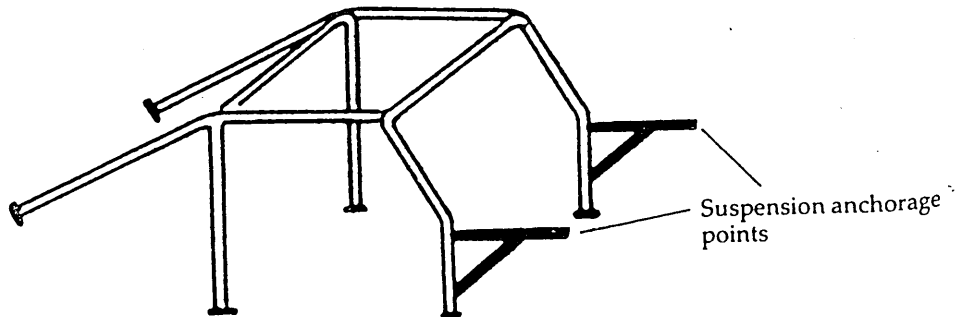
Drawing No. 8



Drawing No. 9

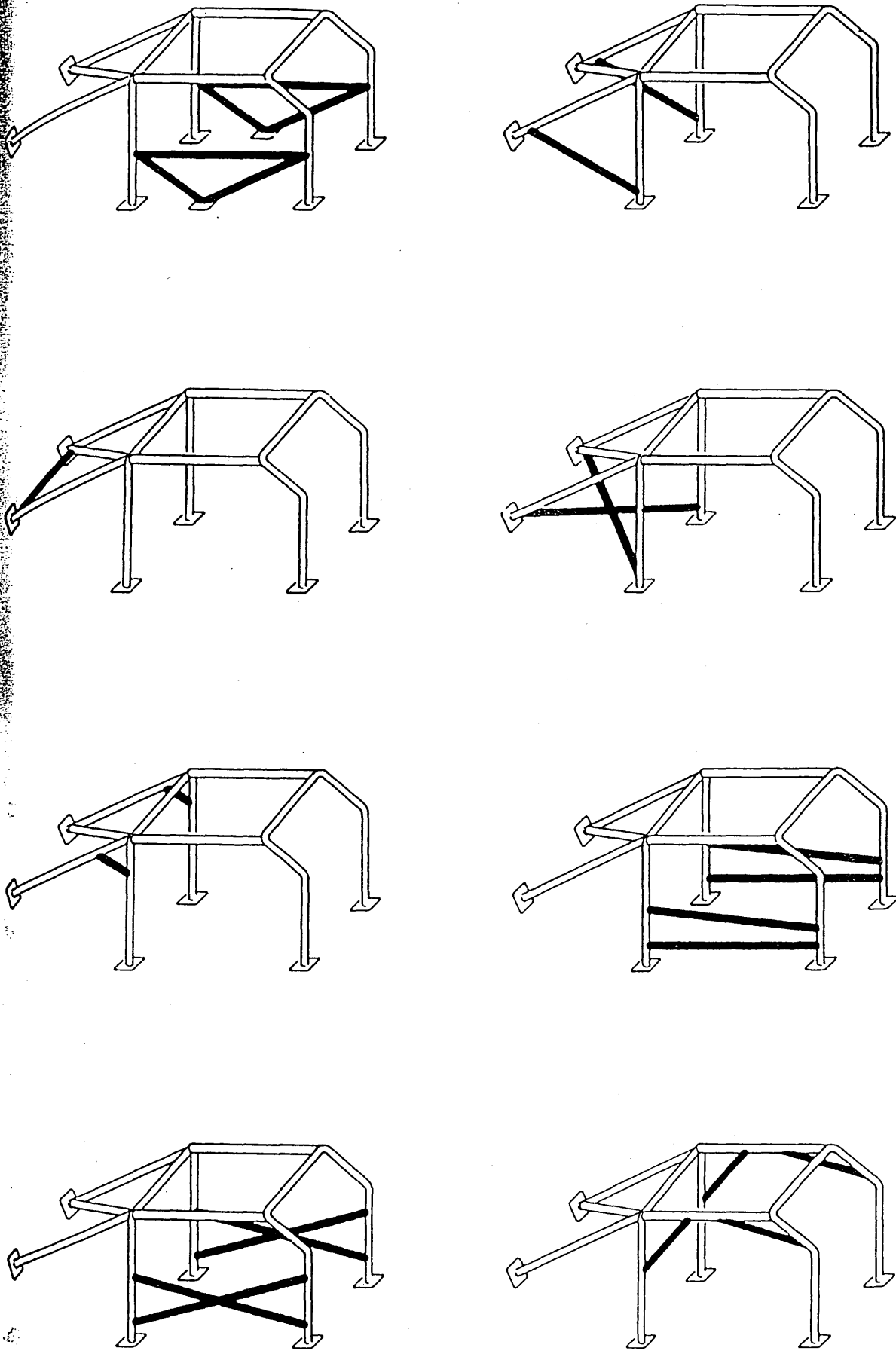


Drawing No. 10



Drawing No. 11

214  
Figure A.1: RAC Approved Roll Cage Designs



Drawing No. 12 Optional Reinforcing Members (1.1.3)

- *Clause 13*

The following technical regulations are mandatory and apply to vehicles in all forms of competition (other than carting). In addition vehicles must comply with the appropriate Specific Technical Regulations. Where there are several regulations concerning any particular subject it shall be taken, as a general principle, that one does not override another unless specifically stated.

All Vehicles must:

- *Clause 13.2.5*

Not have the space normally occupied by passengers encroached upon, but may have the passenger seats removed.

- *Clause 13.2.6*

With the exception of racing cars, or cars built before 1941, have bodywork providing a minimum transverse COCKPIT OPENING width of 81cm. This width may not be interrupted. *Precludes the use of any addition to the roll structure in the vehicle interior to add stiffness as does Clause 13.2.5*

- *Clause 13.2.9*

If originally fitted with driver/passenger doors, hatchback doors, sliding doors, opening boots, or tailgates, these must be secured in the closed position during events. *This allows for the use of door bars which are welded into the roll cage as there is no requirement for the door to open*

## A.2 Specific Technical Regulations for Car Racing - Section J

In addition to complying with Section E, Clause 13 and the appropriate formula Regulations where applicable, all vehicles competing in races must:

- *Clause 20.14.1*

Be fitted with a SAFETY ROLL-OVER BAR complying with RACMSA requirements:

- (a) if required by specific Formula Regulations.
- (b) If a single seater or sports racing car built after 1959.
- (c) If a closed car built after 1959 fitted with a non standard body.  
(eg Lightened body sections, doors or bonnet).
- (d) If an open car built after 1959.

It is strongly recommended that all vehicles be fitted with a SAFETY ROLL-OVER BAR.

- *Clause 20.14.3*

If fitted with lightened non-standard doors be fitted with a HORIZONTAL SAFETY BAR across the door(s) aperture below the line of the window and at a suitable height to protect the driver. *This must not be integral with the door.*

## A.3 Nomenclature and Definitions - Section P

The following definitions are taken from this section of the *Blue Book*:

- **Adequate Strength:**

That the component concerned is of sufficient strength to fulfil the function for which it was intended.

- **Main Chassis Structure:**

(a) Single seater racing cars - the fully sprung structure of the vehicle to which the suspension and/or spring loads are transmitted, extending longitudinally from the foremost front suspension mounting on the chassis to the rearmost one.

(b) Other vehicles - the entire original shell supporting chassis frame of the original body/chassis structure from which nothing may be removed except by normal removal of nuts and/or bolts. No part may be removed by cutting, fracturing or derivetting.

## A.4 Safety Criteria - Section Q

The majority of the relevant information is contained in this section of the *Blue Book* and these are included in full in Appendix H and are summarised in this section.

If a roll cage is designed to the requirements of Section Q then it is deemed to be suitable for racing. If, however, a manufacturer wants to submit his own roll cage design then the construction must be certified to withstand the forces given hereafter in any combination on top of the Safety Cage:

1.5w Lateral

5.5w Fore and Aft

7.5w Vertical

where w = weight of the car + 75kg (for the driver).

- *Clause 1.4.2*

To obtain RACMSA approval, a manufacturer must have demonstrated his consistent ability to design and manufacture safety cages which comply with the specifications approved by the FIA.

- *Clause 1.4.*

Manufacturers recognised by the RACMSA must only supply customers with products designed and manufactured to the approved standards.

- *Clause 1.4.4*

Each RACMSA approved manufacturer must be able to demonstrate to the RACMSA:

(a) That the material used has a certificate of origin or traceability and is kept segregated from other batches of material.

(b) That welding procedures used produce consistent and sound welds and are regularly checked by laboratory tests.

(c) That an auditable in-house quality standards and procedures system is operated and that these are updated regularly.

- *Clause 1.7*

It should be noted that International Safety Roll Over Structure Regulations were issued



by the FIA and became mandatory on 1.1.94. The RACMSA has aligned itself with these regulations where possible.

It was reported to the author that there are nearly no tests carried out on roll cages for sports racing cars. It is generally accepted that if the roll cage is designed according to one of the approved designs and is certified as such by an authorised manufacturer then it is deemed satisfactory.

In an effort to allocate more science to roll cage design it was proposed that a non-linear finite element analysis would give a good indication of the true load carrying capacity and deflection under load of the roll cage/frame. The analysis carried out was verified by physical tests on a full scale chassis.

## Appendix B

# Test Rig Design and Analysis

The chassis test rig was designed using the data from the NASTRAN analyses. These analyses gave estimates of both the loads that needed to be reacted and the collapse loads that needed to be applied to the structure. The design of the test rig to apply the forces at the correct angles is detailed below. In addition the design and stressing of the mountings are detailed.

### B.1 Test Rig Design

The general arrangement of the test rig showing the locations of the mounting points is contained in Figure B.1.

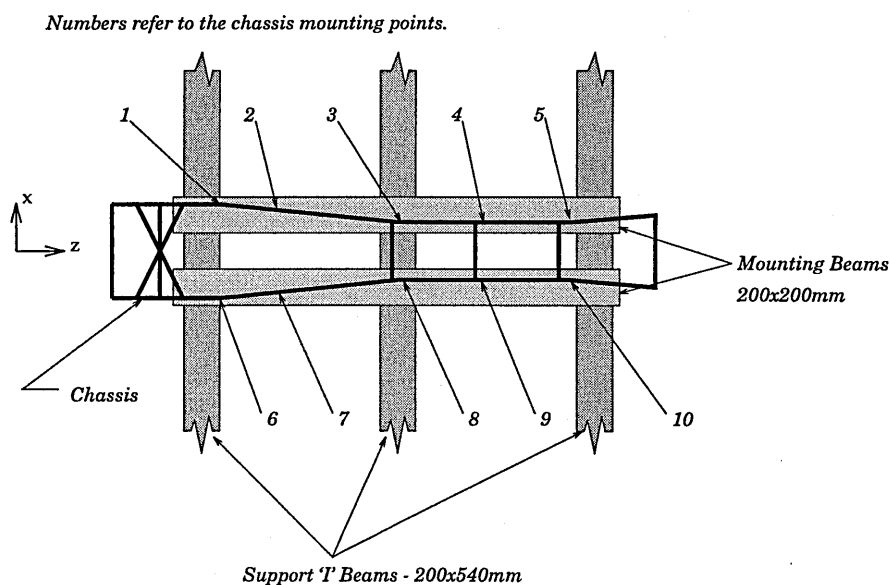


Figure B.1: Chassis Mounting for Tests

Within the College of Aeronautics the Crash Test support frame was the most suitable place to test the chassis. Initially it was hoped to use the 150 ton press, however, the loading of the chassis with an oblique load would not have been feasible due to dimensional constraints. The use of the crash support frame would allow free access around the chassis but the application of the load required some thought. Figure B.1 shows the support frames, the chassis mounting frames and the base

section of the chassis.

### B.1.1 Design of Mounting Beam Clamps

The chassis was located so that the front roll hoop was over the centre support beam as shown in Figure B.2. This was done as the major force component was in the vertical plane and this resulted in its application over the stiffest location on the support frame. Additionally there were the longitudinal and lateral load components to be reacted.

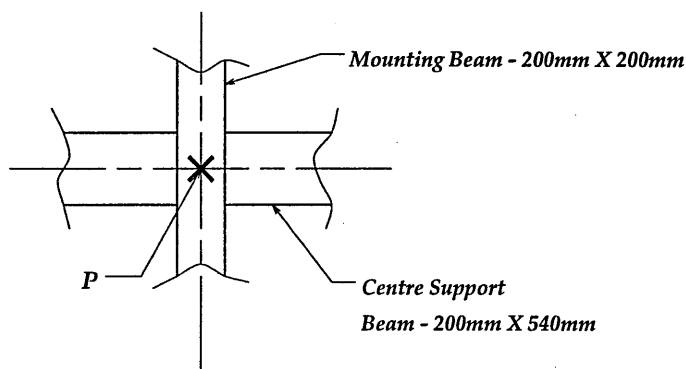


Figure B.2: Relative Location of Load Point to Chassis Mounting Beams for Tests

The final support design consisted of a simple 'clamp' arrangement over the centre beam as shown in the drawings of Appendix J. The calculations for the clamp design are contained below. Simplifications are noted and the reserve factors detailed.

The non-linear finite element analysis was used to predict the collapse load for the structure when loaded at the front windscreen corner. From this analysis the collapse load was 21 kN, however, to be conservative another case was considered with an applied load of 35 kN. The RACMSA requirements state that a load of  $(1.5w \hat{i} + 7.5w \hat{j} + 5.5w \hat{k})$  must be able to be supported at any location on the top of the roll cage. For the TVR chassis analysed,  $w = 1,175 \text{ kg}$ . The resulting load to be carried was 108.6 kN, however, this was not achieved and the calculations for mounting attachments with this load are instructive only.

The load components for each load case are given in Table B.1.

Loads Applied to Chassis				
Case Number	Applied Load kN	$F_x$ N	$F_y$ N	$F_z$ N
1	21	3,344	- 16,718	12,260
2	35	5,573	- 27,864	20,434
3	108.6	17,290	- 86,451	63,397

Table B.1: Load Components Applied to Chassis

From the geometry of the chassis, its mounting and the loaded point we have the situation illustrated in Figure B.3 with simplified mounting attachments as shown. Calculating the forces acting,

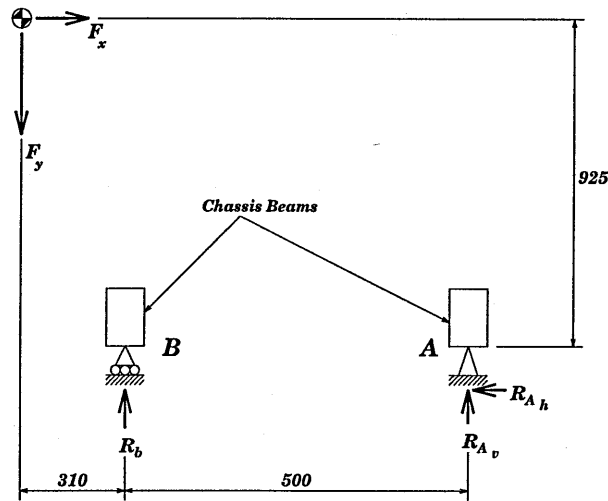


Figure B.3: Chassis Mountings in Relation to the Load

$$\begin{aligned}
 \sum M_A &= 0 \\
 810F_y - 925F_x - 500R_B &= 0 \\
 \therefore R_B &= \frac{810F_y - 925F_x}{500}
 \end{aligned} \tag{B.1}$$

Summation of the vertical forces gives,

$$\begin{aligned}
 + \uparrow \sum V_F &= 0 \\
 -F_y + R_B + R_{A_v} &= 0 \\
 \therefore R_{A_v} &= F_y - R_B
 \end{aligned} \tag{B.2}$$

Summation of the Horizontal Forces,

$$\begin{aligned}
 \rightarrow \sum H_F &= 0 \\
 F_x - R_{A_h} &= 0 \\
 \therefore R_{A_h} &= F_x
 \end{aligned} \tag{B.3}$$

Thus substitution of the loads from Case 1 into equations (B.1), (B.2) and (B.3),

$$\begin{aligned}
 R_B &= \frac{810F_y - 925F_x}{500} \\
 &= \frac{810(16,718) - 925(3,344)}{500} \\
 \therefore R_B &= 20,897 \text{ N } \uparrow
 \end{aligned}$$

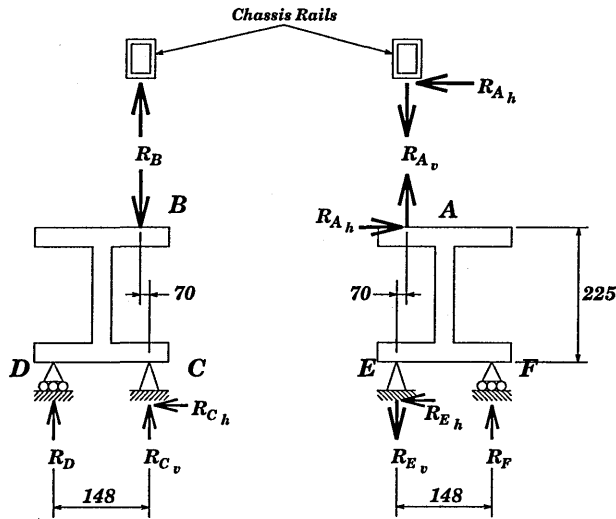


Figure B.4: Mounting Beam Loads

Vertical Forces,

$$\begin{aligned}
 R_{A_v} &= F_y - R_B \\
 &= 16,718 - 20,897 \\
 \therefore R_{A_v} &= -4,179 \text{ N} \\
 \therefore R_{A_v} &= 4,179 \text{ N} \downarrow
 \end{aligned}$$

The resultant load  $R_{A_v}$  thus acts downwards and not upwards as assumed.

Horizontal Forces,

$$\begin{aligned}
 R_{A_h} &= +3,344 \text{ N} \\
 \therefore R_{A_h} &= 3,344 \text{ N} \leftarrow
 \end{aligned}$$

In the direction assumed.

Substituting the relevant values from Case 1, Case 2 and Case 3 gives reactions of,

Reaction Loads on Chassis				
Case Number	Applied Load kN	$R_B$ N	$R_{A_v}$ N	$R_{A_h}$ N
1	21	20,897 ↑	4,179 ↓	3,344 ←
2	35	34,830 ↑	6,966 ↓	5,573 ←
3	108.6	108,064 ↑	21,613 ↓	17,290 ←

Table B.2: Reaction Loads at the Lower Chassis Rails

These reactions can then be translated onto the mounting beams as shown in Figure B.4.

If the reaction B is considered first:

$$\sum M_c = 0$$

$$\begin{aligned}
 70R_B - 148R_D &= 0 \\
 \therefore R_D &= \frac{70R_B}{148}
 \end{aligned} \tag{B.4}$$

Summation of the vertical forces,

$$\begin{aligned}
 + \uparrow \sum V_F &= 0 \\
 -R_B + R_{C_v} + R_D &= 0 \\
 \therefore R_{C_v} &= R_B - R_D
 \end{aligned} \tag{B.5}$$

In the horizontal direction there is no applied force thus,

$$R_{C_h} = 0$$

Substituting the data for Case 1 into equations (B.4) and (B.5),

$$\begin{aligned}
 R_D &= \frac{70(20,897)}{148} \\
 \therefore R_D &= 9,884 \text{ N } \uparrow
 \end{aligned}$$

and, for the vertical forces,

$$\begin{aligned}
 R_{C_v} &= 20,897 - 9,884 \\
 \therefore R_{C_v} &= 11,013 \text{ N } \uparrow
 \end{aligned}$$

Substitution of the relevant values noting that there is no horizontal reaction at  $C$  for each case gives,

Mounting Beam Reactions				
Case Number	Applied Load kN	$R_D$ N	$R_{C_v}$ N	$R_{C_h}$ N
1	21	9,884 $\uparrow$	11,013 $\uparrow$	0
2	35	16,474 $\uparrow$	18,356 $\uparrow$	0
3	108.6	51,111 $\uparrow$	56,953 $\uparrow$	0

Table B.3: Mounting Beam Reaction Loads

Considering the forces applied at A:

$$\begin{aligned}
 \sum M_E &= 0 \\
 70R_{A_v} + 148R_F - 225R_{A_h} &= 0 \\
 \therefore R_F &= \frac{225R_{A_h} - 70R_{A_v}}{148}
 \end{aligned} \tag{B.6}$$

Summation of the vertical forces,

$$\begin{aligned}
 + \uparrow \sum V_F &= 0 \\
 -R_{E_v} + R_{A_v} + R_F &= 0 \\
 \therefore R_{E_v} &= R_{A_v} + R_F
 \end{aligned} \tag{B.7}$$



Summation of the horizontal forces,

$$\begin{aligned} \vec{\uparrow} \sum H_F &= 0 \\ -R_{E_h} + R_{A_h} &= 0 \\ \therefore R_{E_h} &= R_{A_h} \end{aligned} \quad (\text{B.8})$$

Substitution of the forces for Case 1 into equations, (B.6), (B.7) and (B.8),

$$\begin{aligned} R_F &= \frac{225(3,344) - 70(4,179)}{148} \\ \therefore R_F &= 3,107 \text{ N } \uparrow \end{aligned}$$

For the vertical forces,

$$\begin{aligned} R_{E_v} &= 4,179 + 3,107 \\ \therefore R_{E_v} &= 7,286 \text{ N } \downarrow \end{aligned}$$

The horizontal force balance gives,

$$R_{E_h} = 3,344 \text{ N } \leftarrow$$

Substitution of the relevant values for each case gives,

Mounting Beam Reactions				
Case Number	Applied Load kN	$R_F$ N	$R_{E_v}$ N	$R_{E_h}$ N
1	21	3,107 $\uparrow$	7,286 $\downarrow$	3,344 $\leftarrow$
2	35	5,178 $\uparrow$	12,144 $\downarrow$	5,178 $\leftarrow$
3	108.6	16,063 $\uparrow$	37,676 $\downarrow$	17,290 $\leftarrow$

Table B.4: Reactions at Mounting Beam Base

From the preceding analysis the worst case loads were:

Maximum Reaction Loads			
Case Number	Applied Load kN	Tensile Maximum N	Shear Maximum N
1	21	7,286	3,344
2	35	12,144	5,573
3	108.6	37,676	17,290

Table B.5: Tensile and Shear Maximum Loads

In all calculations of the material sizes and the bolt sizes, factors of safety were applied. This was not really necessary for a test rig which had to survive one test only. It was considered good engineering practice to design the test rig to be used many times and as a consequence the factors of safety were applied as detailed.

The bolt sizes required to retain the chassis were calculated using the loads in Table B.5. The yield stress of the mild steel rods was taken to be  $250 \text{ MPa}$  with a factor of safety of 1.5 used to give the allowable working stress,

$$\sigma_a = \frac{\sigma_y}{1.5} = 140 \text{ MPa}$$

As discussed in Section B.2 the maximum shear stress was taken as  $\tau_{max} = 0.577\sigma_y$  and thus the allowable shear stress with a factor of safety of 1.5 is  $\tau_a = 96 \text{ MPa}$ . These allowable stresses were used to calculate the bolt diameters,

Case 1:

$$d_{1t} = \sqrt{\frac{4(7,286)}{140 \times 10^6(\pi)}} = \phi \ 8.1 \text{ mm} \quad (\text{B.9})$$

$$d_{1s} = \sqrt{\frac{4(3,344)}{96 \times 10^6(\pi)}} = \phi \ 6.7 \text{ mm} \quad (\text{B.10})$$

Case 2:

$$d_{2t} = \sqrt{\frac{4(12,144)}{140 \times 10^6(\pi)}} = \phi \ 10.5 \text{ mm} \quad (\text{B.11})$$

$$d_{2s} = \sqrt{\frac{4(5,573)}{96 \times 10^6(\pi)}} = \phi \ 8.6 \text{ mm} \quad (\text{B.12})$$

Case 3:

$$d_{2t} = \sqrt{\frac{4(37,676)}{140 \times 10^6(\pi)}} = \phi \ 18.5 \text{ mm} \quad (\text{B.13})$$

$$d_{2s} = \sqrt{\frac{4(17,290)}{96 \times 10^6(\pi)}} = \phi \ 15.1 \text{ mm} \quad (\text{B.14})$$

In designing the bolted joints the diameter calculated from the stress analysis was for the root diameter of the bolt. This may be somewhat conservative as the threads will carry some of the load. For a metric thread the thread depth [15] is given by,

$$d_m = D - 1.0825p$$

where,  $d_m$  is the minor bolt diameter,  $D$  is the nominal bolt size or major diameter, and,  $p$  is the thread pitch (all dimensions are in mm). Thus rearranging this equation to give a bolt diameter for a given root diameter,

$$D = d_m + 1.0825p \quad (\text{B.15})$$

With a root diameter of  $10.5 \text{ mm}$  substitution gives,

$$D = 10.5 + 1.0825(1.75) = 12.4 \text{ mm}$$

Chassis Mounting Loads			
Mounting Point	Force (x) N	Force (y) N	Force (z) N
1	-336	3,078	-1,939
2	-1,190	2,801	1,966
3	-2,679	6,276	-500
4	494	4,758	4,998
5	6,461	-12,211	-14,059
6	5,043	-11,732	4,852
7	-246	679	-4,825
8	-2,110	-4,776	7,788
9	-1,762	4,205	15,068
10	-284	-10,042	-1,450
Total	3,391	-16,964	12,439

Table B.6: Chassis Mounting Forces for 21kN Applied Load

Which was the minimum bolt size for this application. In this case 1/2" (12.7 mm) bolts were used.

The design calculations assume that one of the bolts in the joint takes the entire load. The clamp actually consisted of four bolts and thus the design assumptions were very conservative. The final arrangement of the clamp is shown in Appendix J.

## B.2 Chassis Attachments to Mounting Frame

The chassis was to be mounted on two 'I' beams (columns) as discussed above. From the nonlinear analysis of the chassis the load for failure of the structure was calculated to be approximately 21kN. This load was applied to the structure and the reactions determined. To allow for any variation between the actual finite element modelling and the test two load cases were investigated. The first was 21kN and the second was 35kN. It was decided that this would be sufficient for the test to be carried out successfully (i.e. and overshoot of 67%).

From the analysis and design of the test rig in Appendix B.1 the locations of the mountings for the lower chassis rails was decided. These are shown in Figure B.1 and the loads acting at the relevant points are tabulated in Table B.6 and Table B.7. In both cases the applied loads could be equated to the reaction forces on the base which was to be expected and verified the loads and reactions.

For these load cases the mountings which reacted combined tensile and shear loads were considered to be critical. All the mountings, however, were analysed for completeness. The lateral and longitudinal forces were added vectorially to give an equivalent shear load with the tensile load being taken on its own. In addition the combined effect of these two stresses is discussed in Appendix B.2.1.

The bolt design was carried out for both grade 8.8 and 4.6 steel. The sample calculation below is for bolt 9 using grade 8.8 steel with a load of 35kN applied to the chassis. The properties for the different bolt material grades are given in Appendix C.

$$\sigma = \frac{P}{A} \quad (\text{B.16})$$

Chassis Mounting Loads			
Mounting Point	Force (x) N	Force (y) N	Force (z) N
1	-549	5,037	-3,173
2	-1,947	4,584	3,217
3	-4,383	10,270	-817
4	809	7,786	8,179
5	10,574	-19,982	-23,005
6	8,252	-19,198	7,937
7	-403	1,111	-7,896
8	-3,453	-7,816	12,744
9	-2,883	6,881	25,541
10	-464	-16,432	-2,373
Total	5,553	-27,759	20,354

Table B.7: Chassis Mounting Forces for 35kN Applied Load

where  $P$  is the applied load and  $A$  is the cross sectional area of the bolt. This equation can be rearranged making  $A$  the subject,

$$A = \frac{P}{\sigma} \quad (\text{B.17})$$

Equation (B.17) was then used to calculate the diameter of the bolt required to carry the load. Writing,

$$A = \frac{\pi d^2}{4} \quad (\text{B.18})$$

Substituting into equation (B.17) yields,

$$\begin{aligned} \frac{\pi d^2}{4} &= \frac{P}{\sigma} \\ \therefore d &= \sqrt{\frac{4P}{\pi\sigma}} \end{aligned} \quad (\text{B.19})$$

From Appendix C, Table C.3 the yield stress of grade 8.8 bolts is 635 MPa and the Ultimate Tensile stress is 830 MPa. The most conservative approximation of the maximum shear yield stress is  $\tau = 0.5(\sigma_y)$ , however, the *von Mises-Hencky or Shear Energy theory* gives the shear yield stress as  $\tau = 0.577(\sigma_y)$  and experiments show this is a more realistic value [15]. A factor of safety of 1.5 is used for all the bolted joints. Thus the allowable yield stress is 425 MPa and the allowable shear yield strength is 245 MPa.

For a tensile load of  $P = 6,881$  N substitution into equation (B.19) gives,

$$d = \sqrt{\frac{4(6,881)}{\pi(425 \times 10^6)}} = 0.0045 \text{ m} = 4.5 \text{ mm}$$

For the shear loads the shear stress is given by,

$$\tau = \frac{P}{A} \quad (\text{B.20})$$

Mounting Bolt Sizing				
Mounting Point	Tensile Load N	Diameter mm	Shear Load $\sqrt{F_x + F_z}$ N	Diameter mm
Grade 8.8 Steel - Allowable Tensile Stress 425 MPa				
1	3,078	3.0	1,968	3.2
2	2,801	2.9	2,298	3.5
3	6,276	4.3	2,725	3.8
4	4,758	3.8	5,022	5.1
5	-12,211	(6.0)	15,473	9.0
6	-11,732	(5.9)	6,998	6.0
7	679	1.4	4,831	5.0
8	-4,776	(3.8)	8,069	6.5
9	4,205	3.6	15,171	8.9
10	-10,042	(5.5)	1,478	2.8
Grade 4.6 Steel - Allowable Tensile Stress 145 MPa				
1	3,078	5.2	1,968	5.1
2	2,801	5.0	2,298	5.5
3	6,276	7.4	2,725	6.0
4	4,758	6.5	5,022	8.2
5	-12,211	(10.4)	15,473	14.3
6	-11,732	(10.1)	6,998	9.6
7	679	2.4	4,831	8.0
8	-4,776	(6.5)	8,069	10.3
9	4,205	6.1	15,171	14.4
10	-10,042	(9.4)	1,478	4.4

Table B.8: Bolt Diameter Results for Grade 8.8 and 4.6 Steel with an applied load of 21kN

As stated above the maximum shear stress is,

$$\tau_{max} = 0.577\sigma_y$$

and with a factor of safety of 1.5 applied the allowable shear stress is,

$$\tau_a = 0.385\sigma_y$$

In a method analogous to that above the diameter of the bolt can be calculated. The equation is derived in a manner similar to that above and,

$$d = \sqrt{\frac{4P}{\pi\tau_a}} \tag{B.21}$$

The shear stress allowable for grade 8.8 steel is  $\tau = 0.385(635) = 245$  MPa. The maximum shear load for bolt 9 is  $P=25,703$  N and substitution into equation (B.21) gives,

$$d = \sqrt{\frac{4(25,703)}{\pi(245 \times 10^6)}} = 0.0116 \text{ m} = 11.6 \text{ mm}$$

The stresses were also calculated as above for steel of grade 4.6 which has a yield stress of 250 MPa. These results are presented along with the results for all the other bolts in Table B.8.

Mounting Bolt Sizing				
Mounting Point	Tensile Load N	Diameter mm	Shear Load N	Diameter mm
Grade 8.8 Steel - Allowable Tensile Strength 425 MPa				
1	5,037	3.9	3,220	4.1
2	4,584	3.7	3,760	4.4
3	10,270	5.5	4,458	4.8
4	7,786	4.8	8,219	6.5
5	-19,982	(7.7)	25,319	11.5
6	-19,198	(7.6)	11,450	7.7
7	1,111	1.8	7,906	6.4
8	-7,816	(4.8)	13,204	8.3
9	6,881	4.5	25,703	11.6
10	-16,432	(7.0)	2,418	3.5
Grade 4.6 Steel - Allowable Tensile Strength 145 MPa				
1	5,037	6.7	3,220	6.5
2	4,584	6.3	3,760	7.1
3	10,270	9.5	4,458	7.7
4	7,786	8.3	8,219	10.4
5	-19,982	(13.2)	25,319	18.3
6	-19,198	(13.0)	11,450	12.3
7	1,111	3.1	7,906	3.8
8	-7,816	(8.3)	13,204	13.2
9	6,881	7.8	25,703	18.5
10	-16,432	(12.0)	2,418	5.7

Table B.9: Bolt Diameter Results for Grade 8.8 and 4.6 Steel with an applied load of 35kN

Using this data and substituting into equation (B.15) for grade 8.8 and grade 4.6 steel respectively,

$$D_{8.8} = 11.6 + 1.0825(1.25) = 12.95 \text{ mm}$$

$$D_{4.6} = 18.5 + 1.0825(2.0) = 20.6 \text{ mm}$$

Neither of these sizes are standard and consequently the nearest size to these would be used, namely 14 mm and 20 mm respectively.

High tensile 1/2" (12.7 mm) diameter bolts were readily available and were consequently used for this application. This was considered suitable as the factor of safety was sufficient to give a reasonable margin.

### B.2.1 Bolts in Combined Shear and Tension

In reference [16] the relationship between the tensile and shear loads in a bolt is expressed as,

$$\frac{x^3}{a^3} + \frac{y^2}{b^2} = 1 \quad (\text{B.22})$$

where,  $x$  is the shear load;  $a$  is the allowable shear load;  $y$  is the tensile load and  $b$  is the allowable tensile load.



Provided the LHS of the equation is under the limiting value of 1 then the bolt design is safe for the applied loads. Using this relationship for bolt 9 with an applied load of 35kN (grade 8.8 steel),

$$\frac{(25,703)^3}{(32,590)^3} + \frac{(6,881)^2}{(65,180)^2} = 0.491 + 0.011 = 0.502 \quad (\text{B.23})$$

Thus it can be seen that the combination of the tensile and shear stresses are not critical in this case.

It has been reported [15] that it is generally sufficient to calculate the stresses in bolts for the tensile and shear loads and use the worst case as the design. The general validity of this can be illustrated using the relationship of equation (B.22). Assuming a design reserve factor of 10% on the maximum shear stress where the maximum shear stress is approximately half of the uniaxial UTS then,

$$\frac{(0.90a)^3}{a^3} + \frac{[0.90(b/2)]^2}{b^2} = 0.95 \quad (\text{B.24})$$

If the tensile maximum stress has a reserve factor of 10% then,

$$\begin{aligned} \frac{x^3}{a^3} + \frac{[0.90(b)]^2}{b^2} &= 1 \\ \frac{x^3}{a^3} &= 1 - 0.81 \\ \therefore \frac{x}{a} &= \sqrt[3]{0.19} = 0.575 \end{aligned}$$

Thus, even when the ultimate stress is approaching the tensile limits, provided the shear stress is less than about 57% of the maximum allowable shear stress the bolt design will be sufficient.

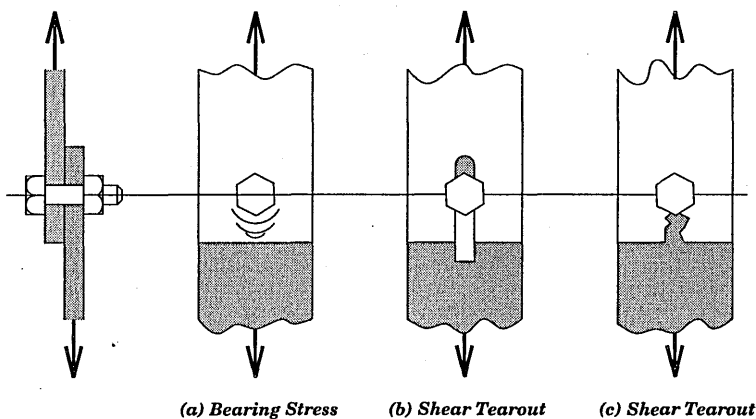


Figure B.5: Loading Plate Failure Modes

### B.3 Sizing of the Chassis Mounting Plates

For a bolted joint loaded in shear there are a number of possible methods of failure. These are,

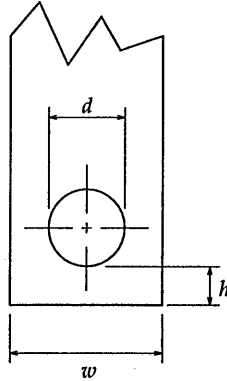


Figure B.6: Loading Plate Dimensions

- Shearing of the bolt
- Failure by crushing of the bolt or plate (bearing failure), Figure B.5 (a),
- Shearing or tearing of the plate end (shear tearout failure), Figure B.5 (b),
- Rupture of one of the connected plates by pure tension (tensile failure), Figure B.5 (c),

The bolt has already been sized to prevent it failing due to shear. The other failure mechanisms are investigated below and the mounting plates sized.

### B.3.1 Bearing Stress

The bearing stress needs to be calculated for the mounting plates and the mounting beam in order to size them for this application. The dimensions of the plate are as shown in Figure B.6. The bearing area is the product of the bolt diameter and the plate thickness. So,

$$A_b = td \quad (\text{B.25})$$

where  $t$  is the thickness of the plate and  $d$  is the bolt diameter. The bearing stress for the plate is given from,

$$\sigma_b = \frac{F}{A_b} \quad (\text{B.26})$$

Substitution of the largest shear load with the relevant bolt diameter gives the relevant bearing stress. For a 12 mm bolt and an assumed plate thickness of 10mm,

$$\begin{aligned} A_b &= 12 \times 10 \\ &= 120 \text{ mm}^2 \\ \therefore A_b &= 120 \times 10^{-6} \text{ m}^2 \end{aligned}$$

$$\begin{aligned} \sigma_b &= \frac{15,473}{120 \times 10^{-6}} \\ \therefore \sigma_b &= 129 \text{ MPa} \end{aligned}$$

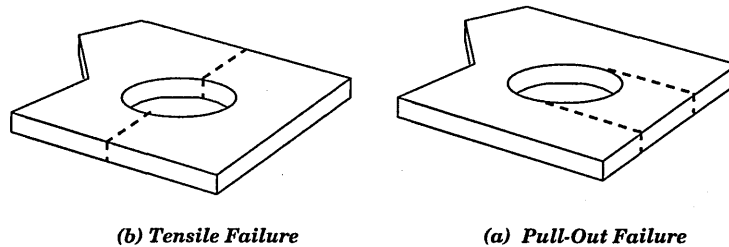


Figure B.7: Loading Plate Failure Modes

With the 35kN loading on the chassis the maximum bearing stress to be expected is,

$$\sigma_b = \frac{25,703}{120 \times 10^{-6}}$$

$$\therefore \sigma_b = 214 \text{ MPa}$$

Standard cold rolled mild steel plate has a yield stress of 280 MPa and the ultimate stress is 410 MPa. Consequently the use of 10mm plate was sufficient in this case and gave a factor of safety of 1.3 based on the yield strength. Additionally the flanges on the mounting beam were 10mm thick and were thus of sufficient thickness to restrain the applied loads.

### B.3.2 Shear Tearout Failure

Overloading of the plate in tension can result in two types of failure as shown in Figure B.7. These are pull-out failure and tensile failure due to normal stresses. Both of these failure modes are investigated below.

Pull out failure occurs when the bolt shears out a section of the plate due to the tensile load. The area that the load acts over is,

$$A = 2ht$$

The thickness of the plate was 10 mm and the area,

$$A = 20h$$

Substituting this into the stress equation with the shear stress of  $\tau_y = 0.577(280) = 162 \text{ MPa}$ . Substituting,

$$\tau = \frac{F}{A}$$

$$162 = \frac{25,703}{20h}$$

$$\therefore h = 7.93 \text{ mm} \quad (\text{B.27})$$

The minimum distance from the end of the plate is 8 mm. The mounting plates were made 200mm long to fit onto the beams. The holes were thus placed further than 16mm from the end of the plates. This was to reduce the bending of the mounting plates and the mounting beam flanges. In the final arrangement the holes were placed 65 mm from the end of the plates.

This type of failure will not occur [15] if the bolt or rivet is kept a minimum of 1.5 hole diameters from the edge of the plate.

### B.3.3 Tensile Failure Stress

The maximum normal stress occurs at the bolt hole sides. This type of failure occurs when the end of the strut shears off. The end of the bar with the 12 mm bolt was critical in this case. The allowable yield stress was  $\sigma_a = 125 \text{ MPa}$ , applying a factor of safety of 2. The area that the stress acts over is calculated from,

$$A = (w - d)t$$

And the diameter of the bolt is 12 mm, the thickness of the plate is 10 mm thus,

$$A = (w - 12)10$$

So the plate width is estimated from the stress equation,

$$\begin{aligned}\sigma &= \frac{F}{A} \\ 125 &= \frac{25,703}{(w - 12)10} \\ \therefore w &= 32.56 \text{ mm}\end{aligned}$$

Again the final plate size was dictated by stores stock and 75 mm wide strip was readily available.

### B.3.4 Weld Design

The chassis was attached to the mounting plates by welding. This welding consisted, where possible, of fillet welds on both sides of the lower chassis rails. It was necessary to calculate the depth of weld required to provide adequate restraint. Both tensile and shear failure were investigated.

#### Tensile Weld Failure

For a weld under tension the load capacity is given by the relationship,

$$P = \frac{\sigma_{yw} Lh}{N} \quad (\text{B.28})$$

where,  $\sigma_{yw}$  is the weld yield stress,  $L$  is the total weld length,  $t$  is the depth of weld required,  $P$  is the load that can be carried, and  $N$  is the safety factor. From the previous load analysis the highest tensile load that the weld is subjected to is 19,982 N. Substitution into equation (B.28) with a safety factor of 2 yields,

$$19,982 = \frac{250 \times 10^6 (2(0.075))h}{2.0}$$

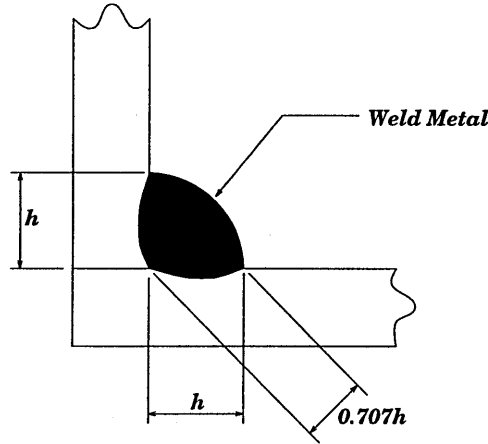


Figure B.8: Fillet Weld Dimensions

$$h = \frac{19,982(2.0)}{250 \times 10^6(2(0.075))}$$

$$\therefore h = 1.10 \text{ mm}$$

Thus the minimum weld thickness is 1.10 mm to resist the tensile loads.

### Shear Weld Failure

For a fillet weld under shear loading the maximum load carrying capacity is,

$$P = \frac{0.707hL\tau_{yw}}{N} \quad (\text{B.29})$$

Where,  $\tau_{yw}$  is the weld shear stress allowable,  $h$  is the weld thickness (see Figure B.8),  $L$  is the total weld length and  $P$  is the allowable load. The factor of safety selected is 2 and the maximum shear load from the mounting analysis is 25,541 N. Substitution yields,

$$25,541 = \frac{0.707h(2(0.075))(0.577(250 \times 10^6))}{2}$$

$$h = \frac{2(25,541)}{0.707(0.15)(0.577(250 \times 10^6))}$$

$$\therefore h = 3.3 \text{ mm}$$

Thus the minimum weld depth to resist the shear load is 3.3 mm. This requirement designs the weld depth required for the chassis mounting.

## B.4 Friction Mounting of Beams

The mounting clamp design in Section B.1.1 relies on friction to hold the entire test rig in position.

From the NASTRAN mounting point loads given in Section B.2 the maximum shear load is taken as the summation of the  $x$  and  $z$  components of the reactions. This was done for each mounting

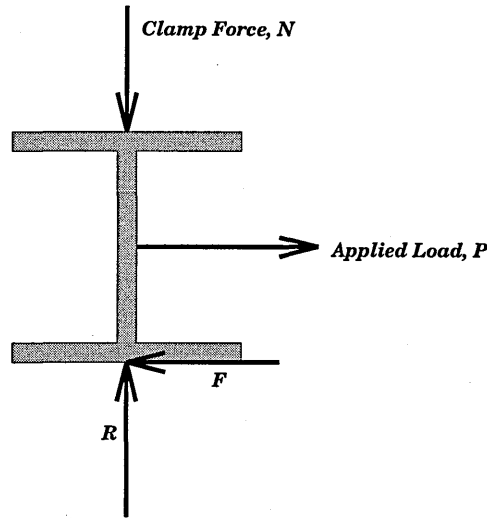


Figure B.9: Forces acting on Mounting Beam

beam and, for the design case, with an applied load of 35 kN,

$$P_a = 35,968 \text{ N}$$

$$P_b = 16,236 \text{ N}$$

where the subscripts  $a$  and  $b$  are used to identify the two mounting beams.

The shear load must be able to be reacted by the resulting friction force from the bolt tension acting on the clamp plate. The friction force acting was calculated from,

$$F_{max} = \mu_s N_0 \quad (\text{B.30})$$

where  $F_{max}$  is the maximum friction force,  $\mu_s$  is the coefficient of friction for the material, and  $N_0$  is the normal force exerted by the bolts. For dry steel on steel the coefficient of static friction  $\mu_s$  is in the range 0.40 - 0.80. For these calculations the value was taken as 0.80 as the steel contact surfaces were quite rough.

For the bolts to hold the beam in position they needed to exert a force sufficient to create the required frictional force. In addition they had to also counteract the tensile forces due to the loading of the chassis. From the analysis in Section B.2 the maximum bolt loads were  $T_a = 7,695 \text{ kN}$  (tensile) and,  $T_b = -35,454 \text{ N}$  (compressive) on the mounting beams.

For the mounting beam to remain in place the friction force needed to be greater than the maximum shear load. The limiting case is when these two forces are equal and substitution into equation (B.30) gives,

$$36,000 = (0.80)N_{0a}$$

$$\therefore N_{0a} = 45,000 \text{ N}$$

$$16,236 = (0.80)N_{0b}$$

$$\therefore N_{0b} = 20,295 \text{ N}$$



In addition the bolt must have a pre-load sufficient to counteract the maximum tensile load of 7.7 kN. The minimum tensile load in the bolt is thus,

$$N_{min} = 20,295 + 7,695 = 27,990 N$$

The load, however, which must be applied to the other side of the mounting beam is still higher and thus this is the design case, i.e.  $N_{0a} = 45 kN$ .

$$\therefore N_{min} = 45,000 N$$

The torque required on one bolt to give this tensile load is given by,

$$T = 0.20F_i d \quad (\text{B.31})$$

where,  $T$  is the required torque,  $F_i$  is the tensile pre-load required, and  $d$  is the bolt diameter. Substitution into this equation,

$$\begin{aligned} T &= 0.20(45,000)(0.012) \\ \therefore T &= 108 Nm \end{aligned}$$

This would be the torque required for one 12 mm bolt and this is clearly not possible. The tensile load would cause the bolt to fail in tension before this load could be realised. There are, however, four bolts carrying the loads and thus the summation of the applied loads is 45 kN. Assuming that each bolt carries an equal proportion of the load,

$$F_1 + F_2 + F_3 + F_4 = 45,000 N$$

thus each bolt carries a tensile load of 11.25 kN. This tensile load would cause a tensile stress of 119 MPa in the bolt and the required torque is,

$$\begin{aligned} T &= 0.20(11,250)(0.012) \\ \therefore T &= 27.0 Nm \end{aligned}$$

#### B.4.1 Load Link Calibration

The load link was calibrated using the Instron 8032 tensile testing machine which was controlled via the Instron 8500 Control panel. The input function to the tensile test machine was a single ramp with a maximum input of 60 kN at a rate of 1kN/sec.

The output from the strain gauges was amplified by 100 and a 0.01kHz filter was used on Channel 1 of the signal conditioning unit.

The load link arrangement is shown in Figure B.10. The output from the load link strain gauges was connected to the strain gauge amplifier which was powered by a 5.1V, 100mA power supply. The output was input into a data logger and the load output from the machine (kN) was logged with the strain load link output in volts.

Three calibrations were carried out and the results are plotted in Figure B.11.

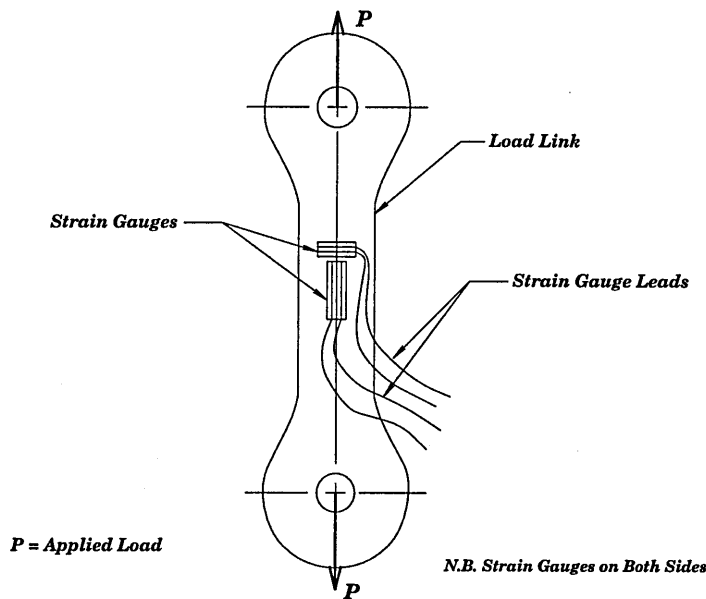


Figure B.10: Loadlink General Arrangement

## B.5 Test Rig Design for Vertical Loading

Analyses were carried out applying vertical loads to the rear hoop of the roll cage. The model was used to predict the onset of yield in the structure. The load case at the onset of yield was then used as the design load for the test rig.

The standard roll cage would be made from high strength T45 tubing, however, that material used in the test chassis roll cage was ERW 1. The modelling was based on the ERW 1 material properties to give the loads and deformations for the tests.

It was decided to carry out the vertical load tests on the same test rig that was to be used for the oblique loading. This meant that the chassis did not have to be moved around and consequently eased the setup changes required. It did, however, mean a lot more design work for the test equipment to carry out the loading. The general arrangement of the loading setup on the rear hoop is shown in Figure 6.1.

### B.5.1 Bolt Diameters in Load Link

The existing load linkage used had high tensile steel 1/2 inch bolts fitted and it was necessary to check the suitability of these for the loads expected. The load linkage bolt was loaded in double shear as shown in Figure B.12.

The bolt was made from aircraft grade high tensile with an ultimate tensile strength of approximately 700 MPa and a yield stress of 620 MPa. The cross sectional area of the bolt was,

$$A = \frac{\pi(12.7)^2}{4} = 126.7 \text{ mm}^2$$

The yield shear stress in the bolt was calculated to be,

$$\tau_y = 0.577\sigma_y$$

# Load Cell Calibration

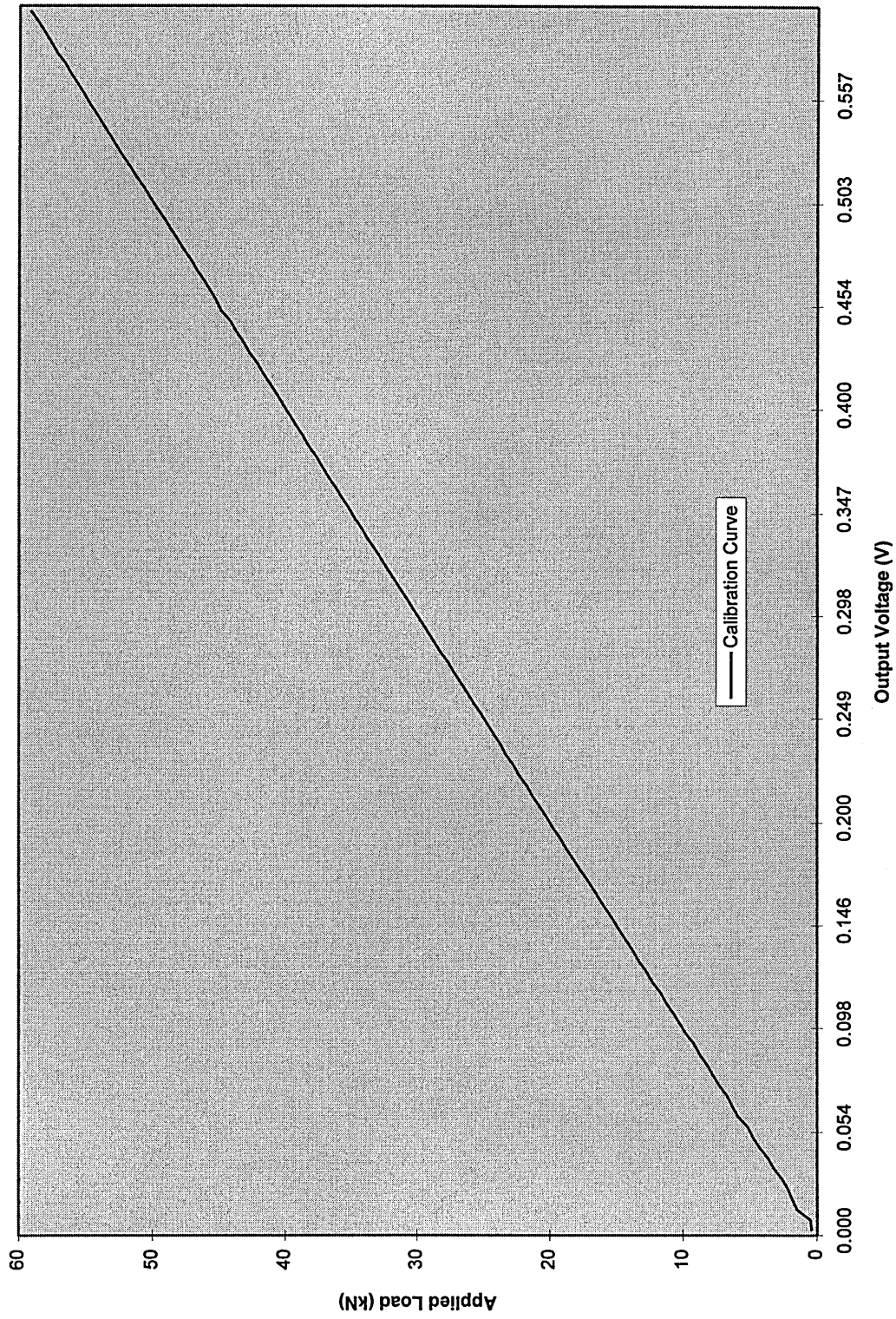


Figure B.11: Load Cell Calibration Curve

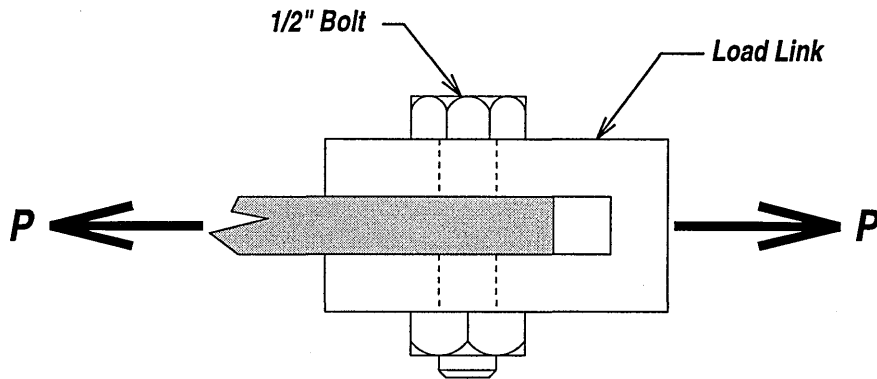


Figure B.12: Loadlink Attachments

$$= 0.577(620)$$

$$\therefore \tau_y = 358 \text{ MPa}$$

Applying a factor of safety of 1.5 on the shear yield stress gives an allowable stress of  $\tau_a = 240 \text{ MPa}$ . The load is taken to be the failure load of 56 kN. The shear stress in the bolt is given by the general formula,

$$\tau = \frac{P}{A}$$

Because the bolt is loaded in double shear the area is in fact twice the cross sectional area of the bolt. It can be seen that this is the area of material resisting the shear loading. Hence,

$$\tau = \frac{56,000}{2(126.7)}$$

$$\therefore \tau = 221 \text{ MPa}$$

Since the allowable stress in the bolt is 240 MPa the 1/2" bolt is suitable for this application. Thus the existing load link could be used.

### B.5.2 Design of Load Bars

The load was to be applied to the top of the rear hoop evenly at two points, one on each side of the hoop. Thus the load application needed to be centralised to ensure even loading. The loading arrangement selected is illustrated in Figure B.13.

From the geometry of the loading bars the angles  $\theta$  and  $\beta$  were calculated:

$$\tan \theta = \frac{18}{24}$$

$$\therefore \theta = 36.9^\circ$$

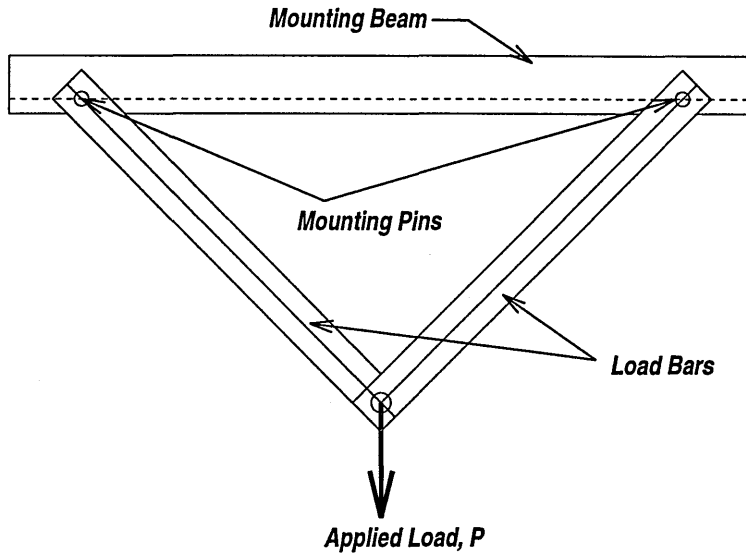


Figure B.13: Loading Arrangement

$$\begin{aligned}\tan \beta &= \frac{24}{18} \\ \therefore \beta &= 53.1^\circ\end{aligned}$$

The Sine Rule was used to calculate the load in the two flat strips. So,

$$\begin{aligned}\frac{A}{\sin A} &= \frac{B}{\sin B} = \frac{C}{\sin C} & (B.32) \\ \therefore \frac{56,000}{\sin 106.2} &= \frac{ac}{\sin \theta} = \frac{bc}{\sin \theta} \\ \therefore ac &= bc = \frac{56,000}{\sin 36.9^\circ} \sin 106.2^\circ \\ \therefore ac &= bc = 35,013 \text{ N}\end{aligned}$$

Hence the load in each of the straps is  $F_{ac} = F_{bc} = 35 \text{ kN}$ .

This load acts on two bars, one on each side of the loading beam. Thus the bolts on each side are subjected to single shear.

The bolts to be used for this application were  $\phi 16 \text{ mm}$  and their suitability is checked below. These bolts were made of a high tensile steel with an ultimate stress of  $700 \text{ MPa}$  and a yield stress of  $620 \text{ MPa}$ . The shear stress is calculated from,

$$\tau = \frac{F_{ac}}{2A}$$

The yield stress in uniaxial tension is  $\sigma_y = 620 \text{ MPa}$  and consequently the allowable shear stress is,

$$\tau_y = 0.577(620) = 358 \text{ MPa}$$

Applying a factor of safety of 1.5 to this gives an allowable shear stress of  $\tau_a = 240 \text{ MPa}$ . The area of the 16 mm bolts is calculated as before,

$$A = \frac{\pi(16)^2}{4} = 201 \text{ mm}^2$$

substitution into the expression for shear stress gives,

$$\begin{aligned} \tau &= \frac{F_{ac}}{2A} \\ &= \frac{35,000}{2(201)} \\ \therefore \tau &= 87.1 \text{ MPa} \end{aligned}$$

Thus the bolts are suitable for the application.

The material of the bars was, however, mild steel with a yield stress of 250 MPa and the pull out shear failure, bearing stress and maximum tensile stress of the bars needed to be calculated.

The other end of the bars were attached to the load cell and the bolt at that end was 25 mm diameter. The stress-check calculation was not carried out for that bolt as it is of sufficient size to carry the loads. The end of the bar with this bolt is critical however and maximum normal stress in the bar is investigated below.

### Bearing Stress

The bearing stress was calculated first as this gave the plate thickness required. It was assumed that the tensile and compressive yield stress were the same, thus, for mild steel,  $\sigma_t = \sigma_c = 250 \text{ MPa}$ . Applying a factor of safety of 1.5 gives an allowable stress of  $\sigma_a = 170 \text{ MPa}$ . The bearing stress is calculated from,

$$\sigma_b = \frac{F}{A}$$

The bolt diameter is 16mm and the bearing stress is developed in the section of plate with an area,

$$A = 16t$$

The thickness is calculated from,

$$\begin{aligned} 16t &= \frac{17,500}{170} \\ \therefore t &= 6.4 \text{ mm} \end{aligned}$$

This is a standard gauge and 1/4" (6.4 mm) mild steel sheet was used.

### Pull-Out Failure

Pull out failure occurs when the bolt shears out a section of the plate due to the tensile load as shown in Figure B.7. The area that the load acts over is,

$$A = 2ht$$



The thickness of the plate was 6 mm and the corresponding area was,

$$A = 12h$$

As before the shear stress at yield is approximately  $\tau_y = 0.577(250) = 144 \text{ MPa}$  and applying a factor of safety of 1.5 gives an allowable stress of  $\tau_a = 96 \text{ MPa}$ . Substituting this into the stress equation with the allowable shear stress,

$$\begin{aligned}\tau &= \frac{F}{A} \\ 96 &= \frac{17,500}{12h} \\ \therefore h &= 15.2 \text{ mm}\end{aligned}\tag{B.33}$$

The minimum distance from the end of the plate was 15.2 mm and the distance was taken as 16mm.

### Normal Stress

The maximum normal stress occurs at the bolt hole sides. The failure occurs when the end of the strut shears off as shown in Figure B.7. The end of the bar with the 25 mm bolt was critical in this case. The area that the stress acts over was calculated from,

$$A = (w - d)t$$

The diameter of the bolt was 25 mm, the thickness of the plate was 6 mm and,

$$A = (w - 25)6$$

So the stress was given by,

$$\begin{aligned}\sigma &= \frac{F}{A} \\ 170 &= \frac{17,500}{(w - 25)6} \\ \therefore w &= 42.2 \text{ mm}\end{aligned}$$

Again the final plate size was dictated by stores stock and 75 mm wide strip was easily available.

## Appendix C

# Material Properties

The material used in the construction of the production chassis is mainly CFS3 and T45 tubing. In the test model T45 was unobtainable at time of manufacture and consequently ERW 1 tubing was used. The material properties of each of these is detailed below.

### C.1 Cold Finished Seamless (CFS) Tubing

This tubing is covered by BS 6323:1982<sup>1</sup> and this replaces the withdrawn standards BS 980:1980, BS 1775:1964 and BS 3014:1958. As a result of the change in standard the old CDS (BS 980) specification tubing is now denoted CFS - cold finished seamless tubing. This tubing is available in a number of differing heat treatments ranging from cold finished to normalised and the relevant properties are contained below.

CFS 3 Tubing - 0.2% Carbon Steel		
Heat Treatment	Yield Strength, $R_e$ MPa	Tensile Strength, $R_m$ MPa
Cold finished/hard (BK)	360	450
Cold finished/soft (BKW)	280	400
Fully Annealed (GBK)	170	340
Normalised (NBK)	215	360

Table C.1: CFS Tubing Material Properties

TVR Engineering quoted the material specification for the chassis as CDS2 (BS 980:1950) which corresponds to CFS3 BK with the relevant properties as detailed above.

### C.2 Carbon Manganese Steel Tube (T.45) Tubing

For the GT Cerbera the roll cage was produced using high strength carbon-manganese steel tubing which is often known as T45 tubing. This material is covered by the British Standard, BS

<sup>1</sup>Seamless and Welded Steel Tubes for Automotive, Mechanical and General Engineering, 1982

4T.45:1972<sup>2</sup>. This tubing is not used in the test chassis, however, the material is used for a series of NASTRAN analyses and the material specification is consequently included. This standard is now classed as obsolete, however, no substitute for this material specification was found.

0.2% Proof Strength 620 MPa  
Tensile Strength 700 (min) - 900 (max) MPa

### C.3 Electrically Resistance Welded (ERW) Tubing

This tubing is covered by BS 6323:1982 and this replaces the withdrawn standards BS 980:1980, BS 1775:1964 and BS 3014:1958. In BS 1775:1964 the tubing is called ERW11 and this is replaced under BS6323 as ERW1 and ERW2 tubing. As with the CFS tubing this material is available in a number of heat treatments, some of which are detailed in the table below.

ERW Tubing Material Properties		
Heat Treatment	Yield Strength $R_e$ MPa	Tensile Strength $R_m$ MPa
ERW 1 Tubing Material Properties		
As welded (KM)	200	300
Subcritically Annealed (GKM)	150	270
Annealed & Descaled (GZF)	150	270
Normalised (NKM)	165	280
Normalised & Descaled (NZF)	165	280
ERW 2 Tubing Material Properties		
As welded (KM)	250	340
Subcritically Annealed (GKM)	160	300
Annealed & Descaled (GZF)	160	300
Normalised (NKM)	195	320
Normalised & Descaled (NZF)	195	320

Table C.2: ERW Tubing Material Properties

In the test chassis the material used for the roll cage is ERW 1 and the properties quoted here are used in the analysis of the chassis with NASTRAN.

A section of the tubing used for the roll cage was subjected to a tensile test to determine the properties of the material used in the test. The results from this test are presented in Figure C.1. The yield strength for the  $\phi 1.75 \times 18$ swg tube (cross sectional area  $166\text{mm}^2$ ) was approximately 151 MPa and the ultimate strength was approximately 271 MPa. These values were very similar to those for the annealed tubing and were lower than the values used in the modelling.

<sup>2</sup>Weldable Carbon-Manganese Steel Tube, Minimum Tensile Strength  $700\text{N}/\text{mm}^2$ , 1972

### Load vs Deflection for ERW 1 Tubing

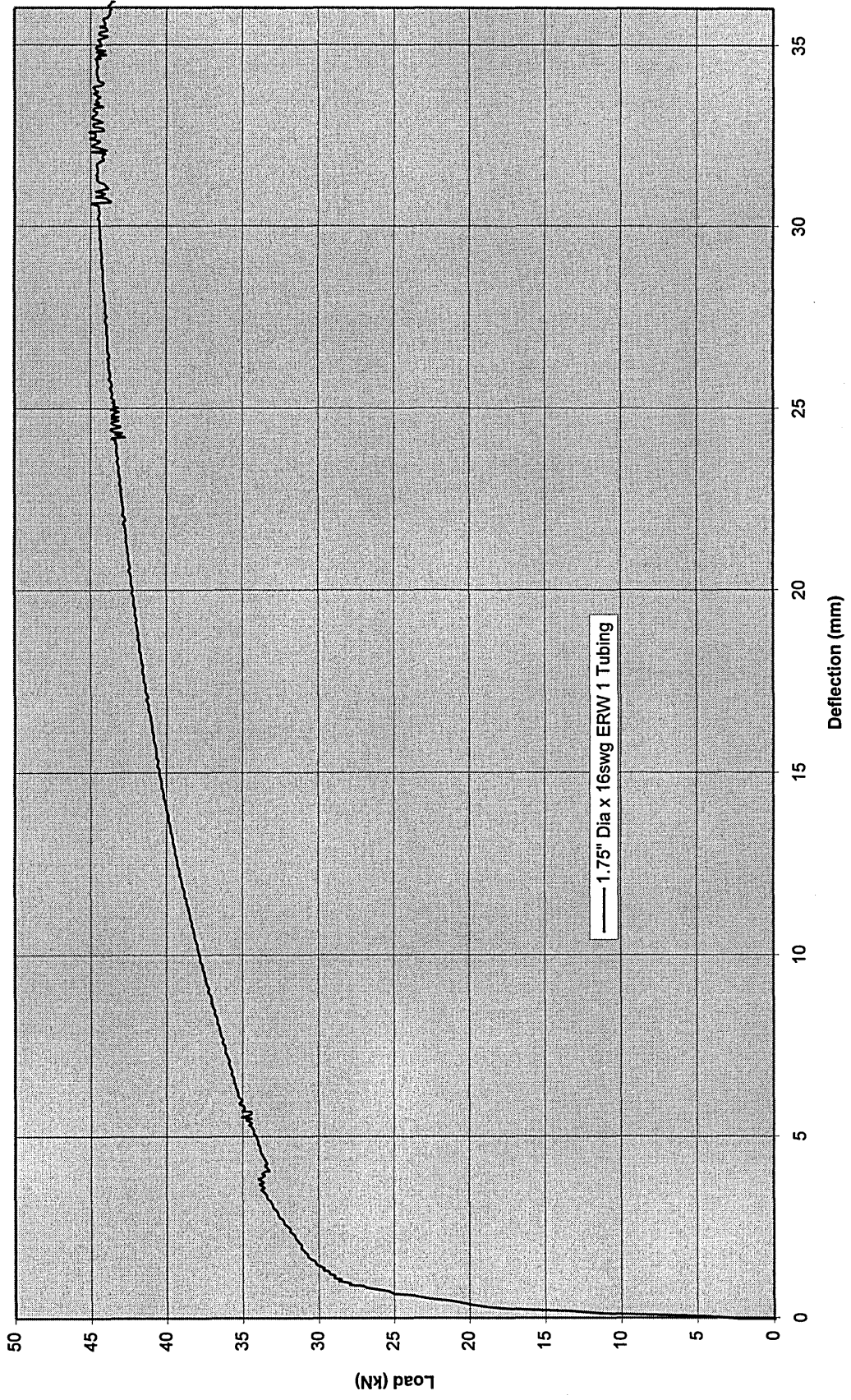


Figure C.1: Tensile Test Results - Chassis Roll Cage Tube.

Figure C.1: Tensile Test Results - Chassis Roll Cage Tube

## C.4 Bolt Grades and Properties

The data in Table C.3 gives the material properties for common classes of bolt. This data was used for the design of the test mountings and all bolted joints.

Metric Steel Bolts			
Property Class	Proof Stress MPa	Yield Stress MPa	Tensile Stress MPa
4.6	225	250	400
4.8	310	340	420
5.8	380	395	520
8.8	600	635	830
9.8	650	710	900
10.9	830	895	1040
12.9	970	1100	1220

Table C.3: Steel Bolt Material Properties

## C.5 Standard Wire Gauges - SWG

The following is an extract of Standard Wire Gauges.

Standard Wire Gauge (SWG)					
SWG	Imperial in.	Metric mm	SWG	Imperial in.	Metric mm
0	0.324	8.23	15	0.072	
2	0.276		16	0.064	1.63
4	0.232	5.89	17	0.056	
6	0.192		18	0.048	1.22
8	0.160	4.06	19	0.040	
10	0.128		20	0.036	0.914
12	0.104	2.64	22	0.028	
13	0.092		24	0.022	0.559
14	0.080		28	0.0148	0.376

Table C.4: Standard and Wire Gauges

## Appendix D

# Plastic Hinge Moment Calculations for Chassis

Plastic hinges are discussed in Chapter 5 and this discussion is not repeated here. The plastic hinge moments needed to be calculated for all the sections of the chassis. A general expression was derived for calculating the plastic moment of a cross section.

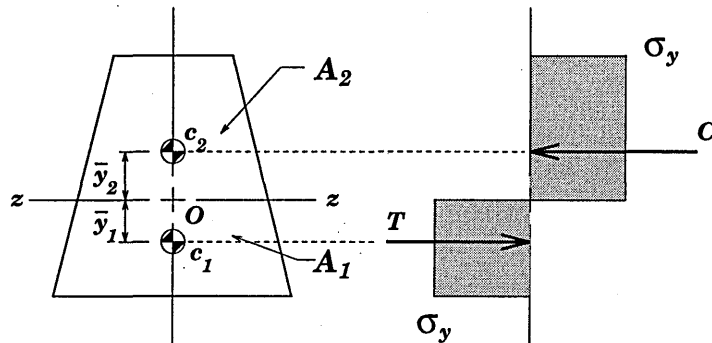


Figure D.1: Plastic Moment for Non-Symmetrical Section

Take a general non-symmetric section as shown in Figure D.1 and assume that the section above the neutral axis is in compression and that below the neutral axis is in tension. At the point of the plastic moment forming the stresses are equal and opposite,  $\sigma_y$ . Thus the tensile force is given by,  $T = \sigma_y A_1$  and the compressive force is,  $C = \sigma_y A_2$ . The resultant force is of course zero. Thus it can be seen that  $T - C = 0$  or  $A_1 = A_2$  and thus the total area is,

$$\begin{aligned} A_t &= A_1 + A_2 \\ \therefore A_1 = A_2 &= \frac{A_t}{2} \end{aligned} \quad (D.1)$$

Thus the neutral axis actually divides the cross section into two equal areas. The neutral axis for the plastic moment is thus often different to that for the elastic moment. Integration over the



surface of the cross section gives the resultant plastic moment,

$$\int \sigma_y dA = M_p \tag{D.2}$$

Alternatively moments can be taken about the neutral axis,

$$M_p = T\bar{y}_1 + C\bar{y}_2 \tag{D.3}$$

where  $\bar{y}_1$  and  $\bar{y}_2$  are the distances from the neutral axis to the centroids,  $c_1$  and  $c_2$  of the areas  $A_1$  and  $A_2$  respectively. Replacing  $T$  and  $C$  by  $\sigma_y(A_t)/2$ ,

$$M_p = \frac{\sigma_y A_t (\bar{y}_1 + \bar{y}_2)}{2} \tag{D.4}$$

Thus the general solution to this problem is to divide the cross section into two equal areas, locate the centroid of each half and use equation (D.4) to calculate  $M_p$ . The equation can be written as,

$$M_p = \sigma_y(z) \tag{D.5}$$

where,

$$z = \frac{A_t(\bar{y}_1 + \bar{y}_2)}{2} \tag{D.6}$$

and  $z$  is known as the plastic modulus of the cross section. The shape factor,  $f$ , is defined as the ratio of the plastic to the elastic moments, so:

$$f = \frac{M_p}{M_y} \tag{D.7}$$

### D.1 Plastic Hinge Moment for a Circular Tube

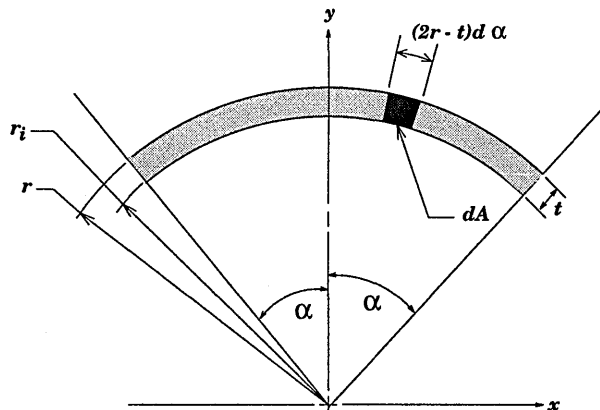


Figure D.2: Circular Tube - Thick Wall

### D.1.1 Thick Walled Tube

Consider the circular tube as show in Figure D.2. Firstly it was necessary to calculate an expression for the elemental area and the location of the centroid of the tube section. The centroid of the tube is given from,

$$\bar{y} = \frac{\int y dA}{\int dA} \quad (\text{D.8})$$

For a thick walled tube as shown in Figure D.2 the area of the shaded sector is given by,

$$A = \alpha r^2 - \alpha r_i^2 \quad (\text{D.9})$$

where,  $r_i = r - t$  and substituting,

$$\begin{aligned} A &= \alpha r^2 - \alpha(r - t)^2 \\ A &= \alpha r^2 - \alpha r^2 + 2\alpha r t - \alpha t^2 \\ \therefore A &= \alpha t(2r - t) \end{aligned} \quad (\text{D.10})$$

Thus the total area of the cross-section is,

$$A_T = 2A = 2\alpha t(2r - t) \quad (\text{D.11})$$

where  $0 \leq \alpha \leq \frac{\pi}{2}$  in radians. An increment of area can be expressed as,

$$dA = t(2r - t)d\alpha$$

and the  $y$  co-ordinate of the centre of the total area is given by,

$$\begin{aligned} y &= \frac{r + r_i}{2} \cos \alpha \\ &= \frac{r + (r - t)}{2} \cos \alpha \\ \therefore y &= \frac{2r - t}{2} \cos \alpha \end{aligned}$$

sustitution of these values into equation (D.8) gives,

$$\begin{aligned} \bar{y} &= \frac{\int y dA}{\int dA} \\ &= \frac{\int_0^\alpha \left(\frac{2r-t}{2}\right) \cos \alpha [t(2r-t)] d\alpha}{\int_0^\alpha t(2r-t) d\alpha} \\ \therefore \bar{y} &= \frac{(2r-t)\sin\alpha}{2\alpha} \end{aligned} \quad (\text{D.12})$$

where,  $0 \leq \alpha \leq \frac{\pi}{2}$ .

The bending moment expression is obtained using equation (D.4). Because the cross section is symmetric the centroidal distance to each half is the same and substituting,

$$\begin{aligned} M_p &= \sigma_y [\alpha t(2r - t)] \left( \frac{(2r - t)\sin\alpha}{2\alpha} + \frac{(2r - t)\sin\alpha}{2\alpha} \right) \\ &= \sigma_y [\alpha t(2r - t)] 2 \left( \frac{(2r - t)\sin\alpha}{2\alpha} \right) \\ \therefore M_p &= t\sigma_y (2r - t)^2 \sin \theta \end{aligned} \quad (\text{D.13})$$

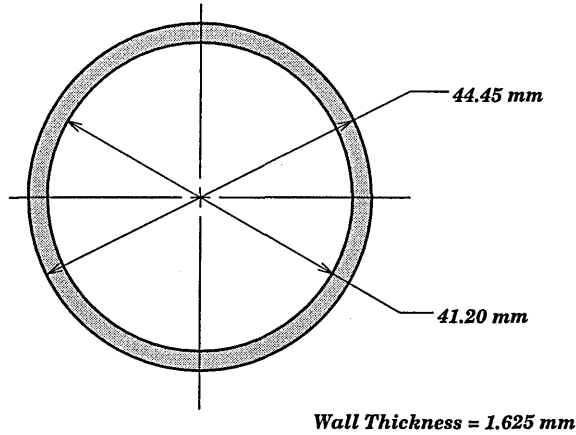


Figure D.3: Circular Chassis Tube

Which is the general expression for the bending moment in the tube.

Consider the complete plastic collapse of the thick walled tube in Figure D.2 by bending. The cross sectional area of one half of the tube from equation (D.10) (i.e.  $\alpha = \frac{\pi}{2}$ ) is,

$$A = \frac{\pi t}{2}(2r - t) \tag{D.14}$$

For complete plastic collapse the centroid of each half of the tube is calculated using equation (D.12) with  $\alpha = \pi/2$  so,

$$\begin{aligned} \bar{y} &= \frac{(2r - t) \sin\left(\frac{\pi}{2}\right)}{2} \left(\frac{\pi}{2}\right) \\ \therefore \bar{y} &= \frac{2r - t}{\pi} \end{aligned} \tag{D.15}$$

The full plastic moment is obtained by substitution into equation (D.13) for  $\alpha = \frac{\pi}{2}$ .

$$\begin{aligned} M_p &= t\sigma_y (2r - t)^2 \sin\left(\frac{\pi}{2}\right) \\ \therefore M_p &= t\sigma_y (2r - t)^2 \end{aligned} \tag{D.16}$$

The above relationships were used to calculate the plastic hinge moments for the tubular members used in the TVR chassis.

**Calculation of the Plastic Hinge Moments for the TVR Chassis**

Equation (D.13) was used to calculate the plastic hinge moments for the tubular chassis members. The sample calculation below is for 1.75 inch, 16swg tube. The results for the other tubes are contained in Table D.1.

**Sample Calculation:** The tube dimensions are given in Figure D.3 and from equation (D.13),

$$\begin{aligned}
M_p &= (1.625)\sigma_y(44.45 - 1.625)^2 \\
&= 2,980.2(200) \text{ Nmm} \\
\therefore M_p &= 596,040 \text{ Nmm}
\end{aligned}$$

As a check of this result the formula from Reference [11] was used which states,

$$\begin{aligned}
M_p &= 1.333\sigma_y(r_o^3 - r_i^3) & (D.17) \\
\therefore M_p &= 1.333\sigma_y \left[ (22.225)^3 - (20.6)^3 \right] \\
&= 2,980.9(200) \text{ Nmm} \\
\therefore M_p &= 596,180 \text{ Nmm}
\end{aligned}$$

which is in good agreement with the derived result.

Plastic Hinge Moments - 200 MPa Yield				
Description	Cross Sectional Area (mm <sup>2</sup> )	Tube Outside Diameter (mm)	Tube Wall Thickness (mm)	Plastic Hinge Moment (Nmm)
Circular Sections				
1.75" × 16swg	219	44.45	1.625	596,040
1.50" × 16swg	186	38.10	1.625	432,388
1.00" × 16swg	121	25.4	1.625	183,706
1.75" × 18swg	166	44.45	1.22	455,995
1.50" × 18swg	141	38.10	1.22	331,873

Table D.1: Plastic Hinge Moments for Roll-Cage Members

## D.2 Axial Force and Bending Moment Interaction

In Section 5 the interaction of axial forces and bending moments was discussed. These interactions were of prime importance in this analysis and the theoretical values were compared to NASTRAN output data. The modelling of plastic hinges in NASTRAN is discussed in Section E.

From Appendix D the centroidal values for the thick wall tube was calculated in equation D.12 and this was,

$$\bar{y} = \frac{(2r - t) \sin \theta}{2\theta}$$

This was used to calculate the plastic hinge moment for the circular tubes.

### Axial Load

Consider the complete plastic collapse of the tube due to an axial force. The stress distribution at collapse is as shown in Figure D.4. The nominal average tube radius  $R_{av}$  is calculated using,

$$R_{av} = \frac{R + (R - t)}{2}$$

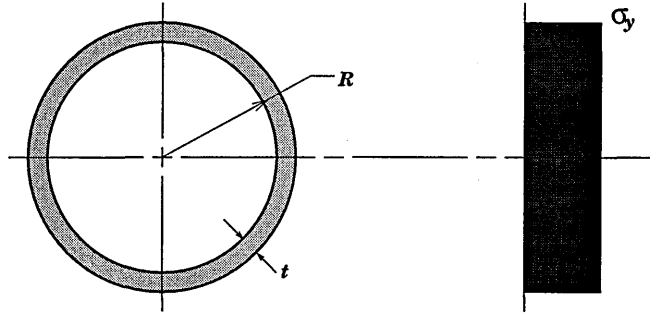


Figure D.4: Tube Subjected to Axial Force - Fully Plastic Collapse

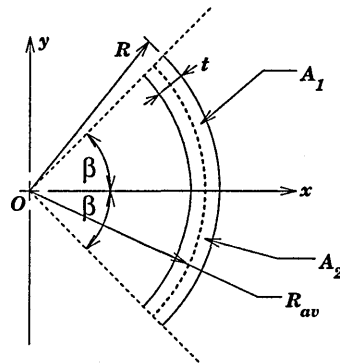


Figure D.5: Tube Subjected to Axial Force

$$\therefore R_{av} = \frac{2R - t}{2}$$

The area of the total cross section, assuming that  $t \ll R_{av}$  is given by,

$$\begin{aligned} A_T &= 2\pi(R_{av})t \\ \therefore A_T &= \pi t(2R - t) \end{aligned}$$

and the maximum load that can be carried or the plastic collapse axial load is,

$$\begin{aligned} P_o &= \sigma_y A_T \\ \therefore P_o &= \pi t(2R - t)\sigma_y \end{aligned} \tag{D.18}$$

General collapse of the tube due to an axial force is given below.

The cross-section subjected to an axial force is given in Figure D.5. From this figure the area of the sector shown is,

$$A = A_1 + A_2 = 2R\beta t - \beta t^2$$

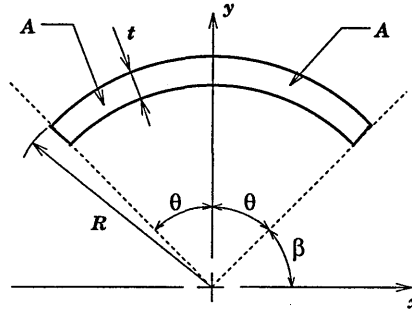


Figure D.6: Tube Subjected to Bending Moment

The load acting on the section is merely the cross-sectional area multiplied by the limiting or yield stress, so with a factor of 2 for the two halves:

$$\begin{aligned}
 P_p &= 2\sigma_y A \\
 &= 2\sigma_y [2R\beta t - \beta t^2] \\
 \therefore P_p &= \sigma_y [4tR\beta - 2t^2\beta]
 \end{aligned} \tag{D.19}$$

Rearranging this equation and substituting from equation (D.18),

$$\begin{aligned}
 P_p &= \sigma_y [2t\beta (2R - t)] \\
 &= [\sigma_y \pi t (2R - t)] \left[ \frac{2\beta}{\pi} \right] \\
 &= P_o \left[ \frac{2\beta}{\pi} \right]
 \end{aligned}$$

Letting  $\left[ \frac{2\beta}{\pi} \right] = n$  the above becomes,

$$\begin{aligned}
 P_p &= nP_o \\
 \therefore n &= \frac{P_p}{P_o}
 \end{aligned} \tag{D.20}$$

### Bending Moment

The complete plastic collapse due to bending is calculated in Appendix D.1. The equation of the collapse moment from equation (D.16) was,

$$M_o = t\sigma_y(2R - t)^2$$

The assumed beam cross section is shown in Figure D.6 and the general collapse of due to bending moment is analysed below.

The area of the sector shown shaded is given by,

$$A = \theta t (2R - t)$$

and the centroidal distance  $\bar{y}$  is given from equation (D.8),

$$\bar{y} = \frac{(2R - t)\sin\theta}{2\theta}$$

Now the plastic moment is calculated by taking moments about the neutral axis,

$$\begin{aligned} M_p &= [A\bar{y}_t\sigma_y] + [A\bar{y}_c\sigma_y] \\ M_p &= 2[A\bar{y}\sigma_y] \\ &= 2\sigma_y [\theta t(2R - t)] \left[ \frac{(2R - t)\sin\theta}{2\theta} \right] \\ \therefore M_p &= (2R - t)^2 t\sigma_y \sin\theta \end{aligned} \quad (\text{D.21})$$

Hence from equation (D.21) substituting for  $M_o$ ,

$$\begin{aligned} M_p &= [t\sigma_y(2R - t)^2] \sin\theta \\ \therefore M_p &= M_o \sin\theta \\ \therefore \frac{M_p}{M_o} &= \sin\theta \end{aligned} \quad (\text{D.22})$$

It can be seen in Figure D.6 that,

$$\theta = \left( \frac{\pi}{2} - \beta \right) \quad (\text{D.23})$$

and thus,

$$\sin\theta = \sin\left(\frac{\pi}{2} - \beta\right)$$

### D.2.1 Combined Bending and Axial Forces

From Appendix D.2 the expression for the ratio of the actual axial force to the maximum allowable axial force is given by,

$$\frac{P_p}{P_o} = \frac{2\theta}{\pi}$$

and substitution for the value of  $\theta$  from equation (D.23),

$$\begin{aligned} \frac{P_p}{P_o} &= \frac{2\left(\frac{\pi}{2} - \theta\right)}{\pi} \\ \therefore \frac{P_p\pi}{P_o} &= 2\left(\frac{\pi}{2} - \theta\right) \\ \frac{\pi P_p}{2P_o} &= \frac{\pi}{2} - \theta \\ \therefore \theta &= \frac{\pi}{2} \left( 1 - \frac{P_p}{P_o} \right) \end{aligned} \quad (\text{D.24})$$

This value for  $\theta$  is substituted into the moment equation (D.22),

$$\therefore \frac{M_p}{M_o} = \sin\left[\frac{\pi}{2} \left( 1 - \frac{P_p}{P_o} \right)\right] \quad (\text{D.25})$$



### Axial Force Ratio vs Bending Moment Ratio

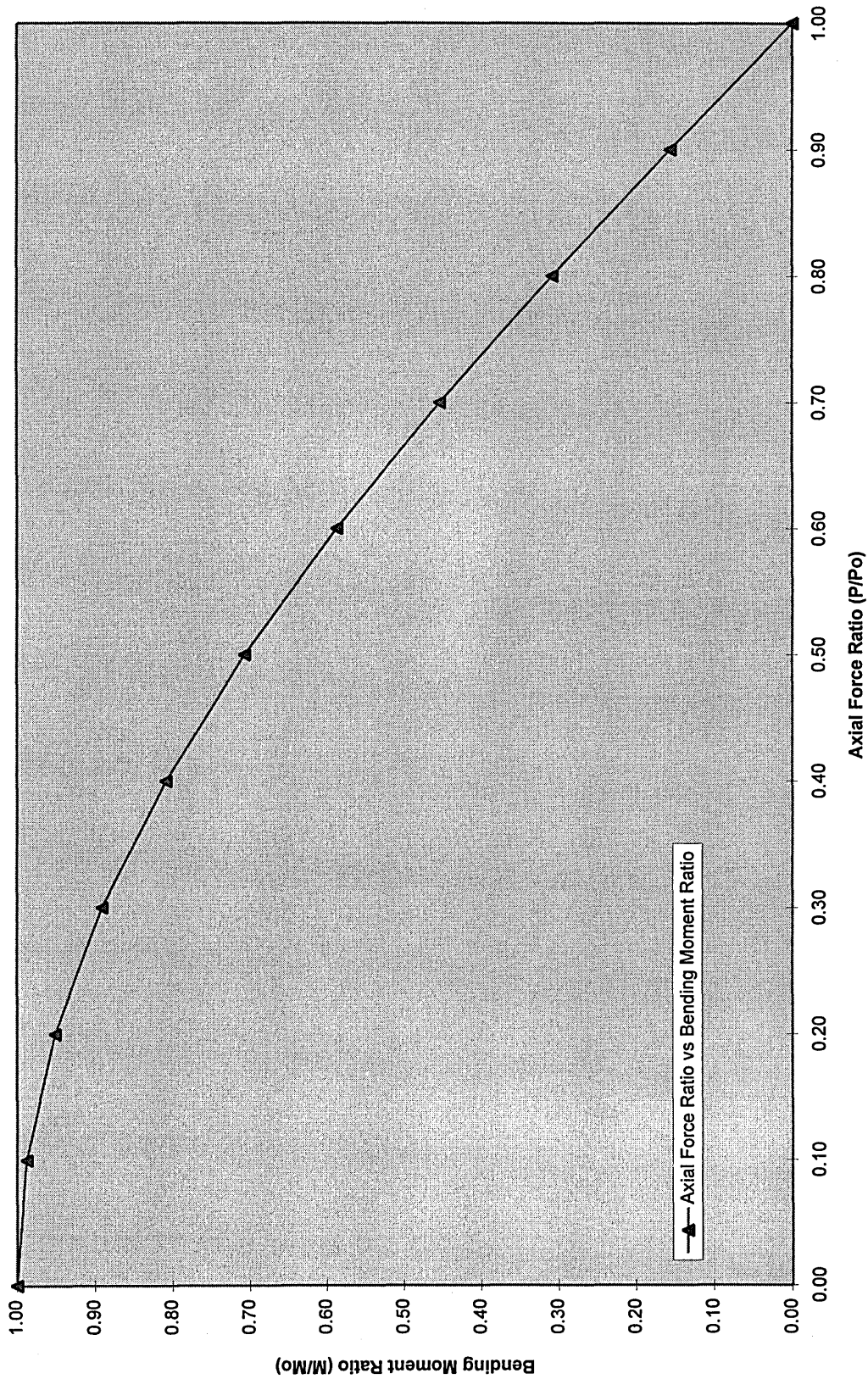


Figure D.7: Yield Surface for Combined Axial and Bending Stresses

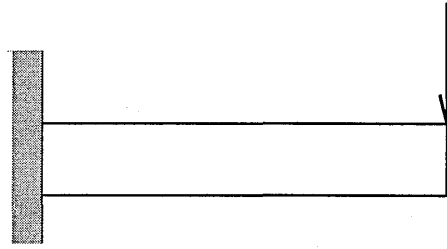
Cantilever Beam  $\phi 25.4 \times 16\text{swg}$ 

Figure D.8: NASTRAN Cantilever Beam

This can be simplified noting,

$$\sin(\theta - \beta) = \sin \theta \cos \beta - \cos \theta \sin \beta \quad (\text{D.26})$$

$$\begin{aligned} \therefore \sin\left(\frac{\pi}{2} - \frac{\pi P_p}{2P_o}\right) &= \sin \frac{\pi}{2} \cos \frac{\pi P_p}{2P_o} - \cos \frac{\pi}{2} \sin \frac{\pi P_p}{2P_o} \\ &= \cos \frac{\pi P_p}{2P_o} \end{aligned} \quad (\text{D.27})$$

From equation (D.25),

$$\frac{M_p}{M_o} = \sin \left[ \frac{\pi}{2} - \frac{\pi P_p}{2P_o} \right]$$

substitution from equation (D.27),

$$\frac{M_p}{M_o} = \cos \frac{\pi P_p}{2P_o} \quad (\text{D.28})$$

And this can then be plotted giving the relationship between the axial load and the bending moment acting. This is plotted in Figure D.7.

### D.3 Comparison of Theoretical Results with NASTRAN Results.

The work carried out in Section D.2.1 gives the theoretical expression for the axial force and bending moment interaction. Data for a tube of  $\phi 25.4 \times 16\text{swg}$  was used to determine the axial and bending moment collapse. This data was then compared to that from a NASTRAN analysis using the same material properties with the same cantilever beam. The cantilever beam is shown in Figure D.8. The results from these two analyses are presented in Figure D.9.

It can be seen that the results from these analyses compare very well and the interaction between the axial force and bending moment were modelled well using the NASTRAN (this was for a symmetric section using the default arrangement of nonlinear rod elements).

Bending Moment Ratio vs Axial Force Ratio - Comparison of NASTRAN and theoretical data.

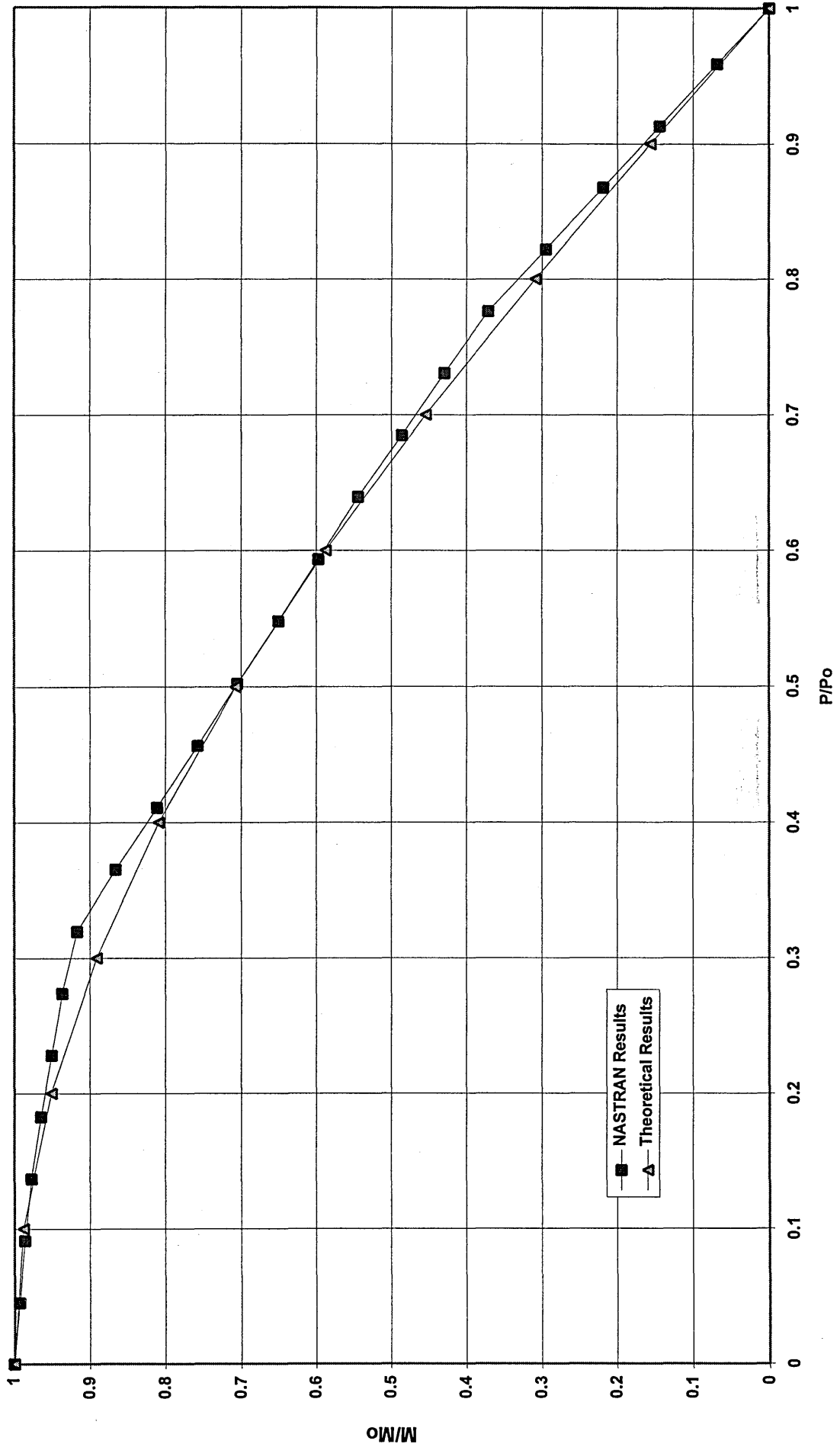


Figure D.9: NASTRAN and Theoretical Results for a Cantilever Beam

## Appendix E

# Nastran Plastic Hinge Model

NASTRAN Beam elements are capable of modelling plastic hinges. In a framework made up of prismatic beams with loads at the joints, the plastic hinges will develop only at the ends of the beam elements, since these are the points where the bending stresses are maximum. In a spaceframe truss the cross sectional axis about which the hinge will develop in any element cannot be determined, in general, by observation. In addition the presence of an axial force will modify the value of the bending moment at which the hinge appears. Once plastic deformation has occurred the plastic hinge angle will remain once the moment load is removed and a subsequent loading may result in the hinge axis becoming rotated to a different orientation.

As the hinges will occur at the ends of the BEAM elements in a space frame truss the modelling used in NASTRAN only allows for the hinges to occur at the end of the beams. This simplifies the formulation used in NASTRAN for determining the plastic hinge and does not require the user to provide detailed geometric descriptions of the beam cross section which would require a complete reformulation of the equations for the linear BEAM element and extensive computation. By making this simplification the user must supply a minimum of geometric information - cross sectional area, second moment of area about the x and y axes and the torsion constant. In addition the standard NASTRAN formulation for the element does not change which made implementation of this element more simple for MSC.

The main purpose for the NASTRAN nonlinear plastic deformation with the BEAM element is to allow the analyst to determine the overall strength and deformation of a spaceframe truss without increasing the complexity of the finite element model. The only additional information, from the users point of view, from a linear analysis is the requirement for the material yield strength.

The plastic section is added to each end of the BEAM element. Each plastic section consists of eight axial rods arranged as shown in Figure E.1. Each axial rod is capable of linear elastic strain and plastic deformation without work hardening. The elastic axial stiffness of each rod is  $\frac{EA}{8l_a}$ , where A is the local cross sectional area of the BEAM and  $l_a$  is equal to  $\frac{1}{6}$  of the length of the BEAM at each end. From Section 5 it can be seen that for a cantilever beam the plastic zone is approximately 1/3 of the beam length and the value used by NASTRAN represented a good approximation for this. In addition the model of the plastic hinge only supports elastic-perfectly plastic behaviour and this is discussed in Section 5 in relation to general engineering structures.

Each of the eight rod elements has an area of 1/8 of the beam cross sectional area and the rods are located as shown in Figure E.1. This is the default arrangement of the rods which gives good results for circular tubes. The default arrangement of rods was chosen to provide the correct neutral axis

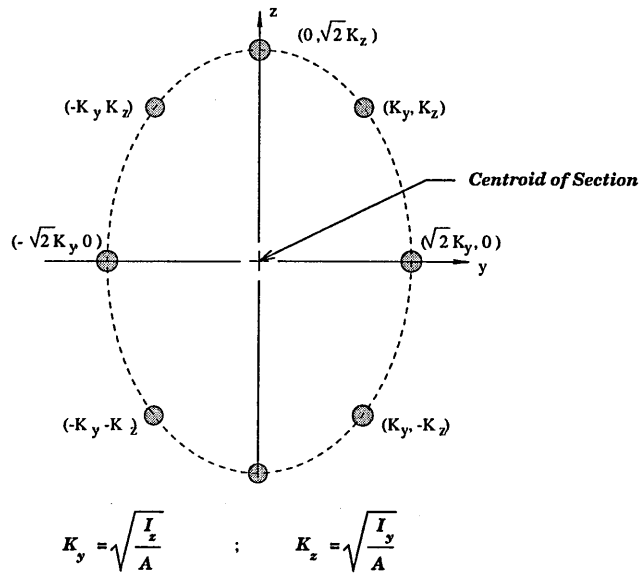


Figure E.1: NASTRAN Plastic Hinge Model

and second moment of area. It is possible to re-arrange these rods for more complex shapes which would yield poor results with the default arrangement.

The rods in the plastic section only couple to the extension and bending of the BEAM and not to the torsion or to the transverse shear. This allows the plastic section to have zero length but finite stiffness. The stiffness matrix for the linear elastic beam between the plastic sections must be modified so that the complete element has the correct elastic stiffness matrix as seen at its ends. Having a finite length of yielded section helps to ensure a gradual transition from the fully elastic state to the fully developed hinge state. Behaviour in between these two states will be plausible, but not accurate, because no means has been provided to compute the actual length of the yielded region.

Due to the problems found with the interaction of the axial and bending moments in the structure and investigation into the modelling of a plastic hinge within NASTRAN was carried out. The main investigation and analysis was the comparison of the results for a simple cantilever beam which was subjected to both axial force and a bending moment. This problem was analysed using NASTRAN as well as by hand and the results were compared. A very close correlation was found and the results are presented in Figure D.9.

As stated above the plastic hinge model consists of eight rod elements, however, in the plastic collapse the model "goes" in stages corresponding to the yield of the outermost rods followed by the incremental yield of the next set of rod elements. Consider the arrangement of the rod elements for the plastic hinge model as shown in Figure E.2. The rods are numbered one to five as shown and the rods located at the same y-location will have the same stress so they can be lumped together. The area of each of these lumped rods and the y-location are given in Table E.1. The areas are taken as a fraction of the total area  $A$  of the beam and the y-location is in terms of the second moment of area of the cross section,  $I$ . All the rods are assumed to have a modulus of  $E$  and a yield stress  $S_y$ .

Consider the strain acting in the cross section at any particular time as shown in Figure E.3. The slope of the strain curve is given by  $D$  and this corresponds to the strain due to the curvature

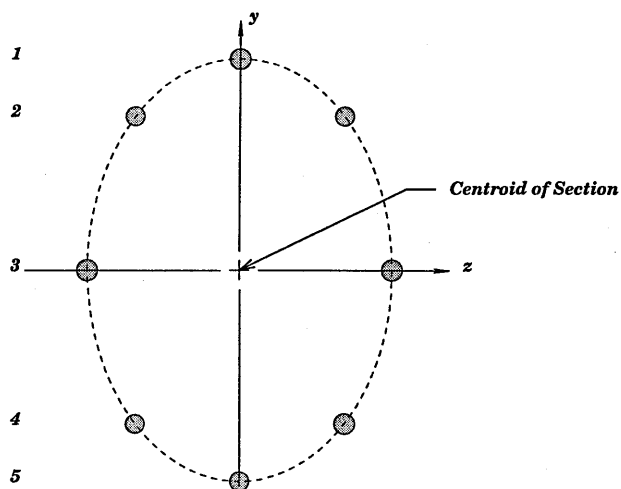


Figure E.2: NASTRAN Plastic Hinge Model Giving Locations of Lumped Masses.

Area $A_i$	Y-location $Y_i$
$A_1 = \frac{A}{8}$	$Y_1 = \sqrt{\frac{2I}{a}}$
$A_2 = \frac{2A}{8}$	$Y_2 = \sqrt{\frac{I}{a}}$
$A_3 = \frac{2A}{8}$	$Y_3 = 0$
$A_4 = \frac{2A}{8}$	$Y_4 = -\sqrt{\frac{I}{a}}$
$A_5 = \frac{A}{8}$	$Y_5 = -\sqrt{\frac{2I}{a}}$

Table E.1: NASTRAN Plastic Hinge Rod Areas and Locations

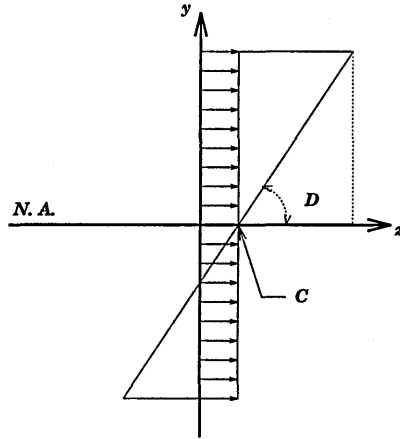


Figure E.3: Axial and Bending Strain on the Cross Section

of the section. The mean strain is represented by  $C$  which is the strain due to the axial forces. Consequently the strain in the cross section can be expressed as,

$$\varepsilon = C + DY_i \tag{E.1}$$

Letting the axial force be represented by  $P$  and the moment by  $M$ , these can be determined from the stress  $S_i$  acting on the section by,

$$P = A_i \times S_i \tag{E.2}$$

$$M = A_i \times S_i \times Y_i \tag{E.3}$$

The overall stress can be expressed as,

$$S_i = \begin{cases} -S_y & \text{for large negative strains} \\ E(C + DY_i) & \text{for intermediate values} \\ +S_y & \text{for large positive strains} \end{cases} \tag{E.4}$$

The neutral axis (N.A.) can be defined from the expression in equation (E.1). Noting that at the neutral axis  $\varepsilon = 0$ ,

$$\begin{aligned} \varepsilon &= C + DY_i \\ \therefore C + DY_i &= 0 \\ DY_i &= -C \\ \therefore Y_i &= \frac{-C}{D} \end{aligned} \tag{E.5}$$

Now if the neutral axis is held at a constant location then several unique zones can be identified.

**Stage 1:**

If the neutral axis remains at the centroid of the cross section then the situation shown in Figure E.4 arises. Thus rods 1 and 2 have a stress of  $+S_y$ ; rods 4 and 5 have a stress of  $-S_y$  and rod 3 has a stress of  $-S_y < S_3 < +S_y$ . Taking moments about rod 3,



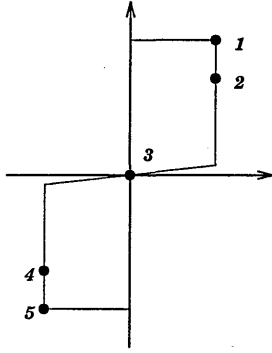


Figure E.4: Bending Failure of Cross Section (Stage 1)

$$\Sigma M_3 = F_1 Y_1 + F_2 Y_2 + F_4 Y_4 + F_5 Y_5 \quad (\text{E.6})$$

Noting from equation (E.2) for yield,

$$P = F = A_i S_y$$

Hence for each rod the force acting on them is,

$$F_1 = \left(\frac{A}{8}\right) S_y$$

$$F_2 = \left(\frac{A}{4}\right) S_y$$

$$F_4 = \left(\frac{A}{4}\right) S_y$$

$$F_5 = \left(\frac{A}{8}\right) S_y$$

(E.7)

Substitution into equation (E.6) yields,

$$\begin{aligned} \Sigma M_3 &= 2 \left[\frac{A}{8}\right] S_y \left[\sqrt{\frac{2I}{A}}\right] + 2 \left[\frac{A}{4}\right] S_y \left[\sqrt{\frac{I}{A}}\right] \\ &= \frac{\sqrt{2I}}{\sqrt{A}} \left[\frac{A}{4}\right] S_y + \frac{\sqrt{I}}{\sqrt{A}} \left[\frac{A}{2}\right] S_y \\ &= S_y \left[\frac{\sqrt{2I}\sqrt{A}}{4} + \frac{\sqrt{I}\sqrt{A}}{2}\right] \\ &= \left[0.25\sqrt{2}\sqrt{AI} + 0.5\sqrt{AI}\right] S_y \\ &= \left[(0.5 + 0.25\sqrt{2})\right] S_y \\ \therefore M &= \left[0.5 + \sqrt{0.125}\right] \left[\sqrt{AI}\right] S_y \end{aligned} \quad (\text{E.8})$$

The axial force in rod three can be expressed as,

$$0 < F < 0.25AS_y$$

Thus a maximum of one rod with area 0.25A has a tensile failure.

**Stage 2:**

When the neutral axis moves below the centroidal axis as shown in Figure E.5 there are again several distinct regions. Rods 1, 2 and 3 have a stress of  $+S_y$  and rods 4 and 5 have stress,  $-S_y$ .

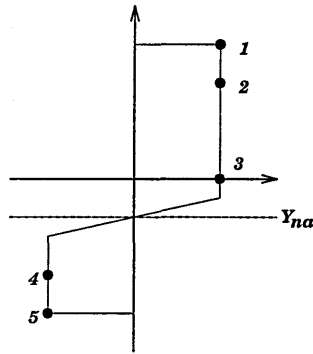


Figure E.5: Bending and Tensile Failure of Cross Section, Stage 2

**Stage 3:**

When the neutral axis moves further down the cross section and is approximately at the y location of rod 4 the following zones appear as shown in Figure E.6. Rods 1, 2 and 3 have a stress of  $+S_y$ , rod 5 has a stress of  $-S_y$  and rod 4 has a stress of,  $-S_y < S_4 < +S_y$ . This situation is illustrated in Figure E.6.

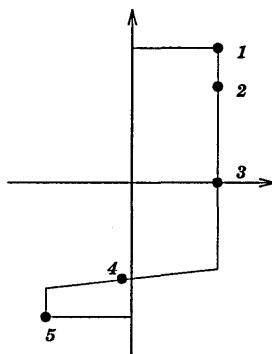


Figure E.6: Bending and Tensile Failure of Cross Section, Stage 3

**Stage 4:**

As the neutral axis moves further down the cross section the situation shown in Figure E.7 arises. Here the neutral axis is between rods 4 and 5 and the stresses in rods 1, 2, 3 and 4 are  $+S_y$  and the stress in rod 5 is  $-S_y$ .

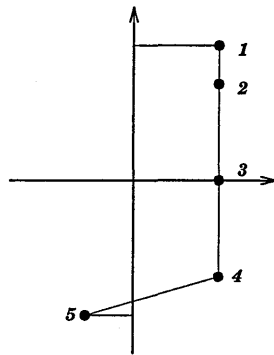


Figure E.7: Bending and Tensile Failure of Cross Section, Stage 4

**Stage 5:**

The final collapse occurs when the neutral axis reaches the extreme fibre as shown in Figure E.8. Here rods 1,2,3 and 4 all have a stress of  $+S_y$ . The force in the remaining rod is expressed as,

$$F = AS_y \tag{E.9}$$

and the moment is,

$$M = 0$$

This corresponds to the axial failure of the cross section.

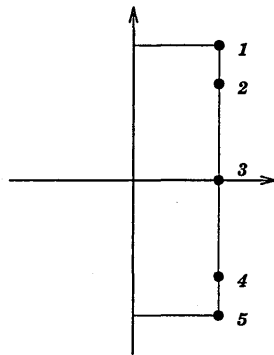


Figure E.8: Tensile Failure of Cross Section (Stage 5)

## Appendix F

# Chassis Member Cross Sectional Properties

The chassis was mainly composed of tubular sections with the exception of the lower chassis rails which were rectangular and one cross member at the front axle which was an open channel section. The cross sectional properties have been calculated below for input into the FE program.

### F.1 Calculation of Cross Sectional Properties

#### F.1.1 Cross Sectional Area

The nomenclature for the calculation of the cross sectional area is contained in Figure F.1.

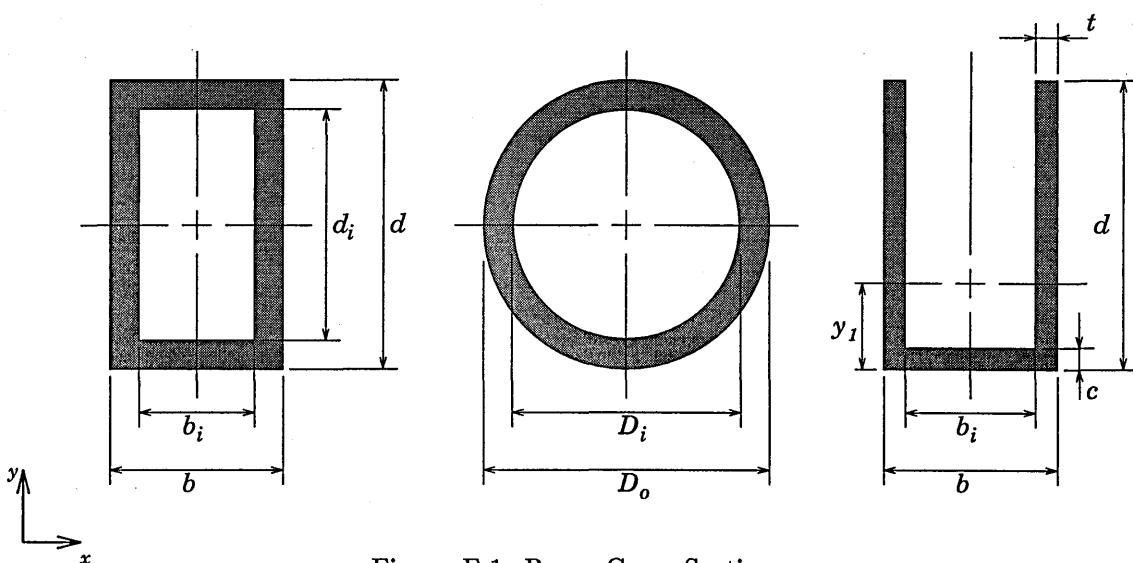


Figure F.1: Beam Cross Sections

For the rectangular cross section, Figure F.1(a), the area can be expressed as,

$$A = bd - b_i d_i \quad (\text{F.1})$$

For the circular cross sections, Figure F.1(b), the area was determined from,

$$A = \frac{\pi(D_o^2 - D_i^2)}{4} \quad (\text{F.2})$$

For the channel section, Figure F.1(c),

$$A = cb + 2t(d - c) \quad (\text{F.3})$$

These formulae were used to calculate the cross sectional areas of the various members. The calculated values are given in Table F.2.

### F.1.2 Second Moments of Area

The nomenclature used for calculation of the second moment of area are contained in Figure F.1. The general form for the Second Moment of Area can be expressed as,

$$I_x = \int y^2 dA \quad (\text{F.4})$$

$$I_y = \int x^2 dA \quad (\text{F.5})$$

#### Rectangular Section

For a rectangular cross section the second moment of area can be expressed as,

$$\begin{aligned} I_x &= \frac{(b)(d)^3}{12} - \frac{(b_i)(d_i)^3}{12} \\ \therefore I_x &= \frac{(b)(d)^3 - (b_i)(d_i)^3}{12} \end{aligned} \quad (\text{F.6})$$

$$\begin{aligned} I_y &= \frac{(b)^3(d)}{12} - \frac{(b_i)^3(d_i)}{12} \\ \therefore I_y &= \frac{(b)^3(d) - (b_i)^3(d_i)}{12} \end{aligned} \quad (\text{F.7})$$

#### Tubular Section

The second moment of area for the circular cross sections is given from the expression,

$$\begin{aligned} I_x &= I_y = \frac{\pi D_o^4}{64} - \frac{\pi D_i^4}{64} \\ \therefore I_x &= I_y = \frac{\pi(D_o^4 - D_i^4)}{64} \end{aligned} \quad (\text{F.8})$$

### Channel Section

The second moment of area for the channel section was computed using,

$$I_x = \frac{b}{3}(d+c)^3 - \frac{d^3}{3}(b-2t) - A(d+c-y_1) \quad (\text{F.9})$$

where, A is the cross sectional area, and  $y_1$  is given by the expression,

$$y_1 = \frac{bc^2 + 2td(2c+d)}{2(cb+2td)} \quad (\text{F.10})$$

For the y-axis,

$$I_y = \frac{(d+c)b^3}{12} - \frac{d(d-2t)^3}{12} \quad (\text{F.11})$$

### F.1.3 Torsion Constants

For closed cross sections the general form for the torsion constant is,

$$J_t = \frac{4A_e^2}{\oint \frac{dS}{t}} \quad (\text{F.12})$$

where,  $A_e$  is the enclosed area of the thin walled section. In all cases it is assumed that the cross sections represent thin walled sections.

### Rectangular Section

For the rectangular hollow section the mean circumference,  $L_m$  is

$$L_m = 2(b+h)$$

and the mean area of the cross section is,

$$A_e = bh$$

This is actually the area enclosed by the centreline of the section wall.

The cyclic integral is evaluated as,

$$\oint \frac{dS}{t} = \int_0^{L_m} \frac{ds}{t} = 2 \int_0^h \frac{ds}{t_1} + 2 \int_0^b \frac{ds}{t_2} = 2 \left( \frac{h}{t_1} + \frac{b}{t_2} \right) \quad (\text{F.13})$$

substitution of these values into equation (F.12) yields,

$$J_t = \frac{2b^2h^2t_1t_2}{bt_1 + ht_2} \quad (\text{F.14})$$

### Tubular Sections

For a circular cross section the torsion constant is the summation of the two second moments of area,

$$J_t = 2 \left[ \frac{\pi(D_o^4 - D_i^4)}{64} \right]$$

$$\therefore J_t = \frac{\pi(D_o^4 - D_i^4)}{32} \quad (\text{F.15})$$

### Open Section 'C' Tube

The thin walled open section of the channel requires a different method for calculating the torsion constant. Equation (F.12) does not apply to open sections. Open sections can be approximated as a long narrow rectangle. The general expression of  $J_t$  for a rectangle of height,  $h$ , and width,  $b$  is,

$$J_t = C \frac{1}{3} \sum_{i=1}^n (h_i)(b_i)^3 \quad (\text{F.16})$$

For cross sections where  $h_i > 10(b_1)$  then  $C = 1$  and if  $h_i < 10(b_1)$  then,  $C = 0.91$  [2]. In the case of a 'C' section the three rectangular sections as shown in Figure F.2 are considered as one of length  $2b + d$  and thickness  $t$ . Substitution into equation (F.16) gives,

$$J_t = (1) \frac{1}{3} [(b)(t)^3 + (b)(t)^3 + (d)(t)^3]$$

$$\therefore J_t = \frac{(2b + d)t^3}{3} \quad (\text{F.17})$$

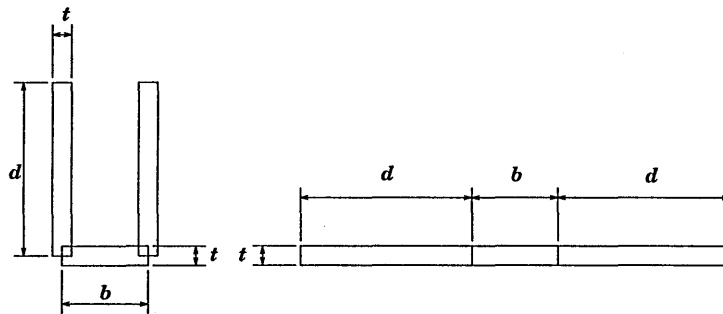


Figure F.2: 'C' Beam Cross Section



Chassis Tubing Sizes				
Description	$b$ (mm)	$b_i$ (mm)	$d$ (mm)	$d_i$ (mm)
Rectangular Section				
$60 \times 40 \times 2$	40	36	60	56
Circular Sections	$D_o$ (mm)		$D_i$ (mm)	
$1.75'' \times 16\text{swg}$	44.45		41.2	
$1.50'' \times 16\text{swg}$	38.10		34.85	
$1.00'' \times 16\text{swg}$	25.40		22.15	
$1.75'' \times 18\text{swg}$	44.45		42.01	
$1.50'' \times 18\text{swg}$	38.10		35.66	
Channel Section	$b$ (mm)	$b_i$ (mm)	$d$ (mm)	$c = t$ (mm)
$29 \times 25 \times 2$	29	25	25	2

Table F.1: Dimensions of the Chassis Tubes

## F.2 Cross Sectional Dimensions and Properties

The dimensions for each of the tubes used in the chassis are given in Table F.1. These dimensions were used for the sample calculations below. The cross sectional properties of the members are given in Table F.2.

### F.2.1 Cross Sectional Area

The following sample calculations were carried out for the rectangular base chassis members ( $60 \times 40 \times 2 \text{ mm}$ ) and one of the tubular chassis members ( $\phi 44.45 \text{ mm} \times 16 \text{ swg}$ ).

For the rectangular cross section the area is calculated using equation (F.1),

$$A = (40 \times 60) - (36 \times 56)$$

$$\therefore A = 384 \text{ mm}^2$$

For the circular cross sections the area is calculated using equation (F.2),

$$A = \frac{\pi((44.45)^2 - (41.20)^2)}{4}$$

$$\therefore A = 219 \text{ mm}^2$$

### F.2.2 Second Moment of Area

For a rectangular cross section the second moment of area was calculated using equations (F.6) and (F.7),

$$I_x = \frac{(40)(60)^3 - (36)(56)^3}{12}$$

$$\therefore I_x = 102,272 \text{ mm}^4$$

$$I_y = \frac{(40)^3(60) - (36)^3(56)}{12}$$

$$\therefore I_x = 193,152 \text{ mm}^4$$

The second moment of area for the circular cross sections was calculated using equation (F.8),

$$I_x = I_y = \frac{\pi((44.45)^4 - (41.20)^4)}{64}$$

$$\therefore I_x = I_y = 50,192 \text{ mm}^4$$

### F.2.3 Torsion Constant

The torsion constant for the rectangular section was calculated using equation (F.14),

$$J_t = \frac{2(40)^2(60)^2(2)(2)}{(40)(2) + (60)(2)}$$

$$\therefore J_t = 202,401 \text{ mm}^4$$

### F.2.4 Tubular Sections

For a circular cross section the torsion constant was calculated using equation (F.15),

$$J_t = \frac{\pi((44.45)^4 - (41.20)^4)}{32}$$

$$\therefore J_t = 100,383 \text{ mm}^4$$

The results of the calculations, along with the details of the cross sections used, are contained in Table F.2.

Cross Sectional Properties				
Description	Cross Sectional Area ( $\text{mm}^2$ )	Second Moment of Area ( $\text{mm}^4$ )		Torsion Constant ( $\text{mm}^4$ )
Rectangular Section	$A$	$I_x$	$I_y$	$J_t$
$60 \times 40 \times 2$	384	102,272	193,152	202401
Circular Sections	$A$	$I_x$	$I_y$	$J_t$
$1.75'' \times 16\text{swg}$	219	50,192	50,192	100,383
$1.50'' \times 16\text{swg}$	186	31,028	31,028	62,057
$1.00'' \times 16\text{swg}$	121	8,616	8,616	17,232
$1.75'' \times 18\text{swg}$	166	38,707	38,707	77,415
$1.50'' \times 18\text{swg}$	141	24,041	24,041	48,081
Channel Section	$A$	$I_x$	$I_y$	$J_t$
	150	9,633	20,862	211

Table F.2: Cross Sectional Properties

## Appendix G

# Torsion Load Calculation

For completeness the method used by Wanke [4] for calculating the torsion load to apply to the chassis is included.

In all the analyses of reference [4] the torsion load applied to the chassis corresponds to that required to unload one wheel. This was determined assuming that the front axle load was 450 kg.

The dynamic forces acting on the chassis were taken to correspond to the formula,

$$F_{dyn} = m \times g \times \frac{a}{g} = m \times g \times j \quad (\text{G.1})$$

where  $m$  is the mass (kg),  $g$  is the gravitational constant ( $\frac{m}{s^2}$ ),  $a$  is the actual acceleration ( $\frac{m}{s^2}$ ), and  $j$  is a dimensionless coefficient for dynamic forces. It has been reported that this dynamic coefficient for private vehicles is 2.5. In ref [4] a dynamic coefficient of 3.0 was assumed for sports cars to cater for their faster speeds and the fact that their suspension is much stiffer than family sedans. In addition a further safety factor for the dynamic forces of  $i = 1.5$  was added.

It was assumed that the total unloading of one wheel at the front of the vehicle represented a suitable torsion load to apply for the testing. The force acting in one of the front suspension mounting points was taken as,

$$\begin{aligned} F_{max} &= F_{bump} = \frac{1}{2} \times i \times j \times m_{axle} \times g \\ \therefore F_{max} &= \frac{1}{2} \times (1.5) \times (3.0) \times (450) \times (9.81) \\ \therefore F_{max} &= 9,932.63 \text{ N} \end{aligned}$$

It was therefore assumed that the load for complete unloading was 10,000 N and with a distance of 600mm between the suspension mounting points a torsion load of,

$$\begin{aligned} M_{max} &= F_{max} \times l \\ \therefore M_{max} &= 6,000 \text{ Nm} \end{aligned} \quad (\text{G.2})$$

This was the load used by Wanke for all his torsion stiffness analyses and is different to that used by the author.

## Appendix H

# RAC Safety Requirements

The following data is taken directly from the RAC *Blue Book* and is the Safety Requirements - Section Q. These are the relevant requirements which must be complied with.

## Q SAFETY CRITERIA

REFERENCE SHOULD BE MADE TO THE TECHNICAL SECTIONS IN THE SPECIFIC REGULATIONS AS TO WHICH OF THE FOLLOWING ARE MANDATORY OR RECOMMENDED FOR ANY PARTICULAR BRANCH OF MOTOR SPORT.

### 1. Safety roll-over structures

#### Introduction

The following are various specifications and configurations that can be used in manufacturing, preparing and installing Rollcages, Rollbars and Safety Cages into Saloon and Sports Cars (1.5.1), Sports Racing Cars (1.5.2), Single Seaters (1.5.3), and other forms of Competition Vehicles (1.5.4).

The details covered in this section give many permutations, the RACMSA mandatory requirements are the minimum acceptable.

Care should be taken to check FIA International requirements for Groups, Classes and Formulae which may not be covered by this section, which is for RACMSA national and lower status events.

#### Definitions

**Safety Cage.** A structural framework designed to prevent serious bodyshell deformation in the case of a collision or a car turning over.

**Rollbar.** Structural frame or hoop and mounting points.

**Rollcage.** Structural framework made up of a main rollbar and a front rollbar (or two lateral rollbars), their connecting members, one diagonal member, backstays and mounting points (see drawings 5 & 6).

**Main Rollbar.** Structure consisting of a near-vertical frame or hoop located across the vehicle just behind the front seats.

**Front Rollbar.** Similar to main rollbar but its shape follows the windscreen pillars and top screen edge.

**Lateral Rollbar.** Structure consisting of a near-vertical frame or hoop located along the right or left hand side of the vehicle. The rear legs of a lateral rollbar must be just behind the front seats. The front leg must be against the screen pillar and dashboard such that it does not unduly impede entry or exit of driver or co-driver.

**Longitudinal Member.** Longitudinal tube which is not a part of the main, front or lateral rollbar, for example, a backstay.

**Diagonal Member.** Transverse tube between a top corner of the main rollbar or upper end of a backstay and a lower mounting point on the opposite side of the rollbar or backstay.

**Framework Reinforcement.** Reinforcing member fixed to the rollcage to improve its structural efficiency.

**Reinforcement Plate.** Metal plate fixed to the bodyshell or chassis structure under a rollbar mounting foot to spread load into the structure.

**Mounting Foot.** Plate welded to a rollbar tube to permit its bolting or welding to the bodyshell or chassis structure, usually onto a reinforcement plate.

**Removable Members.** Structural members of a safety cage which are able to be removed.

#### 1.1. Specifications

1.1.1. Safety cages must be designed and made so that, when correctly installed, they substantially reduce the risk of injury to occupants.

The essential features of safety cages are sound construction designed to suit the particular vehicle, adequate mountings and a close fit to the bodyshell.

The safety cage must not unduly impede the entry or exit of driver or co-driver. Members may intrude into the occupant's space in passing through the dashboard and front side-trim, as well as through the rear side-trim and rear seats. The rear seats may be folded down.

It is not permitted for safety cages to extend beyond the front upper or rear suspension mounting points.

Any modification to a homologated safety cage is prohibited.

1.1.2. **Compulsory Diagonal Member.** Different ways of fitting the compulsory diagonal member (see drawings 5 & 6). The combination of several members is permitted.

1.1.3. **Optional Reinforcing Members.** Each type of reinforcement (see drawings 7 to 12) may be used separately or combined with others.

1.1.4. Tubes must not carry any fluids.

1.2. **Technical Specifications**

1.2.1. **Main, Front and Lateral Rollbars.** These frames or hoops must be made in one piece without joints. Their construction must be smooth and even, without ripples or cracks. The vertical part of the main rollbar must be as straight as possible and as close as possible to the interior contour of the bodyshell.

The front leg of a front rollbar or a lateral rollbar must be straight, or if it is not possible, must follow the windscreen pillars and have only one bend with its lower vertical part.

Where the main rollbar forms the rear legs of a lateral rollbar (see drawing 6), the connection to the lateral rollbar must be at roof level. To achieve an efficient mounting to the bodyshell, the original interior trim may be modified around the safety cage and its mountings by cutting it away or by distorting it. However, this modification does not permit the removal of the complete parts of upholstery or trim. Where necessary, the fusebox may be relocated to enable a rollcage to be fitted.

1.2.2. **Mounting of Rollcages to the Bodyshell.** Minimum mountings are:

1 for each leg of the main or lateral rollbar.

## SAFETY CRITERIA

1 for each leg of the front rollbar.

1 for each backstay (see 1.2.3).

Each mounting foot of the front, main and lateral rollbars must include a reinforcement plate of a material of at least the same thickness as wall of the tube to which it is being welded (minimum 3mm). Each mounting foot must be attached by at least three bolts on a steel reinforcement plate at least 3mm thick and of at least 120cm<sup>2</sup> area which is welded to the bodyshell (see drawings 13 to 18). This does not apply to backstays (see 1.2.3).

Bolts must be at least M8 size and of ISO standard 8.8 or better. Fasteners must be self-locking or fitted with lock-washers. These are minimum requirements. In addition to these requirements, more fasteners may be used, or legs may be welded directly to reinforcement plates. The rollcage may be welded to the bodyshell but must not be welded directly without reinforcement plates.

1.2.3. **Backstays.** These are compulsory and must be attached near the roofline and near the top outer bends of the main rollbar on both sides of the car. They must make an angle of at least 30° with the vertical, must run rearwards and be straight and as close as possible to the interior side panels of the bodyshell. Their materials specification, diameter and thickness must be as defined in 1.3.

Their mountings must be reinforced by plates. Each backstay should be secured by bolts having a cumulative section area at least two thirds of that recommended for each rollbar leg mounting in 1.2.2 above, and with identical reinforcement plates of at least 60cm<sup>2</sup> area (see drawing 19). A single bolt in double shear is permitted, providing it is of adequate section and strength (see drawing 20) and provided that a bush is welded into the backstay.

1.2.4. **Diagonal Members.** At least one diagonal member must be fitted. Their location must be in accordance with drawings 5 or 6 and they must be straight not curved.

The attachment points of the diagonal members must be so located that they cannot cause injuries. They may be made removable but must be in place during events. The lower end of the diagonal must join the main rollbar or backstay not further than 100mm from the mounting foot.

The upper end must join the main rollbar not further than 100mm from the junction of the backstay joint, or the backstay not more than 100mm from its junction with the main rollbar.

They must comply with the minimum specification set out in 1.3. A diagonal member fixed to the bodyshell must have reinforcement plates as defined in 1.2.3.

1.2.5. **Optional Reinforcement of Rollcage.** The diameter, thickness and material of reinforcements must be as defined in 1.3.

They must be either welded in position or installed by means of demountable joints. Reinforcement tubes must not be attached to the bodyshell.

(a) **Transverse Reinforcing Members:**

The fitting of two transverse members as shown in drawing 9 is permitted. The transverse member fixed to the front rollbar must not encroach upon the space reserved for the driver or co-driver. It must be placed as high as possible but its lower edge must not be higher than the top of the dashboard.

(b) **Doorbars (for side protection):**

Longitudinal members must be fitted at each side of the vehicle (see drawings 9 and 12). They may be removable.

The side protection must be as high as possible but not higher than one third of the total height of the door aperture measured from its base.

(c) **Roof Reinforcement:**

Reinforcing the upper part of the rollcage by adding members as shown in drawing 10 is permitted.

(d) **Reinforcement of bends and junctions:**

The reinforcement of the junction between the main rollbar or the front rollbar and the longitudinal members is permitted as shown in drawing 12 as is the reinforcement of the top rear bends of the lateral rollbars.

The ends of these reinforcing tubes must not be more than half way down or along the members to which they are attached.

1.2.6. **Protective Padding.** Where the driver's or co-driver's bodies or crash helmets could come into contact with the safety cage, non-flammable padding must be provided for protection.

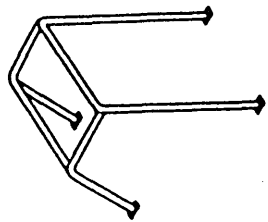
1.2.7. **Removable Members.** Should removable members be used in the construction of a rollcage, the demountable joints used must comply with an approved type (see drawings 21 to 30).



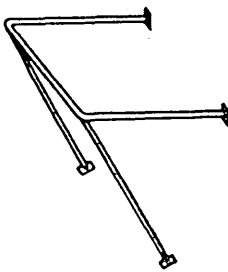
# Rollcentre

Specialists in rollcage design  
and manufacture

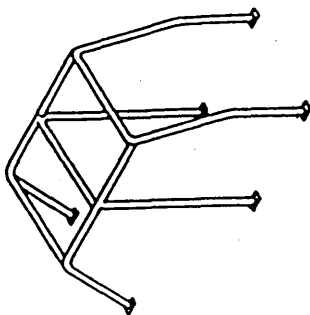
Somersham Road, St Ives, Cambs PE17 4LY  
Tel: 0480 464052 Fax: 0480 494547



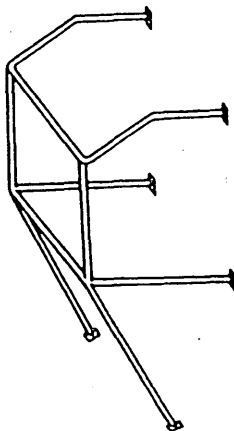
Drawing No. 2



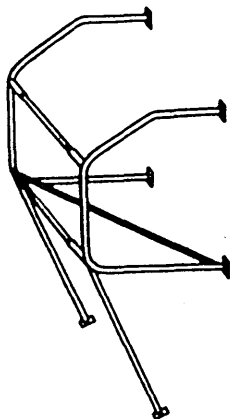
Drawing No. 1



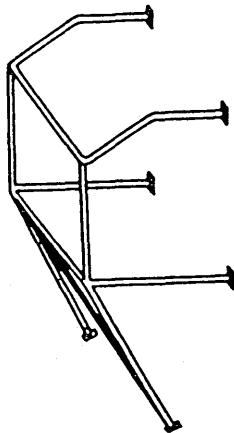
Drawing No. 4



Drawing No. 3



Drawing No. 6



Drawing No. 5

GENERAL REGULATIONS

The screws and bolts must be of adequate diameter and of ISO Standard 8.8 or better. It should be noted that demountable joints must not be used as part of a main, front or lateral rollbar because they act as hinges in the principal structure and allow deformation. Their use is solely for attaching members to the rollbars and for attaching a lateral rollbar to a main rollbar (see drawing 2). In this last case, hinged joints in drawings 21 to 30 must not be used.

1.2.8. **Guidance on Welding.** All welding should be of the highest possible quality with full penetration and preferably using a gas shielded arc. Although good external appearance of a weld does not necessarily guarantee its quality, poor looking welds are never a sign of good workmanship. When using heat-treated steel the instructions of the manufacturer must be followed (special electrodes, gas protected welding). It must be emphasised that the use of heat-treated or medium carbon steels may cause problems and that bad fabrication may result in a decrease in strength (caused by brittle heat-affected zones) or inadequate ductility.

1.3. **Material Specifications**

Specifications of the tubes used:

Minimum Material 350 N/mm<sup>2</sup>

Minimum Yield Strength

38x2.5 or 40x2.0 (EIA 1994 - 45x2.5 or 50x2.0)

Minimum Dimensions (Ø in mm)

In selecting the steel, attention must be paid to obtaining good elongation properties and adequate weldability.

The tubing must be bent by a cold working process and the centreline bend radius must be at least three times the tube diameter. If the tubing is ovalised during bending, the ratio of minor to major diameter must be 0.9 or greater.

1.4. **Exceptions**

The only exceptions to the foregoing requirements for Saloon, Single Seater and Sports Cars are as follows: 1.4.1. Safety cage manufacturers may submit a safety cage of their own design to the RACMSA for approval as regards the quality of the steel used, the dimensions of the tubes, the optional reinforcing members and the mounting to the vehicle, provided that the construction is certified to withstand the forces given hereafter in any combination on top of the Safety Cage:

- 1.5w lateral
- 5.5w Fore and Aft
- 7.5w Vertical

(w=weight of the car+75kg)

## Roll Cages? - Here's just a few.

Alfa Romeo - GTA Junior, GT Junior 2000/1750 GTV, Atlasud, Atlasud Sprint, Alfaetta, GTV Coupe, 33, 75, 164, Giulietta Sprint, Spyder, Audi - 80, 200, Quattro, Austin - A35, A40, Allegro, Maestro, Marina, Maxi, Metro, Mini, Montego, Austin Healey, 3000 4 Seater, Sprite MK1, MKII, BMW - 2002/1502, 3.0 CSL, 3 Series, M3, 5 Series, Caterham - Seven, Citroen - 2CV, AX, Visa, Mahan, Daihatsu - Charade, Spottrak, Fourtrak, Fiat - 124, 124 Coupe, 127, 128, 128 3P, 131, 500, 850 Coupe, Autobianchi, Uno, Strada, X19, Ford - Anglia, Capri I, II, III, Cortina I, II, III, IV, Cougar '86, Escort I, II, III, IV, Escort RS2000, Escort Cosworth, Fiesta I, II, III, Granada, Mkur, Mustang, Orion, Sapphire, Sierra, Sierra Cosworth, Thunderbird '86, Zodiac, Ginetta - G15, G33, GM - Camaro, Grandam, Transam, Fireo, Iroc 2, Hillman - Avenger, Hunter, Imp, Honda - Civic '83, '85, CRX '86, '87, Prelude, Isuzu - Trooper, Jaguar - XJS, Mk 1, 2, XJ6, XJ12, Jansen-Healey, Leda - Nva, Samara, Lancia - Delta, Integrate, Aurelia, Beta Coupe, Fulvia, Montecarlo, Land Rover - Series I, II, IIA, III, Defender 90 110, Range Rover, Discovery, Lotus - Contina, Eilan, Espirit, Europa, Sunbeam, Mazda - RX2, RX3, RX7, 323, MX5, Mercedes-Benz - 190, MG - 1100, 1300, MGB, MGB GT, Maestro, Metro, Midgel, Montego, TD, Mitsubishi - Colt Lancer, Colt Galant, Colt Celeste, Colt Champ, Colt Mirage, Colt Lancer Turbo, Galant GR4, Starion, Shogun, Morgan - Plus 4, Plus 4, Morrifia - 1100, 1300, Mini, Minor, Nissan - 100A, 120A, 120Y, 130, 140Y, 240Z, 240RS, 260Z, Violet A10, 510, 160J, 280Z, 280ZX, 180B, Cherry, Micra, Patrol, Sunny, Peugeot - Avenger, Tiger, Imp, Hunter, Samba, Sunbeam 205, 309, Dodge Charger, Omni, Shadow, Porsche - 911, 911 Targa, Carrera, 914, 924, 944, Reliant - Scimitar, SSI, Renault - 5, 5GT Turbo, Alliance, R8, R10, R12, R14, Clio, Rover - SD1, Montego, 800, 200, 2000 Coupe, Metro, Mini, Seat - Ibiza, Saab - 96, 99, Turbo, 900, M66, SImca - Rally 1000, Skoda - 120, 130 Estelle, Coupe, Favorit, Rapido, Subaru - 1600, 4WD Saicron, RX Turbo, Sunbeam - Alpine, Tiger, Suzuki - Swift Mk1, Mk2, SJ410, SJ413, Vialra, Talbot - Avenger, Samba, Sunbeam, Triumph - Dolomite, Spitfire, G16, 2000, Viessse, Herald, TR2, TR3, TR3A, TR4, TR5, TR6, TR7, Toyota - Celica, Corolla, MR2, Starlet, TVR - 3000M, Vauxhall Opel - Ascona A, Ascona B, Astra Mk1, Mk2, Mk3, Chevrolet, Magnum, Mania B, Monza, Opel GT 1900, Nova Corsa, Viva, Volvo - 120, 140, 240, 340, 340, 540, 544, VW - Beetle, Golf Mk1, Mk2, Scirocco, Polo, Jetta. Plus all the others that we couldn't fit in here... And, we can make bespoke and weld-in cages for any vehicle to any specification!

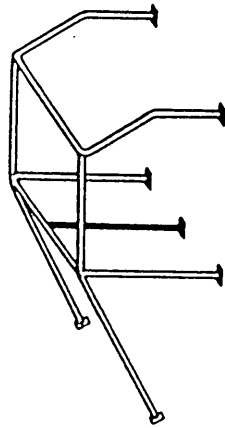
**Safety Devices**  
**JALEYBARSO**

30 Regal Drive, Soham, Cambridgeshire CB7 5BE  
Telephone 0353 624624, Facsimile 0353 624824

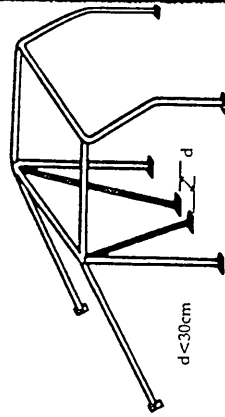


Q

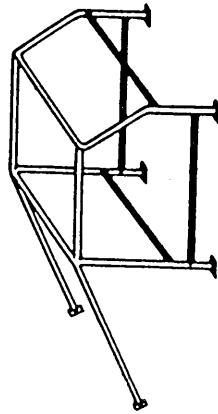
GENERAL REGULATIONS



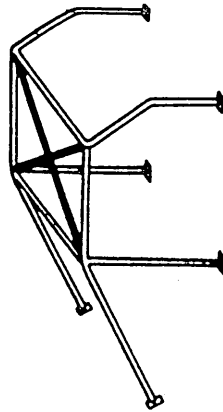
Drawing No. 7



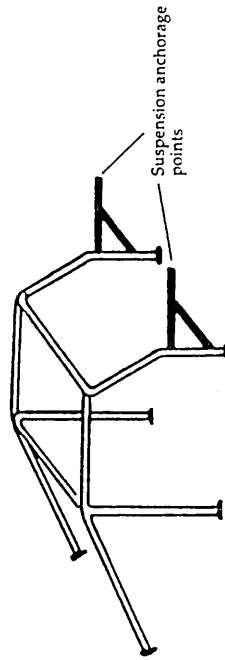
Drawing No. 8



Drawing No. 9



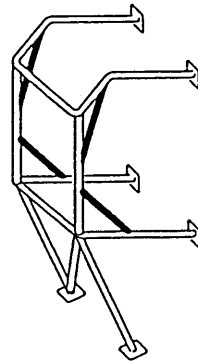
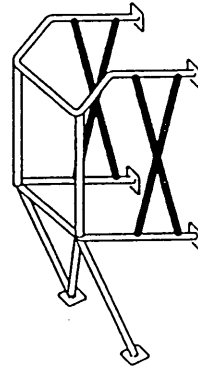
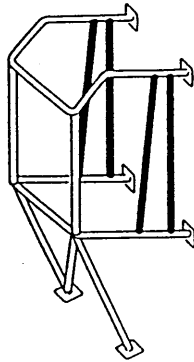
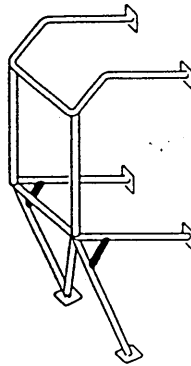
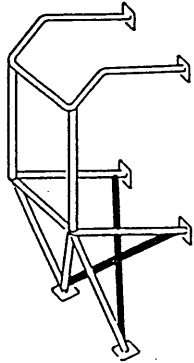
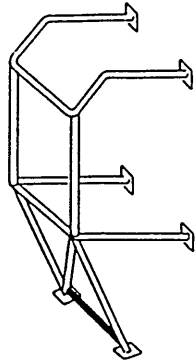
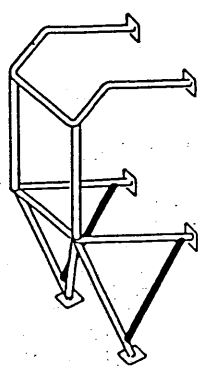
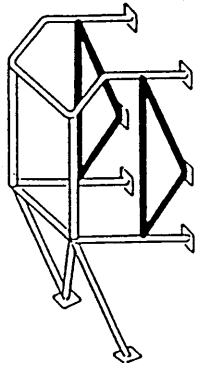
Drawing No. 10



Drawing No. 11

SAFETY CRITERIA

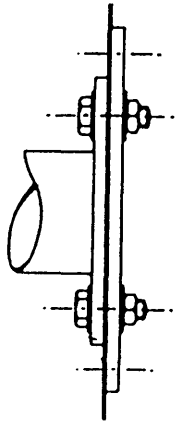
Q



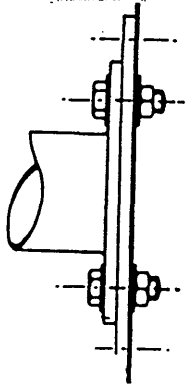


Q

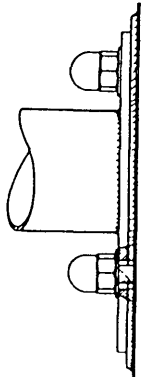
GENERAL REGULATIONS



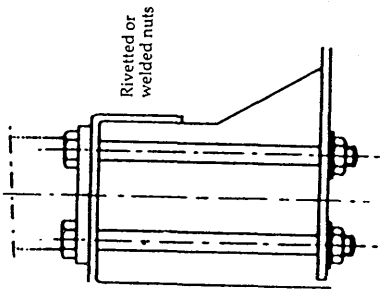
Drawing No. 13



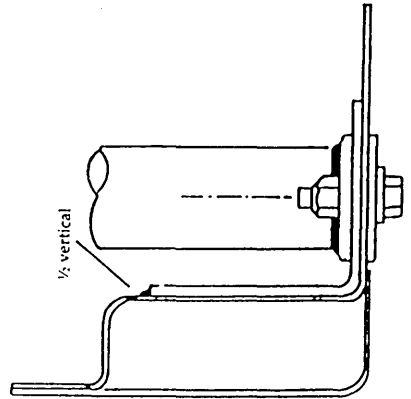
Drawing No. 13(a)



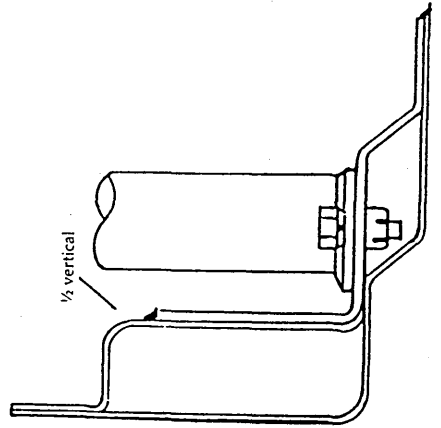
Drawing No. 13(b)



Drawing 14



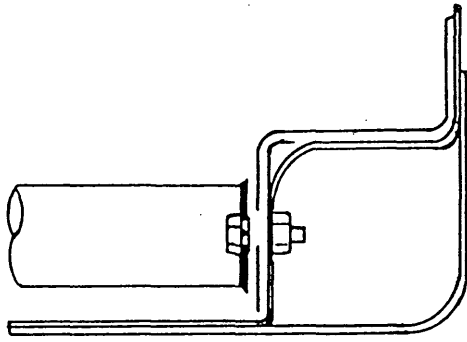
Drawing No. 15



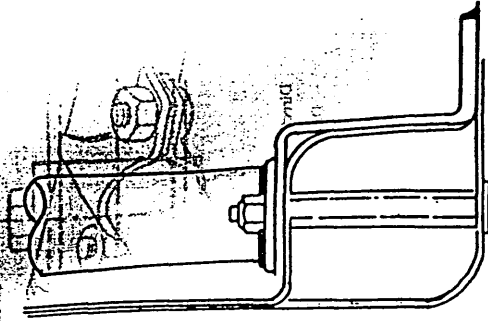
Drawing No. 16

SAFETY CRITERIA/20

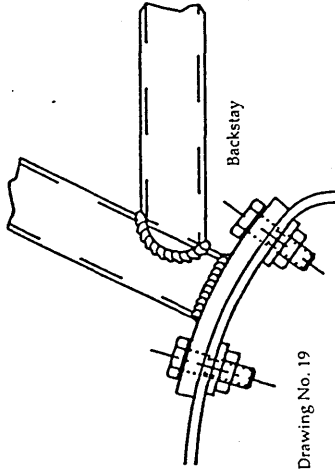
Q



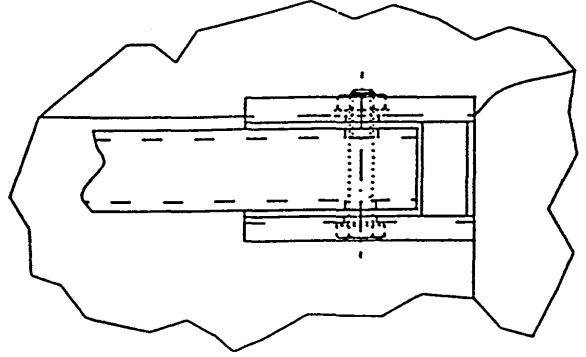
Drawing No. 17



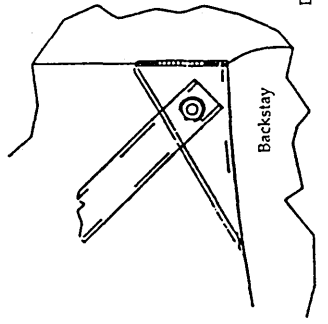
Drawing No. 18



Drawing No. 19

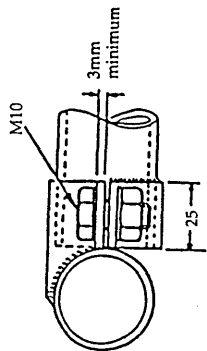
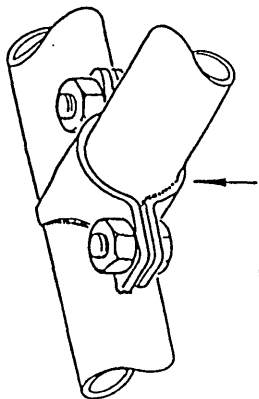


Drawing No. 20



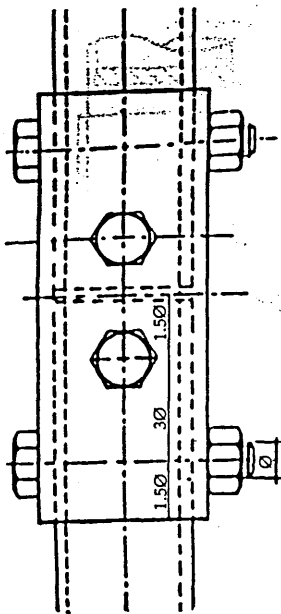
Q

GENERAL REGULATIONS

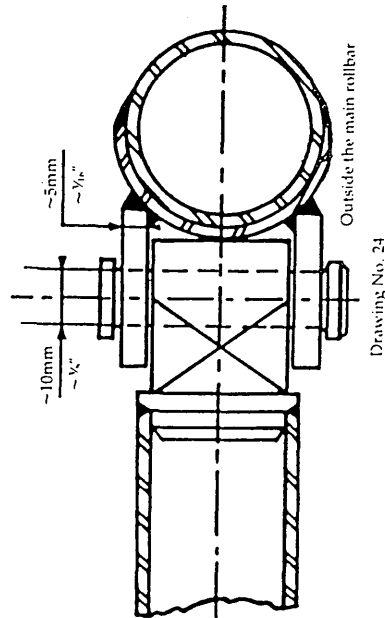
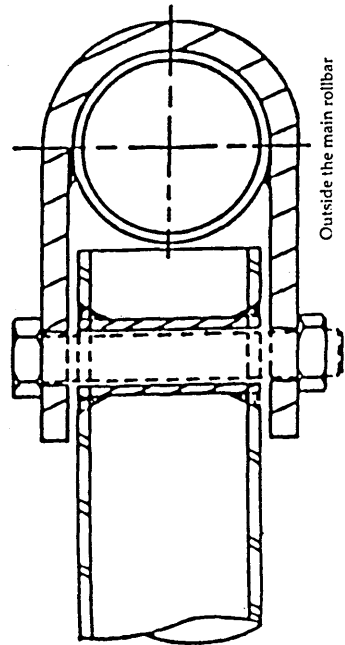
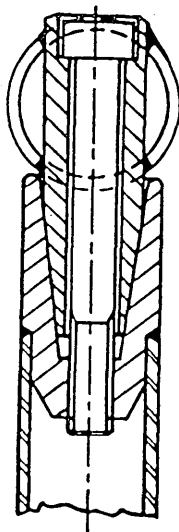
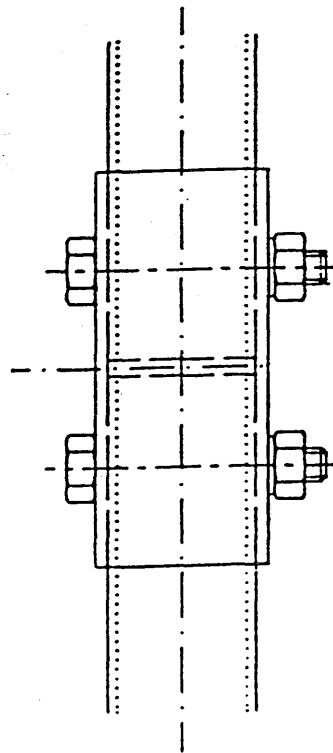


Q

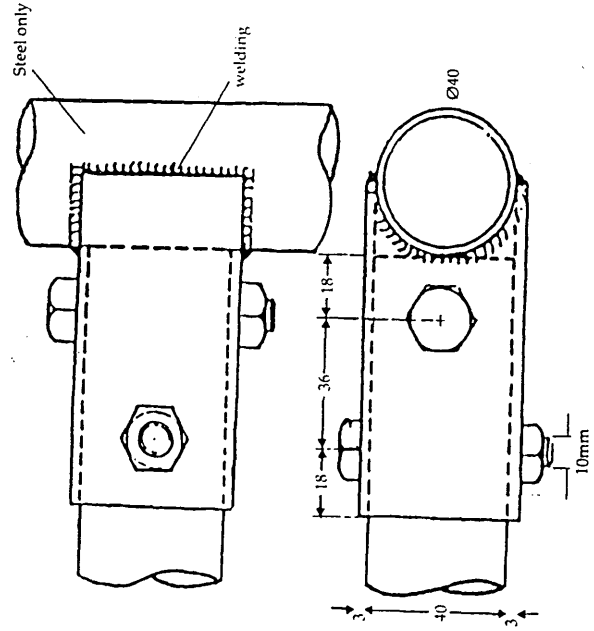
SAFETY CRITERIA



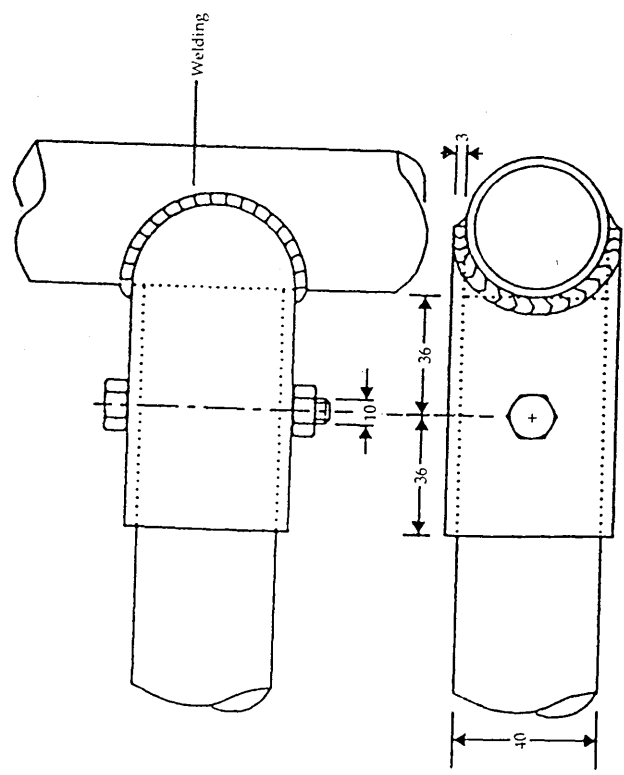
$\varnothing = 14\text{mm}$  (tube  $\geq 40\text{mm}$  <math>\leq 50\text{mm}</math> diam. ext.)  
 $16\text{mm}$  (tube  $\geq 50\text{mm}$  diam. ext.)



GENERAL REGULATIONS

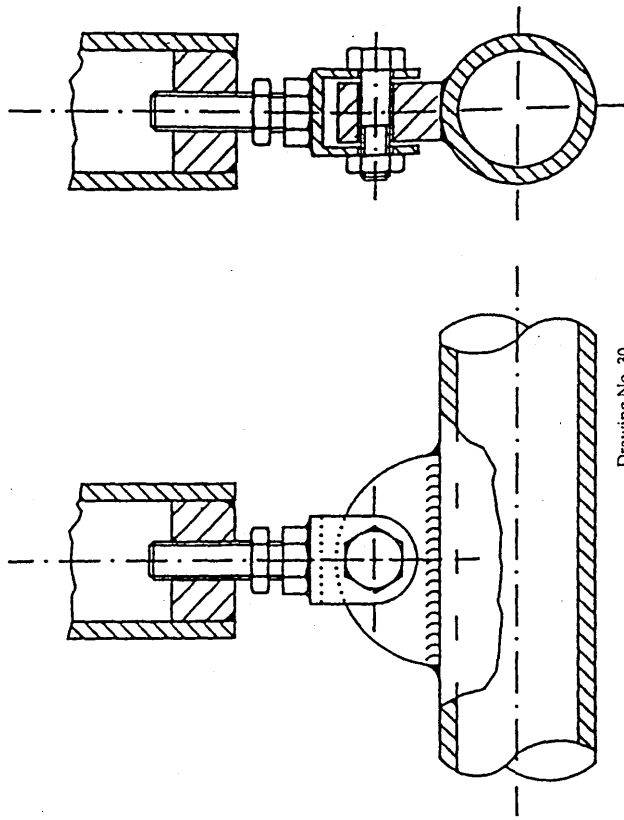


Drawing No. 28



Drawing No. 29

SAFETY CRITERIA



Drawing No. 30

Note: Where a Safety cage manufacturer submits a cage and full documentation to the RACMSA a 'Rollbar' certificate will be raised and issued. Duly authorised copies of this certificate containing a drawing and/or photograph of the Safety cage and a declaration that the rollcage can resist the forces specified must be available to event Scrutineers.

1.4.2. To obtain RACMSA approval, a manufacturer must have demonstrated his consistent ability to design and manufacture Safety cages which comply with the specifications approved by FIA.

1.4.3. Manufacturers recognised by the RACMSA must only supply customers with products designed and manufactured to the approved standards.

1.4.4. Each RACMSA approved manufacturer must be able to demonstrate to the RACMSA:

- (a) That the material used has a certificate of origin or traceability and is kept segregated from other batches of material.
- (b) That welding procedures he uses produce consistent and sound welds and are regularly checked by laboratory tests.
- (c) That he operates and maintains auditable in-house quality standards and procedures which are updated regularly.

1.5. Vehicle Categories Covered

1.5.1. Saloon cars and open sports cars

BASIC ROLLBAR/ROLLCAGE (Drawings 1 and 2) for Production Cars, Touring Cars, Open Sports Cars up to 2000cc.

BASIC ROLLCAGES (Drawings 3 and 4) for Production Cars, Touring Cars, Open Sports Cars over 2000cc. The compulsory diagonal member for all events except rallies can be fixed as illustrated, in all basic rollcages (drawings 5 & 6).

The combination of several diagonal members is permitted.

The different possibilities of installing the optional reinforcing members to the rollcage are shown in drawings 7 to 12.

Each type of reinforcement (drawings 7 to 12) may be used separately or combined with one or several others.

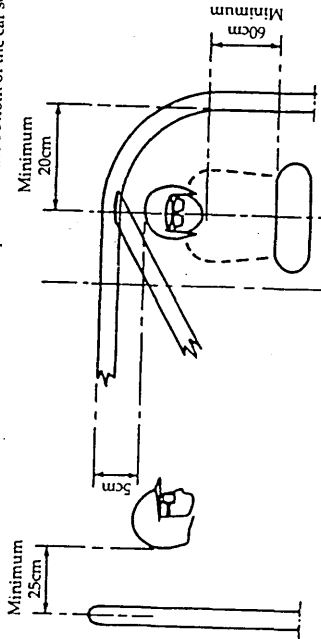
These reinforcements can be installed in each of the basic rollcages (drawings 1-4).

MINIMUM MATERIAL  
As defined in 1.3.

GENERAL REGULATIONS

1.5.2. Sports racing cars

The rollbar must conform to drawing 1 with diagonal brace (drawings 6 and 31). Minimum height 92cm measured along the line of the driver's spine from the bottom of the car seat.



Drawing No. 31

MINIMUM MATERIAL  
Cold drawn seamless  
Carbon Steel 350N/mm<sup>2</sup>

MINIMUM DIMENSIONS  
48.3 x dia x 2.6mm

1.5.3. Single seater racing cars

The rollbar must be symmetrical about the lengthwise centre-line of the car and of minimum height 90cm measured vertically from the base of the cockpit or 92cm measured along the line of the driver's spine from the bottom of the car seat. There must be at least one brace rearwards from the top of the rollbar at an angle not exceeding 60° with the horizontal, this brace must be the same diameter as the rollbar, if two braces are fitted to the tube the diameter may be reduced to 20-26mm the wall thickness being maintained. In addition, forward facing braces should be considered. The width inside the roll-over bar main tubes must be 38cm minimum measured 60cm above the base of the seat. It must incorporate a crossbrace to restrain the driver's head and give rearward support. The top hoop radius must not be less than 10cm measured at the centre line of the tube.

MINIMUM MATERIAL  
Cold drawn seamless  
Carbon steel 350N/mm<sup>2</sup>

MINIMUM DIMENSIONS  
42.4 dia x 2.6 in mm

1.5.4. Other considerations

- (a) An effective rollbar must be fitted with its top edge not less than 5cm above the helmet of the normally seated driver. It must be wider than the driver's shoulders at that height. It must be constructed of good quality seamless steel tubing of minimum 35mm diameter and wall thickness of 2mm. It should have a 6mm hole drilled in the underside for checking the tube thickness. It should have the top bar straight or slightly curved but no tubes meeting in an inverted 'V'. It must be effectively braced to structural members.
- (b) Non-standard cars are advised to fit a rollbar to the following minimum requirements. Minimum height 72cm from the rear of the uncompressed seat cushion. It must have minimum flat width of 38cm running into braced to structural members forward and aft of the cockpit and not less than cockpit width. It must be constructed of good quality seamless steel tubing of minimum 32mm diameter and wall thickness of 1.5mm.

1.5.5. ALL aluminium alloy Roll Cages are prohibited.

1.6. Aerodynamics. The use of a rollbar to achieve or supplement aerodynamic effects is prohibited.

1.7. Future

It should be noted that International Safety Roll Over Structure Regulations are being issued by FIA and will become mandatory 1.1.94. The RACMSA will align itself with these regulations wherever possible.

2. Seat belts

- 2.1. All seat safety belts must be made out of approved materials and anchored securely into the vehicle.
- 2.1.1. Seat belts, in the following specified configurations, must be worn and be correctly adjusted at all times during events.
  - 2.1.1.1. Three point. One diagonal shoulder strap and one abdominal strap, with three fixation points on the chassis/body shell or roll over bar of the vehicle on either side and to the rear of the driver's seat.
  - 2.1.1.2. Four point. Two shoulder straps and one abdominal strap, with four fixation points on the chassis/body shell or roll over bar of the vehicle. On either side of the driver and two to the rear of the driver's seat (or one symmetrical for the two shoulder straps).

The first choice in ...

# LIFELINE fire systems

WHY ARE LIFELINE STILL AT THE FRONT ?

- \* LIFELINE SYSTEMS WORK IN ANY POSITION WITH THEIR UNIQUE FLEXIBLE DIP TUBE
- \* MANUFACTURED IN HIGH QUALITY ALUMINIUM OR CARBON FIBRE
- \* ELECTRICALLY OR MECHANICALLY OPERATED SYSTEMS



# HALON or...

THE WORLD LEADERS IN COMPETITION FIRE PROTECTION ARE FIRST AGAIN WITH ZERO 2000



Save OZONE LAYER BEING THE ENVIRONMENTALLY ACCEPTABLE ALTERNATIVE TO HALON

Save WEIGHT, TYPICALLY 40 - 50% LIGHTER

Save MONEY WHEN YOU NEED TO REFILL

Save INSTALLATION COSTS BEING EASILY FITTED AS A REPLACEMENT FOR A LIFELINE HALON SYSTEM



LIFELINE FIRE & SAFETY LTD. 11 Hurstake Road, Riverway Estate, Newport, I.W., PO30 5UU, UK. Tel. (0)983 521921 Fax. (0)983 522951

GENERAL REGULATIONS

Q

2.1.3. Six point. Two shoulder straps, one abdominal strap and two straps between the legs, with six fixation points on the chassis/body shell or roll over bar of the vehicle. On either side of the driver, two to the rear of the driver's seat (or one symmetrical for the two shoulder straps) and two between the legs.

2.1.4. It is permitted to make a hole in series production seats to allow secure anchoring of seat belts. Notes: It is not permitted to mix parts of seat belts. Only complete sets as supplied by manufacturers should be used.

Only one release mechanism is permitted on each seat belt configuration and this must be available for the wearer to operate whilst seated in the competing position.

The fixation point to the rear should be positioned so that the strap from the shoulder is as near horizontal as possible. It should not be located on the floor directly behind the driver/co-driver.

Seat belts once involved in a serious accident should be discarded. Belts subjected to oil, acid or heat should be replaced.

3. Fire Extinguishers

A fire extinguisher/extinguishing system should be carried on all vehicles, the minimum requirement being that it should be either BCF, or equivalent extinguishant and be operable by the driver whilst normally seated either by manual operation or by a mechanically/electrically assisted triggering system.

3.1. Extinguishers will be classified as Small, Medium or Large, and designated as Hand Held or Plumbed-In. Due to variations in weight and specific gravity of the different extinguishants, lists of manufacturers equivalents will be compiled against the previous Halon weights, and will be available from the RACMSA. Dry powder extinguishers are prohibited.

Note. As replacement extinguishers become available, 'Halons' is being phased out. Every effort should be made to establish the change over by 1 January 1996.

3.1. Capacities

3.1.1. Small, Hand operated.

3.1.2. Medium, Plumbed-In, for discharge into both cockpit and engine compartment.

3.1.3. Large, Plumbed-In, for discharge into both cockpit and engine compartment.

3.1.4. Large, Plumbed-In, for discharge into Engine compartment, plus Medium, Hand Held for Driver or Rally Co-driver use.

3.1.5. Hand operated for cockpit (International).

Table of Equivalents

	BCF	Zero 2000	AFFF
3.1.1	1.5	0.7	0.9
3.1.2	2.5	1.12	TBA
3.1.3	5.0	2.25	TBA
3.1.4	5.0	2.25	TBA
	2.5	-	1.75
3.1.5	4.0	-	2.65

All capacities are minima

Plumbed in Systems

3.2.1. The Large unit it should have two points of triggering one for the driver (and Co-driver in Rallies) and one outside the car for activation by Marshals etc.

3.2.2. The triggering point from the exterior must be positioned close to the Circuit Breaker (or combined with it) and must be marked by the letter "E" in red inside a white circle or at least 10cm diameter with a red edge.

3.2.3. In installing units the direction of nozzles should be carefully considered. Induction, Exhaust, Ignition and Fuel pumping systems being the most likely areas for fire to occur.

3.2.4. Where possible sources of fire exist outside the engine or cockpit areas (ie front mounted fuel tanks) advice should be sought from the RACMSA concerning plumbed-in system installations.

3.2.5. All bottles should discharge simultaneously and must be operable in any position of the car even if inverted.

3.2.6. It is strongly recommended that plumbed-in bottles should be mounted in the fore and aft direction in the vehicle. The fitting of a pressure gauge is recommended.

3.2.7. Method of Operation: The preferred method of operation is electrical which should have its own source of energy for triggering, ideally with provision for checking the integrity of the systems triggering circuit.

3.2.8. Mechanically operated systems, if used, should be fitted with 'Total Discharge' valves (ie ones that continue to discharge even if the operating mechanism should fail after triggering). Hand held extinguishers which have been adapted, by addition of pull-cables, rarely have the capability of being operated in varying positions and are not acceptable.

Publications and equipment available from RACMSA



- PUBLICATIONS**
- 1994 RACMSA Yearbook (British motor sport regulations).....each £18.00
  - 1994 FIA Yearbook of Automobile Sport (international regulations).....each £37.00
  - 1994 FIA Yearbook of Karting Sport (the Karting 'Yellow Book').....each £14.00
  - 1994 RACMSA Motor Sports Directory.....each £3.00
  - 1994 RACMSA Fixture List & Motor Sport Clubs.....each £3.00
  - Starting Motor Sport (28-page booklet).....each £2.50
  - Motor Vehicles (Competition & Trials) Regulations 1969/1974/1976.....each £3.00

**CLUB EQUIPMENT**

- Club membership cards.....200 for £8.00
- Signing-on sheets (Competitors/Officials).....30 for £3.00
- Signing-on sheets (Press).....30 for £3.00
- "Prohibited Area" warning signs (rigid PVC).....per pack of five £28.00
- "Motor Sport Can Be Dangerous" signs (rigid PVC).....per pack of five £28.00
- "Special Stage Warning" (day-glo sign).....each £1.00
- "Special Stage Danger" (day-glo sign).....each £1.00
- Special Stage symbols for road books, etc (Letraset sheet).....per sheet £12.00
- Road/Stage symbols for road books, etc (Letraset sheet).....per sheet £12.00
- Motor Club Manual (ring-binder with regular updates).....£19.00

**HOMOLOGATION & LOG BOOKS, ETC**

- FIA Vehicle Homologation Book for any British car.....each £16.00
- FIA Vehicle Homologation Book for any British car.....each £21.00
- FIA Group A Vehicle Homologation Book for any non-UK car.....each £26.00
- FIA Group N Vehicle Homologation Book for any non-UK car.....each £21.00
- FIA Homologation Papers — Extension.....each £11.00
- RACMSA Competition Vehicle Log Book.....each £16.00
- RACMSA Historic Vehicle Identity Form.....each £21.00

All prices are current at the date of publication, but may be changed without notice.  
Send cheque or postal order with order to: Tina Donnelly, Corporate Services,  
RAC Motor Sports Association Ltd, Motor Sports House, Riverside Park, Colnbrook,  
Slough SL3 0HG

GENERAL REGULATIONS

- 3.2.9. Weight checking: Extinguisher systems should be capable of being dismantled for the purpose of checking the weight of the extinguisher and the integrity of the cylinder, also to enable the operating system to be serviced without discharging the contents. The tare weight of the unit must be marked on the cylinder.
- 3.2.10. Installation: Particular attention should be paid to the installation and maintenance of any system, especially if it is mechanically operated. Pull cables should be fitted in such a way that no kinks or 'S' bends are formed which could cause malfunction.
- 3.3. During events:
- 3.3.1. All plumbed-in extinguisher systems must be in an 'ARMED' condition (ie be capable of being operated without the removal of any safety device) at all times whilst competing or practising in races or speed events (including during post-event scrutineering), and at all times that crash helmets are worn on rallies (ie. on Stages etc.).
- 3.3.2. Any plumbed-in extinguisher system found to be incapable of being operated will be the subject of a report to the Clerk of the Course/Stewards for possible penalisation as an offence against Safety Regulations.
- 3.3.3. Checking for correctly 'Armed' extinguisher systems, should only be carried out by RACMSA Scrutineers, and/or Judges of Fact nominated for that purpose.
- 3.4. Hand held extinguishers
- 3.4.1. Must not be carried loose but should be retained in positive quick release brackets, secured to the vehicle by a minimum of two 6mm bolts.
- 3.4.2. Extinguishers with pressure gauges are recommended.
- 3.4.3. The tare weight of the unit must be clearly marked on the cylinder.
- 3.5. General
- It is recommended that all fire extinguisher bottles be securely mounted within the main structure of the vehicle. It is prohibited to mount bottles of over the medium capacity outside the main structure.
4. Safety Fuel Cells
- The FIA approved standard for Safety Fuel Cells is FIA/Spec/FT 3. These fuel cells are only manufactured by authorised companies and bear the name of the company, specification, code and date of manufacture stencilled on each cell. No other cells are approved. Cells of over five years old are deemed obsolete.
5. Red Warning Light
- A rearward facing red warning light of a minimum of 21 watts, with surface area minimum 20cm<sup>2</sup>, maximum 40cm<sup>2</sup>, or of 21 watts with a surface area minimum of 50cm<sup>2</sup> and with lens and reflector to EC Standards, must be located within 10cm of the centre line of the vehicle and be clearly visible from the rear. The warning light must be switched on when visibility conditions are reduced or when instructed by the Clerk of the Course.
6. Tank fillers, vents and caps
- Tank fillers and caps must not protrude beyond the bodywork or be situated within the driver/passenger compartment. The caps must have an efficient locking action to reduce the risk of opening during an accident and to ensure closing after refuelling (14.1.2). Air vents must be at least 25cm to the rear of the cockpit.
7. Crushable structure
- The entire fuel tank area 'Licked by the open air stream' must incorporate a crushable structure as follows:
- 7.1.1. The crushable structure should be a sandwich construction based on a fire resistant core of minimum crushing strength 25lb/sq.in. It is permitted to pass water pipes through this core.
- 7.1.2. The minimum thickness of the sandwich construction must be 10mm. The fore and aft fuel tank area, however, must provide for a crushable structure of at least 100mm thickness at its thickest point, the position of this widest point to be at the constructor's discretion, over a length of at least 35cm after which it may be generally reduced to 10mm.
- 7.1.3. The sandwich construction must include two sheets of 1.5mm thick aluminium sheet having a tensile strength of 14 tons/sq.in and minimum elongation of 5%.
- 7.1.4. All oil tanks mounted outside the main chassis structure must be surrounded by crushable structure of minimum thickness 10mm.
8. External circuit breaker
- The circuit breaker, when operated, must isolate all electrical circuits with the exception of those that operate fire extinguishers. The triggering system for the circuit breaker on saloons should be situated at the lower part of the windshield mounting, preferably on the driver's side or below the rear window. On Open Cars it should be situated on the lower main hoop of the Roll-over Bar on the driver's side or at the lower part of the windshield mounting (as above).
- Alternatively on Historic Cars, the mounting point may be mounted approximately vertically below the line of the scuttle on the driver's side.
- The location to be identified by a Red Spark on a White edged Blue triangle, and the 'On' and 'Off' positions clearly marked.
9. Overalls
- Clean Flame-Resistant overalls, must be worn. Flame resistant overalls may be manufactured from Nomex III, or Proban treated materials. Competitors are also strongly advised to wear Flame Resistant gloves, socks, balacavas and underwear. Plastic shoes (such as trainers) should be avoided.

SAFETY CRITERIA

Q

- From 1st January 1994 a standard of BS 6249 part 1 Index A or B, or FIA standard overalls will be mandatory, (note Index C is not acceptable). This standard will be clearly marked on the label within the garment. Overalls manufactured to other European standards which have FIA approval are acceptable, and will display an FIA label and number stitched into the collar or waist band of the garment.
- BS 6249 part 1 was formerly expressed under standard BS 3120, this standard was withdrawn in 1982. Garments displaying BS 3120 will be acceptable for RACMSA events until 31 December 1995.
- As with any item of safety equipment, evidence of damage or excessive wear can render it unsuitable for use. In the case of overalls this could include over frequent, or incorrect, washing, broken seams or stitching and worn patches. Two piece overalls should be avoided, but if worn must overlap and provide flame resistant coverage.
- Due to the complex nature of national test standards and variations of detailed testing it is not possible to quote 'equivalents' from foreign national standards unless they are FIA approved as detailed above. National test standards will eventually be superseded by European norms (CE Marks), which will provide a common standard throughout Europe.
- Individual competitors are responsible for ensuring their own safety and that appropriate flame resistant overalls are worn when mandatory.
10. Crash Helmets
- 10.1. Crash helmets bearing an RACMSA approval sticker must be worn at all times during training, practice and competition. The user must ensure that the helmet is to a standard currently specified [10.3.1.1], that it fits properly, is secured properly and that it is in a serviceable condition. It is strongly recommended that a flame resistant balacava, helmet bib or face mask also be worn.
- 10.2. Total protection can never be given by any headgear, and the best of crash helmets may not entirely prevent head injury or death in a severe accident. Helmet users must understand that helmets are deliberately constructed so that the energy of a severe blow will be absorbed by the helmet and thereby partially destroy it. The damage may not be readily apparent; it is essential therefore that any helmet receiving a blow in an accident is either replaced or returned to the manufacturer for competent inspection - this of necessity must be the responsibility of the helmet user, who will have been aware of the circumstances under which the helmet was struck. It is not possible nor indeed reasonable to expect the scrutineer, in every case, to observe significant damage. Where there is any doubt about the helmet's fitness for its intended purpose then the Chief Scrutineer is empowered to remove the RACMSA Approval Sticker and impound the helmet for the duration of the meeting. This should be a rare occurrence since competitors must appreciate that, once a helmet has served its purpose, it is not only sensible but necessary to replace it. It is the competitor himself who must ensure that the helmet which he uses is fully fit for its purpose; it is clear that this is a small insurance to pay for one's life. The competitor also might consider that, should he survive an accident, but receive head injuries having knowingly used a previously damaged helmet, he could be placing an enormous burden of care upon his family.
- 10.2.1. Impounding of helmets:
- Case 1 Pre-Event. If the helmet does not conform with the required Standards or is in a poor or dangerous condition, the Chief Scrutineer will impound the helmet for the duration of the Meeting, removing the RACMSA sticker. At the close of the Meeting the helmet will be returned, as received with the exception of the RACMSA sticker, to the competitor concerned.
- Case 2 Accident during the Event. If the competitor is injured and the helmet is damaged, the Chief Scrutineer will impound the helmet and remove the RACMSA sticker then seek the advice of the Steward as to further action.
- Case 3 Accident during Event and competitor evacuated to hospital with head injuries. The Chief Scrutineer will make sure that the helmet has been seen by the Chief Medical Officer, he will then impound the helmet and remove the Authorisation Sticker. Unless the Chief Medical Officer wishes to retain the helmet it must be despatched to the Technical Department at the RACMSA. Unless specifically called for by the competitor it will be disposed of after six weeks.
- 10.3. The competitor is reminded of the following essential criteria when buying or using his helmet:
- (a) Correct Fit.
- (b) Correct Fit.
- (c) Security.
- (d) Condition.



2 and 3 layer suits, FIA Approved for International Motor Sport.  
 RACMSA approved helmets stocked BELL · SHOEI · ARAI · SIMPSON · TOP-TEC  
 Send for 1994 catalogue and list of stockists  
 Dept. MSY, 363 Dogthorpe Road, Peterborough PE1 3RE. Tel. 0733 68247. Fax 0733 68249.

\*Clean Flame-Resistant overalls, to a minimum standard of BS6249 Part 1 Proban, must be worn. Competitors are also strongly advised to wear Flame-Resistant gloves, socks, balacavas and underwear. Plastic shoes (such as trainers) should be avoided.

Q

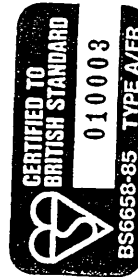
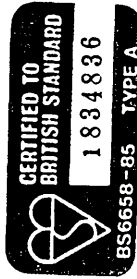
GENERAL REGULATIONS

# INTERNATIONAL HELMET STANDARDS

B.S.I. (Great Britain)

- BS6658-85 Type A

- BS6658-85 Type A/FR



Snell Foundation (USA)

-SA85\*

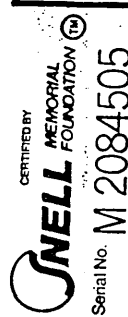
-SA90



-M85\*



-M90\*



\*Valid until 31st December 1995.

## SAFETY CRITERIA

Q

10.3.1. Standard. Helmets bearing one of the undermentioned 'standards' may be approved by the RACMSA subject to other criteria being met.

### ACCEPTABLE HELMET STANDARDS

BS 6658 - 85 'A' (Type 'B' is not acceptable)

BS 6658 Type A/FR

SNELL SA 85, M 85, M 90 SA 90, (NB SA 85, M 85 and M 90 may be phased out from 31 December 1995)

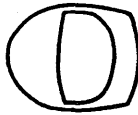
See also colour chart on page 228.

Note\*, for FIA Events must have fire resistant standard.

Part of the approval procedure is to affix an RACMSA sticker to the outside of the helmet in the approximate location of the driver's right ear. Stickers may only be affixed by selected scrutineers, by the RACMSA at Motor Sports House, or by selected manufacturers, after the helmet has been checked for conformity with the standard required and is considered to be in a satisfactory condition. RACMSA approval stickers, for which a fee of £1 is charged, are printed on foil, and once individually affixed, cannot be reapplied. Note that helmet standards are regularly reviewed and updated, and superseded. Standards will periodically cease to be acceptable; hence an element of 'lifing' will always remain.

Approval sticker

Colour: Fluorescent yellow

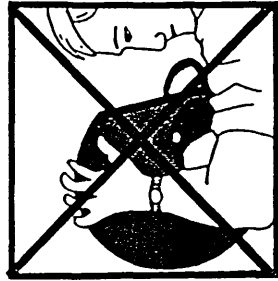
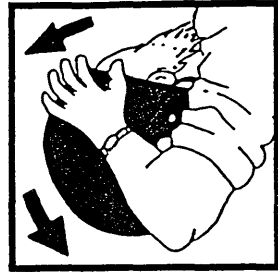
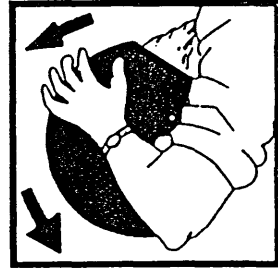


10.3.2. Fit and Security. To ensure satisfactory fit and security of your helmet, proceed as follows:

- Obtain correct size by measuring the crown of your head.
- Check that there is no side-to-side movement; a helmet should be as closely fitting as possible consistent with comfort.
- Tighten straps securely - the chin strap must be under tension at all times; ensure therefore that the strap cannot slip. Chin cups are prohibited.
- With head forward attempt to pull up the back of the helmet, as shown in the diagram below, to ensure the helmet cannot be removed in this way.
- Ensure you can see clearly over each shoulder.
- Make sure nothing impedes your breathing in the helmet and never cover your nose or mouth other than with a flame resistant balaclava or face mask. Helmets with life-support attachments must only be worn if they are connected to a life-support system.
- Never wear a scarf, tie or other loose clothing which could come loose and possibly cause an accident.
- Ensure that the visor can be opened with one gloved hand.
- Satisfy yourself that the back of the helmet provides protection for your neck.
- Do not buy from mail order unless you can satisfactorily carry out the above checks; return a helmet unused if it does not fit.

10.3.3. Condition and Care of Helmet

- The user himself must bear the prime responsibility for ensuring that his helmet is fit for the purpose intended, since significant damage to the helmet may have been sustained without this being apparent to the scrutineer.
- Anything other than minor superficial damage is likely to result in the scrutineer removing the RACMSA sticker and impounding the helmet for the event.
- It is in everyone's interest for the competitor to buy the best helmet he can and to look after it (the best is not necessarily the most expensive). A helmet bag should always be used.
- There must be no alteration to the structure of a helmet. Where a radio intercom is fitted this should only be done in accordance with the helmet manufacturer's instructions.





## Q

### SAFETY CRITERIA

- 14.1.6. **Headrests.** On all vehicles where it is not mandatory (13) it is strongly recommended that a head restraint in the form of a headrest be fitted, as near to the driver's/co-driver's helmet as possible, to prevent whiplash of the neck and spine in case of impact. It is recommended that they comply with 13.
- 14.1.7. **Radiator Caps.** These caps should be positioned or shielded in such a way that hot water or steam cannot scald the driver of the vehicle if they become opened or broken in an accident.
- 14.1.8. **Clutch and Bell Housing Protection.** It is recommended that a shield be placed to guard the clutch/bellhousing and to protect in case of clutch/bellhousing derangement. This can be a 1/8in steel plate, or sandbag type absorber as used in drag racing.
- 14.1.9. As a general principal, competitors are advised to replace any safety item, helmet, safety harness, seats etc., should they have been involved in a severe accident.

### GENERAL REGULATIONS

- (e) Use only a weak solution of soft soap and water to clean the interior and exterior of the helmet; do not get the interior too wet.
- (f) Some moulded plastic helmets although they meet approved standards can be seriously damaged by substances such as petrol, paint, adhesives, cleaning agents and stickers (not the RACMSA Stickers) - such damage may not always be apparent; however, crazing or obvious dulling of the surface finish could indicate serious structural weakening of the helmet and is likely to result in the scrutineer removing the RACMSA sticker and impounding the helmet for the event.
- (g) The helmet should be stored, preferably in a helmet bag, in a cool dry place away from sunlight when not in use. Do not strap the helmet to the roll cage or allow other unrestrained movement which could cause the helmet to be damaged.
- (h) A good helmet, properly cared for, is one very important link in a long chain of safety measures. Do not allow it to become the weak link. Do not rely on others. You are responsible for your own safety. Do not, through your own fault, become a grave burden to others.

#### 11. Goggles or Visor

Either goggles or a visor must be worn at all times during training practice and competing, unless in a closed vehicle.  
Recommended visor standard (minimum) BS4110Y.

#### 12. Front Engine Cars

With front engine cars a propellor shaft restraint should be fitted. Either safety hooks or a rigidly fixed steel panel of not less than 18swg.

#### 13. Head Restraints

Head restraints must be fitted, capable of restraining a 17kg mass decelerating at 5g. Dimensions to be 10cm x 10cm and located such that the driver's/passenger's head/helmet is restrained and cannot move past it under rearward forces, or be trapped between the rollbar and the head restraint. It is recommended that it be within 5cm of the driver's/passenger's helmet when they are normally seated.

#### 14. General Safety Recommendations

14.1. Owing to the widely varying nature of competitions and the vehicles taking part in them, the RACMSA takes the view that it would not be in the best interests of the competitors to cover all aspects of safety precautions with mandatory regulations. Inevitably such regulations could not necessarily provide for the most appropriate safety precautions in all foreseeable circumstances.

The RACMSA therefore draws attention to the following points so that the competitors can consider them and take precautions as seem appropriate to their own particular requirements.

##### 14.1.1. Electrical

(a) **Batteries** - precautions should be taken to reduce the possibility of acid burns from batteries in case of accidents. Batteries should be sealed in a leak-proof non-conductive insulated compartment.

(b) **Electrical System** - all wiring should be secured and well protected to reduce the risk of fire from electrical short circuits.

##### 14.1.2. Fuel

(a) **Fuel Tanks and Pipes** - every effort should be made to isolate fuel tanks and pipes from the driver/passenger compartment. The risk of fuel spillage from accident damage can be reduced by use of bag type tanks or by coating metal tanks with GRP. Tanks should be located so that they are given maximum protection by the structure of the vehicle. Vents should be designed to avoid spillage if the vehicle becomes inverted.

(b) **Fuel Fillers** - these should be designed and located to reduce risk of damage. Filler caps should not be liable to open in the case of an accident. Simple screw caps are effective. The positive locking of the fuel filler caps is recommended. The filler pipe to the tank should be of minimum possible length and not protrude beyond the bodywork (6).

14.1.3. **Steering Wheels** - the types least likely to inflict injuries due to breakage should be selected. Uncovered wooden rims should be avoided.

14.1.4. **Fire Extinguishers** - even small extinguishers carried in a vehicle can extinguish or contain fires before they develop seriously. Minimum recommendation is for a 1.5kg extinguisher. More sophisticated equipment is required in many events and full vehicle systems are highly recommended (see 3).

14.1.5. **Seats** - all seats should be correctly located and securely anchored in such a way as to allow no movement in squab or backrest.

When installing a Competition Seat, carry out the following checks before selection or purchase:

- (a) Study the requirements of the vehicle concerned and ask the manufacturers advice and recommendations.
- (b) Check that the seat is suitable for the type of forces to which it could be subjected. These will include fore and aft and lateral loadings.
- (c) Check that the seat carries full instructions for installation in your vehicle.
- (d) Check that suitable mounting installations are available from the manufacturer.
- (e) Ask the manufacturer to confirm that the seat frame is suitable for your Motor Sport discipline.
- (f) If the original seat attachments and supports are changed, the following minimums should be applied - 4 attachments per seat using 8mm bolts - steel reinforcement plates/brackets 3mm, or light alloy 5mm - surface area for each mounting point (brackets and counterplates) 40cm<sup>2</sup>

## **Appendix I**

# **NASTRAN Data Files**

Non-Linear Data File with Force Load.

ID MSC-XL, MSC-NASTRAN  
 SOL 101  
 TIME 5000  
 CEND  
 TITLE = MSC/NASTRAN ----- MSC/XL  
 SUBTITLE = Extended Chassis including front extension and extra width  
 LABEL = Mounted on base and restrained in 123 direction  
 \$ FILENAME: EXTLONGFRONTLOAD.DAT  
 \$ Plate is removed to speed up analysis, load is in aft direction  
 \$ Model is made up of both elastic and plastic elements  
 \$ Roll cage is to Neil andersons drawing.  
 \$ Load applied to front corner of the roll cage  
 MAXLINES=200000  
 DISP = ALL  
 OLOAD = ALL  
 SPCFORCE = ALL  
 ELSTRESS = ALL  
 ELFORCE = ALL  
 STRAIN = ALL  
 SEALL = ALL  
 ESE = ALL  
 SPC = 1

SUBCASE 1  
 LOAD = 1  
 SUBCASE 2  
 LOAD = 2  
 SUBCASE 3  
 LOAD = 3  
 SUBCASE 4  
 LOAD = 4  
 SUBCASE 5  
 LOAD = 5  
 SUBCASE 6  
 LOAD = 6  
 SUBCASE 7  
 LOAD = 7  
 SUBCASE 8  
 LOAD = 8  
 SUBCASE 9  
 LOAD = 9  
 SUBCASE 10  
 LOAD = 10  
 SUBCASE 11  
 LOAD = 11  
 SUBCASE 12  
 LOAD = 12  
 SUBCASE 13  
 LOAD = 13  
 SUBCASE 14  
 LOAD = 14  
 SUBCASE 15  
 LOAD = 15  
 SUBCASE 16  
 LOAD = 16  
 SUBCASE 17  
 LOAD = 17  
 SUBCASE 18  
 LOAD = 18  
 SUBCASE 19  
 LOAD = 19  
 SUBCASE 20  
 LOAD = 20  
 BEGIN BULK  
 PARAM POST 0  
 PARAM AUTOSPC YES  
 \$  
 \$

\$ THIS SECTION CONTAINS ALL DEFINED COORDINATE SYSTEMS

CORD2C	1	0	1731.	45.	30.	1731.	45.	31.	+
	1732.	45.	30.						
CORD2C	2	0	2065.	-45.	30.	2065.	-45.	31.	+
	2066.	-45.	30.						

\$ THIS SECTION CONTAINS BULK DATA FOR SE 0

GRID	1	2500.	750.	30.
GRID	2	2959.	400.	72.3
GRID	3	850.	750.	262.
GRID	4	1600.	750.	320.
GRID	5	2300.	750.	310.
GRID	6	2850.	750.	310.
GRID	7	-50.	-248.	30.
GRID	8	28.	-248.	30.
GRID	9	106.	-248.	30.
GRID	11	122.5	-248.	30.
GRID	12	139.	-248.	30.
GRID	14	219.5	-248.	30.
GRID	15	300.	-248.	30.
GRID	17	388.	-248.	30.
GRID	18	526.	-248.	30.
GRID	20	535.75	-248.	30.

MULTIPLE LINES REMOVED FROM HERE.....  
 GRID 1671 2055.644486.1075937.9016  
 GRID 1674 -413.5 950.  
 GRID 1677 2055. 413.5 950.  
 \$

CBAR	1	7	8	1
CBAR	2	1	9	1
CBAR	3	1	11	1
CBAR	4	1	12	1
CBAR	5	1	14	1
CBAR	6	1	14	1
CBAR	7	1	15	1
CBAR	8	1	17	1
CBAR	9	1	18	1
CBAR	10	1	20	1
CBAR	11	20	21	1

MULTIPLE LINES REMOVED FROM HERE.....

CBAR	116	3	165	166	1.
CBAR	117	3	166	167	1.
CBAR	118	3	167	129	1.
CBAR	119	3	170	21	1.
CBAR	120	3	170	171	1.
CBAR	121	3	171	172	1.
CBAR	122	3	172	173	1.
CBAR	123	3	173	174	1.
CBAR	124	3	174	175	1.
CBAR	125	3	36	177	1.
CBAR	126	3	177	178	1.
CBAR	127	3	178	179	1.
CBAR	128	3	179	180	1.
CBAR	129	3	180	181	1.

MULTIPLE LINES REMOVED FROM HERE.....

CBAR	1277	3	1674	1608	1.
CBAR	1278	3	1430	1877	1.
CBAR	1279	3	1677	1603	1.

\$ THIS SECTION CONTAINS THE LOADS, CONSTRAINTS, AND CONTROL BULK DATA ENTRIES

FORCE	1000	1475	0	108590.	5.5	1.5	-7.5
LOAD	1	1.	0.02	1000			
LOAD	2	1.	0.05	1000			
LOAD	3	1.	0.07	1000			
LOAD	4	1.	0.1	1000			
LOAD	5	1.	0.12	1000			

LOAD 6	1.	0.15	1000
LOAD 7	1.	0.17	1000
LOAD 8	1.	0.20	1000
LOAD 9	1.	0.22	1000
LOAD 10	1.	0.25	1000
LOAD 11	1.	0.27	1000
LOAD 12	1.	0.30	1000
LOAD 13	1.	0.32	1000
LOAD 14	1.	0.35	1000
LOAD 15	1.	0.37	1000
LOAD 16	1.	0.40	1000
LOAD 17	1.	0.42	1000
LOAD 18	1.	0.45	1000
LOAD 19	1.	0.47	1000
LOAD 20	1.	0.50	1000
\$ SPC 1	1	123456	0.0
\$ SPC 2	2	123456	0.0
\$ SPC 3	3	123456	0.0
\$ SPC 4	4	123456	0.0
\$ SPC 5	5	123456	0.0
\$ SPC 6	6	123456	0.0
\$ SPC 7	7	123	0.0
\$ SPC 8	8	123	0.0
\$ SPC 9	9	123	0.0
\$ SPC 10	10	123	0.0
\$ SPC 11	11	103	0.0
\$ SPC 12	12	106	0.0
\$ SPC 13	13	43	0.0
\$ SPC 14	14	44	0.0
\$ SPC 15	15	45	0.0
\$ SPC 16	16	46	0.0
\$ SPC 17	17	48	0.0
\$ SPC 18	18	49	0.0
\$ SPC 19	19	50	0.0
\$ SPC 20	20	51	0.0
\$ SPC 21	21	73	0.0
\$ SPC 22	22	74	0.0
\$ SPC 23	23	79	0.0
\$ SPC 24	24	80	0.0
\$ SPC 25	25	81	0.0
\$ SPC 26	26	82	0.0
\$ SPC 27	27	89	0.0
\$ SPC 28	28	93	0.0
\$ SPC 29	29	94	0.0
\$ SPC 30	30	58	0.0
\$ SPC 31	31	59	0.0
\$ SPC 32	32	60	0.0
\$ SPC 33	33	61	0.0
\$ SPC 34	34	63	0.0
\$ SPC 35	35	64	0.0
\$ SPC 36	36	65	0.0
\$ SPC 37	37	66	0.0
\$ SPC 38	38	68	0.0
\$ SPC 39	39	69	0.0
\$ SPC 40	40	70	0.0
\$ SPC 41	41	71	0.0
\$ SPC 42	42	76	0.0
\$ SPC 43	43	77	0.0
\$ SPC 44	44	84	0.0
\$ SPC 45	45	85	0.0
\$ SPC 46	46	86	0.0
\$ SPC 47	47	87	0.0
\$ SPC 48	48	91	0.0
\$ SPC 49	49	95	0.0
\$ SPC 50	50	96	0.0
\$ SPC 51	51	98	0.0
\$ SPC 52	52	99	0.0
\$ SPC 53	53	100	0.0
\$ SPC 54	54	101	0.0

\$ THIS SECTION CONTAINS THE PROPERTY AND MATERIAL BULK DATA ENTRIES

\$ PBAR 1	1	384.	193152.	102272.	207016.				
\$ PBAR 2	1	247.3	74810.	74810.	149620.				
\$ PBAR 3	1	183.4	30539.	30539.	61078.				
\$ PBAR 4	1	119.5	8462.	8462.	16924.				
\$ PBAR 5	1	233.6	51968.6	51968.6	79720.6				
\$ PBAR 6	1	370.2	89687.9	201241.3809.8					
\$ PBEAM 3	1	183.4	30539.	30539.	61078.				+
\$ PBEAM 5	1	233.6	51968.6	51968.6	79720.6				+
\$ PBEAM 1	1	213.	47962.	47962.	95924.				+
\$ PBEAM 6	1	370.2	89687.9	201241.3	809.8				+
\$ PBEAM 1	1								+
\$ MAT1 1	1	207000.	PLASTIC	0.0	7.85-6	1	250.		
\$ SMATS1 1	1			.33					
\$ SFLPARM 1	5			AUTO					NO
\$ SFLPARM 2	30			AUTO					NO
\$ ENDDATA									

Non-Linear Data File with Displacement Load

Nonlinear Data File

```

ID      MSC-XL, MSC-NASTRAN
SOL 106
TIME 10000
CEND
TITLE = Non Linear Test File of TWR Chassis - 8/3/95
SUBRTIE = load applied to the front windscreen corner of the roll cage
          load applied acting in an aft direction in this case.
LABEL = SPC applied on tunnel base
$Bar element added to the load point to apply displacements at the front $windscreen c
orner.
$
$ Additional spcd cards and subcases added for complete collapse - 11/3/95
$
$ Additional spcd cards and subcases added to displace the loaded corner
$ 200mm - 13/3/95
$
$ File based on nonlinear_data_fns_w_lgdisp.dat - in this model the restraints
$ are changed to model those used for the test. The rest of the model is
$ unchanged.
$
$ This model is set up with web gussets as was the test model - this represents the test
chassis 20/10/95
$
$ This model uses two materials to estimate the collapse mode of the chassis
$ the chassis elements are taken as CDS 3 with a yield of 350 MPa whereas
$ the roll cage is ERW 11 with a yield of 200 MPa.
$
MAXLINES = 40000000
DISP = ALL
LOAD = ALL
SPCFORCE = ALL
ELSTRESS = ALL
ELFORCE = ALL
STRAIN = ALL
SEALL = ALL
ESE = ALL
SPC = 100
SUBCASE 1
LOAD = 100
NLPARM = 1
SUBCASE 2
LOAD = 101
NLPARM = 1
SUBCASE 3
LOAD = 102
NLPARM = 1
SUBCASE 4
LOAD = 103
NLPARM = 1
Subcase 5 to 70 removed....
$
$
SUBCASE 71
LOAD = 162
NLPARM = 3
SUBCASE 72
LOAD = 163
NLPARM = 3
SUBCASE 73
LOAD = 164
NLPARM = 3
SUBCASE 74
LOAD = 165
NLPARM = 3
SUBCASE 75

```

LOAD = 166  
NLPARM = 3  
Additional subcases removed.....  
\$  
\$

```

BEGIN BULK
PARAM IGDISP 1
PARAM POST 0
PARAM AUTOSPC YES
SPCD 100 10002 1 0.159 10002 2 -0.796
SPCD 101 10002 3 0.584
SPCD 101 10002 1 0.318 10002 2 -1.592
SPCD 101 10002 3 1.168
SPCD 102 10002 1 0.478 10002 2 -2.388
SPCD 102 10002 3 1.751
SPCD 103 10002 1 0.637 10002 2 -3.184
SPCD 103 10002 3 2.335
SPCD 104 10002 1 0.796 10002 2 -3.981
SPCD 104 10002 3 2.919
SPCD 105 10002 1 0.955 10002 2 -4.777
SPCD 105 10002 3 3.505
SPCD 106 10002 1 1.115 10002 2 -5.573
SPCD 106 10002 3 4.087
SPCD card 107 to 149 removed for clarity....
SPCD 150 10002 1 15.126 10002 2 -75.631
SPCD 150 10002 3 55.463
SPCD 151 10002 1 15.922 10002 2 -79.612
SPCD 151 10002 3 58.382
SPCD 152 10002 1 16.719 10002 2 -83.593
SPCD 152 10002 3 61.301
SPCD 153 10002 1 17.515 10002 2 -87.573
SPCD 153 10002 3 64.220
SPCD 154 10002 1 18.311 10002 2 -91.554
SPCD 154 10002 3 67.139
SPCD 155 10002 1 19.107 10002 2 -95.534
SPCD 155 10002 3 70.058
SPCD 156 10002 1 19.903 10002 2 -99.515
SPCD 156 10002 3 72.978
SPCD 157 10002 1 20.699 10002 2 -103.495
SPCD 157 10002 3 75.897
SPCD 158 to 169 removed.
SPCD 170 10002 1 31.845 10002 2 -159.224
SPCD 170 10002 3 116.764
PBEAM 1 2 384. 193152. 102272.
+ + YESA 1.
+ PBEAM 2 2 186. 31028. 31028. 62057.
+ + YESA 1.
+ PBEAM 3 2 121. 8616. 8616. 17232.
+ + YESA 1.
+ PBEAM 4 1 154. 17497. 17497. 34993.
+ + YESA 2.
+ PBEAM 5 2 150. 9633. 20863. 211.
+ + YESA 1.
+ PBEAM 10 1 166. 38707. 38707. 77415.
+ + YESA 1.
+ PBEAM 11 1 166. 38707. 38707. 77415.
+ + YESA 1.
+ PBEAM 12 1 166. 38707. 38707. 77415.
+ + YESA 1.
+ PBEAM 13 1 141. 24041. 24041. 48081.
+ + YESA 1.

```

```

PBEAM 14 1 166. 38707. 38707. 77415. +
+
+ YESA 1. 166. 38707. 38707. 77415. +
+
+ YESA 1. 141. 24041. 24041. 48081. +
+
+ YESA 1. 166. 38707. 38707. 77415. +
+
+ YESA 1. 141. 24041. 24041. 48081. +
+
+ YESA 1. 141. 24041. 24041. 48081. +
+
+ YESA 1. 141. 24041. 24041. 48081. +
+
+ YESA 1. 93. 6790. 6790. 13581. +
+
+ YESA 1. 141. 24041. 24041. 48081. +
+
+ MATS1 1. PLASTIC 0.0 1 1 200. +
+ MATS1 2. PLASTIC 0.0 1 1 350. +
$
$
$ THIS SECTION CONTAINS ALL DEFINED COORDINATE SYSTEMS
$
$
CORD2R 1 0 0.0 0.0 0.0 0.0 0.0 1. +
1. 0.0
CORD2R 3 0 -560. 925. 1310. -560.812925.35321310.465+
-560.093924.13591310.495
$
$ THIS SECTION CONTAINS BULK DATA FOR SE 0
$
$
GRID 1 0.0 30. -200.
GRID 2 -268. 30. -330.
GRID 3 -268. 30. -296.
GRID 5 -268. 30. -236.8
GRID 6 -268. 30. -177.6
GRID 7 -268. 30. -118.4
GRID 8 -268. 30. -59.2
GRID 9 -268. 30. 0.0
Grid Points Removed.....
GRID 11009 0 -525. 925. 1407.8570
GRID 11012 0 525. 925. 1407.8570
GRID 11015 0 553.3744775.61732132. 0
GRID 11018 0 -553.3744775.61732132. 0
$
CBAR 10002 2 9674 10002 1. 1.
+
456 456
CBEAM 11001 10 9808 11000 1. 1.
CBEAM 11002 10 11000 9729 1. 1.
CBEAM 11004 10 11001 9737 1. 1.
CBEAM 11005 10 9816 11001 1. 1.
CBEAM 11008 10 11003 9724 1. 1.
CBEAM 11011 10 11006 9714 1. 1.
CBEAM 11014 10 11006 11009 1. 1.
CBEAM 11017 10 11003 11012 1. 1.
CBEAM 11022 10 11015 9696 1. 1.
CBEAM 11023 10 11018 9709 1. 1.

```

```

$
CBEAM 1 1 2 3 1 1
CBEAM 2 1 3 5 1 1
CBEAM 3 1 5 6 1 1
CBEAM 4 1 6 7 1 1
CBEAM 5 1 7 8 1 1
CBEAM 6 1 8 9 1 1
CBEAM 7 1 9 11 1 1
CBEAM 8 1 11 12 1 1
CBEAM 9 1 12 13 1 1
CBEAM 10 1 13 14 1 1
CBEAM Cards Removed.....
CBEAM 11020 12 9570 11018 1. 1.
CBEAM 11021 12 11018 9568 1. 1.
$
$ THIS SECTION CONTAINS THE LOADS, CONSTRAINTS, AND CONTROL BULK DATA ENTRIES
$
$
FORCE 100 10002 100 1.5 -7.5 5.5
FORCE 101 10002 101 1.5 -7.5 5.5
FORCE 102 10002 102 1.5 -7.5 5.5
FORCE 103 10002 103 1.5 -7.5 5.5
FORCE 104 10002 104 1.5 -7.5 5.5
FORCE 105 10002 105 1.5 -7.5 5.5
FORCE 106 10002 106 1.5 -7.5 5.5
FORCE 107 10002 107 1.5 -7.5 5.5
FORCE 108 10002 108 1.5 -7.5 5.5
FORCE 109 10002 109 1.5 -7.5 5.5
FORCE 110 10002 110 1.5 -7.5 5.5
FORCE 111 10002 111 1.5 -7.5 5.5
$
SPC 100 1 123456 0.0
SPC 100 17 123 0.0
SPC 100 80 123 0.0
SPC 100 10002 123456 0.0
SPC 100 36 123 0.0
SPC 100 99 123 0.0
SPC 100 45 123 0.0
SPC 100 108 123 0.0
SPC 100 54 123 0.0
SPC 100 117 123 0.0
SPC 100 120 123456 0.0
SPC 100 160 123456 0.0
SPC 100 215 123456 0.0
SPC 100 245 123456 0.0
SPC 100 890 123456 0.0
SPC 100 900 123456 0.0
SPC 100 910 123456 0.0
SPC 100 920 123456 0.0
$
$ THIS SECTION CONTAINS THE PROPERTY AND MATERIAL BULK DATA ENTRIES
$
$
PBAR 2 1 219. 50192. 50192. 100383.
$
MAT1 1 207000. .33 7.85-9
MAT1 2 207000. .33 7.85-9
$
NLFARM 1 5 AUTO PW NO
NLFARM 2 15 AUTO PW NO
NLFARM 3 25 AUTO PW NO
ENDDATA

```





CORD2R 1 0 0.0 0.0 0.0 0.0 1. +  
 1. 0.0 0.0 -560. 925. 1310. -560.812925.35321310.465+  
 CORD2R 3 0 -560. 925. 1310. -560.812925.35321310.465+

\$ THIS SECTION CONTAINS BULK DATA FOR SE 0  
 \$ \$ \$ \$ \$

GRID 1 0.0 30. -200.  
 GRID 2 -268. 30. -330.  
 GRID 3 -268. 30. -296.  
 GRID 5 30. -236.8  
 GRID 6 -268. 30. -177.6  
 GRID 7 -268. 30. -118.4  
 GRID 8 -268. 30. -59.2  
 GRID 9 -268. 30. 0.0

Grid cards deleted from here.....  
 GRID 15088 0 -299.591402.5 2641.5450  
 GRID 15089 0 -287.727375. 2668.3640  
 GRID 15090 0 -275.864347.5 2695.1820

\$ \$ \$ \$ \$  
 CBEAR 1 1 2 3 1  
 CBEAR 2 1 3 5 1  
 CBEAR 3 1 5 6 1  
 CBEAR 4 1 6 7 1  
 CBEAR 5 1 7 8 1  
 CBEAR 6 1 8 9 1  
 CBEAR 7 1 9 11 1  
 CBEAR 8 1 11 12 1  
 CBEAR 9 1 12 13 1  
 CBEAR 10 1 13 14 1

CBEAR Cards Deleted from here.....  
 CBEAR 7855 2 8913 8914 1. 1.  
 CBEAR 7856 2 8914 293 1. 1.  
 CBEAR 10002 200 9570 10002 1. 1.  
 + 456 456

\$ \$ \$ \$ \$  
 CBEAM 7933 70 222 8997 1. 1.  
 CBEAM 7934 70 229 8999 1. 1.  
 CBEAM 7935 70 9001 9001 1. 1.  
 CBEAM 7936 70 9001 9002 1. 1.  
 CBEAM 7937 70 9002 9003 1. 1.  
 CBEAM 7938 70 9003 9004 1. 1.  
 CBEAM 7939 70 9004 9005 1. 1.  
 CBEAM 7940 70 9005 9006 1. 1.  
 CBEAM 7941 70 9006 9007 1. 1.  
 CBEAM 7942 70 9007 9008 1. 1.  
 CBEAM 7943 70 9008 9009 1. 1.  
 CBEAM 7944 70 9009 9010 1. 1.

CBEAM Cards Deleted from here.....  
 CBEAM 15085 13 15088 15089 1. 1.  
 CBEAM 15086 13 15089 15090 1. 1.  
 CBEAM 15087 13 15090 307 1. 1.

\$ \$ \$ \$ \$  
 SPC 1 1 123456 0.0  
 SPC 2 1 123456 0.0  
 SPC 3 1 123456 0.0  
 SPC 4 1 123456 0.0  
 SPC 10 1 123456 0.0  
 SPC 1 120 123456 0.0  
 SPC 11 1 123456 0.0  
 SPC 2 120 123456 0.0  
 SPC 100 2 123 0.0  
 SPC cards deleted from here.....  
 SPC 100 10002 123456 0.0  
 \$ \$ \$ \$ \$

\$ THIS SECTION CONTAINS THE PROPERTY AND MATERIAL BULK DATA ENTRIES

\$ \$ \$ \$ \$  
 PBAR 1 1 384. 193152. 102272. 202401.  
 PBAR 2 1 186. 31028. 31028. 62057.  
 PBAR 3 1 121. 8616. 8616. 17232.  
 PBAR 4 1 154. 17497. 17497. 34993.  
 PBAR 5 1 150. 9633. 20863. 211.  
 PBAR 200 1 219. 50192. 50192. 100383.

\$ \$ \$ \$ \$  
 MATI 1 1 207000. .33 7.85-9  
 NLFARM 1 5 AUTO PW NO  
 NLFARM 2 15 AUTO PW NO  
 NLFARM 3 28 AUTO PW NO  
 ENDDATA

\$ THIS SECTION CONTAINS THE LOADS, CONSTRAINTS, AND CONTROL BULK DATA ENTRIES

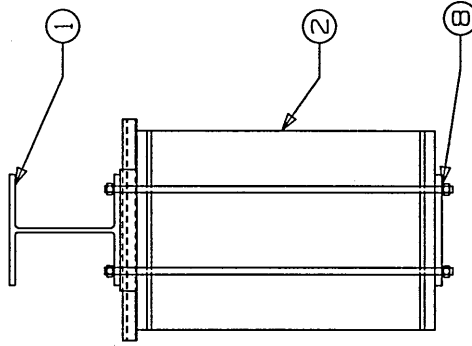
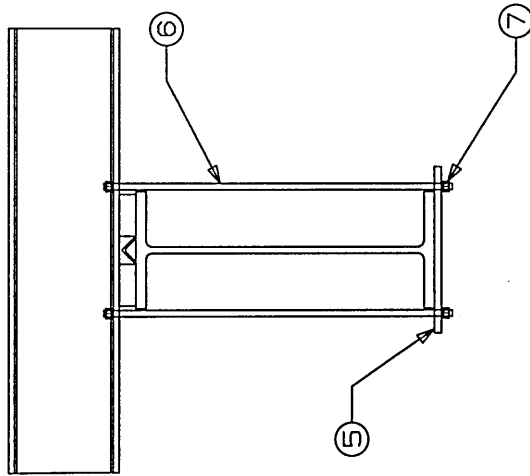
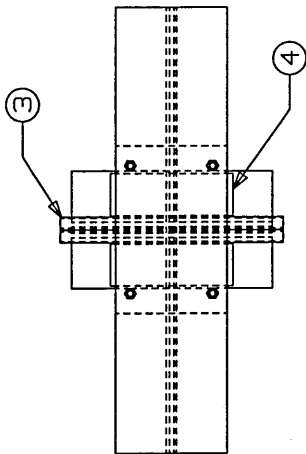
## Appendix J

# Drawings

ITEM	DRWG. No.	DESCRIPTION	QTY.	MATERIAL
1	NOT DRAWN	CHASSIS MOUNTING BEAM	2	STEEL I BEAM 200x200
2	NOT DRAWN	TEST RIG SUPPORT BEAM	3	STEEL I BEAM 210x540
3	NOT DRAWN	GUIDE RAIL	1	STEEL ANGLE 38x38
4	TVR004	PACKING PLATE	4	STEEL 220x75x30
5	TVR002	CLAMPING PLATE	2	STEEL 200x300x12
6	TVR003	CLAMPING ROD	8	STEEL $\phi$ 12
7	TVR003	NUT	16	STEEL 12x1.75
8	TVR003	PLAIN WASHER	16	STEEL

NOTES:

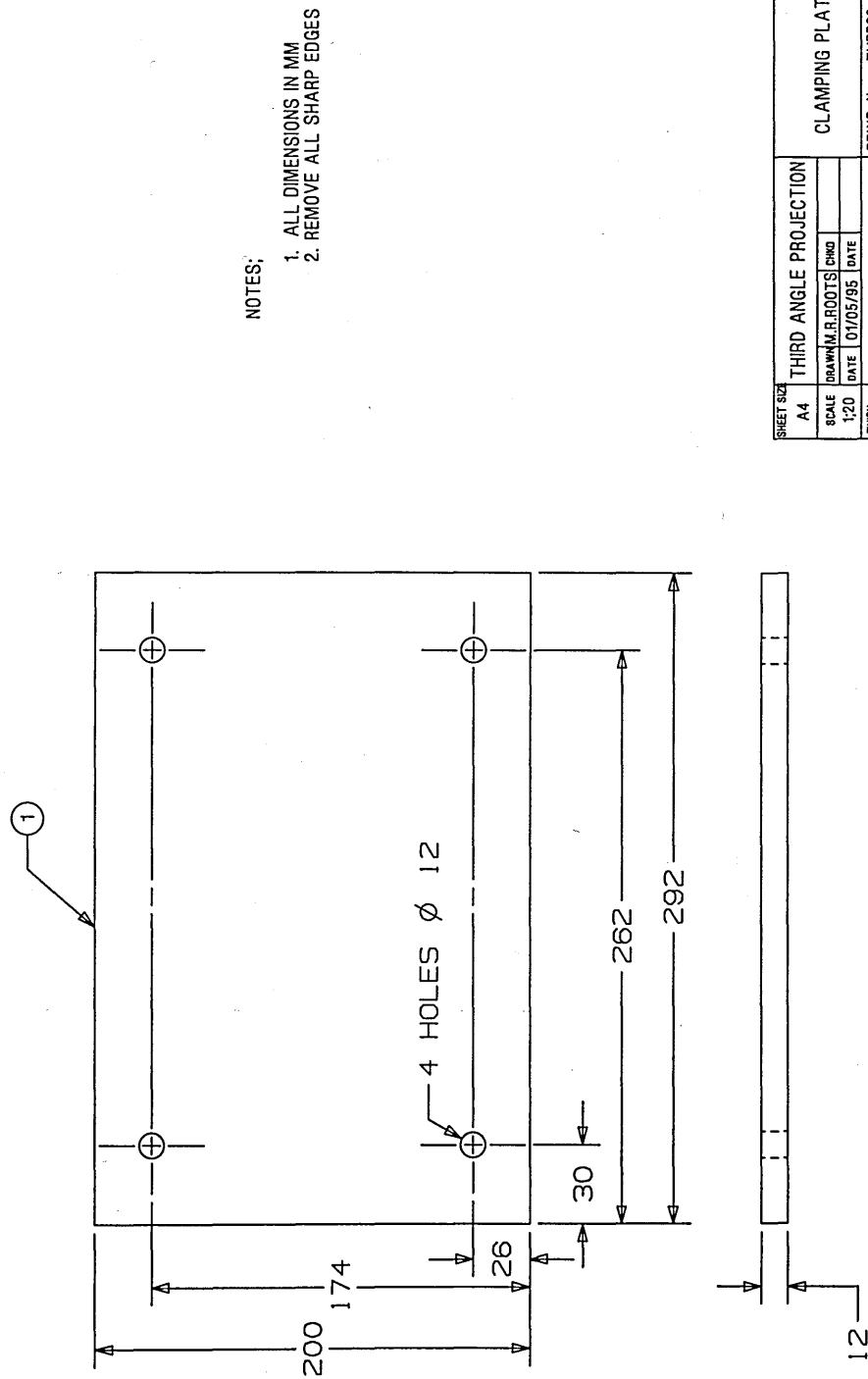
1. ALL DIMENSIONS IN MM
2. MOUNTING BEAMS AND GUIDE RAIL NOT SHOWN TRUE LENGTH.
3. CHASSIS NOT SHOWN



SHEET SIZE		THIRD ANGLE PROJECTION		TVR CHASSIS TEST MOUNTING GENERAL ARRANGEMENT	
A4	SCALE	DRWN	M.R.ROOTS	CRD	
1:10	1:10	DATE	07/05/95	DATE	
FINISH		CRANFIELD UNIVERSITY		DRWG. NO. TVR001	
		COLLEGE OF AERONAUTICS		SHEET OF SHEETS	

DO NOT SCALE

ITEM	DRWG. No.	DESCRIPTION	QTY	MATERIAL
1	TYR002	CLAMPING PLATE	2	COLD FORMED MILD STEEL



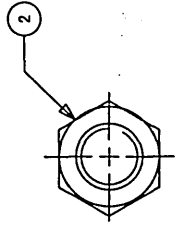
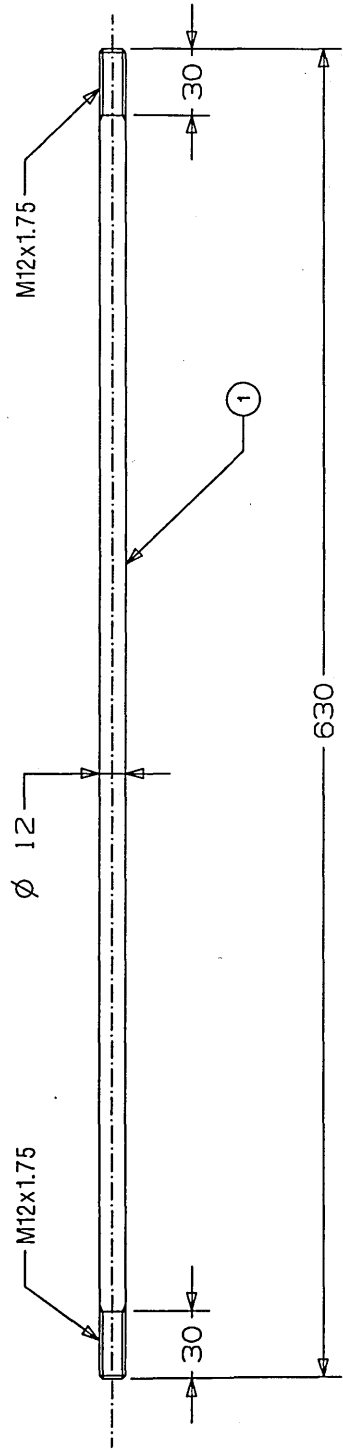
NOTES:  
 1. ALL DIMENSIONS IN MM  
 2. REMOVE ALL SHARP EDGES

SHEET SIZE		THIRD ANGLE PROJECTION		CLAMPING PLATE	
A4	SCALE	DRAWN	R ROOTS	CHKD	
1:20	DATE	10/05/95	DATE		
FINISH	CRANFIELD UNIVERSITY		COLLEGE OF AERONAUTICS		DRWG. No. TYR002
					SHEET OF SHEETS

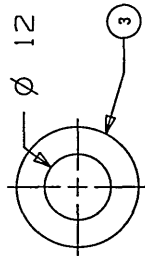
DO NOT SCALE

DO NOT SCALE

ITEM	DRWG No.	DESCRIPTION	QTY	MATERIAL
1	TVRD03	THREADED STEEL ROD	8	STEEL - GRADE 4.8 MIN.
2	TVRD03	M12x1.75 NUT	16	STEEL - GRADE 4.8 MIN.
3	TVRD03	FLAT STEEL WASHER	16	MILD STEEL



GRADE 4.8 STEEL NUT  
M12x1.75 - 4 OFF

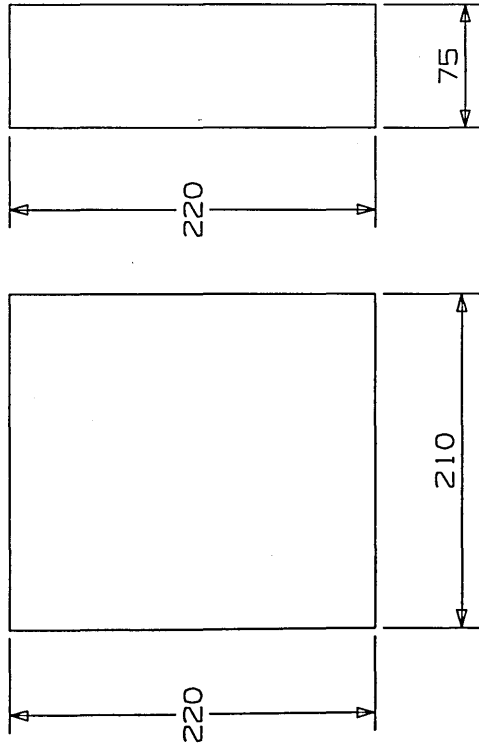


MILD STEEL FLAT WASHER  
4 OFF

SHEET SIZE		TVR TEST EQUIPMENT		CLAMPING ROD, NUTS AND WASHERS	
A4	SCALE	DRAWN (M.R.ROOTS)	CHKD		
1:2.5	DATE	01/05/95	CATE		
FINISH	CRANFIELD UNIVERSITY		DRWG NO: TVRD03		
	COLLEGE OF AERONAUTICS		SHEET OF SHEETS		

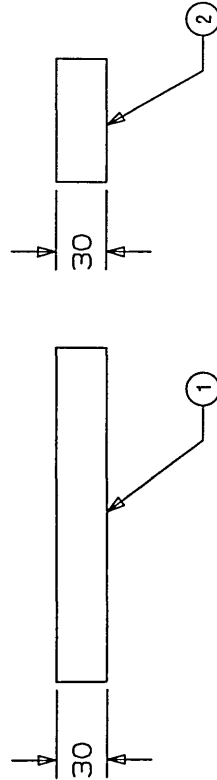
ITEM	DRWG No.	DESCRIPTION	QTY	MATERIAL
1	TVR004	PACKING PIECE	2	MILD STEEL 210X220X30
2	TVR004	PACKING PIECE	4	MILD STEEL 75X220X30

DO NOT SCALE



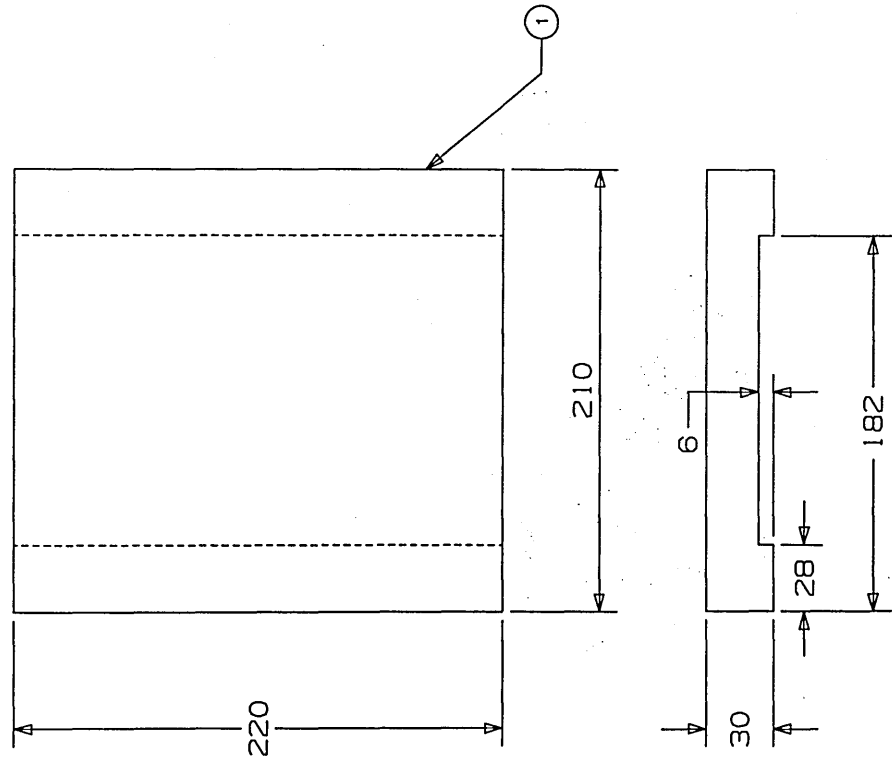
NOTES:

1. ALL DIMENSIONS IN MM
2. REMOVE ALL SHARP EDGES



SHEET SIZE		THIRD ANGLE PROJECTION		PACKING PIECE	
A4	DRW/M.R.ROOTS	CRD	DATE	02/05/95	DRWG NO: TVR004
SCALE	1:5	FINISH	CRANEFIELD UNIVERSITY	COLLEGE OF AERONAUTICS	SHEET OF SHEETS

DO NOT SCALE				
ITEM	DRWG No.	DESCRIPTION	QTY	MATERIAL
1	TVRD05	PACKING PIECE	2	MILD STEEL 220X200X30



NOTES  
 1. ALL DIMENSIONS IN MM  
 2. REMOVE ALL SHARP EDGES

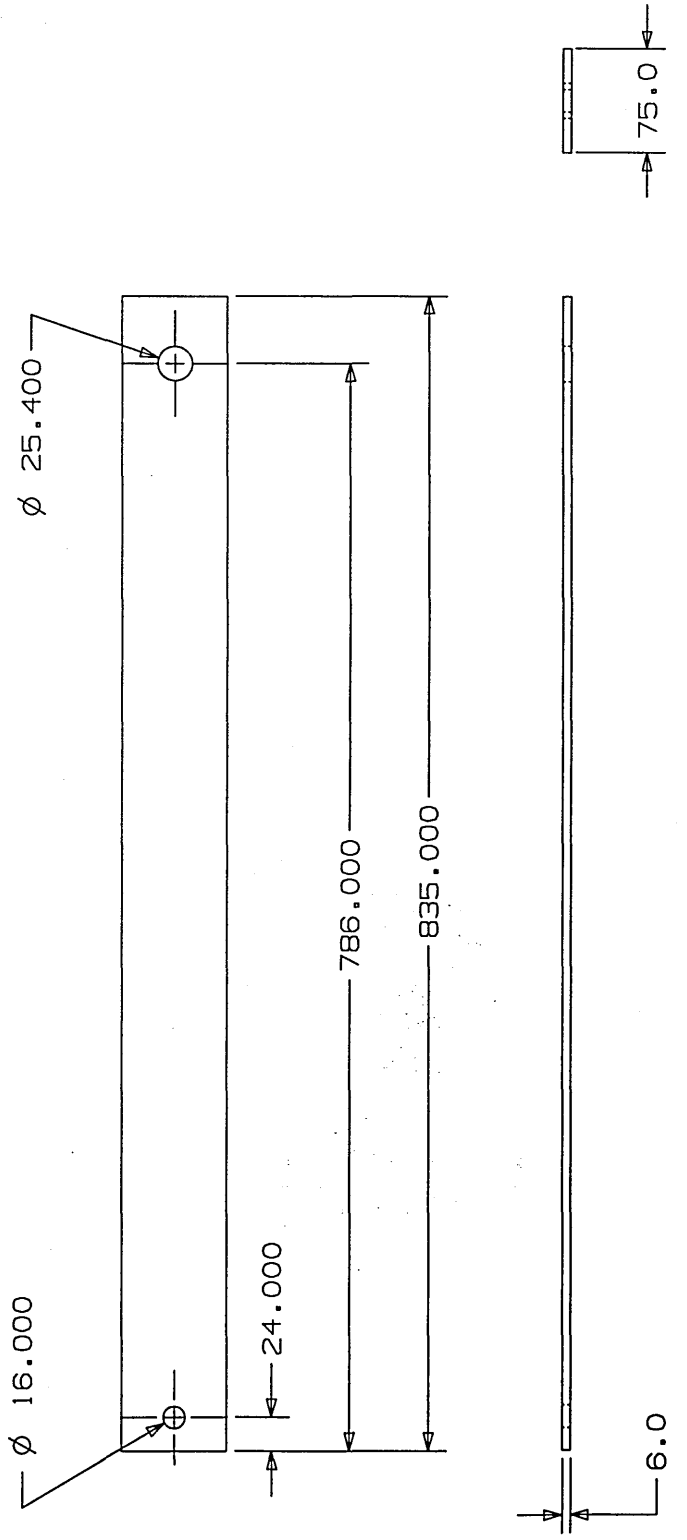
SHEET SIZE	THIRD ANGLE PROJECTION		PACKING PIECE	
A4	DRAWN	M.R.ROOTS	CHD	
SCALE	1:2.5	DATE	02/05/95	DRWG NO: TVRD05
FRSB	CRANFIELD UNIVERSITY		SHEET OF SHEETS	
	COLLEGE OF AERONAUTICS			





ITEM	DRWG No.	DESCRIPTION	QTY	MATERIAL
1	TVR007	LOADING BAR	4	MILD STEEL FLAT BAR
2				
3				
4				

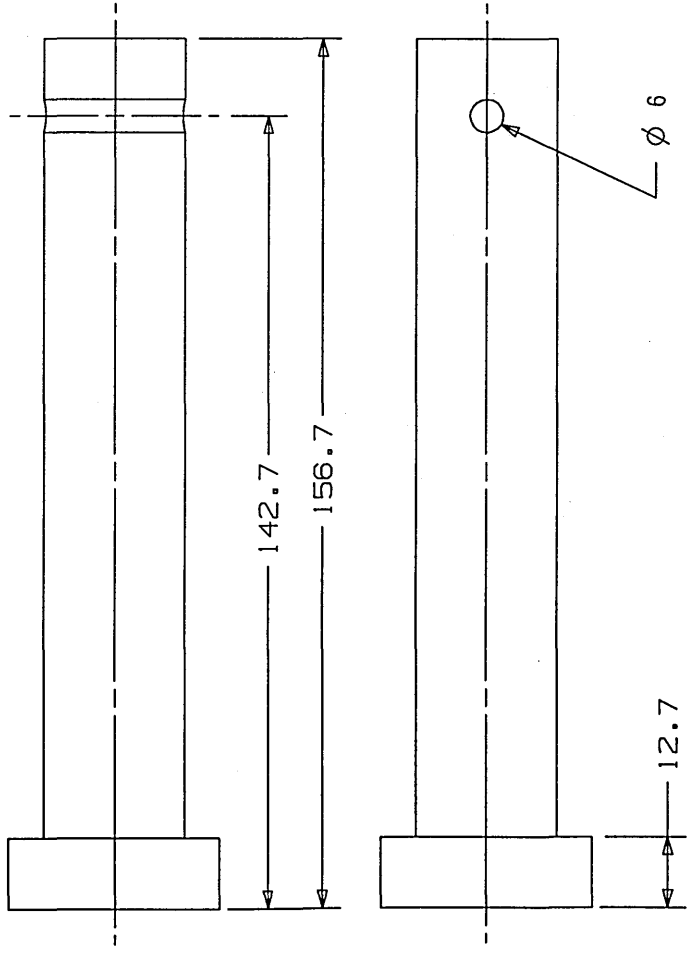
DO NOT SCALE



SHEET SIZE		THIRD ANGLE PROJECTION	
SCALE	DRAWN	M. ROOTS	CHD
FR81	DATE	31/08/95	DATE
		CRANFIELD UNIVERSITY	
		COLLEGE OF AERONAUTICS	
		DRWG NO. TVR007	SHEET OF SHEETS

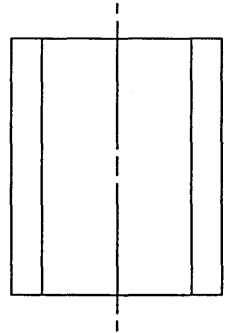
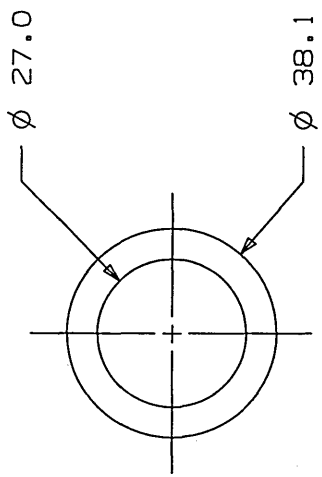
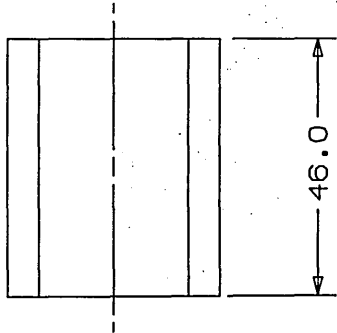
TVR TEST RIG  
LOADING BAR

ITEM	DRWG No.	DESCRIPTION	QTY	MATERIAL
1		LOAD PIN	1	MILD STEEL



SHEET SIZE		THIRD ANGLE PROJECTION		TVR TEST RIG LOAD PIN	
SCALE	DRAWN	R. ROOTS	CHD		
FINISH	DATE	31/08/95	DATE		
CRANFIELD UNIVERSITY COLLEGE OF AERONAUTICS				DRWG NO:	TVR008
				SHEET	OF SHEETS

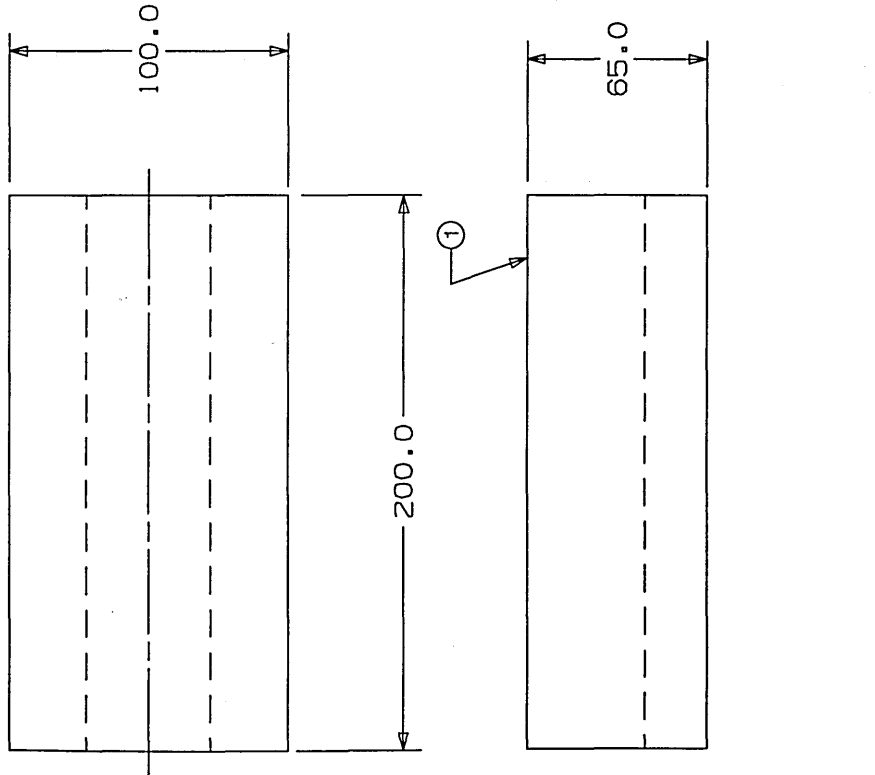
ITEM	DRWG No.	DESCRIPTION	QTY	MATERIAL
	TVR009	LOAD CELL SPACER	2	MILD STEEL



SHEET SIZE		THIRD ANGLE PROJECTION		TVR TEST RIG SPACER	
SCALE	DRWN	M.P.ROOTS	CHKD		
	DATE	31/09/95	DATE		
FINISH	CRANFIELD UNIVERSITY			DRWG NO: TVR009	
	COLLEGE OF AERONAUTICS			SHEET OF SHEETS	

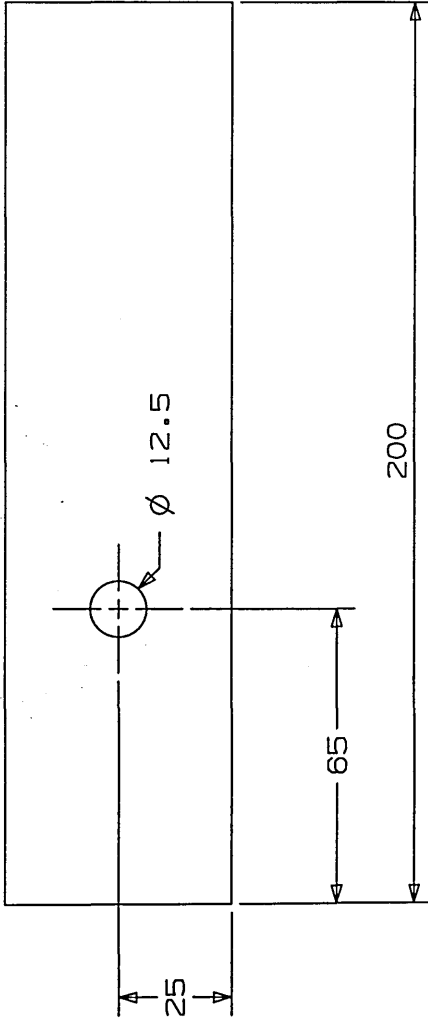
ITEM	DRWG No.	DESCRIPTION	QTY	MATERIAL
1	TVRD10	MOUNTING FORM BLOCK	2	HARDWOOD

NOTES:  
 1. GRAIN DIRECTION ACROSS WIDTH  
 2. RADIUS IN BLOCK TO SUIT 1.75" OD TUBE



SHEET SIZE		THIRD ANGLE PROJECTION		TVR TEST RIG MOUNT BLOCK	
SCALE	FINISH	DATE	DATE	DRWG NO.	SHEET OF SHEETS
1:2		1/9/95		TVRD10	
		CRANFIELD UNIVERSITY COLLEGE OF AERONAUTICS			

ITEM	DWG NO.	DESCRIPTION	QTY	MATERIAL
1		MOUNTING PLATE	10	MILD STEEL STRIP
2	NOT DRAWN	BOLT	10	M10, GRADE 8.8
3	NOT DRAWN	WASHER	10	MILD STEEL TO SUIT
4	NOT DRAWN	NUT	10	M10, GRADE 8.8



NOTES

1. MINIMUM MATERIAL THICKNESS 10MM
2. MINIMUM BOLT DIAMETER 10MM
3. REMOVE ALL SHARP EDGES
4. HOLE IN PLATE TO SUIT BOLTS
5. MINIMUM PLATE WIDTH 50MM

